UNIVERSIDADE DE SÃO PAULO
DEPARTMENT OF MECHANICAL ENGINEERING – POLYTECHNIC SCHOOL
CONCENTRATION AREA OF THERMAL AND FLUIDS ENGINEERING

DANILO BRITO STECKELBERG

DEVELOPMENT OF AN INTERNAL COMBUSTION ENGINE FUEL MAP MODEL BASED ON ON-BOARD ACQUISITION

São Paulo
2016

DANILO BRITO STECKELBERG

DEVELOPMENT OF AN INTERNAL COMBUSTION ENGINE FUEL MAP MODEL BASED ON ON-BOARD ACQUISITION

Dissertation submitted to Polytechnic School of São Paulo University (*Escola Politécnica da Universidade de São Paulo*) to obtain the degree of Master of Science in Engineering.

Concentration area of Thermal and Fluids engineering.

ADVISOR: Antônio Luiz Pacífico

São Paulo

2016

Este exemplar foi revisado e corrigido em relação à versão original, sob responsabilidade única do autor e com a anuência de seu orientador.

São Paulo, _____ de _____ de _____

Assinatura do autor: _____

Assinatura do orientador: _____

Catalogação-na-publicação

Steckelberg, Danilo
Development of an Internal Combustion Engine Fuel Map Model Based on On-board Acquisition / D. Steckelberg -- versão corr. -- São Paulo, 2016.
171 p.

Dissertação (Mestrado) - Escola Politécnica da Universidade de São Paulo. Departamento de Engenharia Mecânica.

1.Automotive Engineering 2.Vehicle Dynamics 3.Fuel Consumption 4.Engine Fuel Map I.Universidade de São Paulo. Escola Politécnica. Departamento de Engenharia Mecânica II.t.

DEDICATION

This work is dedicated to my parents, who have granted me all support during my whole student life and onwards, despite of the fact that I would live far from them.

All my friends are also remembered, since this work has occupied a good part of my time.

I also dedicate this work to Maressa, my love, who has always supported me, despite of all difficulties we found on the course of this work.

ACKNOWLEDGEMENTS

I thank my professor Antônio Luiz Pacífico who has helped with patience and attention.

I also acknowledge the Polytechnic School of São Paulo University for the opportunity to study such a fascinating field.

RESUMO

É apresentada uma metodologia para descrever o mapa de desempenho (ou mapa de consumo de combustível) de um motor de combustão interna como função de suas condições de operação (rotação e torque) baseados em medições embarcadas. É utilizada para este levantamento a combinação de medições via GPS (para a velocidade longitudinal e inclinação de pista) e OBD-II para aquisição de sinais da rede CAN, como rotação do motor e consumo de combustível.

É desenvolvida uma metodologia para o cálculo do torque líquido do motor baseado na medição de velocidade e aceleração longitudinal do veículo com uma margem de incerteza de 2% a 5% no cálculo do torque em condições normais de operações. É realizado um detalhamento da origem das incertezas para avaliar a contribuição individual de cada parâmetro.

Um modelo de regressão polinomial é utilizado para descrever o mapa de consume de combustível do motor cujos coeficientes característicos são determinados experimentalmente através da metodologia proposta para cinco veículos diferentes a fim de comprovar a eficácia da metodologia. Os coeficientes de correlação variam de 0.797 a 0.997, sendo que em três de cinco veículos o coeficiente de correlação é maior que 0.910, comprovando a robustez da metodologia.

Palavras-chaves: mapa de desempenho, consumo de combustível, rede CAN, porta OBD-II.

ABSTRACT

It is presented a methodology to describe the engine performance map (or the engine fuel map) for an internal combustion engine as a function of its operating conditions (engine speed and torque) based on on-board measurements. It is used a combination of GPS measurements for vehicle speed and road grade together with a OBD-II acquisition system in order to acquire information provided by CAN network, such as engine speed and fuel consumption.

A methodology to calculate the engine torque based on speed and acceleration measurements is shown with an average uncertainty in the range of 2% to 5% for torque calculation in normal operating conditions. It is presented a detailed breakdown of the contribution of individual parameters in torque calculation uncertainty.

A polynomial regression model to describe the engine fuel map is presented and the coefficients for this model is calculated based on on-road measurements for 5 different vehicles to prove the accuracy of the proposed methodology. The correlation coefficients obtained for these measurements are within the range of 0.797 to 0.997 and three out of five vehicles with correlation coefficient higher than 0.910, proving the methodology robust.

Keywords: engine performance map, fuel consumption, CAN network, OBD-II.

SUMMARY

TABLE OF FIGURES

TABLE OF TABLES

TABLE OF ACRONYMS (ALPHABETIC ORDER)

ABNT	Brazilian Association of Technical Normatization
ABS	Anti-lock Brake System
AI	Artificial Intelligence
ANN	Artificial Neural Networks
ASA	Adaptative Simulated Annealing algorithm
BMEP	Brake Mean Effective Pressure
BQM	Backward Quasi-static Model
BSFC	Brake Specific Fuel Consumption
CAN	Controller Area Network
CFD	Computational Fluid Dynamics
CG	Center of Gravity
CH	Chassis Block
CO2	Carbon Dioxide
DE	Differential Evolutionary algorithm
DFT	Discrete Fourier Transform
DOP	Dillution of Precision
DR	Driver Block
DTC	Diagnostic Trouble Code
ECU	Electronic Control Unit
EN	Engine Block
EPA	Environmental Protection Agency
FBD	Free Body Diagram
FDM	Forward Dynamic Model
FFT	Fast Fourier Transform
FTP-75	Federal Test Procedure-75
GA	Genetic Algorithms
GHG	Greenhouse Gases

GPS	Global Positioning System
HC	Hydrocarbons
HMI	Human-Machine Interface
HRR	Heat Rejection Rate
ICE	Internal Combustion Engine
IDM	Inverse Dynamic Model
IIR	Infine Impulse Response
IMEP	Indicated Mean Effective Pressure
INMETRO	Brazilian Institute of Metrology, Quality and Tecnology
ISFC	Indicated Specific Fuel Consumption
ISO	International Organization for Standardization
JC08	Japanese speed cycle
LPG	Liquefied Petrol Gas
MA	Moving Average filter
MAF	Mass Air Flow
MAP	Manifold Absolute Pressure
NEDC	New European Drive Cycle
NHTSA	National Highway and Traffic Safety Agency
NOX	Nitrous Oxides
OBD-II	On-Board Diagnosis II
ORNL	Oak Ridge National Laboratory
PEMS	Portable Emission Monitoring System
PM	Particulate Material
RMSE	Root Mean Square Errors
RPM	Revolutions Per Minute
SAE	Society of Automotive Engineers
SC03	Air conditioning speed cycle
SSE	Sum of Square Errors
THC	Total Hydrocarbons
TR	Transmission Block
US06	High power speed cycle
WH	Wheel Block
WOT	Wide Open Throttle

TABLE OF SYMBOLS (ORDER OF APPEARANCE)

t_t	Total time
D_t	Total distance
P_i	Percentage of time in idle
P_a	Percentage of time in acceleration
P_c	Percentage of time in cruise
P_d	Percentage of time in deceleration
v	Vehicle speed
a	Vehicle acceleration
$\bar{v}$	Mean speed
v_{max}	Maximum speed
$\bar{a}_+$	Average positive acceleration
$FE_{combined}$	Laboratory combined fuel economy
FE_{city}	Laboratory city fuel economy
$FE_{highway}$	Laboratory highway fuel economy
FE^*_{city}	Adjusted highway city fuel economy
$FE^*_{highway}$	Adjusted highway fuel economy
θ	Road grade
VSP	Vehicle specific power
V_p	Piston speed
ω_e	Engine rotational speed
f_c	Fuel consumption
τ_e	Engine torque
A_{eff}	Throttle effective area
τ_w	Wheel torque
ω_w	Wheel rotational speed
W, W_f, W_r	Weight force (W) acting on front wheel (W_f) and rear wheel (W_r)
F, F_{xf}, F_{xr}	Tractive force (F) acting on front wheel (F_f) and rear wheel (F_r)

R_{hx}, R_{hz}	Trailer towing force (R_h) acting on front wheel (R_{hf}) and rear wheel (R_{hr})
D_A	Aerodynamic drag force
τ_c	Clutch torque
I_e	Engine rotational inertia
α_e	Engine rotational acceleration
τ_d	Differential torque
I_t	Transmission rotational inertia
N_t	Transmission gear ratio
τ_a	Axle torque
N_f	Differential gear ratio
r	Tire dynamic radius
I_w	Wheel rotational inertia
α_w	Wheel rotational acceleration
α_d	Differential rotational acceleration
η_{tf}	Transmission and Differential combined efficiency
M_r	Rotational equivalent mass
M_e	Equivalent mass
M	Vehicle curb mass
$f_r, f_\emptyset, f_s$	Coefficients of tire rolling resistance
F_z	Force acting on z direction
F_{z0}	Reference force acting on z direction
R_x	Tire resistive force acting on x direction
R_{x0}	Reference tire resistive force acting on x direction
c_p	Pressure proportional coefficient (constant)
p_0	Reference inflation pressure
p	Inflation pressure
ρ	Air density
C_d	Aerodynamic drag coefficient
A_F	Frontal area
v_r	Relative speed between vehicle and wind
v_w	Wind speed

ψ	Wind drift angle
R_{Tx}	Resistive force on x direction
f_0	Resistive force regression constant coefficient
f_2	Resistive force regression quadratic coefficient
Δt	Time interval
$\overline{v_i}$	Mean speed on interval i
a_i	Acceleration on interval i
v_i	Speed on interval i
f_o'	Corrected resistive force regression constant coefficient
f_2'	Corrected resistive force regression quadratic coefficient
$(A/F)_{stoic}$	Air-fuel ratio in stoichiometric condition
$(A/F)_{actual}$	Actual Air-fuel ratio
λ	Equivalence ratio
$\sigma_{f_0}, \sigma_{f_2}, \sigma_x, \ldots$	Standard deviation of variable f_0, f_2, x, …
$\mu_{f_0}, \mu_{f_2}, \mu_x, \ldots$	Sample mean of variable f_0, f_2, x, …
k	Moving average filter periods
$H(\Omega)$	Signal amplitude
Ω	Frequency
Ω_c	Filter Cut-off frequency
N	Filter order
s_x,s_z, …	Space covered in $x, z,$ ... direction
$\dot{s_x}$,$\dot{s_z}$, …	Derivative of space covered in $x, z,$ ... direction with respect to time
$\dot{m}_f$	Fuel mass flow
λ_{comm}	Commanded equivalence ratio
$\dot{m_{air}}$	Air mass flow (equivalent to MAF)
λ_{stoic}	Stoichiometric equivalence ratio
P_{kin}	Kinetic power
P_{res}	Resistive power
P_g	Grade power
P_{wheel}	Power acting on wheel
P_e	Engine power
$a_{00}, a_{10}, \ldots, a_{ij}$	Polynomial regression coefficients

R^2	Correlation coefficient
$RMSE$	Root mean square errors
SSE	Sum of square errors
F_{test}	Statistical F test
$\sum \dot{m}_{f_c}$,	Total fuel mass flow calculated
$\sum \dot{m}_{f_m}$	Total fuel mass flow measured
$\Delta_{m/c}$	Relative difference between measured and calculated fuel mas flow

1 INTRODUCTION

The Transportation sector is a major energy consumer worldwide. Brazilian's Company for Energetic Research (*Empresa de Pesquisas Energéticas – EPE)* presents in its yearbook the energy consumption by different sources and also by sectors. Figure 1.1 presents the final consumption by source:

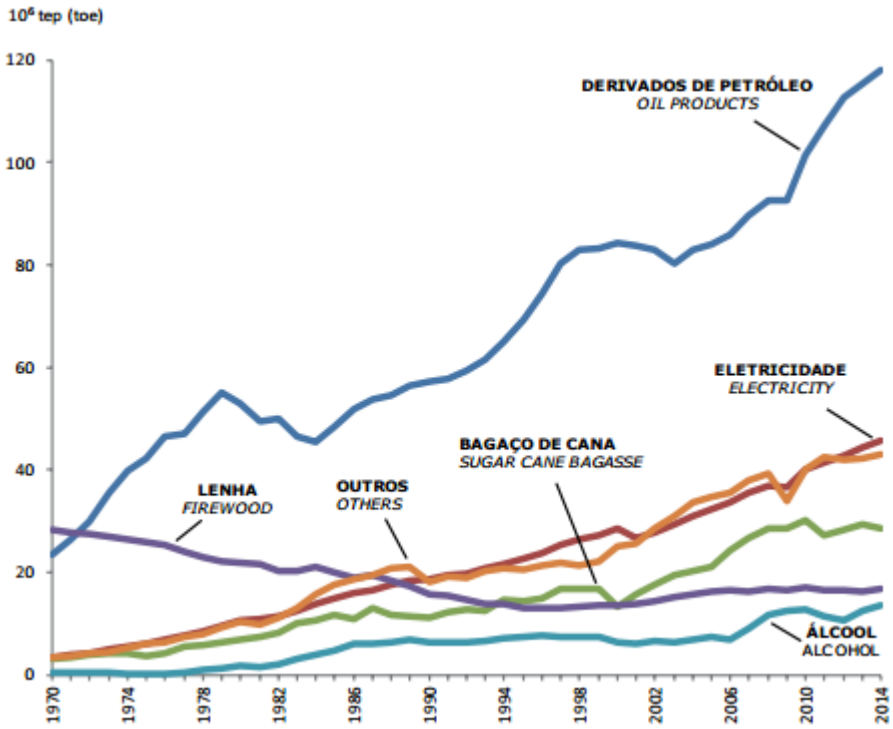

Figure 1.1 - Energy consumption by source (EPE, 2015)

It can be observed that the increase in energy consumption by oil products is higher than the increase for other sources. According to EPE (2015), between the year of 2005 and 2014 the energy consumption by oil products share went from 42.9% to 44.5%; for gasoline, the share went from 7.0% to 9.7%; for Diesel, from 16.7% to 18.8%. The ethylic alcohol, which is also used as fuel for vehicles in Brazil, went from 3.7% to 5.1%.

This report presents the oil products consumption by sector, presented in Figure 1.1:

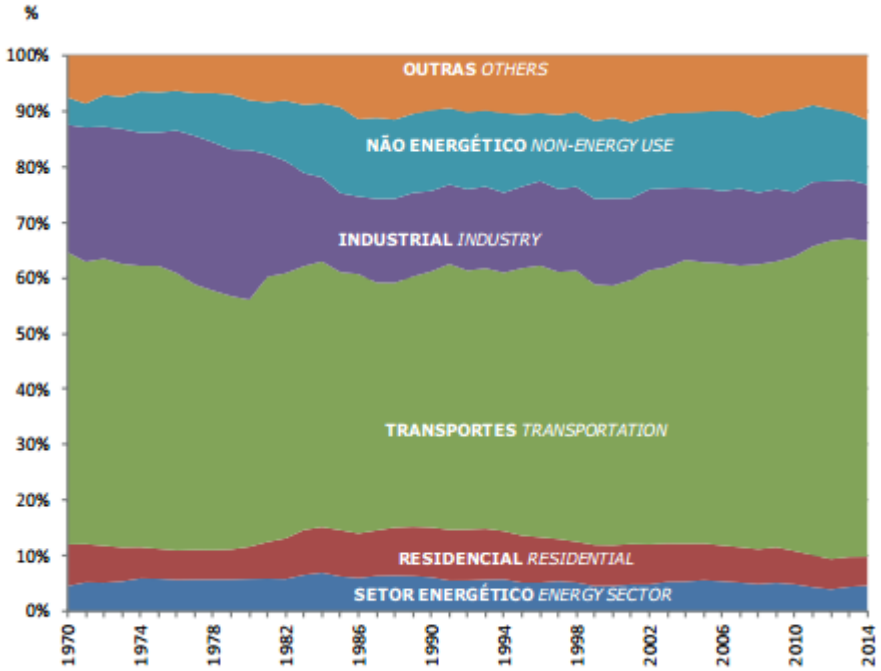

Figure 1.1 - Oil products consumption by sector (EPE, 2015)

From Figure 1.1 one can conclude that the transportation sector is the main oil products consumer. In 2005, the consumption relative to this sector accounted for 50.6% of total oil products consumption, and went to 56.9% in 2014.

The U.S. Energy Information Agency (EIA) presented in its 2011 yearbook a similar analysis (EIA, 2012). Figure 1.2 presents the energy consumption by source from 1949 to 2011:

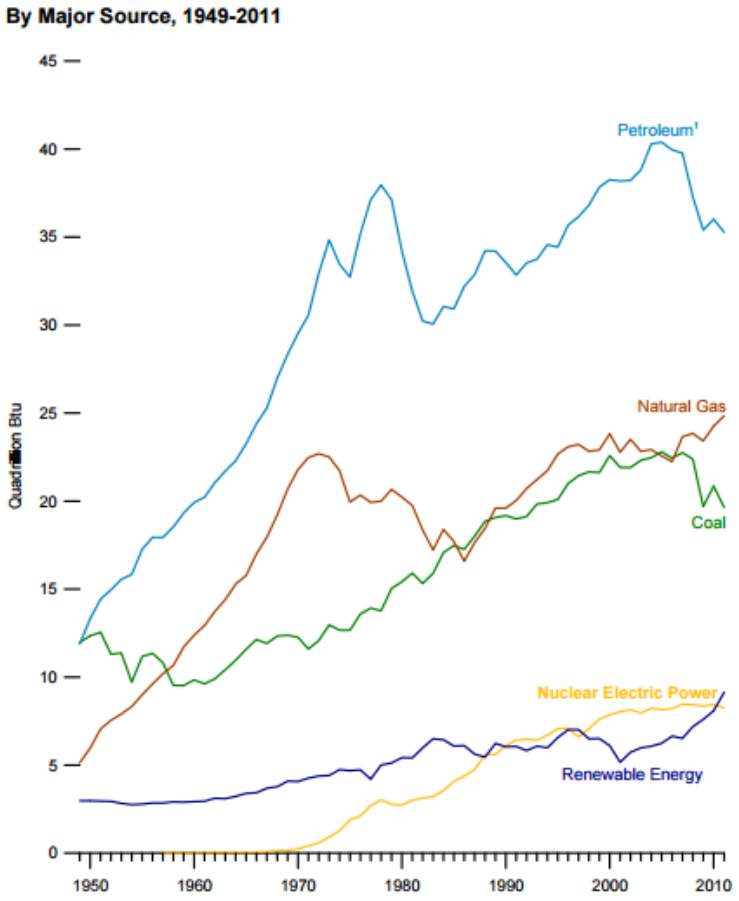

Figure 1.2 – Energy consumption by source (EIA, 2012)

From Figure 1.2, it can be observed that petroleum consumption is higher than all other sources. The relationship between different sectors and the primary energy source is presented in Figure 1.3. From Figure 1.1 to Figure 1.3, it can be concluded that Petroleum is the most important fuel source in the transportation sector, and that the transportation sector is one of the major players in total energy consumption.

In order to reduce the transportation sector from Petroleum, many countries worldwide have adopted regulations to monitor and control carbon dioxide (CO_2) emissions from passenger and light commercial vehicles In the United States of America (US), the National Highway Traffic Safety Administration (NHTSA), a subsidiary of US Department of Transportation (DOT) set standards for Corporate Average Fuel Economy (CAFE), measured in miles per gallon, that should be met from 1978 onwards (NHTSA, 1978). The European Union (EU), through the European Community (EC), has also created a regulation based on CO_2 emissions from 1999 onwards (EC, 1999).

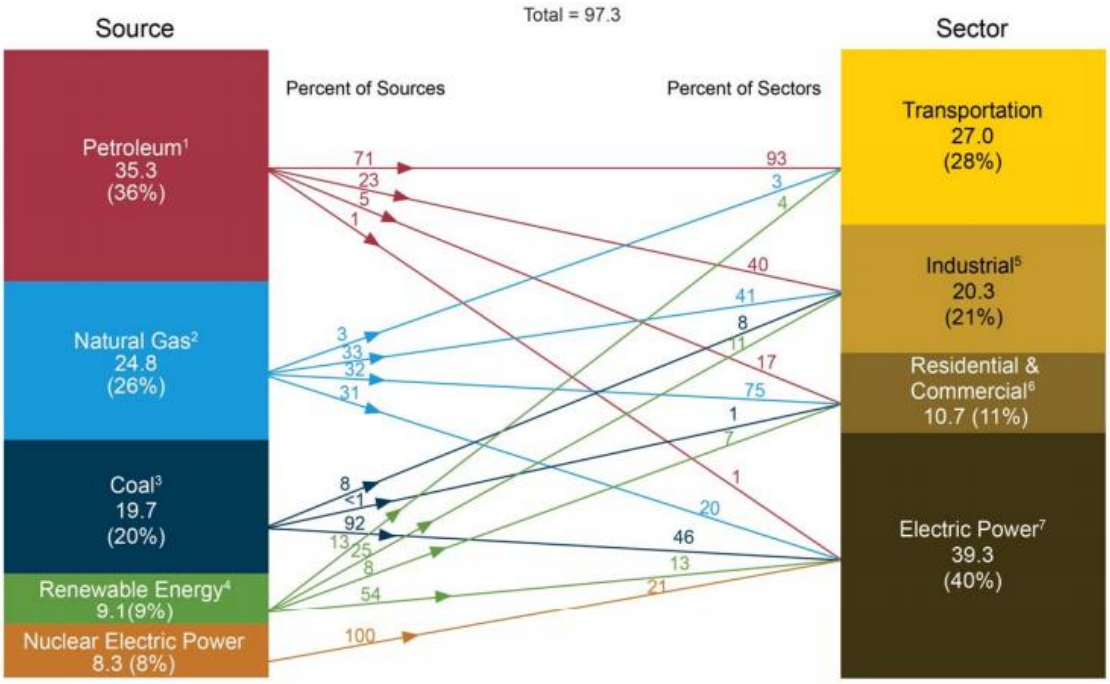

Figure 1.3 – Primary energy consumption by source and sector (EIA, 2012)

Since the procedures to measure vehicle CO_2 emissions or their Fuel Economy (typically measured in kilometers per liter or miles per gallon) differ from country to country, it makes it difficult to compare vehicles from different countries, and also average figures for each country.

The main technical differences between these procedures are: 1) the test cycle – the speed by time cycle that is used to represent a typical driving style (US uses a cycle developed by the Environmental Protection Agency – EPA – known as EPA 75, while EU uses a different cycle, known as NEDC – New European Drive Cycle); 2) how the fuel consumption is assessed (fuel consumption, fuel economy or CO_2 emissions); and 3) the structure to set the standard (in the US, the individual standard is set according to vehicle's footprint – the area inside the four wheels – while in Europe, the standard is set according to vehicle's weight.

The International Council on Clean Transportation (ICCT) has presented a methodology to make feasible these comparisons. Their results are presented normalized to the European procedure (ICCT, 2014), shown in Table 1.1 and Figure 1.4:

Table 1.1 – Overview of Regulation Specifications for Passenger cars (ICCT, 2014)

Country or Region	Target Year	Standard Type	Unadjusted Fleet Target/Measure	Structure	Test Cycle
EU	2015 2021	CO_2	130 gCO_2/km 95 gCO_2/km	Weight-based corporate average	NEDC
China	2015 2020 (proposed)	Fuel consumption	6.9 L/100km 5 L/100km	Weight-class based per vehicle and corporate average	NEDC
U.S.	2016 2025	Fuel economy/ GHG	36.2 mpg[i] or 225 gCO_2/mi 56.2 mpg[ii] or 143 gCO_2/mi	FP-based corporate avg.	U.S. combined
Canada	2016 2025 (proposed)	GHG	217 gCO_2/mi[iii] N/A[iv]	FP-based corporate avg.	U.S. combined
Japan	2015 2020	Fuel economy	16.8 km/L 20.3 km/L	Weight-class based corporate average	JC08
Brazil	2017	Fuel economy	1.82 MJ/km	Weight-based corporate average	U.S. combined
India	2016 2021	CO_2	130 g/km 113 g/km	Weight-based corporate average	NEDC for low-powered vehicle
South Korea	2015	Fuel economy/GHG	17 km/L or 140 gCO_2/km	Weight-based corporate average	U.S. combined
Mexico	2016	Fuel economy/GHG	39.3 mpg or 140 g/km	FP-based corporate avg.	U.S. combined

[i] Assumes manufacturers fully use A/C credit
[ii] Proposed CAFE standard by NHTSA. It is equivalent to 163g/mi plus CO2 credits for using low-GWP A/C refrigerants.
[iii] In April 2010, Canada announced a target for light-duty vehicle fleet of 246 g/mi for MY2016. The separated targets for car and light truck fleet are estimated by ICCT based on the overall target.
[iv] Canada follows the US standards in the proposal, but the final target value would be based on the projected fleet footprints.
FP: footprint

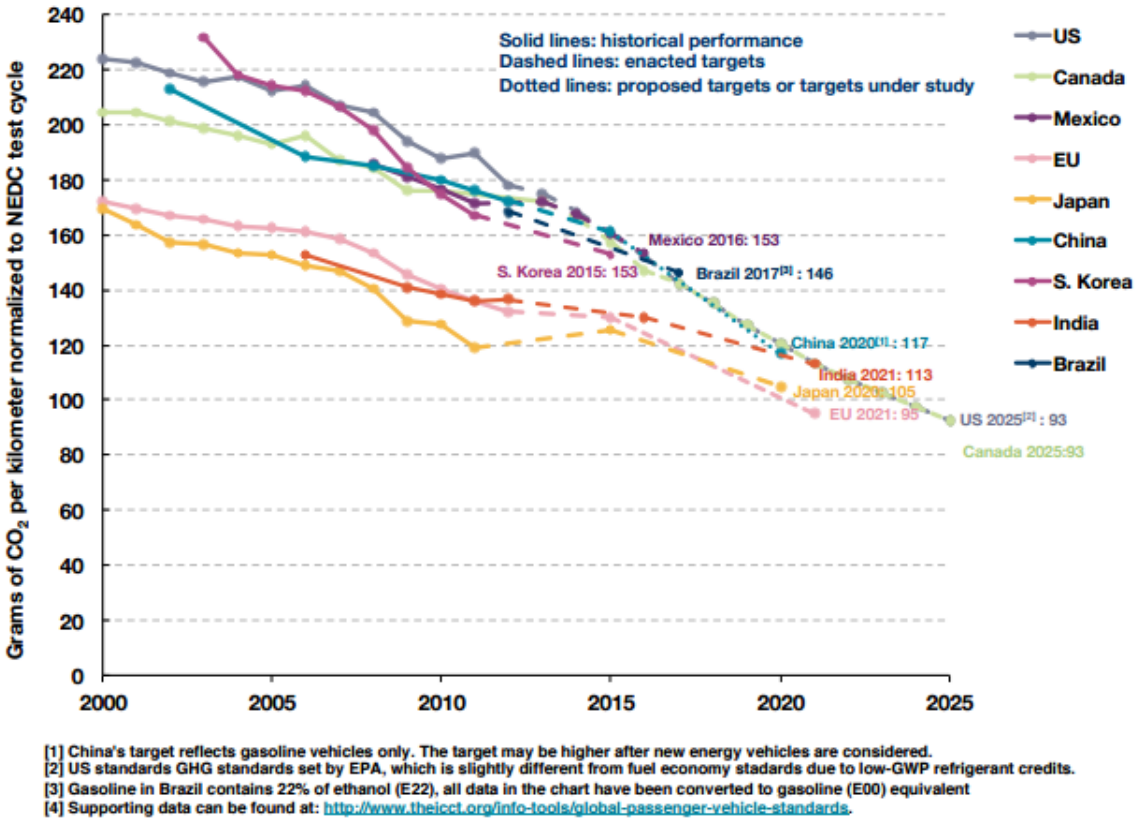

[1] China's target reflects gasoline vehicles only. The target may be higher after new energy vehicles are considered.
[2] US standards GHG standards set by EPA, which is slightly different from fuel economy stadards due to low-GWP refrigerant credits.
[3] Gasoline in Brazil contains 22% of ethanol (E22), all data in the chart have been converted to gasoline (E00) equivalent
[4] Supporting data can be found at: http://www.theicct.org/info-tools/global-passenger-vehicle-standards.

Figure 1.4 – Global Standards for Passenger Cars (ICCT, 2014)

Despite of the efforts governments, vehicle manufacturers (also known as Original Equipment Manufacturers – OEMs) and their suppliers have applied, consumers are struggling to achieve the same path of fuel consumption reduction observed in laboratory measured tests (Ntziachristos et al., 2014). This behavior suggests that vehicles are driven in different conditions than the conditions observed in standardized tests performed in laboratories.

Internal Combustion Engines (ICE) operate in a range of loads (described often as mean effective pressure – MEP – and also as torque), and revolution speeds (described usually in revolutions per minute – RPM). The ICE efficiency (mostly often expressed in break specific fuel consumption – BSFC) is dependent of the operating conditions (Heywood, 1988). These conditions are determined by a wide range of parameters, including, but not limited to: vehicle total mass and inertia (including occupants and luggage); vehicle aerodynamic; transmission, driveline and tires rolling resistance; driving operating mode (idling, acceleration, deceleration and cruise); transmission and driveline gear ratios (Gillespie, 1992).

The engine performance map relates the engine efficiency over its operating range, as presented in Figure 1.5. This map is often derived from dynamometer test stands.

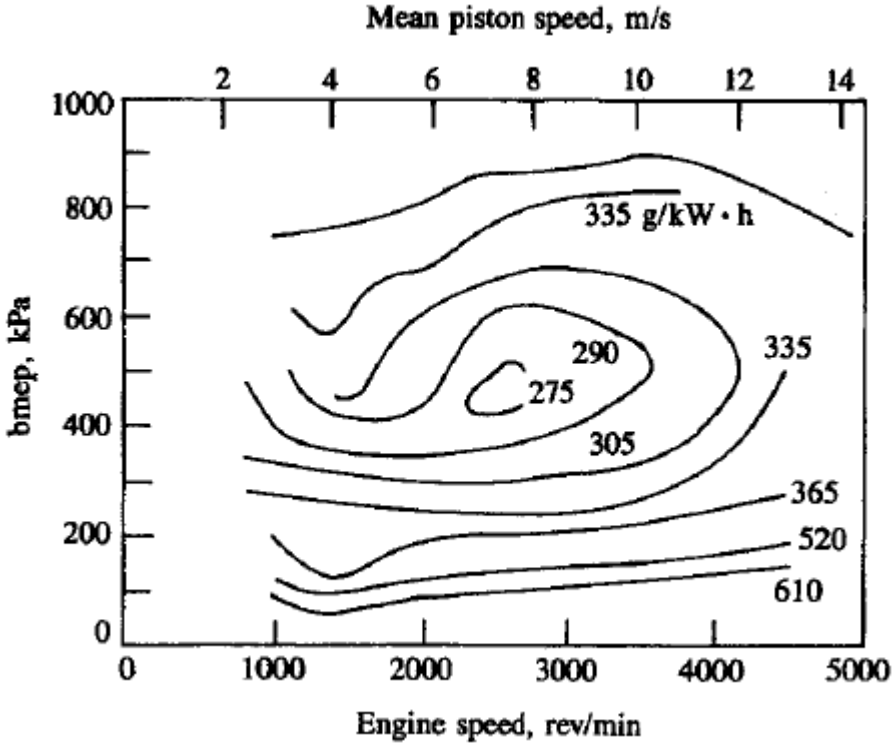

Figure 1.5 – Engine performance map (Heywood, 1988)

However, dynamometer test stands are expensive, and require the engine to be removed from the vehicle. The engine is tested in steady-state operation over a wide range of engine speeds and loads (SAE, 1995). This work presents a cost effective method to measure the engine performance map in-vehicle, without the use of engine dynamometer tests, reducing the difficulties and the cost to raise this information.

The state-of-the-art of engine fuel consumption measurement are mostly works that measure the engine fuel consumption in test benches rather than in-vehicle testing, focusing on engine technology and efficiency capability. Some of the most important works are categorized and listed below:

- Compare engine efficiency for different fuels (Cheikh, et al, 2016; Loftan, et al, 2016);
- Fuel Consumption optimization (Guzzella, 2007; Saerens, et al, 2009)
- Use of artificial neural networks and genetic algorithms to predict fuel consumption (Togun and Baysec, 2010; Sayin et al, 2006);
- Thermodynamic and chemical reaction models (Lopes and Ferreira, 2014; Maroteaux et al, 2015);
- Mathematic models to describe the engine fuel map (Jahns, 1983; McKiernan et al, 1987; Goering and Cho, 1988; Çelik and Arcaklioglu 2005; Keller, 2014).
- Performance feel and fuel economy multi-objective optimization Maloney, Nursilo, 2011);
- Compare different engines (Zhao, Xu, 2013);
- Estimating potential benefits of innovative technologies (Earleywine et al., 2011)
- Shift Schedule model-based optimization (Blagojević et al., 2012; Kumar, Pandey, 2015; Eckert, et al., 2014);

There are also researches focused on vehicle fuel consumption. Instead of analyzing the engine as a component, these researchers are concerned about the impact of fuel consumption on gases emissions, the energy matrix, public health and other issues related to fuel consumption. The state-of-the art works in vehicle fuel consumption measurement is categorized and presented below:

- Analysis of on-road emissions and fuel consumption (Weiss et al, 2011; Johnson et al, 2009; Tong, Hung and Cheung, 2011; Zhang et al, 2014; Birrell et al, 2014);
- Indirect vehicle fuel consumption measurement (Skog and Händel, 2014);
- Real-world drive cycle development (Frey et al, 2012; Wu et al, 2015; Hu et al, 2012; Kent et al, 1977; Tong et al, 1999; Liu, Wang and Khattak, 2016; André et al, 2006).

Although there is many other authors and works that were not cited in this brief summary, the combination of the development of a mathematical model to describe engine fuel consumption as a function of its operating conditions and on-board vehicle measurement. This work intends to use on-board measurements to obtain the engine operating conditions and instantaneous fuel consumption in order to apply a mathematical model that will be capable of predicting fuel consumption in other conditions that do not extrapolate the conditions that were used to fit the mathematical model.

2 OBJECTIVES

This work aims to obtain the operating conditions of a passenger car engine through on-board measurements and apply a mathematical model to generate the engine performance map.

The methodology proposed aims to be: 1) simple, in order to be accessible to OEMs, Universities, and to critic customers with little access to equipment and resources; and 2) to use only on-board acquisition, thus, fostering the level of information raised for a broader range of vehicles and increasing the sample size of measurements. To validate the methodology proposed, four different vehicles will be tested under the proposed process. Only Otto cycle engines will be tested since it is the majority of passenger vehicles in Brazil.

The engine maps raised following this proposal will be submitted to fuel economy simulations, and the methodology will be considered successful if it can predict the fuel economy within 10% difference if compared to a simulation with a known engine performance map. A second tracking metric will be the correlation coefficient, which will be considered successful if it is greater than 0.9.

3 LITERATURE REVIEW

3.1 A REVIEW ON FUEL ECONOMY AND GREENHOUSE GAS EMISSION TEST CYCLES

According to Mahlia et al. (2012), the essential steps to establish a fuel economy and greenhouse gas (GHG) standard: 1) the test procedure; 2) set up fuel economy standards based on the fuel economy test data; 3) to develop uniform fuel economy labels; 4) develop incentive programs for more efficient vehicles.

The test procedure standardizes how the tests are run in order to establish a unique procedure for a specific market. Fuel Economy standards define which vehicles should be tested, how the vehicles are classified and compared, how the tested data should be reported, and target definition for each manufacturer or vehicle. Fuel Economy labels have the aim to inform final customers how much fuel each vehicle consumes to run a given distance and the vehicle emissions – in order words, for final customers awareness. Incentive programs try to benefit more efficient vehicles in order to reduce overall average fleet fuel consumption.

The test procedure normally consists of: 1) place the vehicle drive wheels on a dynamometer to simulate driving environment (temperature, vehicle total rolling resistance, vehicle weight); 2) a professional driver or programmed robot to drive the vehicle in a prescribed standard driving routine, i.e. speed by time cycle (Mahlia et al., 2012).

A layout of the test cell is presented in Figure 3.1:

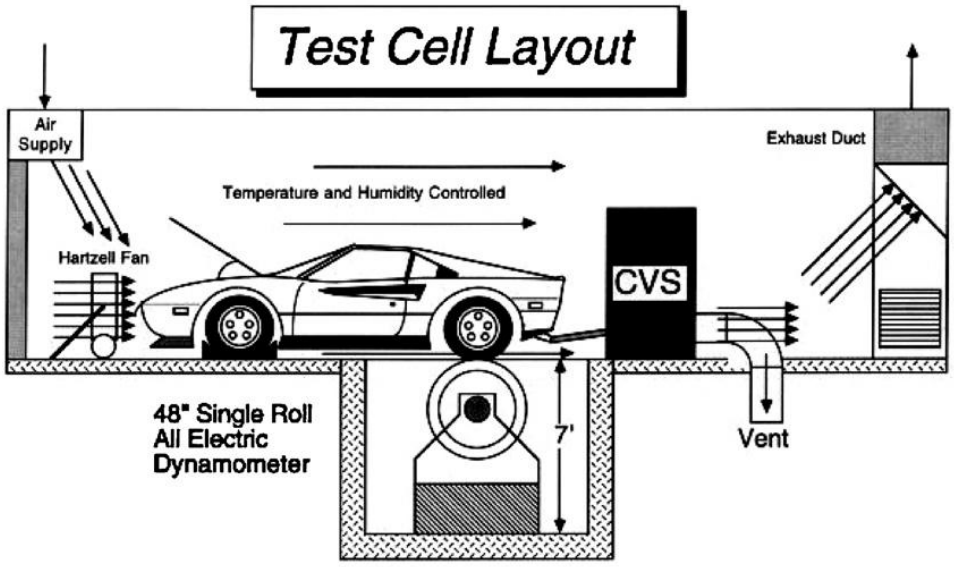

Figure 3.1 – Layout of fuel economy and emissions testing (Mahlia et al., 2012)

3.1.1 Fuel Economy test cycles

The Fuel Economy test cycles are standardized speed by time routines that aim to simulate a typical driving style. These cycles must be followed by the driver that is conducting the test. Different test cycles are used to represent different driving patters, such as urban drive, extra-urban drive, local roads drive, etc. The most used test cycles are the ones used for fuel economy certification in US, EU and Japan. The characterization of driving cycles is usually done by a wide range of parameters, as presented by Liu et al. (2016). The most commonly used are total time, distance traveled, average speed and idling percentage. For comparison purposes, in this work it will be considered the following parameters:

- Total time (t_t): represents the total time used to perform the test cycle;
- Total distance (D_t): represents the total scheduled distance that should be traveled during the test;
- Idle (P_i), acceleration (P_a), cruse (P_c) and deceleration (P_d) percentages: represents the portion that each of these conditions is visited during the test;
- Average speed ($\bar{v}$): represents the constant speed that one should maintain to travel scheduled distance within total time;
- Maximum speed (v_{max}): represents the higher speed achieved on the test schedule;
- Mean average positive acceleration ($\bar{a}_+$): represent the level of aggressiveness of the accelerations.

a) EPA City cycle:

The EPA City cycle is used in US certification for fuel economy, and represents a typical city driving style. This test is known as FTP-75, and its driving schedule is shown in Figure 3.2:

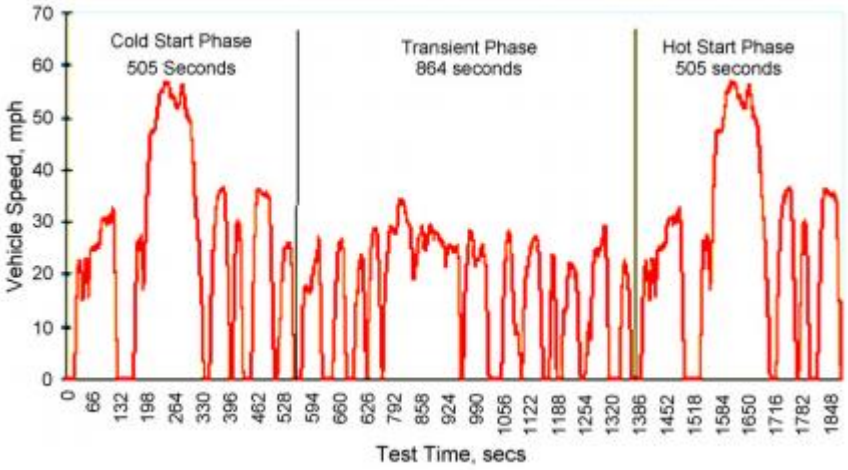

Figure 3.2 – FTP-75 test cycle schedule (Mahlia et al., 2012)

b) EPA Highway cycle:

The EPA Highway cycle is also used in US fuel economy certification, but represents an extra-urban driving style. Its speed by time schedule is presented in Figure 3.3:

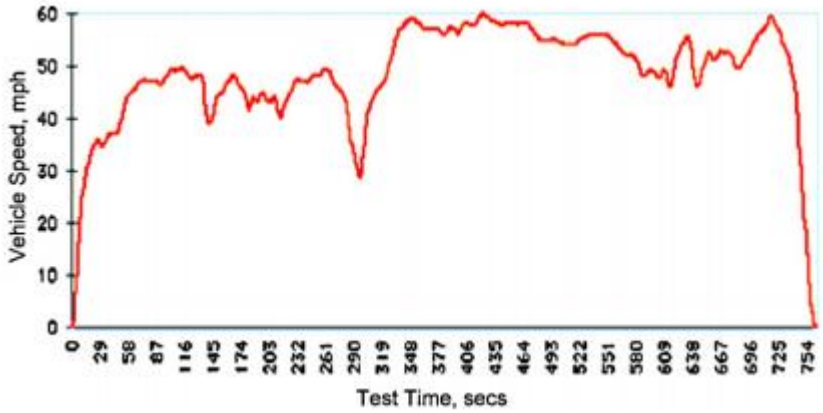

Figure 3.3 – FTP highway test cycle (Mahlia et al., 2012)

c) EPA high speed aggressive test cycle (US06) :

This driving schedule is used to represent aggressive driving styles, in order to account higher speed and acceleration levels than cycles a) and b), as presented in Figure 3.4:

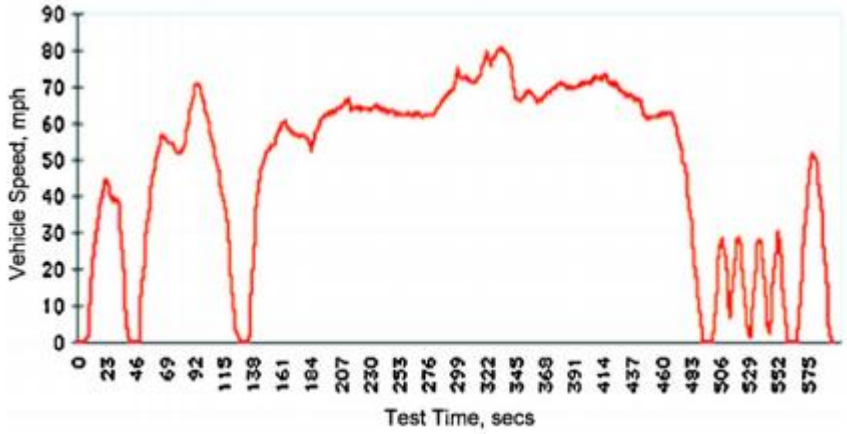

Figure 3.4 – US06 test cycle (Mahlia et al., 2012)

EPA air conditioning test cycle (SC03)

The air conditioning test cycle is a specific test cycle in order to evaluate the effect of air conditioning in vehicle's fuel economy. It is done in higher test temperature and with simulated solar radiation. The driving schedule is shown in Figure 3.5:

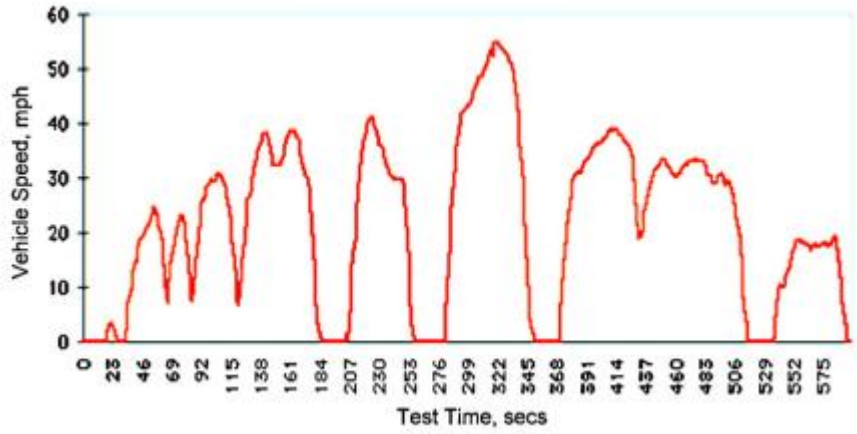

Figure 3.5 – SC03 air conditioning test cycle (Mahlia et al., 2012)

d) NEDC:

The NEDC schedule simulates a combined city and highway driving style, as presented in Figure 3.6:

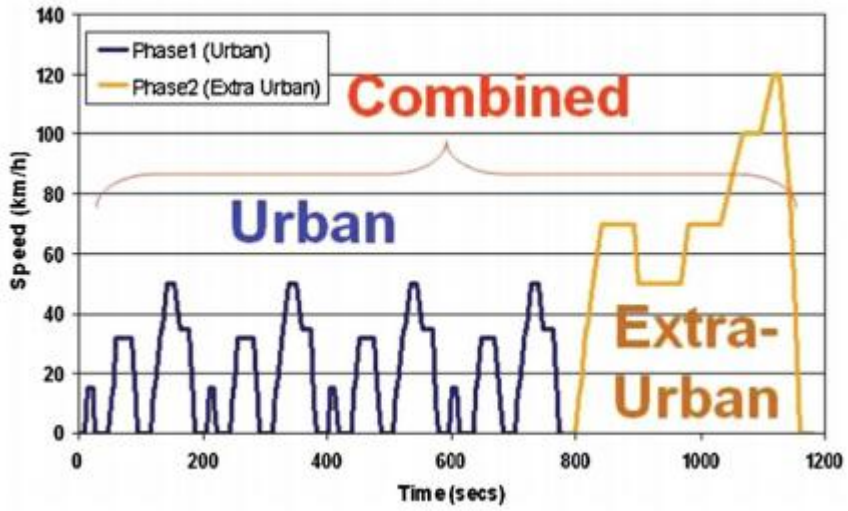

Figure 3.6 – NEDC test cycle (Mahlia et al., 2012)

e) Japanese drive cycle (JC08):

The JC08 test cycle is used for certification purposes in Japan, and, as NEDC, simulates a combined city and highway driving style, as shown in Figure 3.7:

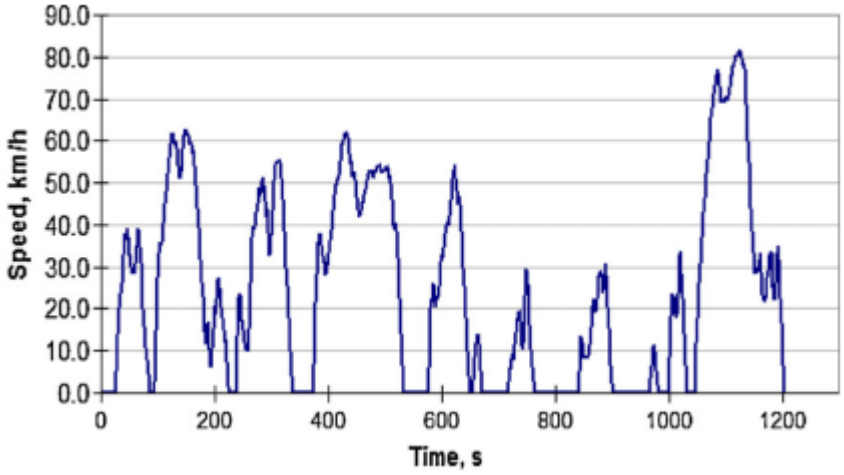

Figure 3.7 – JC08 test cycle (Mahlia et al., 2012)

Standardized fuel economy tests aim to represent typical ambient conditions, as well as typical driving behaviors in order to submit the tested vehicle to the same conditions it would be used on regular conditions. In the US, EPA is responsible to certify vehicle's fuel economy and approve fuel economy labels that vehicle manufacturers will disclose. Current EPA label layout is presented on Figure 3.8:

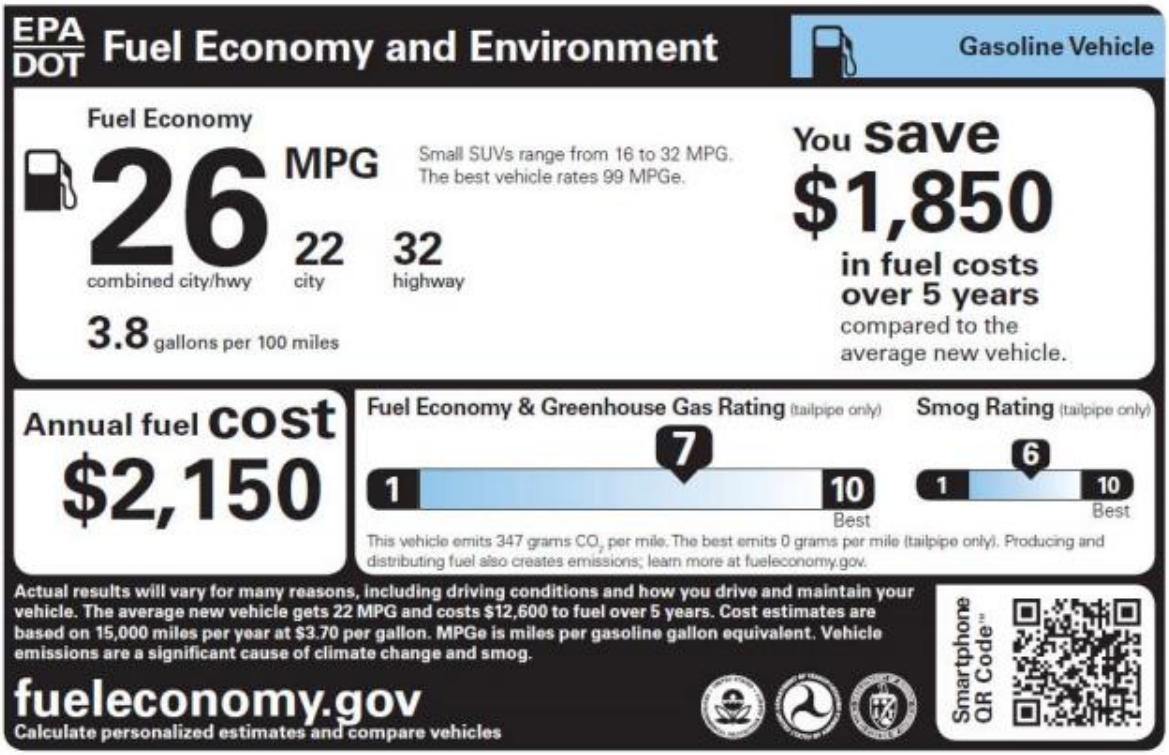

Figure 3.8 – Example of EPA fuel economy label (EPA, 2013)

In this example, the vehicle can run 22 miles with one gallon in a city route, while it can run 32 miles with one gallon in a highway route. The combined city/highway considers a harmonic mean weighed 55% for city cycle and 45% for highway cycle, based on a sample of daily driving commute measured by U.S. National Highway Traffic Safety Administration, as described in Eq. 3.1:

$$FE_{combined} = \frac{1}{\frac{0.55}{FE_{city}} + \frac{0.45}{FE_{highway}}} \tag{3.1}$$

Similarly to US, other countries have adopted a fuel economy labeling procedure. In Brazil, the National Institute for Metrology, Quality and Technology (INMETRO), has established the fuel economy labeling procedure. Brazilian fuel economy label is presented in Figure 3.9:

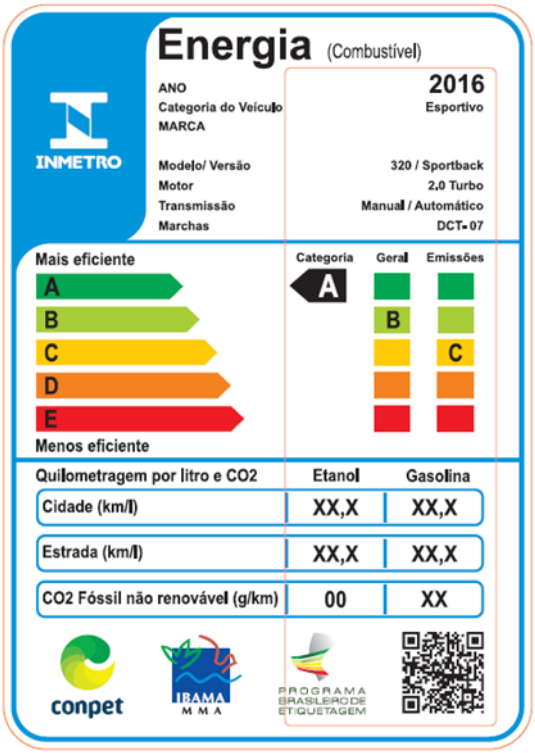

Figure 3.9 – Brazilian fuel economy label (INMETRO, 2011)

One issue observed by manufacturers and certification governmental organizations such as EPA and INMETRO is that consumers have a hard time to achieve laboratory test fuel economy numbers. In US and Brazil it is used an adjustment factor to laboratory test numbers in order to reduce the difference observed in road conditions against certification tests (NHTSA, 1978 and INMETRO, 2011). Few details are given by NHTSA and INMETRO on how the adjustment factors were raised. The adjustment factor for both Brazil and US are the same, and are presented in Eq.3.2a and Eq. 3.2b:

$$FE^{*}_{city} = \frac{1}{0.0076712 + \frac{1.18053}{FE_{city}}} \tag{3.2a}$$

$$FE^{*}_{highway} = \frac{1}{0.0032389 + \frac{1.34660}{FE_{highway}}} \tag{3.2b}$$

The adjustment factors for city and highway fuel economy are presented in Figure 3.10:

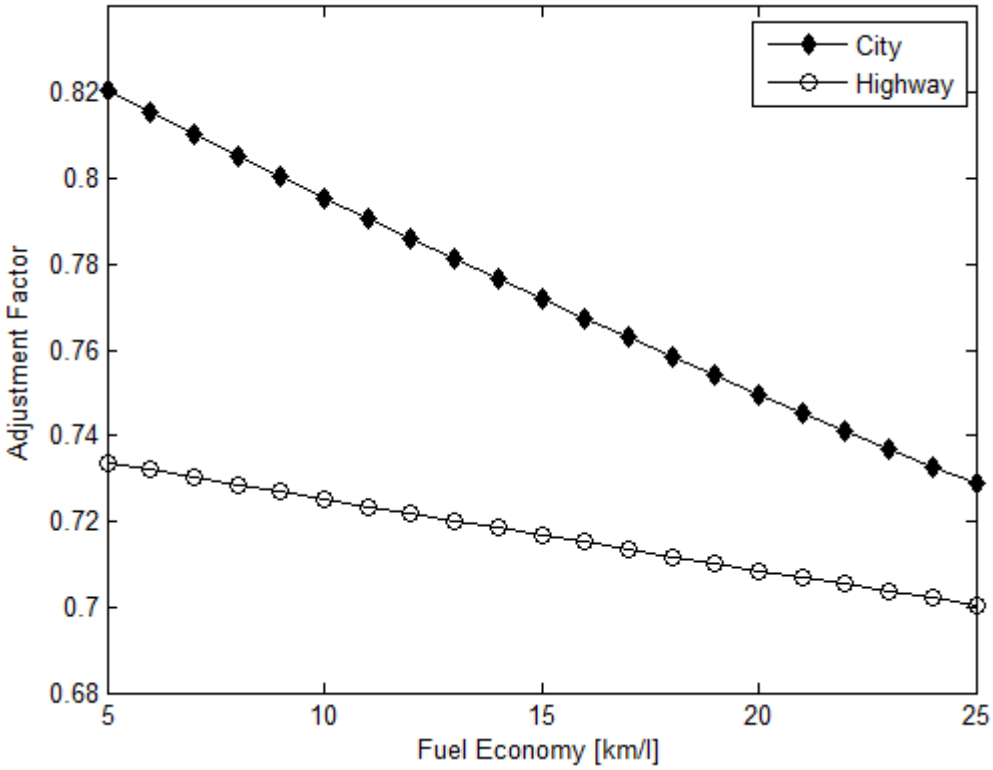

Figure 3.10 – Adjustment factors for city and highway fuel economy

3.1.2 A review on real world fuel economy testing

One controversy regarding fuel economy measurements using test benches and unique standardized test cycles is that different vehicles could be tested and used in considerable different conditions as those observed in these standardized tests (André et al, 2006). Standardized tests are run in controllable conditions and do not take into account a wide range of factors that jeopardize fuel consumption. Among these factors, the most important are:

- The presence of road grades, that requires extra power from the engine during uphill to compensate a gain in potential energy, however, this energy is not entirely converted into vehicle movement during downhill, which means that part of the potential energy is dissipated;
- The presence of different ambient temperature, ambient pressure, track temperature, wind;
- More aggressive driving behavior than standardized speed schedule (higher levels of speed and acceleration);

- Standardized test schedules demand similar power delivery independently of vehicle class, which does not reflect real use conditions.

CO_2 and other tail pipe emissions gases measured in on-road conditions are found to be significant higher than laboratory tests (Tong, Hung and Cheung, 2011). Large discrepancies between real world usage and laboratory numbers were presented by Huo, et al. (2011), Mellios, et al. (2011) and Mock, et al. (2012). Ntziachristos et al. (2014) and Oh et al. (2014) claim that informed drivers recognize that vehicle manufacturers' fuel consumption numbers are hard to achieve. In their study, many different sources to assess in-use fuel consumption (i.e., real world or on-road fuel consumption), in a total of 313 vehicles. The difference observed between type approval (vehicle manufacturer number, obtained through laboratory tests) and in use fuel consumption is presented on Figure 3.11:

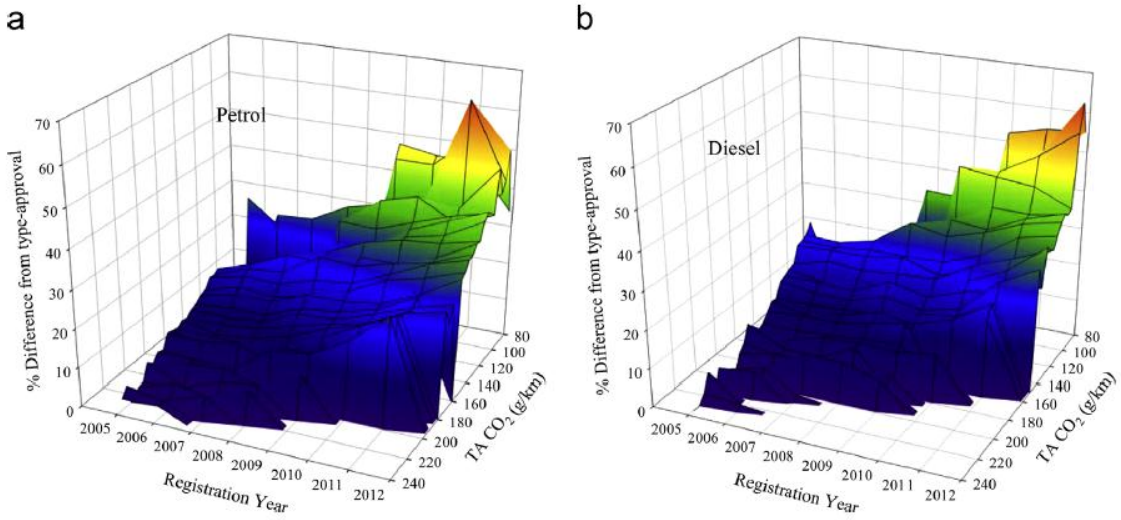

Figure 3.11 - Relative difference of in-use over the type-approval CO2 emissions, as a function of the type-approval CO2 bin and the registration year for (a) petrol, and (b) diesel passenger cars (Ntziachristos et al., 2014)

Real world fuel economy test can be used for development of new driving cycles that aim, mainly, to:

- Capture specific driving style (Tong, Hung and Cheung, 1999; Kent, Allen and Rule, 1977; Wang et al, 2008);
- The benefit of a technology in different conditions (Xu et al, 2015; Fontaras, Pistikopoulos and Samaras, 2008);
- Assess fleet fuel efficiency (Yu, Li and Li, 2016, Wu et al, 2015); and to measure the quality of a drive – regarding fuel efficiency (Sivak and Schoettle, 2012).

Different authors use different characteristic parameters to compare real word driving cycles. Liu et al (2016) compared the different assessments done by 7 other researchers and themselves, as presented in Table 3.1:

Table 3.1 – Comparison of cycle characteristic parameters for different authors (Liu, J. et al., 2016)

	EPA (1995)	Tong et al. (1999)	Q. Wang et al. (2008)	Kamble et al. (2009)	Brady and O'Mahony (2013)	Kent et al. (1978)	Lyons et al. (1986)	This study
Distance	✓				✓	✓	✓	
Total duration	✓			✓	✓	✓		✓
Driving duration	✓	✓		✓	✓	✓		✓
Total average speed	✓	✓	✓	✓	✓	✓	✓	✓
Driving average speed		✓	✓					✓
Maximum speed	✓				✓		✓	✓
Average acceleration	✓	✓	✓	✓	✓		✓	✓
Average deceleration	✓	✓	✓	✓	✓		✓	✓
Maximum acceleration	✓			✓	✓		✓	✓
Maximum deceleration	✓			✓	✓		✓	✓
Root mean square accel./decel.		✓	✓			✓	✓	✓
Average positive vehicular jerk	✓						✓	✓
Average negative vehicular jerk								✓
Maximum positive vehicular jerk								✓
Maximum negative vehicular jerk								✓
Root mean square jerk								✓
Acceleration/deceleration events		✓	✓					✓
Percent time on idling	✓	✓	✓	✓	✓	✓	✓	✓
Percent time on acceleration		✓	✓	✓	✓			✓
Percent time on deceleration		✓	✓	✓	✓			✓
Percent time on stable driving		✓	✓	✓	✓		✓	✓
Percent time on extreme accel./decel.								✓
Percent time on extreme veh. jerk								✓
Kinetic intensity/energy/power	✓	✓	✓				✓	✓

As this work will use on-road measurements, it is important to compare the real-world cycle to the standardized cycles that are used for fuel economy certification. Some of the parameters described in Table 3.1 will be used for these comparisons.

3.2 On-board measurement of vehicle speed, engine torque, fuel consumption and exhaust gas emission

This work aims to provide an accessible procedure to measure engine fuel consumption and propose a model for the fuel consumption as a function of the engine operating conditions. It is important that this measurements are done in-vehicle, eliminating the need of an engine test bench, which is expensive and not accessible to most vehicle users. The most important source of measurements are global positioning system (GPS), vehicle on-

board diagnosis (OBD) system and portable emission measurement system (PEMS), that provides a wide range of parameters that will be used in the development of the present work. In this section a brief description of these sources will be presented for didactical purposes. In the methodology section (Section 4) it will be given more details on what parameters will be used and their sources.

3.2.1 Global Positioning System

Global Positioning Systems have been extensively used to monitor drivers and analyze their behaviors (Smith et al, 2011). GPS technology can accurately measure vehicle speed and determine its position. The applicability of GPS usage in fuel economy studies is very wide and many authors have based their studies with GPS speed logging. These works cover:

- Generating new driving cycles (Smith et al, 2011;)
- Evaluating drive behaviors (Sivak and Schoettle. 2012);
- Comparing different drive cycles and procedures (Liu, Wang and Khattak, 2016);
- Evaluating real-world fuel economy (Smith et al, 2011);
- Determining optimal route and vehicle operation (Smith et al, 2011);
- Speedometer calibration (Igarashi, 2011).

GPS is a satellite-based system that aims to give users their accurate position (Leica, 1999). The GPS provides user's position by measuring the distance from the satellite to the GPS receiver. The user distance to the satellite narrows the possible user position to a sphere, i. e., the receiver could be anywhere within the sphere with a radius equal to the distance measured by the satellite. A second satellite also measures its distance to the GPS receiver, narrowing the possible user position to a second sphere that intersects with the first sphere, which narrows the possibility to a circle (the circle represented by the intersection of the two spheres).

The addition of a third satellite (hence, a third intersecting sphere) narrows the possible position to two points. A fourth sphere solves this ambiguity. This fourth sphere is Earth itself (the possible position can only be located in Earth). In practice, more satellites are often used in order to increase accuracy. Figure 3.12illustrates this concept:

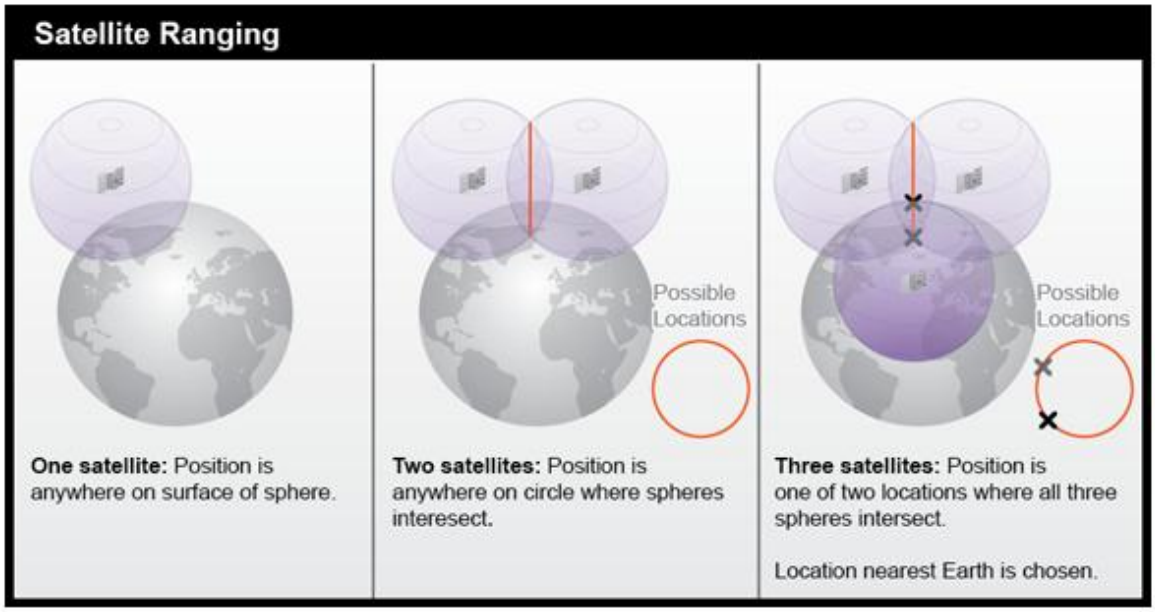

Figure 3.12 – Illustration of the spheres defined by satellite measured distances (Pennstate, 2016)

Although GPS have been extensively used for diverse purposes, several factors can degrade GPS performance (Lasky et al, 2006). GPS receivers require a clear line-of-sight to the satellite, and any object (including tall trees, buildings and terrain features) in this path can affect and weaken the signal.

3.2.2 CAN Network and on-board diagnostics

Automotive electronic subsystems have become numerous and independent, requiring an interdependent subsystem for communication (Ribbens, 2002). The need for this intercommunication system led to the development of a communication protocol called Controller Area Network (CAN). This network is used to connect vehicles' many computers, called ECUs (Electronic Control Units). These ECUs are responsible for controlling most aspects of modern vehicles, including engine, transmission, emissions control, human-machine interface (HMI), infotainment, brakes, airbags, lights, and many other systems in a vehicle (Foster and Koscher, 2015).Figure 3.13 presents an example of ECUs available in a vehicle:

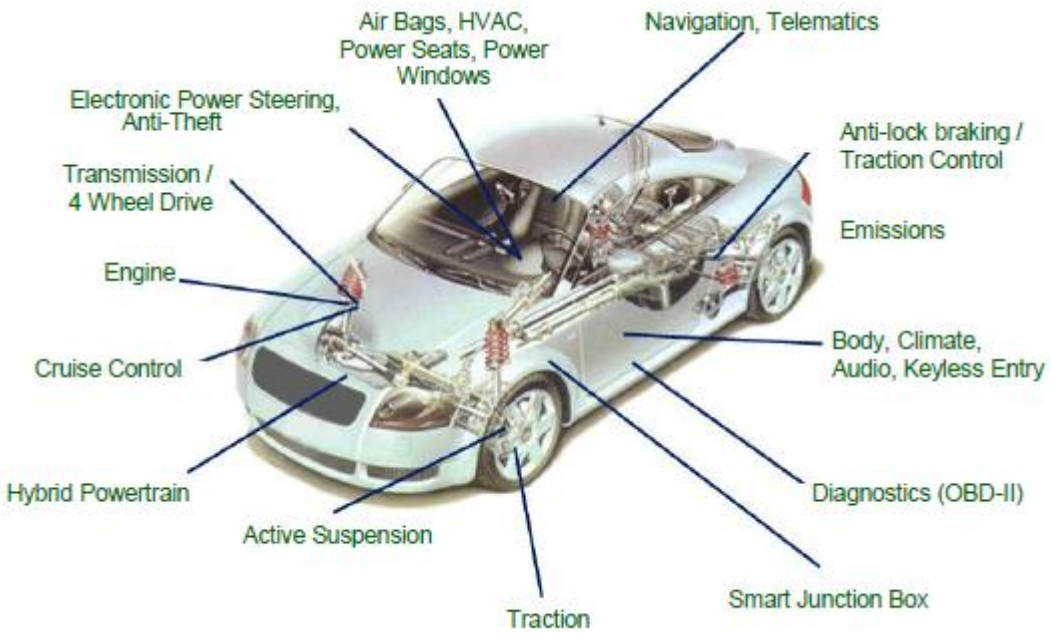

Figure 3.13 – Example of Electronic Control Units in a vehicle (Walter, 2014)

The communication between different ECUs is done through CAN, a serial data communications bus for real-time applications (Guo, Ang, and Wu, 2009). Each ECU works as a node on the network, providing and receiving information, and all messages are shared with all nodes, as shown in Figure 3.14:

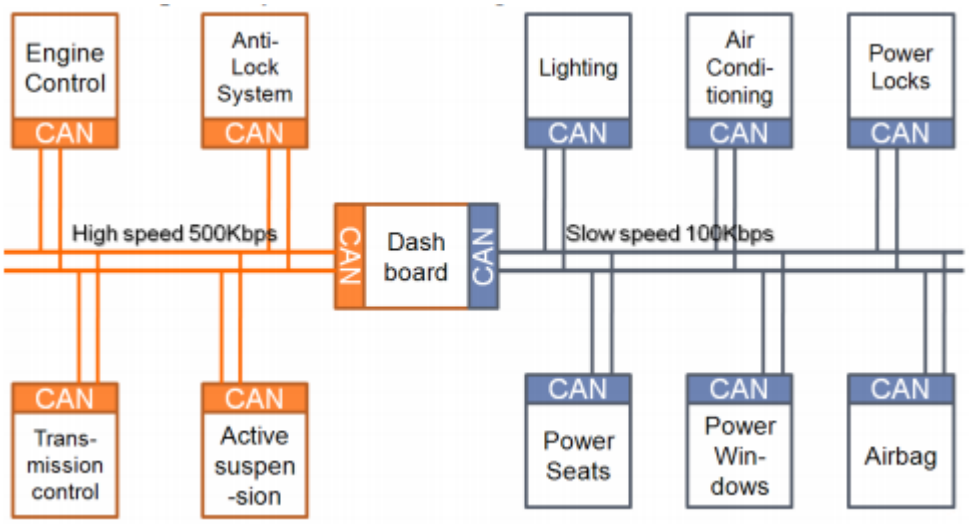

Figure 3.14 – Example of CAN topology (Guo, Ang and Wu, 2009)

Most of the information flow through the CAN network is used for vehicle operation only, and most of the information is not directly available to users; however, this information can be accessed through the On-Board Diagnostics-II (OBD-II) connector. This connector

was introduced in 1996, regulated by SAE J1979 Standard, and is mandatory in many countries (Teixeira, F. C. R., Tournier, D. R., 2015), including USA, Brazil and EU countries. OBD-II protocol aims to provide diagnosis for failure modes such as engine malfunction, catalyst system failure, active and passive safety systems failure (Navet and Simonot-Lion, 2008). However, additional information on traffic from an ECU to another ECU could be gathered and stored for further processing. These sensors may include (Ribbens, 2013):

- Fuel quantity;
- Fuel pump pressure;
- Fuel flow rate;
- Vehicle speed;
- Oil pressure;
- Oil quantity;
- Coolant temperature;
- Outside ambient temperature;
- Windshield washer fluid quantity;
- Brake fluid quantity.

As this information flows from one ECU to another, it allows this signal to be intercepted and recorded through the OBD. The OBD connector layout is presented in Figure 3.15:

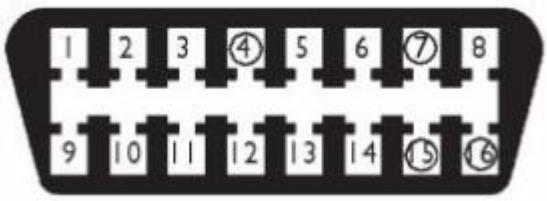

Figure 3.15 - Layout of OBD-II connector (Denton, 2009)

Each pin presented in Figure 3.15 has a standard signal type, shown in Table 3.2:

Table 3.2 – Pin configuration (Denton, 2009)

Pin	**Configuration**
Pin 1	Manufacturer`s discretion
Pin 2	Bus + Line, SAE J1850
Pin 3	Manufacturer`s discretion
Pin 4	Chassis Ground

Pin 5	Signal Ground
Pin 6	Manufacturer`s discretion
Pin 7	K Line, ISO 9141
Pin 8:	Manufacturer`s discretion
Pin 9:	Manufacturer`s discretion
Pin 10	Bus – Line, SAE J1850
Pin 11	Manufacturer`s discretion
Pin 12	Manufacturer`s discretion
Pin 13	Manufacturer`s discretion
Pin 14	Manufacturer`s discretion
Pin 15	L line, ISO 9141
Pin 16	Vehicle battery positive

OBD-II protocol is able to read only information that flows through central CAN. Some parameters are only used within a specific ECU and are not available on CA, according to each manufacturer interests. Walter (2014) classifies some parameters as acquirable a non-acquirable, as shown in Table 3.3:

Table 3.3 – Parameters classification according to Walters (2014)

Parameters acquirable	**Parameters non-acquirable**
Engine speed	Odometer
Vehicle speed	Torque
Mass air flow (MAF)	ABS
Manifold air pressure (MAP)	Ride and handling parameters
Temperatures (ambient, coolant, etc.)	Air-bag parameters
Accelerator pedal and throttle position	Hybrid operating parameters
Oxygen sensors	Fuel consumption from injectors (in most cases)
Fuel trims	
Diagnostic trouble codes (DTCs)	

One of the three inputs presented in Table 3.3 can be directly acquired (speed), but the other inputs (fuel consumption and engine torque) must be inferred from the available parameters. This procedure will be discussed in the Methodology section.

3.2.3 Portable emission measurement system (PEMS)

PEMS has been used mainly by heavy-duty vehicles for on-road evaluation of the conformity to Euro V and Euro VI (Bonnel, Kubelt and Provenza, 2011). PEMS has been developed as an alternative to measurement in test cells (Weiss et al, 2011), since it was impractical to remove the engine from the vehicle to be tested. They defend that PEMS could be extended to light-duty vehicles as well, based on the success of its application in heavy-duty vehicles.

PEMS are compact equipment coupled to vehicle's exhaust system, capable of collecting exhaust and measure the concentrations of the regulated pollutants: total hydrocarbons (THC), carbon monoxide (CO, nitrous oxides (NO_2) and carbon dioxide (CO_2) (Bonnel, Kubelt and Provenza, 2011 and Weiss et al, 2011). Figure 3.16 shows an example of a vehicle equipped with a PEMS:

Figure 3.16 – Vehicle equipped with PEMS (Weiss et al, 2011)

PEMS are usually integrated to a GPS and vehicle OBD system, so it can mutually log vehicle speed, exhaust gas emissions in real-time and vehicle CAN parameters, providing valuable and complete information. These devices, however, present high cost for most possible users.

3.3 ENGINE BRAKE SPECIFIC FUEL CONSUMPTION (BSFC) MODELING AND TESTING

The engine is responsible to convert chemical energy (stored in form of fuel) into mechanical energy (transmitted to the rest of the vehicle through engine crankshaft rotation). Engines can operate under a wide range of crankshaft rotating speeds (also called engine speed) and load (Çelic, V.; Arcaklioglu, E., 2005). The engine BSFC is the fuel flow rate divided by the brake power. It is dependent of the piston speed and the engine brake mean effective pressure (BMEP). Generically, one could write Eq. 3.3a:

$$BSFC = f(BMEP, V_p) \tag{3.3a}$$

In Eq. 3.1 V_p is the piston speed.

The piston speed is directly related to engine speed (ω_e), while BMEP is directly related to the engine torque (τ_e), and BSFC to fuel consumption (f_c). Therefore, Eq. 3.3a can be modified into Eq. 3.3b:

$$f_c = f(\tau_e, \omega_e) \tag{3.3b}$$

The relationship between fuel consumption, engine torque and engine speed is often presented in the form of the engine performance map, as presented in Figure 3.17:

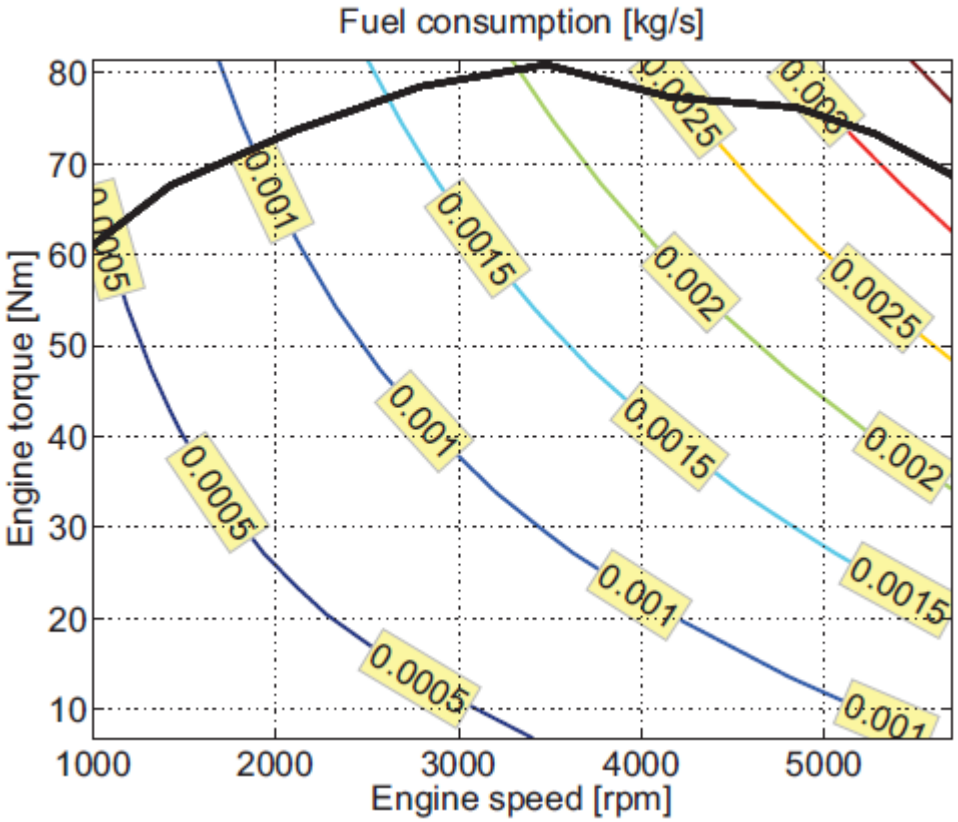

Figure 3.17 – Example of an engine performance map (Hofman and van Leeuwen, 2009)

The engine performance map can be obtained both by analytical modeling, and by measurements in test benches. Engine performance map measurement in test benches is regulated by SAE J1312 (1995). The procedure detailed in this standard states that the engine shall be tested in steady torque and engine speeds, varying the test points from idle engine speed to max engine speed, and from minimum stable torque to maximum engine brake torque, as presented in Figure 3.18:

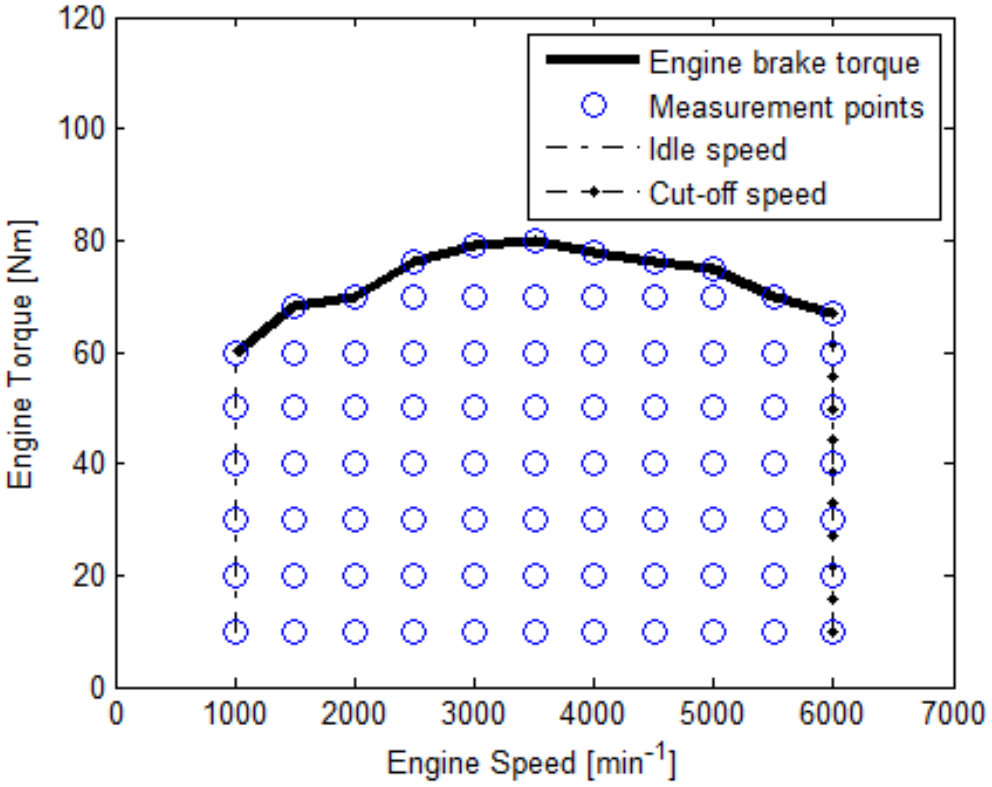

Figure 3.18 – Example of measurement points of engine performance map bench test as recommended by SAE J1312 standard

The advantage of the methodology is that each point is measured in steady state condition and in controlled ambient conditions, providing an accurate result. Also, as ambient conditions are controllable, unlike during on-road tests, the effect of ambient conditions on engine performance can be evaluated by varying these conditions. The main disadvantages are that: 1) it requires the engine to be removed from the vehicle; 2) it requires a long time of testing due to the large amount of measurement points; and 3) hourly cost of engine test benches is expensive because a large number of sensors, instruments and control devices are used to increase accuracy.

Authors have combined engine performance map measurements in test benches with artificial intelligence (AI) for diverse researches purposes. Chakraborty, A., et al. (2016) used

artificial neural networks to predict BSFC, NO_x, HC, CO and particulate material (PM) emissions in Diesel engines operating in dual-mode with diesel and liquefied petrol gas (LPG) using injection duration and engine load as input variables. The engine test bench used in this work and the experimental test setup are presented in Figure 3.19 and Figure 3.20, respectively.

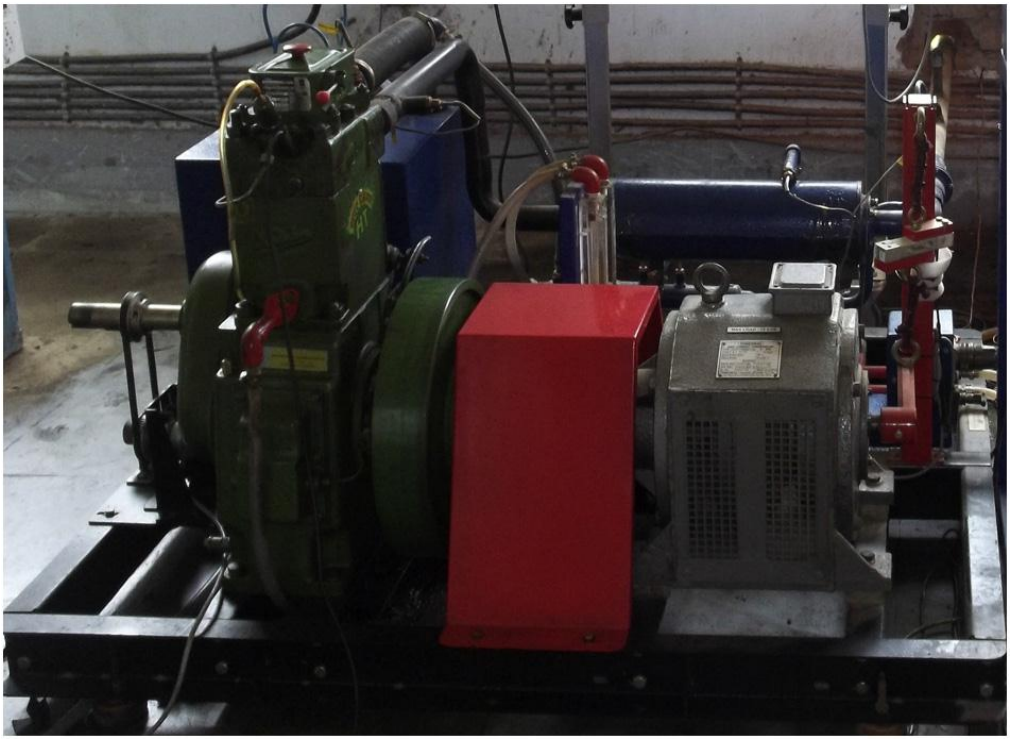

Figure 3.19 – Engine test bench used by Chakraborty et al (2016)

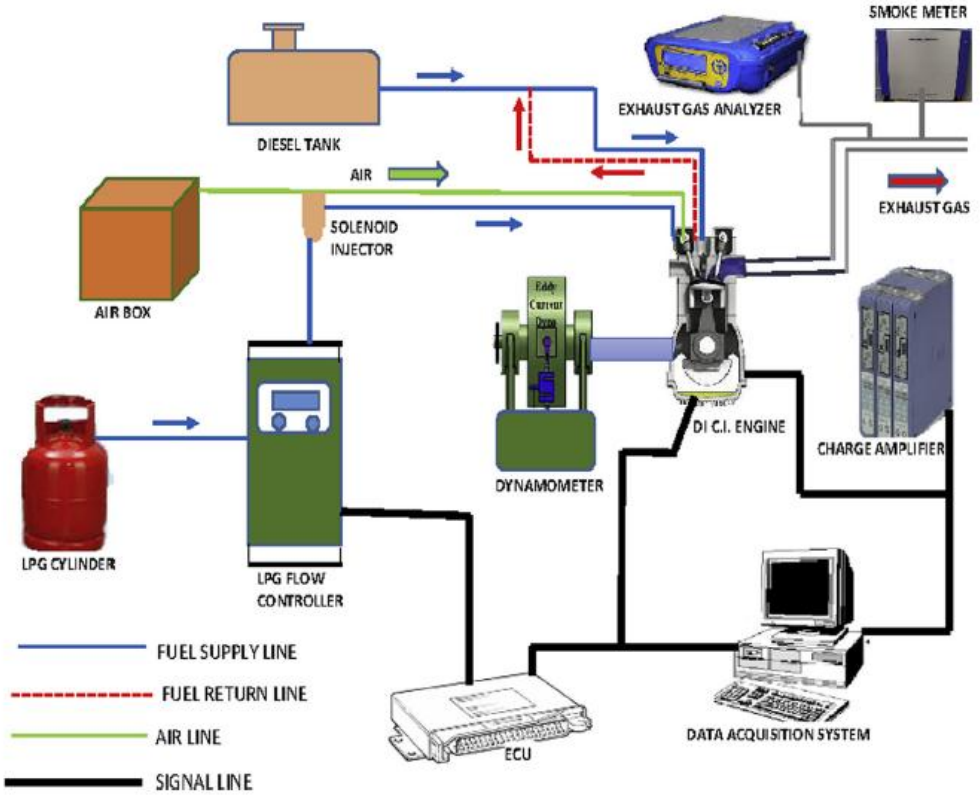

Figure 3.20 – Schematic view of Chakraborty et al (2016) experimental setup

The engine map was measured in diverse conditions of LPG injection pressure and diesel injection duration, and for engine speeds and loads. These measurements were used as inputs for artificial neural networks (ANNs). In this work, authors used ANNs to predict exhaust gas emissions and BSFC in other conditions different than the measured ones. The results obtained are presented in Figure 3.21:

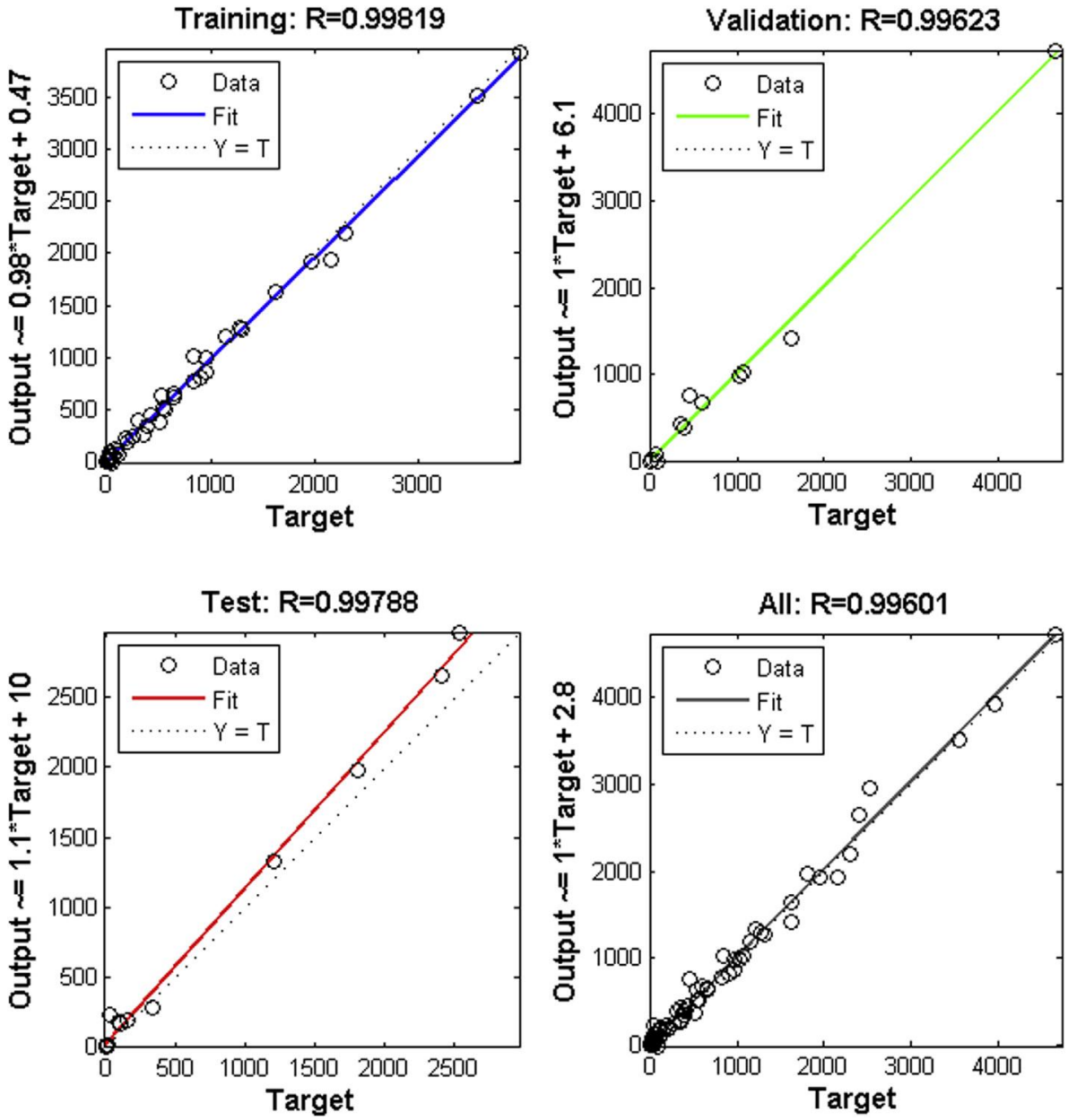

Figure 3.21 – Results obtained by Chakraborty et al (2016)

The results observed through ANN present overall correlation coefficient (R^2) above 0.992, which means that a large portion of the overall variation within data are explained by the model.

Togun and Baysec (2010) studied the use of ANNs to predict engine torque and fuel consumption using as inputs spark advance, throttle position and engine speed for a gasoline fueled spark-ignition engine. The results obtained in this work are shown in Figure 3.22:

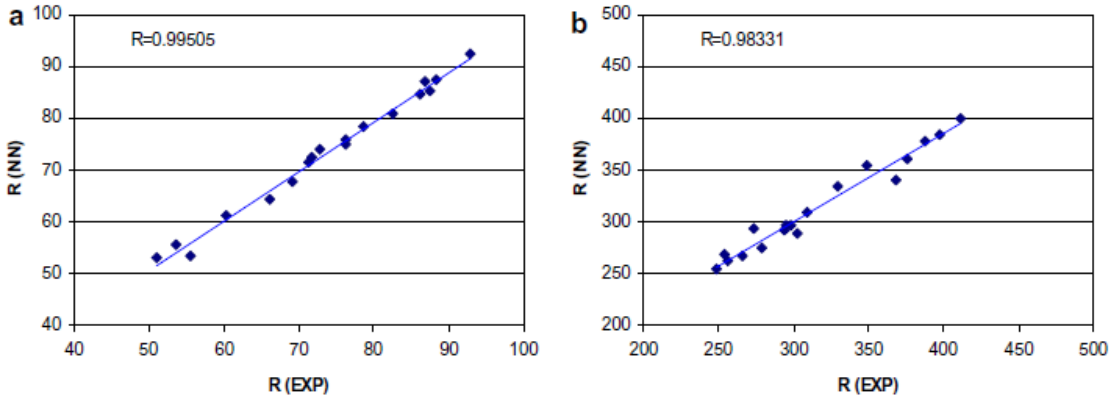

Figure 3.22 – Prediction of ANN and actual results for testing sets: a) Torque and b) BSFC

The results presented in Figure 3.22 also show high correlation coefficient for the ANN model, and the authors claimed that the results are in agreement with experimental results.

Other authors have used ANNs to predict a specific engine performance characteristic. Çay et al (2012) uses ANNs to predict engine power, BSFC and exhaust temperature using the following inputs: engine speed, torque, fuel flow, intake manifold mean temperature and cooling water entrance temperature. They presented results with $R^2 > 0.99$ and with mean errors less than 3.8% for the testing data.

Çay (2013) raised the engine fuel map using ANN. The inputs he used were the same used by Çay et al (2012). Figure 3.23 presents the BSFC map obtained in this study. Additional works using ANNs include, but are not limited to:

- Evaluation of engine performance fueled with gasoline-ethanol blends (Kapusuz et al, 2015);
- Minimizing dual fuel engine emission (Lotfan et al, 2016);
- Engine calibration development and emissions control (Turkson et al, 2016); soot emissions in diesel engines (Ghazikhani and Mirzaii, 2011);
- A diversity of non-emissions related works.

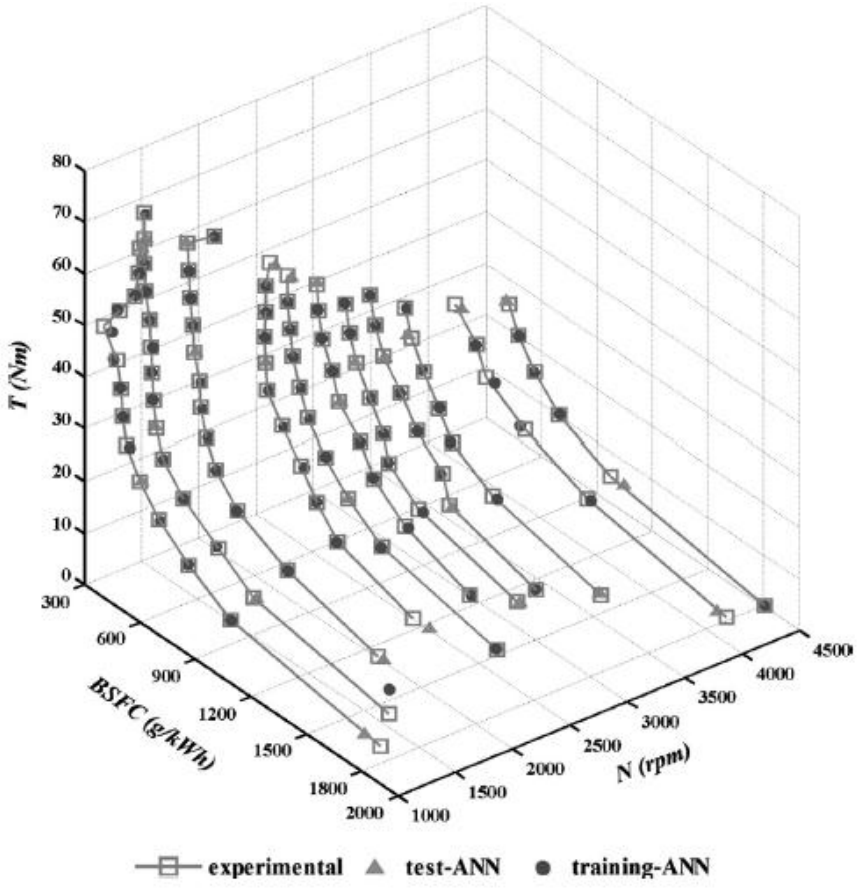

Figure 3.23 – Engine BSFC map obtained by Çay (2013)

Other models rather than ANN are used for modeling engine performance map. Togun and Baysec (2010) have used genetic algorithms (GA) to predict engine BSFC and torque using spark advance, throttle position and engine speed as input parameters. This study used measurement data as input to train and test the GA, and the results of experimental data compared to GA are presented in Figure 3.24:

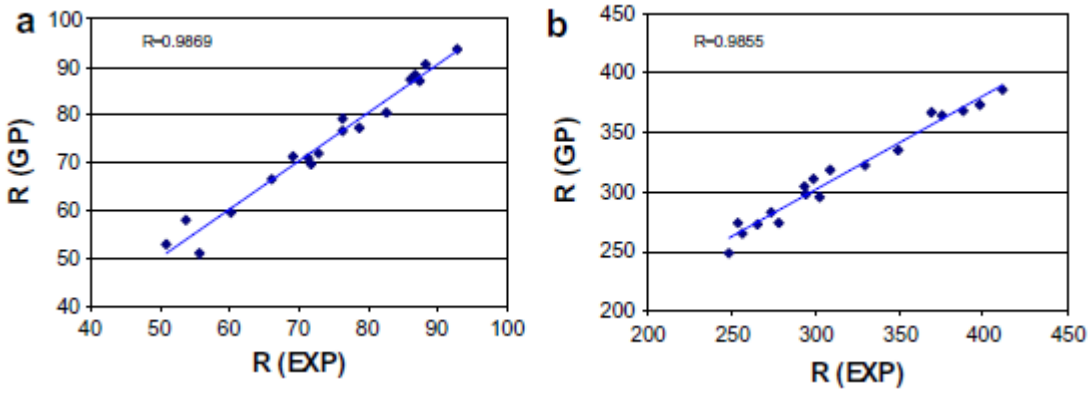

Figure 3.24 – Comparison of experimental results with GA for test set data for: a) engine torque and b) BSFC (Togun and Baysec, 2010)

Luo, et al. (2016) have combined different multi-objective algorithms to optimize output power in a Stirling engine. Authors used differential evolutionary (DE) algorithm, GA, and adaptive simulated annealing algorithm (ASA), and compared their results. The optimal results obtained in this study are presented in Figure 3.25. It can be seen that the optimal results obtained from the three methods are similar.

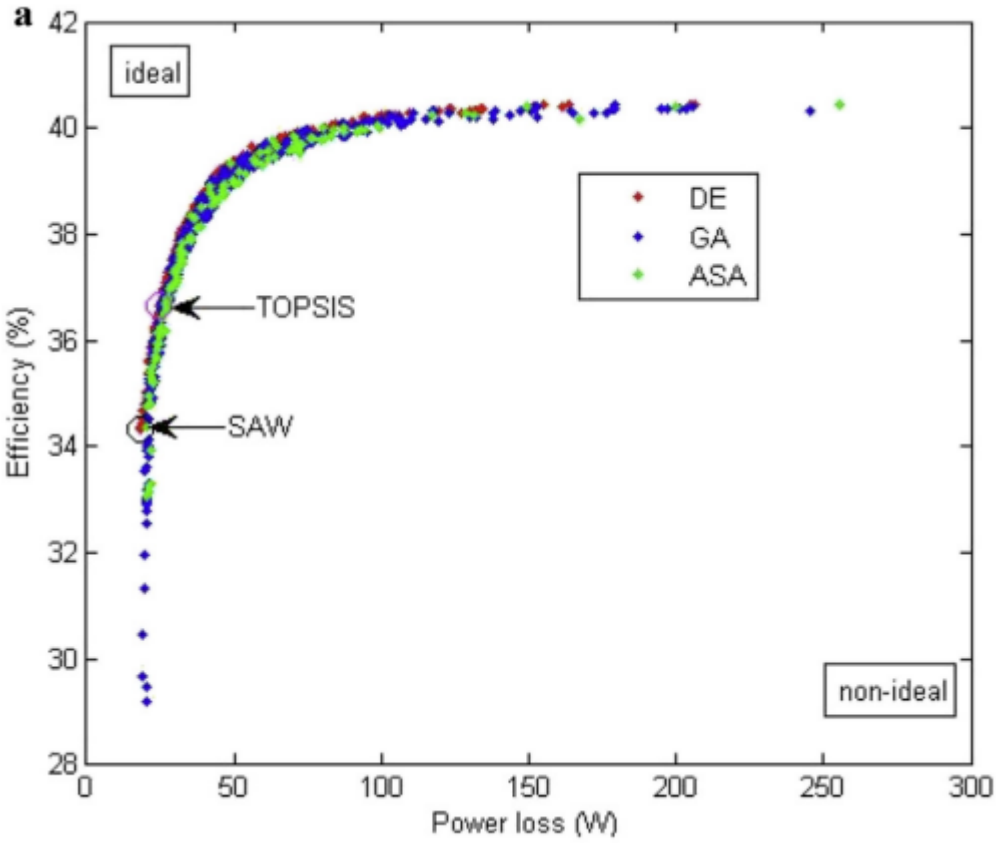

Figure 3.25 – Optimal results obtained by three different optimization algorithms (Luo et al, 2016)

The engine map obtained in this work relates the output power as a function of efficiency and power loss, as presented in Figure 3.26. This representation is different from the map presented in Figure 3.17, but it can be considered an engine performance map as well.

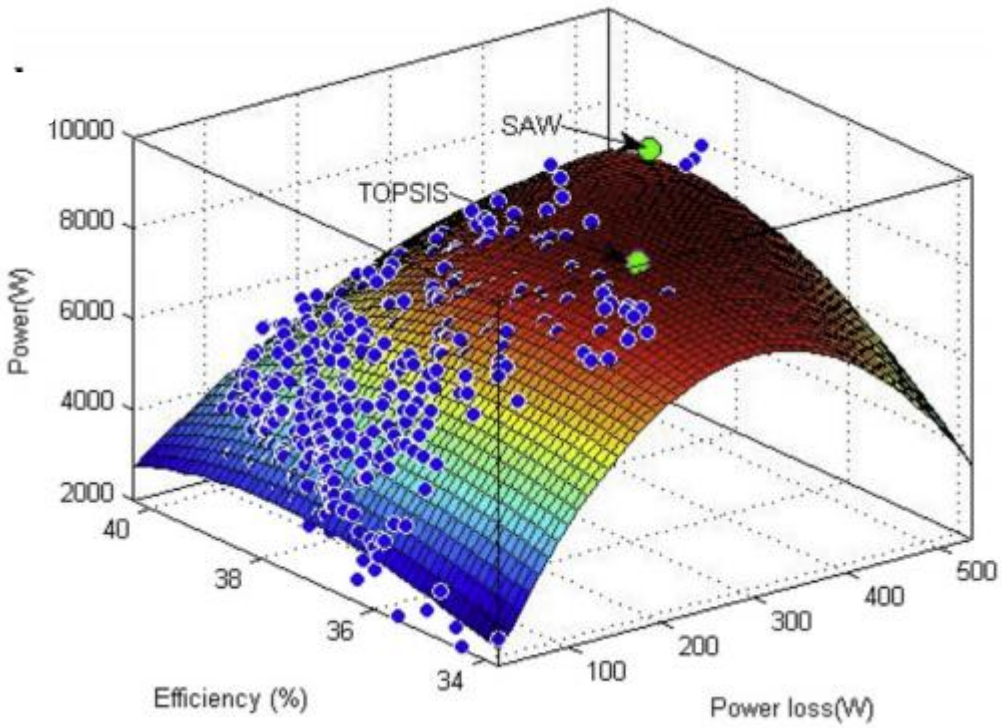

Figure 3.26 – Engine map representing power output as function of efficiency and power loss (Luo et al, 2016)

Other modeling technique used to estimate engine fuel consumption is computational fluid dynamics (CFD). This technique provides numerical approximation to the equations that govern fluid motion (Ashgriz and Mostaghimi, 2002). The steps used to solve problems using CFD consists of:

- Write mathematical equations that describe fuel flow;
- The studied domain is discretized to produce a numerical model analogue of the equations;
- Initial and boundary conditions of the specific problem are used to solve these equations, either directly or iteratively.

Benajes, et al. (2016) combined experimental results and CFD modeling with GA to optimize diesel engine combustion chamber. Experimental results were used to validate the CFD model, ensuring it would represent the physical phenomena. The comparison between experimental and CFD presented by the authors for 1200, 1600 and 1800 RPM are shown in Figure 3.27, Figure 3.28 and Figure 3.29:

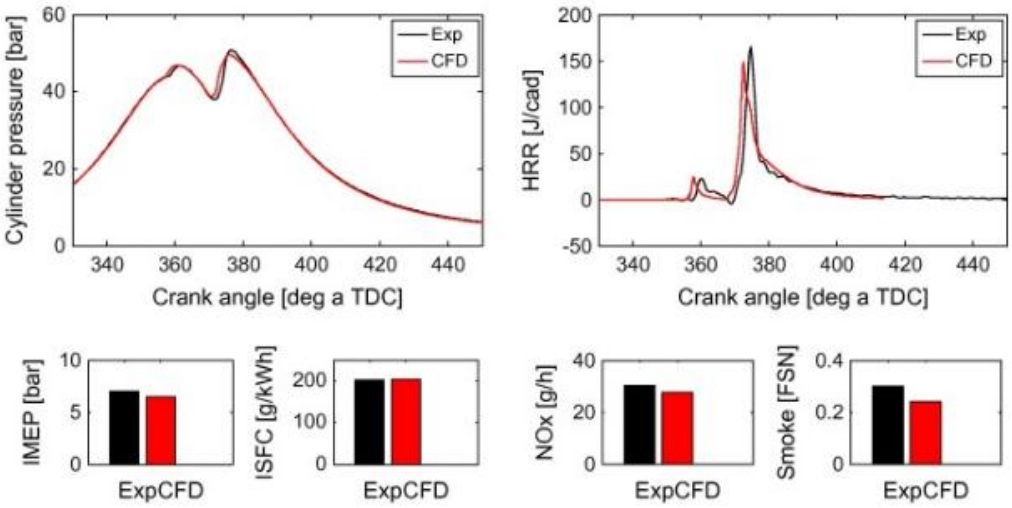

Figure 3.27 - Experimental vs CFD results for 1200 RPM (Benajes et al, 2016)

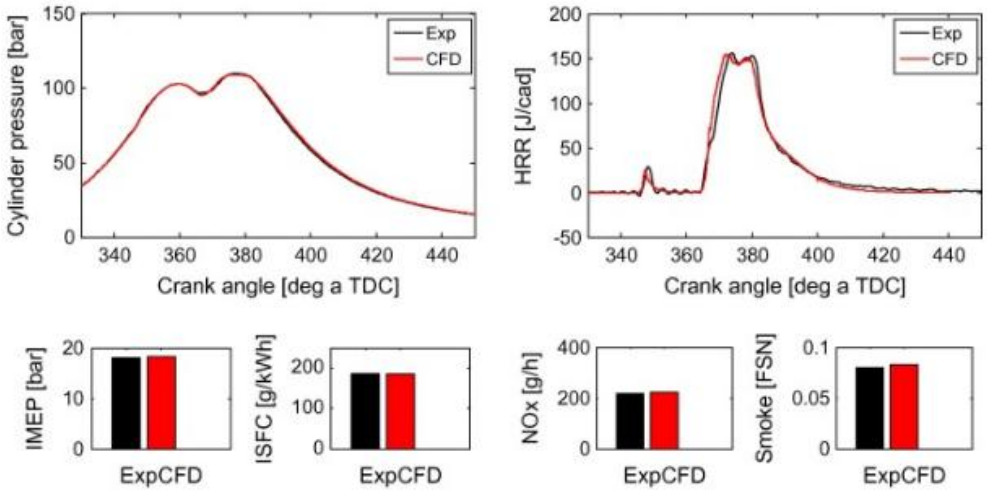

Figure 3.28 - Experimental vs CFD results for 1600 RPM (Benajes et al, 2016)

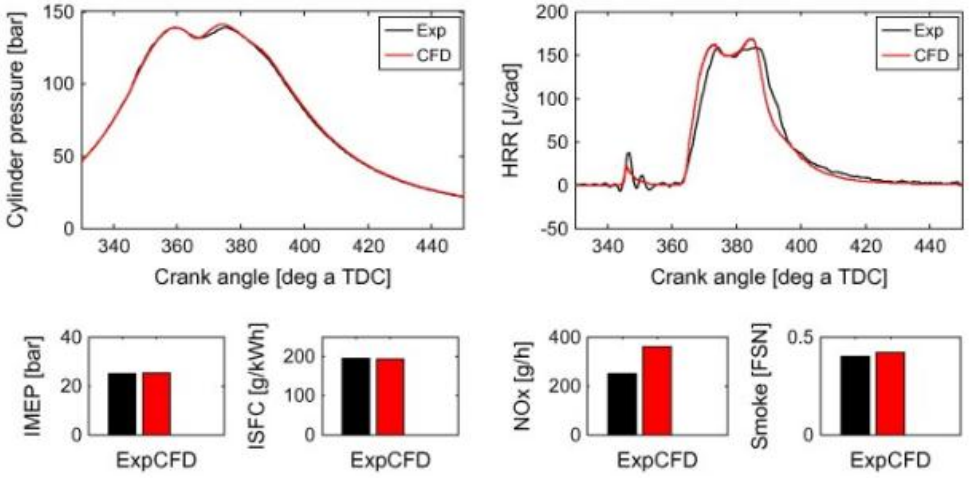

Figure 3.29 - Experimental vs CFD results for 1800 RPM (Benajes et al, 2016)

It can be seen that CFD results presented similar results for cylinder pressure (top left chart in Figure 3.27, Figure 3.28 and Figure 3.29), heat rejection rate (HRR – top right chart in Figure 3.27, Figure 3.28 and Figure 3.29), indicated mean effective pressure (IMEP – botton left chart in Figure 3.27, Figure 3.28 and Figure 3.29), indicated specific fuel consumption (ISFC - second chart from left to right in bottom plots in Figure 3.27, Figure 3.28 and Figure 3.29). The results diverged slightly more for NO_x and smoke emissions.

After the validation of the CFD model, GA was used for parameters optimization. Authors used multi-objective optimization methodology to minimize ISFC and NO_x emissions. They concluded that studied cylinder geometry has limited influence in ISFC, but it affects more significantly NO_x emissions. For low loads, they were able to achieve 15% reduction in NO_x while only 0.5% improvement was observed in ISFC.

Tatschla et al. (2014) studied engine cycle-to-cycle variation intrinsic to spark ignition (SI) engines on fuel consumption using CFD modeling. They studied the effect of spark advance and elevating compression ratio, and generated an engine map with the fuel economy benefit as a function of BMEP and engine speed, presented in Figure 3.30:

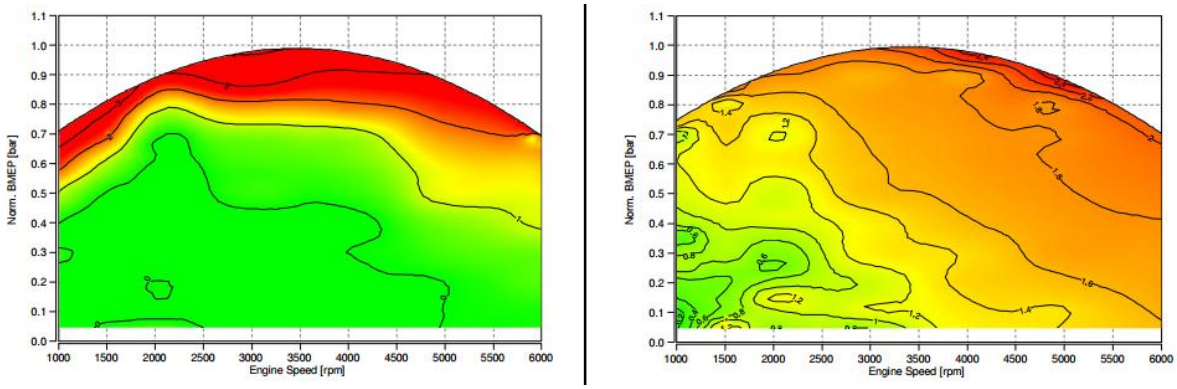

Figure 3.30 - Fuel consumption benefit for optimized spark timing (left) and for elevated compression ratio (right) (Tatschla et al., 2014)

Wallner et al. (2011) have combined optical monitoring of combustion inside an ICE engine with CFD modeling in order to optimize a hydrogen fueled engine performance and emissions. Engine optical measurements were used to validate CFD model in order to ensure its representativeness and simulate parameters that would be difficult to evaluate in physical models. The parameters used in optimization study were the engine geometry, injection system, nozzle design and injection strategy.

From the examples seen in this section, it can be seen that a diversity of models (ANN, GA, polynomial models, CFD numerical models, etc.) can be used successfully to describe

the fuel consumption behavior as a function of the engine operating conditions. The main issue lies on the obtaining quality data for developing and calibrating those models. Usually, quality data are obtained in dynamometers and test benches, which is not widely accessible.

3.4 FUEL CONSUMPTION AND EXHAUST GAS EMISSIONS MODELS

According to Bosgra (2010), there are essentially two different approaches to obtain dynamic models: experimental modeling and theoretical modeling. Experimental modeling is obtained by finding systematic relationships of a real system through the design and setup of a well-planned experiment to measure this system's characteristic variables. Theoretical models rely on the use of accepted theories of underlying sciences and the equations that describe a system behavior.

Vehicle models are typically a combination of these two approaches. The application of physical laws generates specific equations that describe vehicle motion, while experimental modeling are used to account for simplifications in the physical model. These approaches are combined to develop a complete vehicle model (Hofman and van Leeuwen, 2009). Vehicle models, according to this author, can be classified as forward looking and backward facing model according to the direction of the calculation (engine to wheel or wheel to engine). Hofman and van Leeuwen (2009) compared forward dynamic model (FDM), a backward quasi-static model (BQM) and an inverse dynamic model (IDM), presenting their intrinsic differences.

The dynamic models (IDM and FDM) blocks diagram are presented in Figure 3.31:

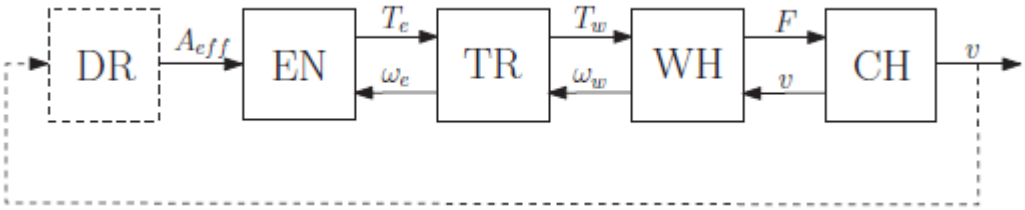

Figure 3.31 – diagram block of a dynamic vehicle fuel economy model (Hofman and van Leeuwen, 2009)

Follows below the legend for the blocks in Figure 3.31:

- DR: Driver block;
- EN: Engine block;
- TR: Transmission block;

- WH: Wheel block;
- CH: Chassis block.

The variables are described as follows: A_{eff} is the effective throttle area; τ_e is the engine brake torque; ω_e is the engine speed; τ_w is the wheel torque; ω_w is the wheel rotational speed, F is the wheel force, v is the vehicle translational speed.

In dynamic models, the powertrain is modeled using a set of ordinary differential equations in state-space form (Guzzella and Sciaretta, 2013). In these models, the inputs are the same signals that are present in the real system. This means that a driver model block (utterly referred as DR) has to be added to the simulation, which will allow the speed (essentially the output of the vehicle model) to be used as a feedback signal.

Quasi-static models directly calculate the engine operating conditions based on the desired speed (i. e., the vehicle will follow the prescribed cycle speed perfectly). Based on vehicle speed, acceleration and road grade the force required to run a chosen profile is calculated for a short period of time. The engine torque and speed are calculated based on vehicle`s parameters such as gear ratios and losses, driveline ratio and losses. Based on the engine speed and torque for each time step, the fuel consumption (obtained through the engine performance map) is calculated and integrated for the whole trip duration in order to calculate the total fuel consumption.

The IDM, unlike the other simulation methods, do not use modular approach. Instead, it uses a set of equations in the affine form, writing the inputs as a function of the outputs (Hofman and van Leeuwen, 2009). An excerpt of speed trace for the simulations using the three methods presented by Hofman and van Leeuwen (2009) is presented in Figure 3.32:

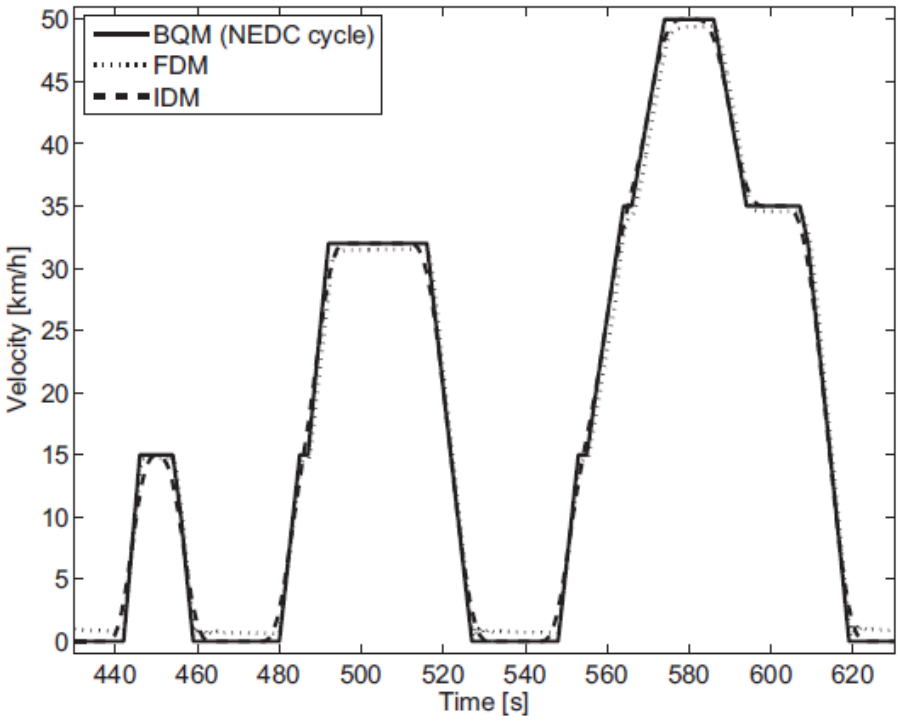

Figure 3.32 – Speed trace in NEDC cycle for three different simulation methods (Hofman and van Leeuwen, 2009)

It can be seen from Figure 3.32 that BQM speed trace is identical as NEDC cycle presented in Figure 3.6, including its discontinuities. The dynamic models (IDM and FDM) present smooth speed trace, similarly to the trace observed in real laboratory tests. The fuel flow comparison is presented graphically in Figure 3.33, and the simulation results for 2 different driver models for each method is presented in Table 3.4:

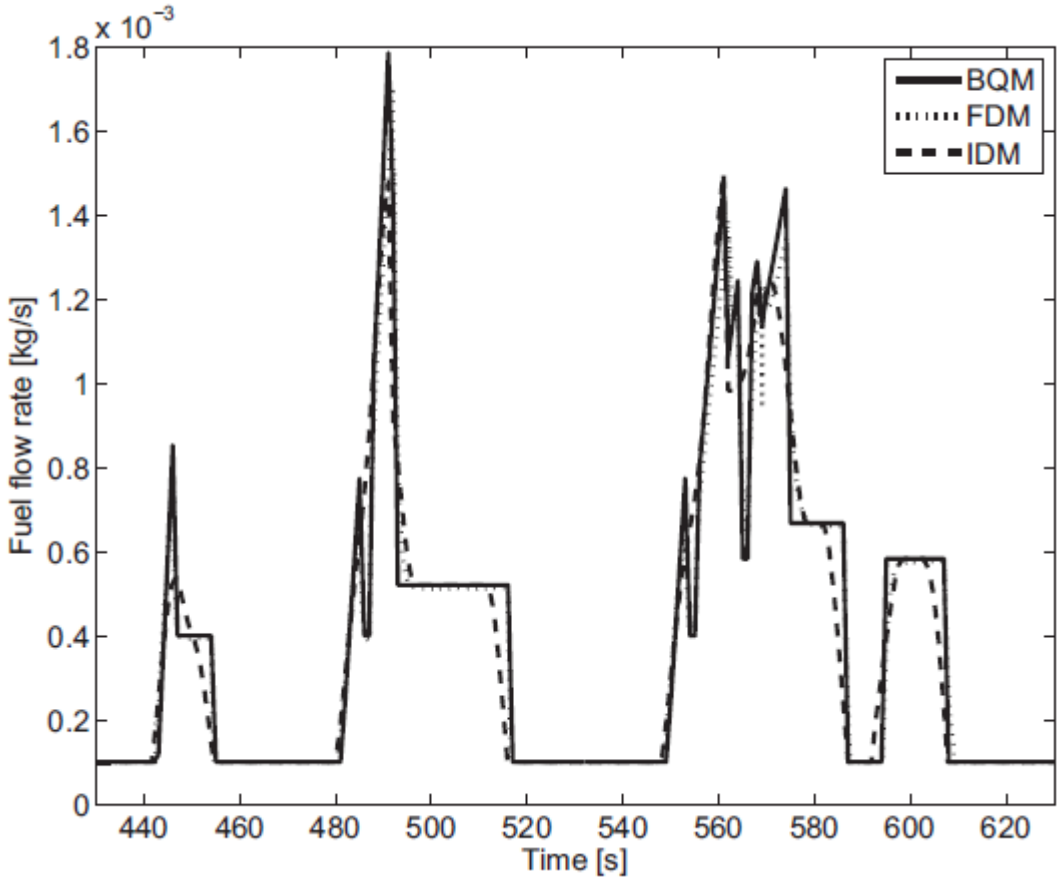

Figure 3.33 – Fuel mass flow during a part of NEDC (Hofman and van Leeuwen, 2009)

Table 3.4 – The influence of driver model and simulation method in fuel consumption (Hofman and van Leeuwen, 2009)

Method	Driver model	NEDC [L/100km]		FTP [L/100km]	
Forward	1	8.37	98.4%	8.44	101.4%
Inverse	1	8.36	98.2%	8.39	100.9%
Forward	2	8.56	100.4%	8.64	103.9%
Inverse	2	8.51	100.1%	-	-
Quasi-static	n.a.	8.51	100.0%	8.32	100.0%

Hofman and van Leeuwen state that quasi-static simulations are suitable whenever the dynamic effects are negligible. The results observed in this study showed a maximum of 1.8% difference from quasi-static to dynamic modeling, which is a reasonable difference for a large number of applications. The dynamic effects are particularly important in studies regarding drivability and driver comfort in which transient effects can affect the user perception of quality. The human intrinsic sensors are sensitive to acceleration and jerks, in other words, the

derivative of speed and the derivative of acceleration, which require high definition measurement of transient behaviors. These effects in general have short duration and low peaks, consuming low levels of energy, and in general, are of relative low importance for fuel consumption measurements.

The engine fuel map obtained in Hofman and van Leeuwen's study is presented in Figure 3.34:

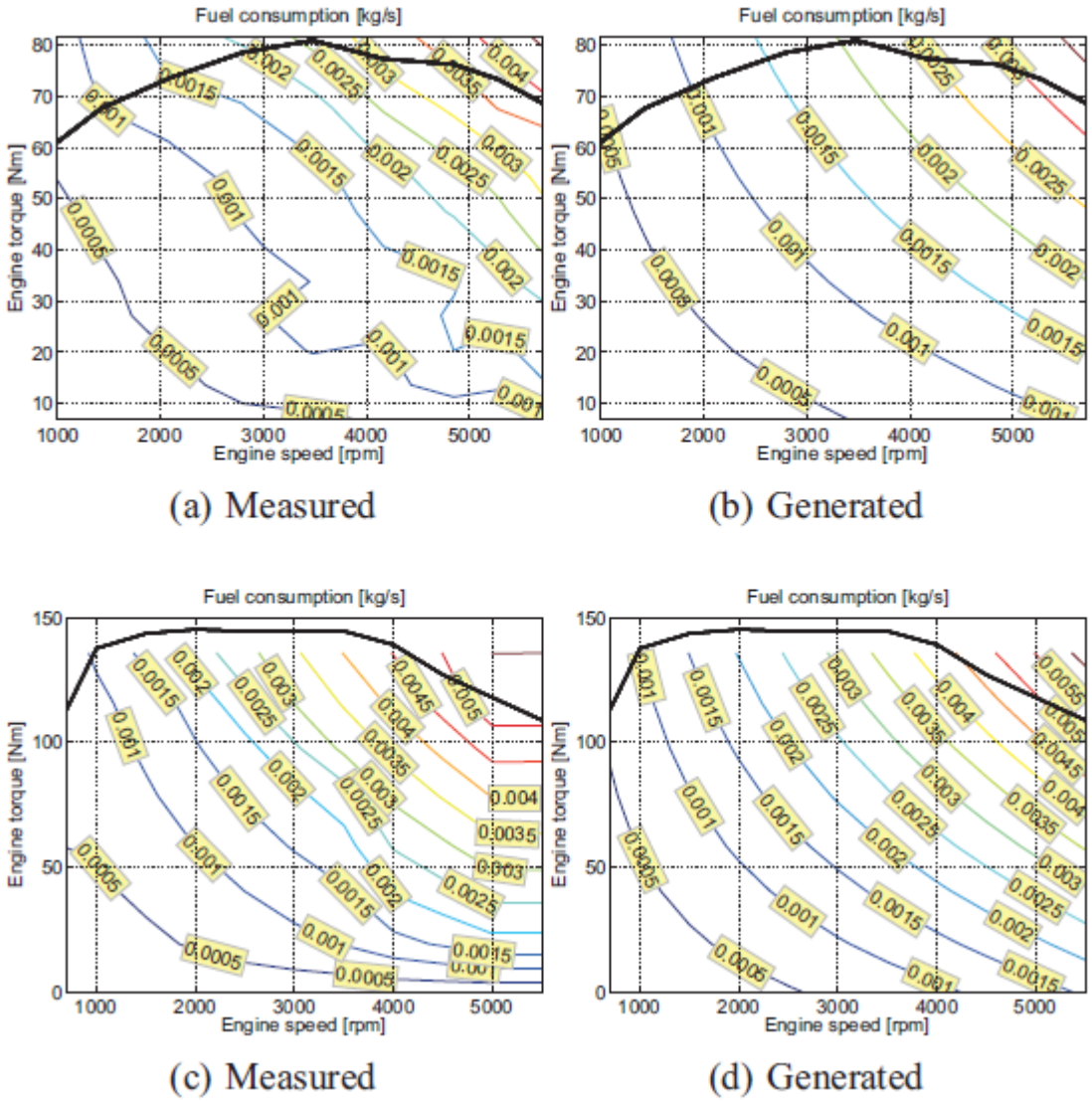

Figure 3.34 - Engine maps for 1.0l engine (top) and 1.9l engine (bottom) (Hofman and van Leeuwen, 2009)

According to Manzoli (2009), there are two different mathematical approaches currently used to estimate second-by-second fuel consumption: modal models based on vehicle speed vs acceleration profile and power-based models. Modal modeling approach does not take into account vehicle's characteristics, but instead, it creates a relationship in the

form $f_c = f(vehicle\ speed, vehicle\ acceleration)$, while power-based models develops a mathematical model based on vehicle's characteristics and physical laws. A brief review of these models is presented in the next section.

3.4.1 Modal fuel consumption modeling

Barth et al. (1996) states that a model based on the vehicle operating conditions (idle, acceleration, deceleration and cruise modes of operation) is required for traffic evaluations in both micro scale and macro scale evaluations. These models are called modal models and they propose to characterize the operating modes as a matrix of speed and acceleration, as presented in Figure 3.35:

	DECELERATION/ACCELERATION (mph/s)												
Speed (mph)	-6	-5	-4	-3	-2	-1	0	1	2	3	4	5	6
0							IDLE						
5													
10													
15													
20													
25													
30							CRUISE						
35													
40													
45													
50													
55													
60													
65													

Figure 3.35 – Example of speed/acceleration matrix containing modes of idle, acceleration, deceleration and cruise (Barth et al., 1996)

The objective is to evaluate the emission for exhaust gases emission for each bin of the matrix. The more sophisticated the instruments used to acquire speed and exhaust emissions, the finer the grid, and better the quality of the model.

It is important to notice that these models do not take into account vehicles characteristics, such as vehicle mass, vehicle resistive forces, gear ratios, etc. Modal models are not based on physical modeling, unlike the models presented by Hofman and van Leeuwen, and instead, are based on evaluating the fuel consumption of a vehicle based on the driving pattern.

Ahn (1998) used this methodology to develop a micro scale emission model based on acceleration and speed levels. Ahn developed his model based on Oak Ridge National

Laboratory (ORNL) in USA, using a sample of eight vehicles. The base data used in this work for fuel consumption is shown in:

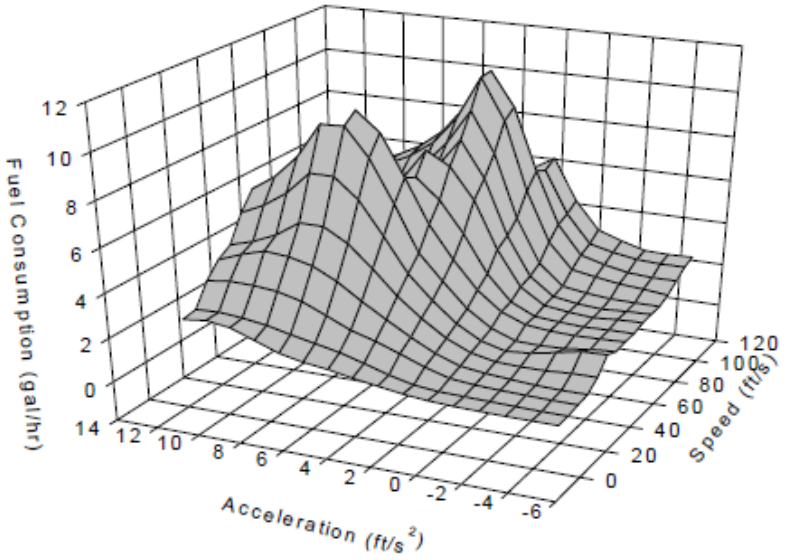

Figure 3.36 – Surface plot of fuel consumption as function of speed and acceleration (Ahn, 1998)

Ahn studied 2 different modeling approaches in a total of 15 different parameters configuration and compared the difference between the models and the measured values. The two different modeling techniques used are non-linear regression models and neural network models.

The first regression model used to predict the expected fuel consumption is a combination of cubic and quadratic equations (which results in polynomial equations) fitted using minimum correlation coefficient criteria to adjust the equation coefficients and to choose the best combination of quadratic and cubic equations. Figure 3.37 presents the predicted fuel consumption for the best fit model:

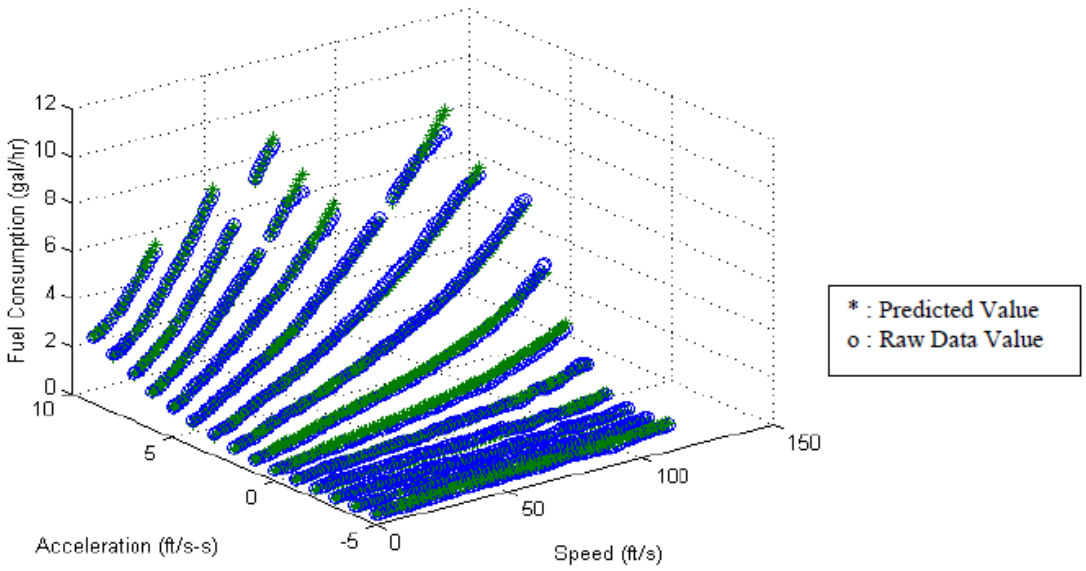

Figure 3.37 – Predicted fuel consumption for best fit polynomial regression (Ahn, 1998)

The second model used is a neural network model that uses the measured data for test and train sets of data. A three layered neural network model was used, as shown in Figure 3.38:

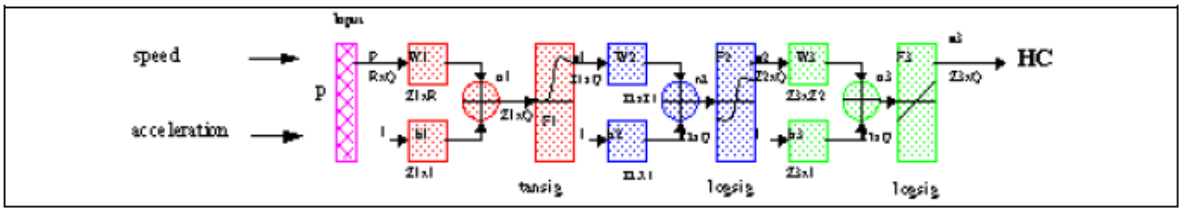

Figure 3.38 – Three layered network used by Ahn (1998)

The fuel consumption map generated by neural network model presented high correlation and is presented in Figure 3.39:

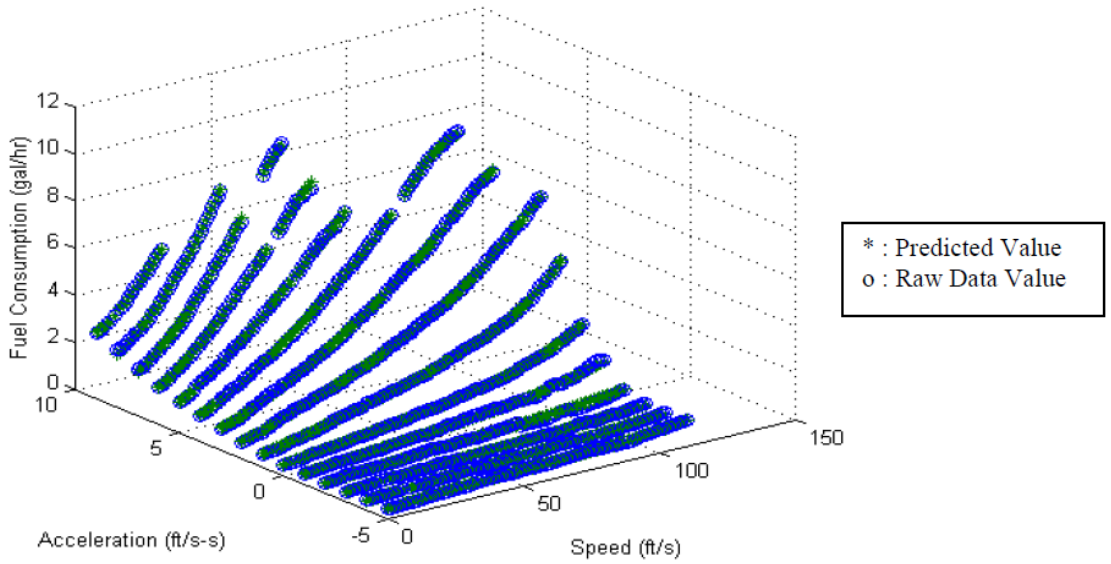

Figure 3.39 – Predicted fuel consumption from neural network model (Ahn, 1998)

In order to validate these models, the author used second-by-second data from FTP 75 city cycle (presented in Figure 3.2) and the US06 cycle (presented in Figure 3.4) and compared the modal fuel consumption obtained through the presented models and the fuel consumption from measured points. The results obtained are presented in Table 3.5 and Table 3.6:

Table 3.5 - Summary of FTP-75 cycle test of fuel consumption models (Ahn, 1998)

	Regression Models				Neural Net Model
	Model C	Model E	Model M	Model N	Model O
CPU Time (seconds)	0.0056	0.0162	0.0315	0.0306	0.0884
Total Error	6.26	4.6306	4.1949	0.5758	2.3707
1-s Based Error	14.1	9.3541	8.6548	5.5316	4.2164
Standard Deviation	0.75	0.78	0.784	0.72478	0.7239
Correlation Coefficient	0.985	0.989	0.994	0.995	0.992

Table 3.6 - Summary of US06 cycle test of fuel consumption models (Ahn, 1998)

	Fuel Consumption Modeling	
	Model N	Model O
CPU Time(seconds)	0.0118	0.032
Total Error	2.1662	2.0857
1-s Based Error	4.4050	14.0092
Standard Deviation	2.0144	1.9084
Correlation Coefficient	0.97605	0.97042

The models comparison for FTP-75 showed that regarding total error was model N (3rd order polynomial regression), which was also the model with higher correlation

coefficient (0.995). Neural network model (Model O) was the second in both ranks (total error and correlation coefficient). For the US06 cycle, both models presented similar performance for both total error and correlation coefficient.

3.4.2 Vehicle specific power modeling

The vehicle specific power approach is based on a simplification of the forces applied to a vehicle (Duarte et al, 2015). This model relates a calculated demand power based on vehicle simplified characteristics (such as aerodynamic drag coefficient, frontal area, tire rolling resistance), with fuel consumption. This methodology takes into account the physic phenomena that drives the energy and power requirements for a given drive test. The equation used for a typical light-duty vehicle is presented in Eq. 3.4 (Coelho et al, 2009):

$$VSP = v \cdot (1.1a + 9.81 \sin(\theta) + 0.132) + 0.000302\, v^3 \quad (3.4)$$

Where VSP is the vehicle specific power, v us vehicle speed, a is vehicle acceleration and θ is the road grade. However, as this model used simplifications and constant parameters and is not specific to the tested or simulated vehicle since it assumes constant parameters to fit the power required to move the vehicle. This model, therefore, has limited applications to simulate a specific vehicle and it is more suitable to evaluate fuel consumption for a fleet or traffic management, and not for a specific vehicle.

A full model for vehicle power demand is presented in Section 4, which will be the model used in the development of this work.

4 METHODOLOGY

This section will explain the methodology used to measure selected vehicles, data processing required to obtain all necessary data and the models used to generate engine performance map. In order to develop the methodology, a clear understanding of the physics behind vehicle motion is required. The first part of the methodology consists of a brief explanation of vehicle longitudinal dynamics, which will relate vehicle acceleration capability to the power generated by the engine. The basic methodology development flowchart is presented in Figure 4.1:

Figure 4.1 – Basic methodology development flowchart

Vehicle longitudinal dynamics model will help understand what parameters can be obtained in order to ensure that all required input data for the engine performance map model are available. The vehicle longitudinal dynamics model describes vehicle motion as a function of its physical characteristics and parameters. The approach used in current work is based on model presented by Gillespie (1992).

Gillespie adopts the SAE coordinate system, where x axis is parallel to vehicle longitudinal motion, y axis is transversal to vehicle longitudinal motion and parallel to the ground, and z axis is perpendicular to the ground. This coordinate system is presented in Figure 4.2:

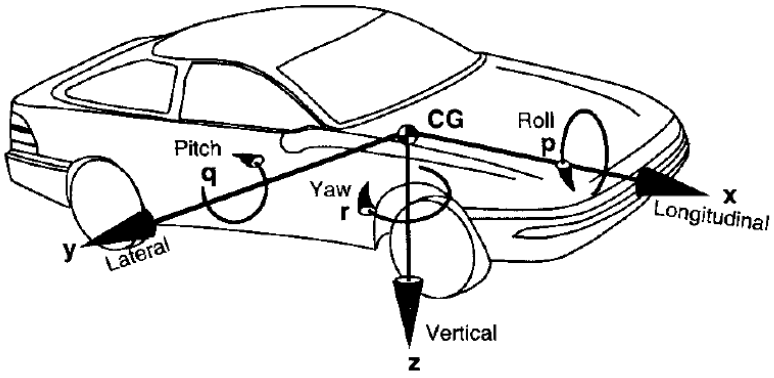

Figure 4.2 – SAE Coordinate system adopted by Gillespie (1992)

4.1 PHYSICAL MODELING

This section aims to provide detailed information on how the vehicle will be measured, the instruments and equipment used and what parameters need to be acquired. The outputs of this section are the raw data recorded measurements, which will be the basis for the engine map model development. A vehicle dynamics model is used to extract the most important parameters required for acquisition and empirical coefficients assessment. A procedure to avoid error states and variability sources is also presented in order to improve repeatability of the experiments.

4.1.1 Vehicle dynamics longitudinal model

The main forces acting on vehicle direction x (longitudinal direction) are obtained through the free body diagram (FBD) presented by Gillespie (1992), as shown in Figure 4.3:

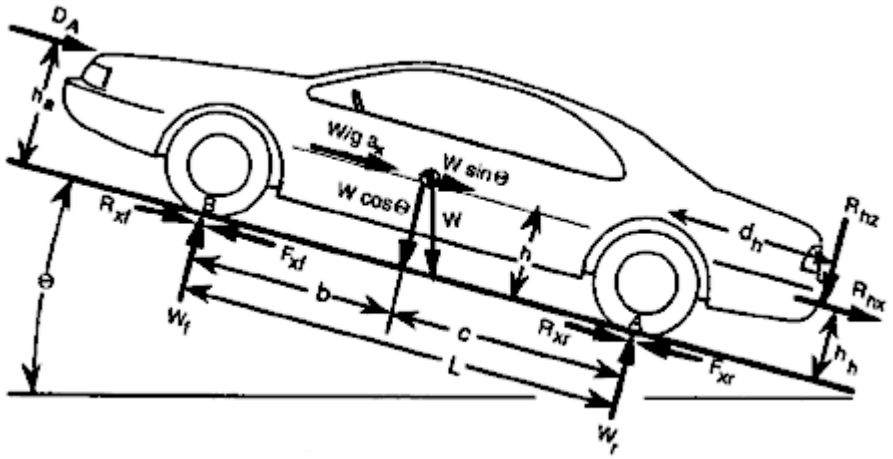

Figure 4.3 – Arbitrary forces acting on a vehicle – FBD (Gillespie, 1992)

Force symbols presented in Figure 4.3 are described in Table 4.1:

Table 4.1 – Description of forces presented in Figure 4.3

Force Symbol	Description
W, W_f, W_r	Weight force (W) acting on front wheel (W_f) and rear wheel (W_r)
F, F_{xf}, F_{xr}	Tractive force (F) acting on front wheel (F_f) and rear wheel (F_r)
R_{hx}, R_{hz}	Trailer towing force (R_h) acting on front wheel (R_{hf}) and rear wheel (R_{hr})
R_{xf}, R_{xr}	Tires resistive force (R_x) acting on front wheel (R_{xf}) and rear wheel (R_{xr})
D_A	Aerodynamic drag force

When vehicle is on uphill or downhill condition, i.e., when $\theta \neq 0$, weight force can be decomposed into a component parallel to the ground ($W \sin\theta$) and a component perpendicular to the ground ($W \cos\theta$), acting on vehicle center of gravity (CG).

In order to develop a proper vehicle dynamics modeling, it is important to understand the power flow through powertrain system (presented in Figure 4.4).

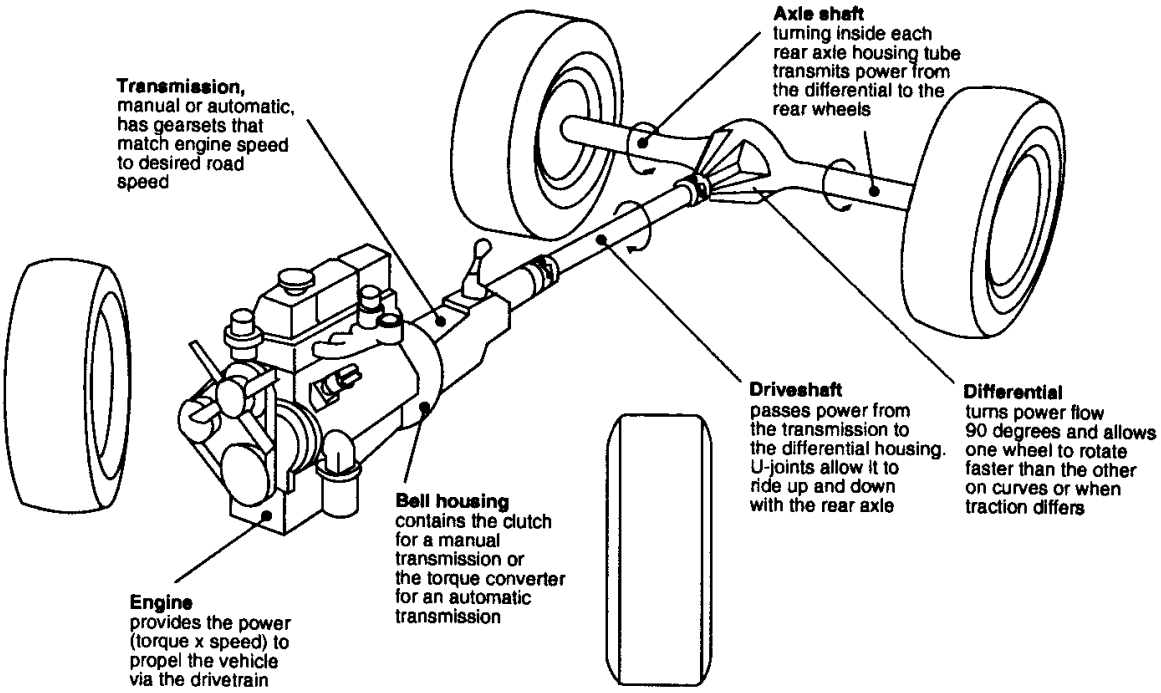

Figure 4.4 – Primary elements in the powertrain system (Gillespie, 1992)

The engine is responsible to convert fuel energy (chemical energy) into thermal energy through a combustion process. The pressure created by combustion (thermal energy) forces engine pistons to turn engine crankshaft, generating a rotational motion (mechanical energy). This motion is then transferred to the transmission through the clutch (in manual transmission vehicles) or through the torque converter (in automatic transmission vehicles). Transmission is responsible to multiply engine torque through a gearing system, thus, reducing rotational speed. This motion is transferred to the differential, that turns power flow 90 degrees to the axle shafts and to the wheel. Differential also allows one wheel to rotate in different speed from the other, which is required during turning maneuvers. The power flow for a typical ICE powered engine is presented in Figure 4.5:

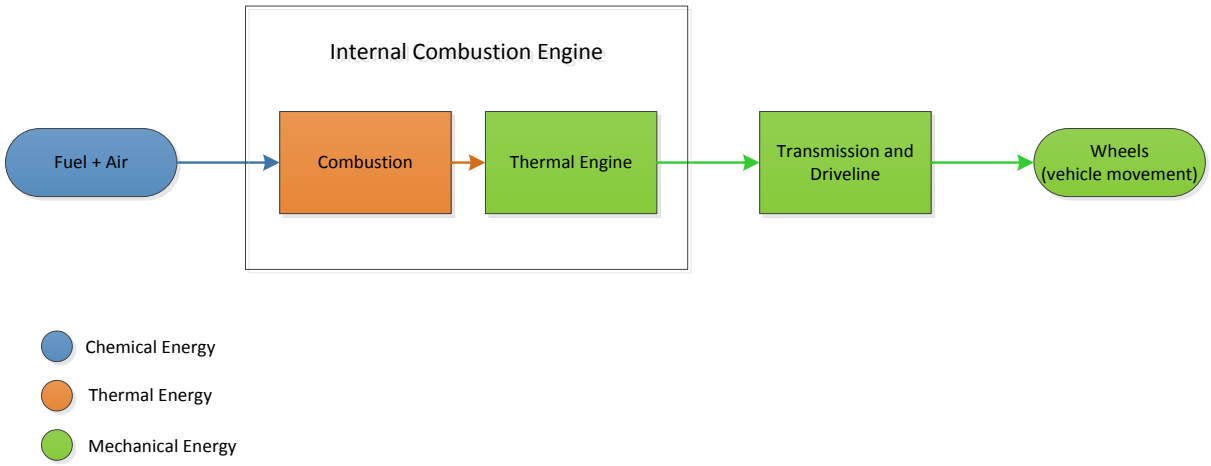

Figure 4.5 – Power flow from tank to wheel

Longitudinal vehicle dynamics considers only mechanical power components of Figure 4.5. The engine torque is transmitted to transmission through the clutch (considering a manual transmission vehicle). Details of clutch mechanisms are presented in Figure 4.6.

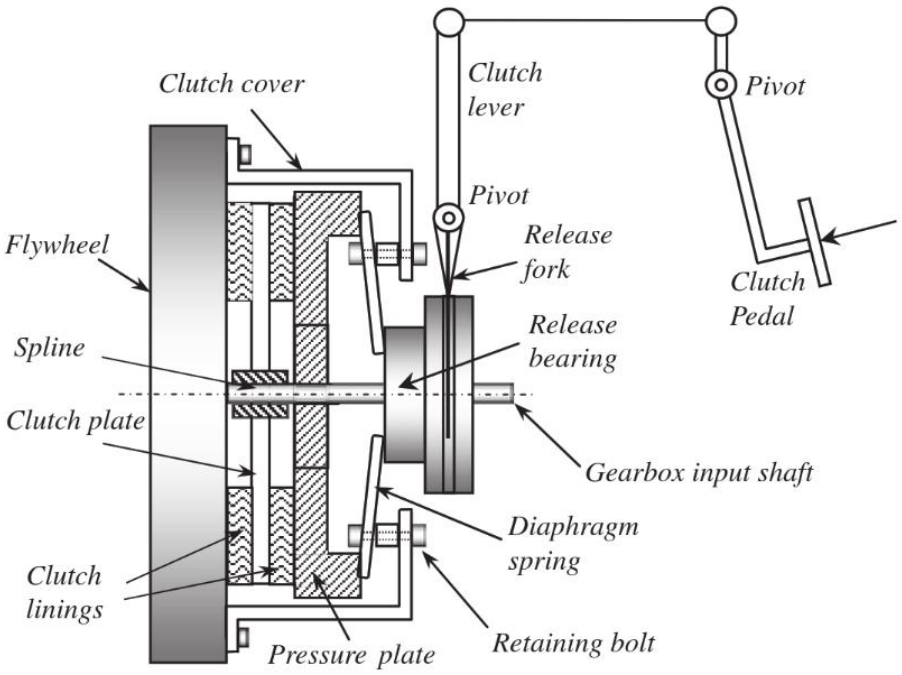

Figure 4.6 Details of clutch mechanisms (Mashadi and Crolla, 2011)

Clutch has function to decouple engine and transmission when vehicle is in idle condition or during gear shifting. The output torque in the clutch is given by Eq. 4.1:

$$\tau_c = \tau_e - I_e \cdot \alpha_e \tag{4.1}$$

where τ_c is the clutch output torque, τ_e is the engine torque (i.e., clutch input torque), I_e is the engine overall rotational inertia and α_e is engine rotational acceleration. This torque will be transmitted to transmission (also called gearbox) and the output torque will be multiplied. A schematic example of a 5 speed manual transmission is presented in Figure 4.7:

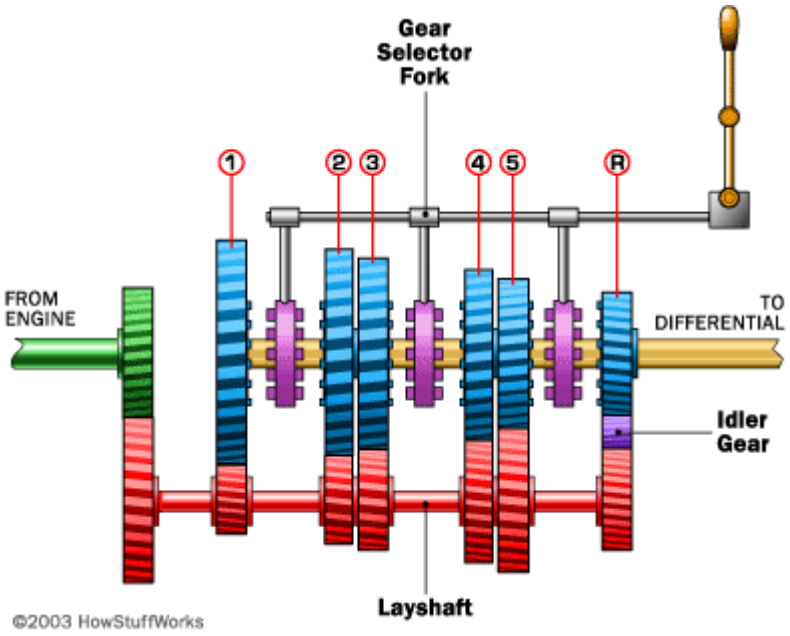

Figure 4.7 – Schematic example of a 5 speed manual transmission (How Stuff Works, 2016)

The output torque in transmission is given by Eq. 4.2:

$$\tau_d = (\tau_c - I_t \cdot \alpha_e)N_t \tag{4.2}$$

where τ_d is the torque delivered to the driveline, I_t is the transmission rotational inertia and N_t is the gear multiplication ratio. The schematic exaple of a differential is presented in Figure 4.8:

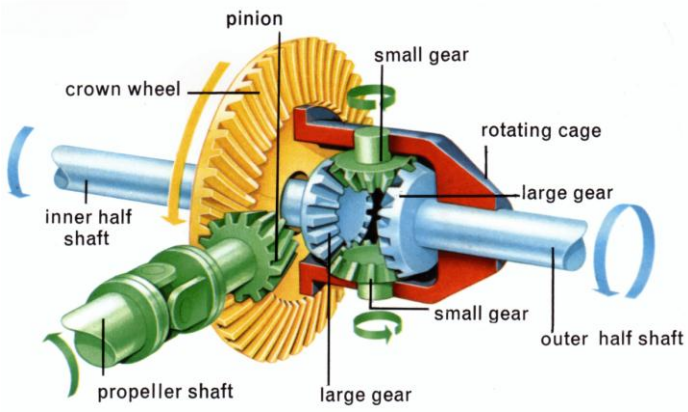

Figure 4.8 – Schematic example of a differential (Mr. Clutch, 2016)

Similarly, the axle torque is given by Eq. 4.3:

$$\tau_a = (\tau_d - I_d \cdot \alpha_d) N_f \tag{4.3}$$

where τ_a is the axle torque, I_d is the differential rotational inertia, α_d is the rotational acceleration of the differential and N_f is the differential gear ratio. The axle torque is the torque that is directly transmitted to the wheels and move the vehicle. Vehicle motion equation can be, thus, described in Eq. 4.4:

$$\tau_a = F_x r + I_w \alpha_w \tag{4.4}$$

where F_x is the tractive force, presented in Figure 4.3, r is the dynamic radius of the tires, I_w is the tire and wheels combined inertia, and α_w is the wheels rotational acceleration.

The rotational acceleration for the engine, differential and wheel are given by Eq. 4.5 and Eq. 4.6:

$$\alpha_e = N_t \alpha_d \tag{4.5}$$

$$\alpha_d = N_f \alpha_w \tag{4.6}$$

Combining Eq. 4.5 and 4.6:

$$\alpha_e = N_t N_f \alpha_w = N_{tf} \alpha_w \tag{4.7}$$

where N_{tf} is the combined gear ratios. Combining Eq. 4.1 to Eq. 4.7 and solving for tractive force one can obtain:

$$F_x = \frac{\tau_e N_{tf}}{r} - \frac{\left((I_e + I_t) N_{tf}^2 + I_d N_f^2 + I_w\right) a_x}{r^2} \tag{4.8}$$

Introducing a factor to account for transmission and differential inefficiencies, as proposed by Gillespie (1992):

$$F_x = \frac{\tau_e N_{tf} \eta_{tf}}{r} - \frac{\left((I_e + I_t) N_{tf}^2 + I_d N_f^2 + I_w\right) a_x}{r^2} \tag{4.9}$$

The Eq. 4.9 can be interpreted as follows: the longitudinal tractive force acting on the vehicle (F_x) is caused by the engine torque (τ_e), that is multiplied by the overall transmission and differential ratio (N_{tf}) and overall drivetrain (transmission and differential) efficiency (η_{tf}) and divided by tire dynamic radius (r), discounted the effort necessary to accelerate rotating components (which includes all negative elements in Eq. 4.9). When vehicle is operating in steady speed regime, i.e., $a_x = 0$, the discounted effort due to rotational inertias is null.

Applying Newton's second law considering the FBD presented in Figure 4.3, one can obtain Eq. 4.10:

$$\sum F_i = M \cdot a_i \therefore M \cdot a_x = F_x - R_x - D_A - R_{hx} - W \cdot \sin\theta \tag{4.10}$$

Replacing F_x by the tractive force presented in Eq. 4.9:

$$M \cdot a_x = \frac{\tau_e N_{tf} \eta_{tf}}{r} - \frac{\left((I_e + I_t)N_{tf}^2 + I_d N_f^2 + I_w\right) a_x}{r^2} - R_x - D_A - R_{hx} - W \cdot \sin\theta \quad (4.11)$$

Grouping the terms that multiply the acceleration, the Eq. 4.12 can be obtained:

$$M \cdot a_x + \frac{\left((I_e + I_t)N_{tf}^2 + I_d N_f^2 + I_w\right) a_x}{r^2} = \frac{\tau_e N_{tf} \eta_{tf}}{r} - R_x - D_A - R_{hx} - W \cdot \sin\theta \quad (4.12)$$

For simplification matter, an equivalent translational inertia can be defined:

$$M_r = \frac{\left((I_e + I_t)N_{tf}^2 + I_d N_f^2 + I_w\right)}{r^2} \quad (4.13)$$

Combining Eq. 4.13 and Eq. 4.12:

$$(M + M_r) \cdot a_x = \frac{\tau_e N_{tf} \eta_{tf}}{r} - R_x - D_A - R_{hx} - W \cdot \sin\theta \quad (4.14)$$

In current work, vehicles will not be tested with a trailer attached, and the term R_{hx} in Eq. 4.14 will be null. This equation is the basis for the present work development, since it relates the tractive force, the resistive forces and the engine torque. The next sections will present a model for the tire resistive forces and aerodynamic force.

4.1.2 Tire resistive force

Pneumatic tires in contact to the ground and subject to vehicle weight is deformed, losing its round shape. The action of a driving torque causes the contact patch between tire and the ground to be shifted in front of the wheel center (Eriksson and Nielsen, 2014), as presented in Figure 4.9:

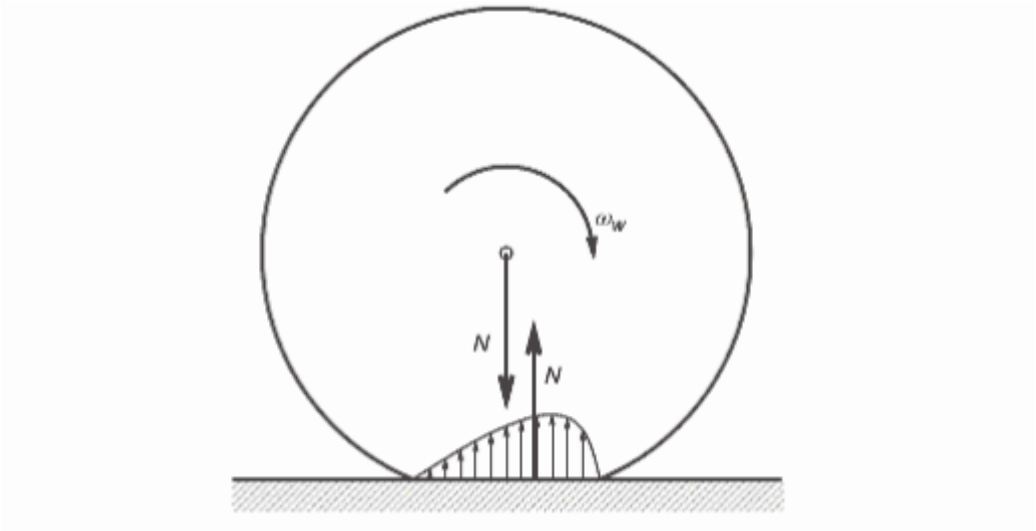

Figure 4.9 – Tire deformation under driving torque (Eriksson and Nielsen, 2014)

This shifting in contact patch causes the normal force to act shifted from wheel center, generating a torque contrary to vehicle movement, which is the origin of the rolling resistance. The more rigid the tire, less deformation and, thus, less rolling resistance.

It is usually to define the rolling resistance force as a function of a rolling resistance coefficient (f_r). Eriksson and Nielsen (2014) presented the following generic equation:

$$R_x = f_r(T, p, \tau, v, \dots) \cdot M \cdot g \cdot \cos\theta \tag{4.15}$$

where T is the tire temperature, p is the inflation pressure, τ is the driving torque applied on the wheel and v is vehicle speed. For small angles, the approximation $\cos(\theta) \approx 1$ is valid and in most literatures this term is omitted. Gillespie (1992) proposed the following model for passenger vehicles rolling resistance coefficient:

$$f_r = 0.01 \cdot \left(1 + \frac{v[\text{mi/h}]}{100}\right) \tag{4.16}$$

Another model is proposed by Schmid (1938), presented in Eq. 4.17:

$$f_r = f_\emptyset + f_s \left(\frac{v[\text{mi/h}]}{100}\right)^{2.5} \tag{4.17}$$

where $f_\emptyset$ is the non-speed dependent term of the rolling resistance and f_s is the speed-dependent term. Eriksson and Nielsen (2014) presented these terms graphically (shown in Figure 4.10) as a function of tire inflation pressure.

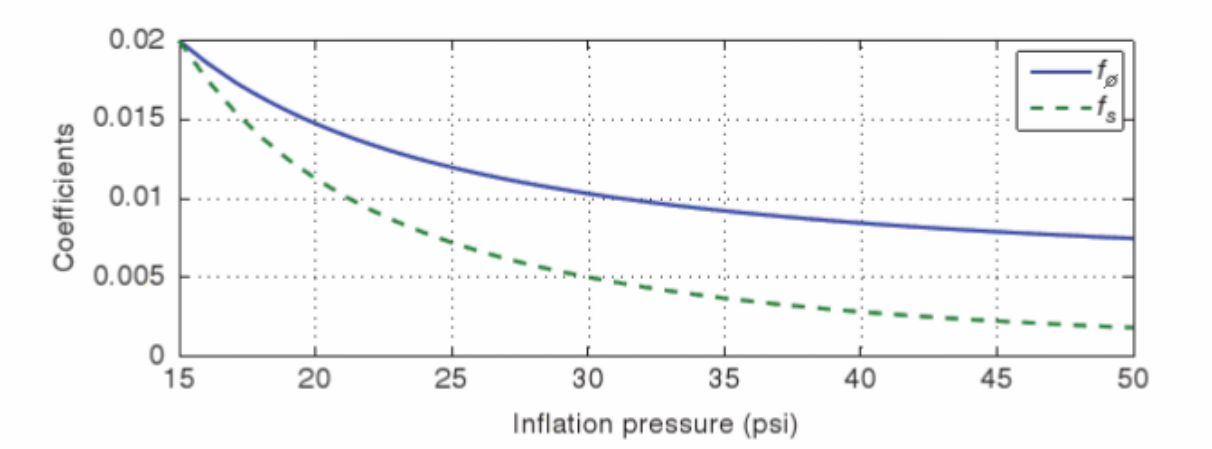

Figure 4.10 - $f_\emptyset$ and f_s as function of inflation pressure (Eriksson and Nielsen, 2014)

Clark and Dodge (1979) evaluated tire rolling resistance subject to different conditions of load, speed, temperature, inflation pressure and warm-up times. The results for rolling resistance versus speed for five different tires are presented in Figure 4.11:

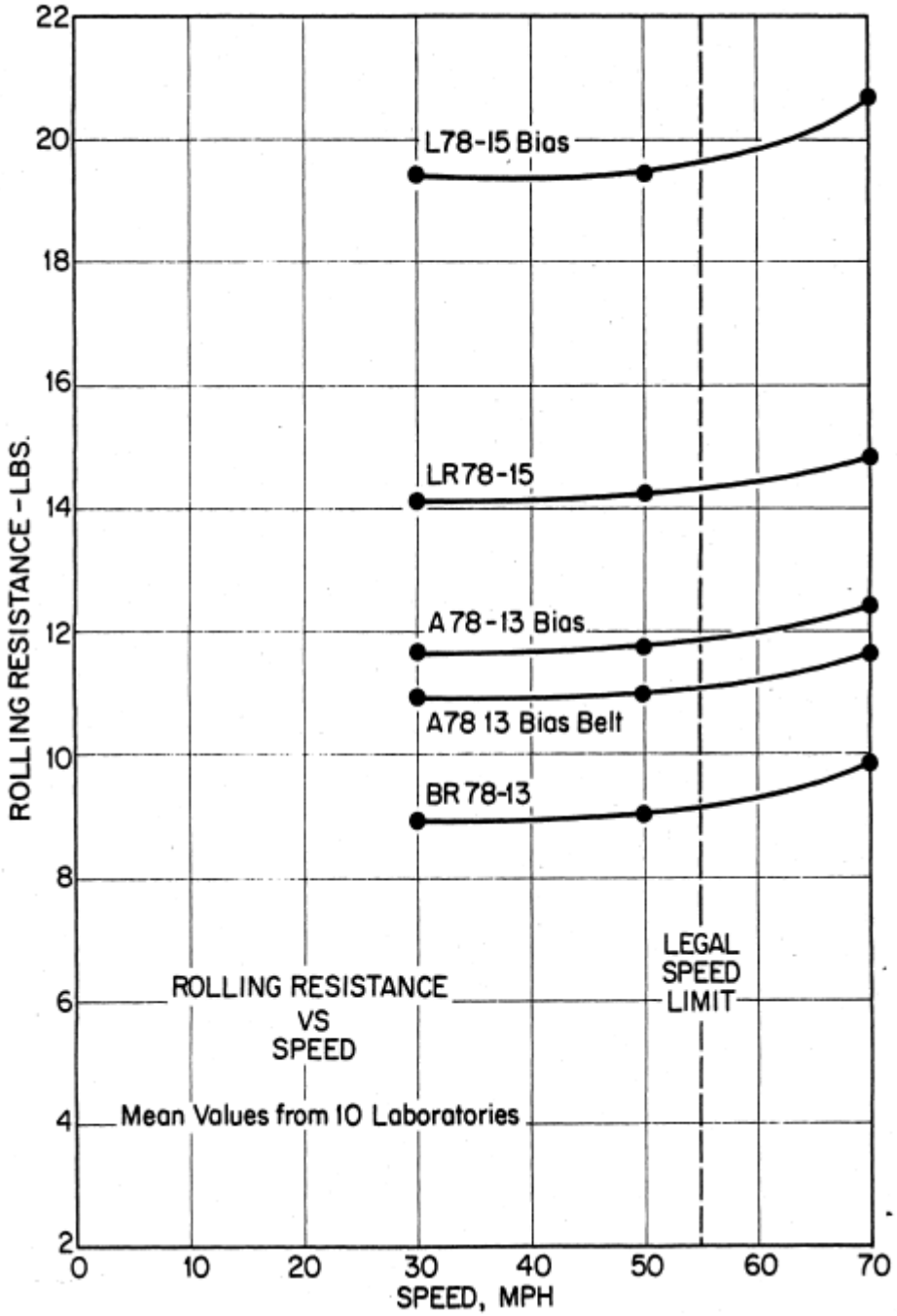

Figure 4.11 – Rolling resistance force vs. speed for five different passenger car tires (Clark and Dodge, 1979)

It can be seen that for speeds lower than 50 mi/h (around 80 km/h) the rolling resistance force is almost independent of speed, and starts to rise after this speed. The influence of warm-up time is presented in Figure 4.12:

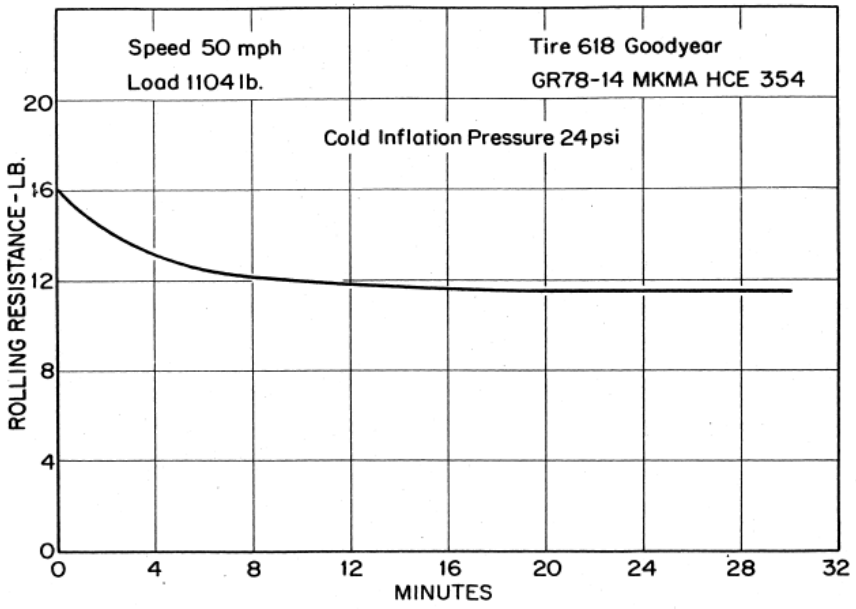

Figure 4.12 - Typical rolling resistance versus warm-up time (Clark and Dodge, 1979)

Figure 4.12 shows that after 20 minutes of constant speed riding at 50 mph is sufficient to achieve a steady rolling resistance value. The rolling resistance coefficient as a function of vertical load is presented in Figure 4.13:

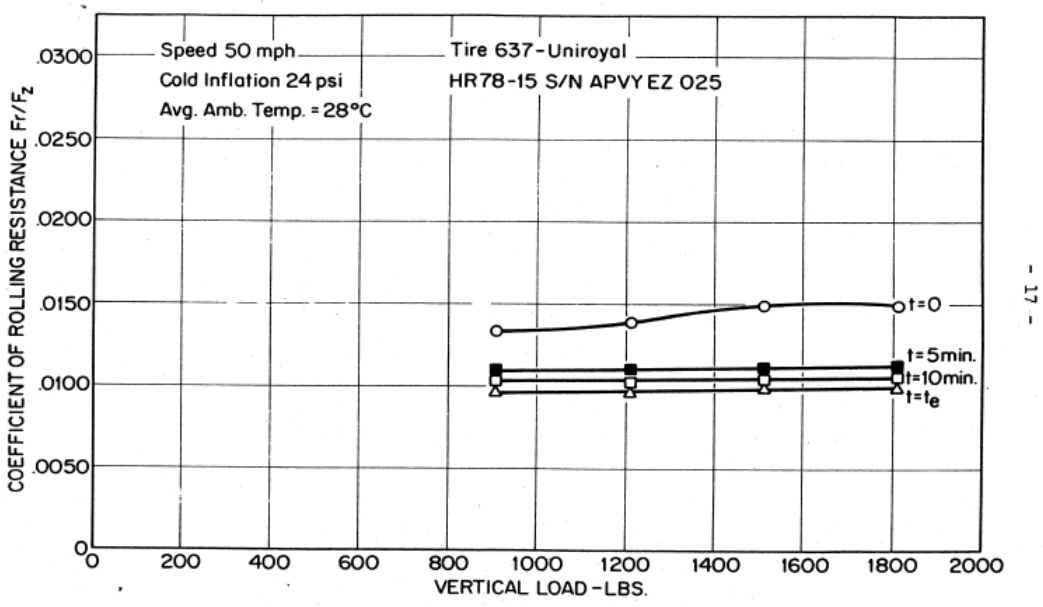

Figure 4.13 – Coefficient of rolling resistance as function of warm-up time and vertical load (Clark and Dodge, 1979)

For warm-up times greater than five minutes the coefficient of rolling resistance does not depend on the vertical load, which means that rolling resistance force will rise linearly with load increase.

Rolling resistance force and coefficient versus the reciprocal of inflation pressure is presented in Figure 4.14:

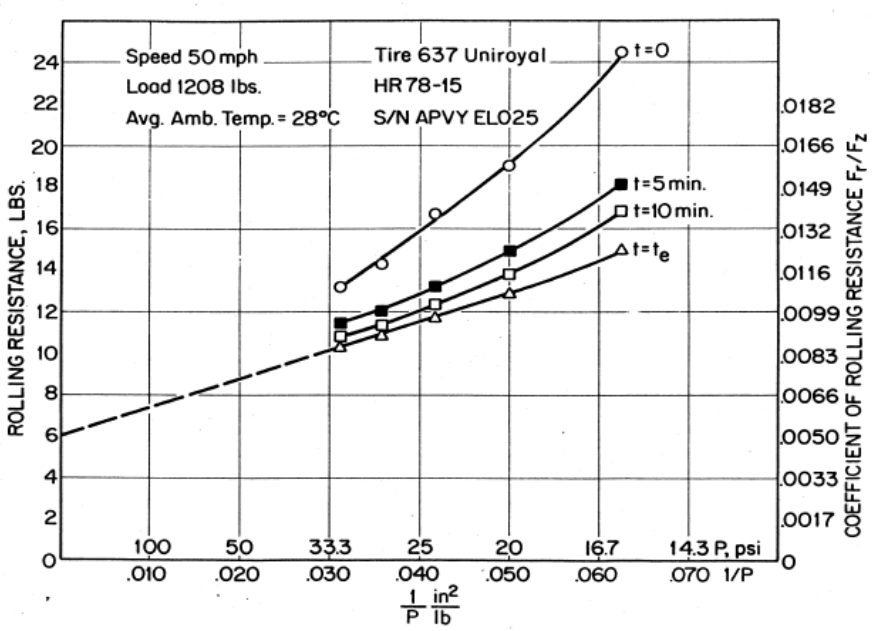

Figure 4.14 – Rolling resistance force and coefficient as a function of warm-up time and reciprocal of inflation pressure (Clark and Dodge, 1979)

Rolling resistance increases almost linearly with reciprocal of tire pressure for $t = t_e$ (where t_e is the warm-up time required to stabilize rolling resistance). The authors proposed an equation for the resistive force as function of tire properties, load and pressure inflation:

$$R_x = R_{x0}.\left(\frac{F_z}{F_{z0}}\right).\left[1 + c_p.\left(\frac{p_0}{p} - 1\right)\right] \tag{4.18}$$

Knowing that $f_r \equiv R_x/F_z$, Eq. 4.18 can be rearranged:

$$\frac{R_x}{F_z}\frac{F_{z0}}{R_{x0}} = \frac{f_r}{f_{r0}} = \left[1 + c_p.\left(\frac{p_0}{p} - 1\right)\right] \tag{4.19}$$

The mathematical model used in this work will consider a standard inflation pressure recommended by vehicle manufacturer and that f_r is independent of vehicle speed. Therefore, vehicle measurement speeds must not be greater than 100 km/h.

4.1.3 Aerodynamic drag

Aerodynamic forces are a result of fluid viscosity, which causes a resistive force when fluid is sheared. Katz (1995) states that unlike tire rolling resistance, which can be considered as independent of vehicle speed, aerodynamic forces are largely dependent of vehicle speed. Aerodynamic drag force is given by Eq. 4.20:

$$D_A = \frac{1}{2}\rho \cdot C_d \cdot A_F \cdot v_r^2 \tag{4.20}$$

where ρ is air density, C_d is the drag coefficient, A_F is vehicle frontal area and v_r is relative air speed in vehicle longitudinal direction, as presented in Figure 4.15:

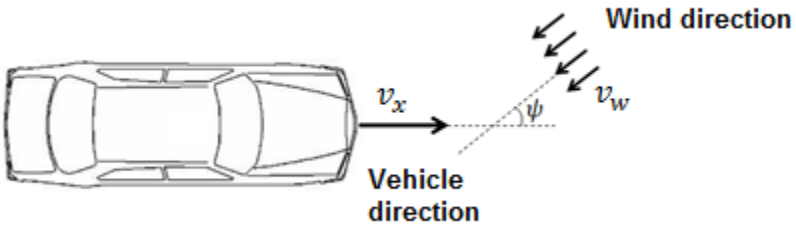

Figure 4.15 – Generic representation of a vehicle moving subjected to wind

where ψ is known as yaw angle (angle between wind direction and vehicle movement direction) and v_w is wind speed and v_x is vehicle speed in x direction (which will be referred also by a simpler form of v). In this case, the relative speed is given by Eq. 4.21:

$$v_r = v_x + v_w \cos(\psi) \tag{4.21}$$

Lucas and Emtage (1987) and Yasin (1978) states that the aerodynamic drag coefficient (C_d) is dependent of yaw angle. Also, air density is dependent of ambient temperature and ambient pressure, and Eq. 4.20 can be modified into Eq. 4.22:

$$D_A = \frac{1}{2}\rho(p_{atm}, T_{atm}) \cdot C_d(\psi) \cdot A_F \cdot v_r^2 \tag{4.22}$$

The generic relationship between the yaw angle and aerodynamic drag coefficient is presented by Yasin (1978) as proportional to the square of yaw angle, and is presented graphically in Figure 4.16:

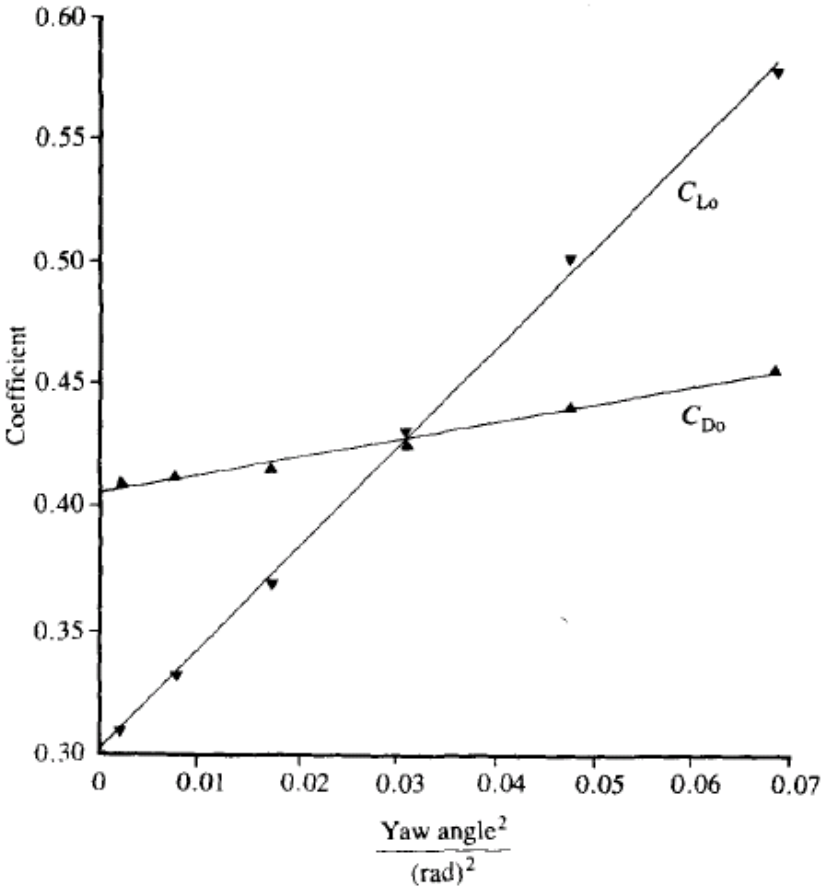

Figure 4.16 – Corrected aerodynamic coefficients of drag (C_{D0}) and lift (C_{L0})

In practical applications, it is difficult to precisely measure wind speed at the vehicle (usually, it is measured in meteorological stations nearby vehicle test site), as well as its direction. It is of common practice to consider the wind speed module null. However, for real world testing conditions, vehicle are subject to wind in a wide range of speeds and directions, which will cause an error on the calculated aerodynamic forces when compared to wind tunnel tests, where wind speed and directions are controlled.

4.1.4 Vehicle road load force measurement

Combining the resistive forces in Eq. 4.14, one can obtain Eq. 4.23:

$$R_{Tx} \equiv R_x + D_A + R_{hx} + W \sin\theta \tag{4.23}$$

As seen in section 4.1.2 and section 4.1.3, $R_x = R_x(f_r, v, p)$ and $D_A = D_A(v, C_d, A_F, \psi, p_{amb}, T_{amb})$, and, therefore, R_{Tx} is also dependent of the same parameters as its composing forces. Some of these parameters are controllable (for example, f_r, since one can choose the tires to be used during the tests and can measure it prior to vehicle testing, as well as C_d and A_F); some parameters can be measured and corrected in

post-processing, such as p_{amb} and T_{amb} (further detail on this correction will be given in this section); and some parameters are variable (in this case, the only variable parameter is vehicle speed). As these tests are conducted without trailer, R_{hx} is equal to zero, and at flat tracks, $\sin\theta$ is also zero, and the resistive force is composed by rolling resistance and aerodynamic drag only.

Considering vehicle speed as the only variable parameter, it is convenient to state that $R_{Tx} = R_{Tx}(v)$ and defining an effective mass as Eq. 4.24:

$$M_e \equiv M + M_r \tag{4.24}$$

Substituting Eq. 4.23 and 4.24 in Eq. 4.14:

$$M_e \cdot a_x = \frac{\tau_e N_{tf} \eta_{tf}}{r} - R_{Tx}(v) \tag{4.25}$$

Through Eq. 4.25, it is simple to relate vehicle acceleration and engine torque, however, the total resistive force needs to be known. There are two different approaches to determine the resistive force as a function of vehicle speed. The first methodology consists of measuring the torque required to maintain a constant speed (i.e., $a_x = 0$). The resistive force will be given by Eq. 4.26:

$$R_{Tx}(v) = \frac{\tau_e N_{tf} \eta_{tf}}{r} \tag{4.26}$$

By measuring the required torque for different speeds, the resistive force as a function of speed can be obtained.

The second methodology, known as coastdown methodology, consists of accelerating the vehicle up to a defined start speed (in many cases $100\ \mathrm{km/h}$ or $120\ \mathrm{km/h}$), put the vehicle in neutral gear and let the vehicle decelerate without any engine torque applied up to a final speed (in many cases $30\ \mathrm{km/h}$ or $20\ \mathrm{km/h}$). The resistive force in this case is given by Eq. 4.27:

$$M_e \cdot a_x = -R_{Tx}(v) \tag{4.27}$$

Ahlawat et al (2013) compared these two methodologies, as presented in Table 4.2:

Table 4.2 – Comparison of coastdown and torque methodologies (Ahlawat et al, 2013)

	Coastdown	**Torque**
Pros	Less instrumentation	Driveline losses test excluded
Cons	Time consuming tests, including driveline losses.	Difficult to install on current production vehicles.

The comparison between torque estimated using coastdown method and torque method presented by Ahlawat et al. (2013) shows a correlation coefficient of 0.928 for the

coastdown method and 0.993 for the torque method. Also, it was observed that coastdown method tends to underestimate the resistive force, as can be seen in Figure 4.17and Figure 4.18:

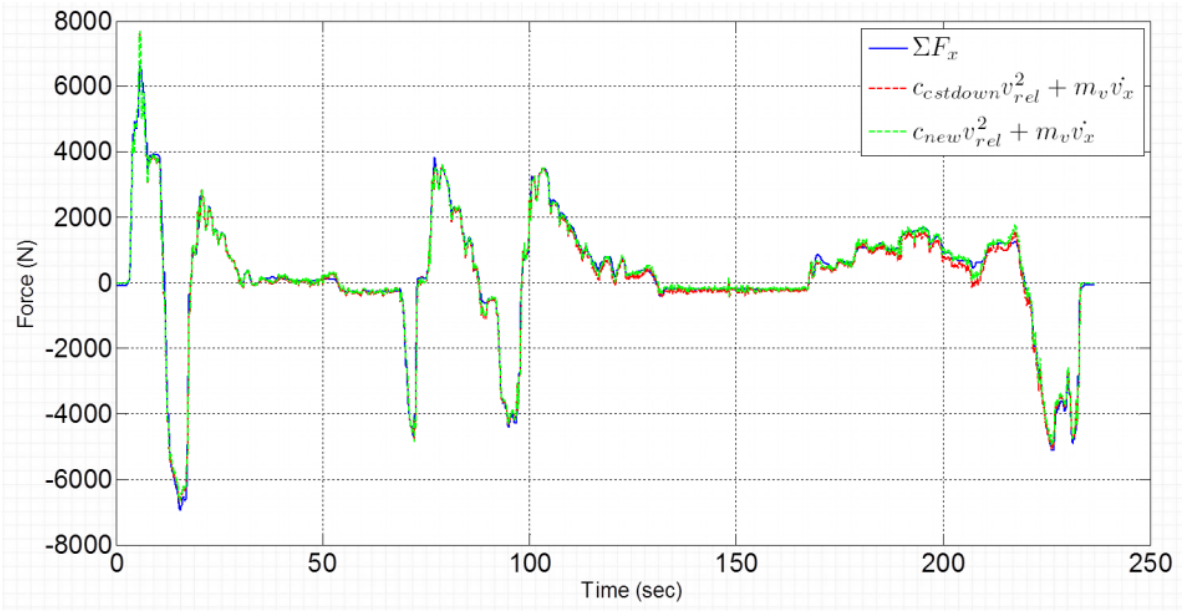

Figure 4.17 – Force acting on wheels measured (blue line), estimated through coastdown (red line) and estimated through torque measurement (green line) (Ahlawat et al., 2013)

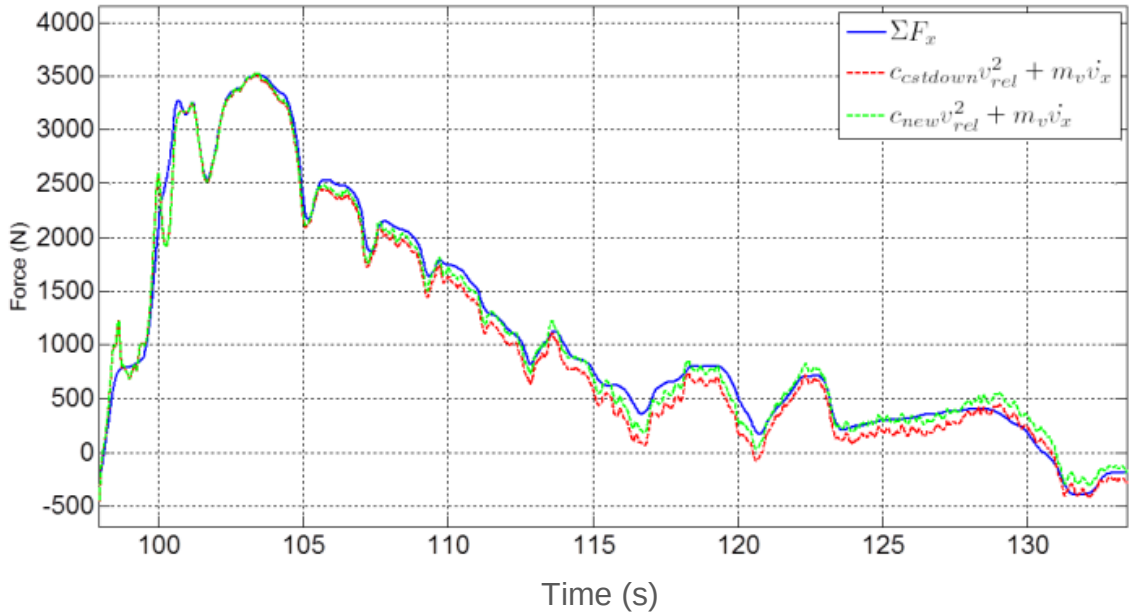

Figure 4.18 –Figure 4.17 excerpt from 100s to 130s (Ahlawat et al., 2013)

In the present work, the coastdown method will be used for the following reasons:

- It is easier to instrument the vehicle and to test, and the instrumentation can be used on public roads;
- Although correlation coefficient for coastdown method is lower than correlation coefficient from torque method, it is still a high correlation coefficient and can be used to estimate resistive force.
- Brazilian standard for determining resistive force uses the coastdown methodology.

The standard used in Brazil to determine road load resistance force is ABNT 10312:2012. This standard requires that the vehicle is tested from an initial speed of 100 km/h to a final speed of 30 km/h in neutral gear, in order to satisfy Eq. 4.27. This standard requires that the following physical quantities should be measured complying the requirements for accuracy and resolution presented in Table 4.3:

Table 4.3 – Requirements for physical quantities measurement (ABNT, 2012)

Quantity	**Accuracy**	**Resolution**
Vehicle speed	± 0.4 km/h	± 0.2 km/h
Time	± 0.1 s	± 0.1 s
Ambient temperature	± 1 ℃	± 1 ℃
Atmospheric pressure	± 0.7 kPa	-
Wind speed	± 0.4 m/s	-
Vehicle mass	± 5 kg	-
Tire pressure	± 4 kPa	-

In order to avoid influence of ambient conditions mentioned in the beginning of the current section, this standard determines that the coastdown test should be run only within the ranges of ambient temperature, atmospheric pressure and wind speed presented in Table 4.4:

Table 4.4 – Accepted range of ambient conditions for a coastdown test according to ABNT (2012)

	Minimum condition	**Maximum condition**
Ambient temperature	5 ℃	35℃
Atmospheric pressure	91 kPa	104 kPa
Wind speed	0 m/s	3.0 m/s (average) 5.0 m/s (peak) 2.0 m/s (transversal

		direction)

The standard proposes the following equation to represent vehicle road load resistive force (Eq. 4.28):

$$R_{Tx}(v) = f_0 + f_2 \cdot v^2 \tag{4.28}$$

where f_0 is the constant coefficient for the resistive force and f_2 is the quadratic coefficient. The test procedure consists of measuring the vehicle deceleration from the initial speed to final speed, computing the time required to run fixed speed intervals, obtain the acceleration for each interval, calculate the force and use a minimum square regression technique to obtain the f_0 and f_2 coefficients.

The maximum speed interval allowed is $5\,\mathrm{km/h}$. A generic example for the speed intervals time measurement is presented in Table 4.5:

Table 4.5 – Example of coastdown measurement intervals

Speed [km/h]	100.0	95.0	90.0	85.0	80.0	75.0	70.0	65.0	60.0	55.0	50.0	45.0	40.0	35.0	30.0
Time [s]	0.0	3.8	7.9	12.2	16.6	21.7	27.1	33.1	40.6	48.9	56.6	64.3	72.7	83.1	94.5

From this data, the mean acceleration for each interval is given by Eq. 4.29:

$$a_i = \frac{v_{i+1} - v_i}{3.6 \cdot \Delta t} \tag{4.29}$$

where a_i is the mean acceleration for interval i, v_i is the speed for interval i, and Δt is the time difference between two speed intervals. The factor 3.6 is used to obtain the acceleration in SI units ($\mathrm{m/s}$). It is important to obtain an average interval speed for the regression technique. The mean speed (in SI units) is obtained by Eq. 4.30:

$$\overline{v_i} = \frac{v_{i+1} + v_i}{2 \cdot 3.6} \tag{4.30}$$

The regression coefficients are given by Eq. 4.31 and Eq. 4.32, respectively:

$$f_0 = \frac{D \times A - C \times E}{(n-1) \times D - C^2} M_e \tag{4.31}$$

$$f_2 = \frac{(n-1) \times E - C \times A}{(n-1) \times D - C^2} M_e \tag{4.32}$$

The terms A, B, C, D and E are presented in Table 4.6, and n is the number of intervals.

Table 4.6 – Coefficients used in f_0 and f_2 calculation

A	B	C	D	E

$\sum_i a_i$	$\sum_i \overline{v_i}$	$\sum_i \overline{v_i}^2$	$\sum_i \overline{v_i}^4$	$\sum_i a_i \cdot \overline{v_i}^2$

For the data used as example in Table 4.5 the calculation procedure to find f_0 and f_2 would lead to the values presented in Table 4.7:

Table 4.7 – Calculation procedure for example presented in Table 4.5

Acceleration	Mean speed	Squared of mean speed	Fourth power of mean speed	Acceleration times mean speed squared
-0.3694	27.083	733.5	538032	-270.95
-0.3388	25.694	660.2	435870	-223.65
-0.3200	24.306	590.8	348997	-189.06
-0.3121	22.917	525.2	275807	-163.91
-0.2756	21.528	463.4	214781	-127.71
-0.2591	20.139	405.6	164491	-105.09
-0.2296	18.750	351.6	123596	-80.71
-0.1862	17.361	301.4	90847	-56.12
-0.1659	15.972	255.1	65082	-42.33
-0.1806	14.583	212.7	45230	-38.41
-0.1808	13.194	174.1	30308	-31.48
-0.1655	11.806	139.4	19424	-23.07
-0.1338	10.417	108.5	11774	-14.52
-0.1219	9.028	81.5	6642	-9.94

M_e	A	B	C	D	E
1050	-3.239	252.8	5003	2370884	-1377

f_0 [N]	**101.8**
f_2 [N/(m/s²)]	**0.3950**

Comparing Eq. 4.28 with Eq. 4.23, one can conclude that:

$$R_{Tx}(v) = f_0 + f_2 \cdot v^2 = R_x + D_A + R_{hx} + W \sin\theta \tag{4.33}$$

As aforementioned, it will be considered that no trailer is attached, thus $R_{hx} = 0$ and as the coastdown test is done in a flat road, $\sin\theta = 0$, reducing Eq. 4.33 to Eq. 4.34:

$$R_{Tx}(v) = f_0 + f_2 \cdot v^2 = R_x + D_A \tag{4.34}$$

For speeds lower than 100 km/h the assumption of tire resistive force independent of speed is reasonable, and therefore the following relationships can be made:

$$R_x = f_r \cdot M \cdot g = f_0 \tag{4.35}$$

$$D_A = \frac{1}{2}\rho \cdot C_d \cdot A_F \cdot v_r^2 = f_2 \cdot v^2 \tag{4.36}$$

In order to avoid a bias on resistive force, the coastdown test is made considering 10 runs, i.e., 10 measurements for the times required for the speed intervals showed in Table 4.5, with 5 runs done in opposite way as the other 5 ones. The wind direction is not important anymore since it will produce a random error instead of a biased error. Eq. 4.36 can be modified into Eq. 4.37:

$$D_A = \frac{1}{2}\rho \cdot C_d \cdot A_F \cdot v^2 = f_2 \cdot v^2 \tag{4.37}$$

which leads to the relationship presented in Eq. 4.38:

$$f_2 = \frac{1}{2}\rho \cdot C_d \cdot A_F \tag{4.38}$$

The influence of ambient temperature and pressure is captured by Brazilian standard ABNT 10312:2012 through the following relationships:

$$f_o' = f_0 \cdot [1 + K_T(T - T_0)] \tag{4.39}$$

$$f_2' = \left(\frac{p_o \cdot T}{p \cdot T_0}\left(f_2 - K_p \cdot f_0\right) + K_p \cdot f_o'\right) \tag{4.40}$$

where K_T is a temperature correction factor for f_0 ($K_T = 8.6 \cdot 10^{-3}$ K^{-1}); K_P is an f_0 correction factor for f_2 ($K_P = 2.503 \cdot 10^{-4}$ [m/s]^2); p_0 is a reference pressure ($p_0 =$ 101.325 kPa) and T_0 is a reference temperature ($T_0 = 293.15$ K). These corrections will be used to estimate the resistive force.

These relationships given by Eq. 4.34 to Eq. 4.36 can be used in Eq. 4.25, and the result follows in Eq. 4.41:

$$M_e \cdot a_x = \frac{\tau_e N_{tf} \eta_{tf}}{r} - f_0 - f_2 \cdot v^2 - W \cdot \sin\theta \tag{4.41}$$

The term $W \cdot \sin\theta$ was once again included since it is important when testing in real world conditions. Knowing that $\dot{v} = a_x$, the engine torque can be obtained by rearranging Eq. 4.41, leading to Eq. 4.42:

$$\tau_e = \frac{(M_e \cdot \dot{v} + f_0 + f_2 \cdot v^2 + W \cdot \sin\theta) \cdot r}{N_{tf} \cdot \eta_{tf}} \tag{4.42}$$

4.1.5 Vehicle instrumentation and data acquisition

The parameters that need to be acquired in order to identify the engine operating condition are the engine speed and the engine torque. The engine speed can be directly acquired from OBD measurements (see Table 3.3), since it is a required diagnostic parameter.

Engine torque, however, is not a required parameter, so it relies on each manufacturer interest to provide it or not. This demands the engine torque to be calculated indirectly through the use of Eq. 4.42.

In Eq. 4.42 it can be seen that one require to know the following parameters to calculate the engine torque:

- Vehicle mass (M_e);
- Vehicle acceleration ($\dot{v}$) and vehicle speed (v);
- Constant coefficient of resistive force regression (f_0);
- Quadratic coefficient of resistive force regression (f_2);
- Road grade (θ);
- Tire rolling radius (r);
- Total transmission and differential ratio (N_{tf});
- Total transmission and differential efficiency (η_{tf}).

These parameters will be classified in time-variant parameters and constant parameters, as presented in Table 4.8:

Table 4.8 – Constant and time-variant parameters for engine torque calculation

Constant parameters	Time-variant parameters
Vehicle mass	Vehicle speed
Constant coefficient of resistive force regression	Vehicle acceleration
Quadratic coefficient of resistive force regression	Road grade
Tire rolling radius	-
Total transmission and differential ratio	-
Total transmission and differential efficiency	-

The procedure to obtain the constant parameters is described below:

1. The vehicle mass can be measured through the use of a weighing-machine with a resolution of 5 kg. This machine is presented in Figure 4.19:

Figure 4.19 – Weighing machine used to obtain vehicle mass

2. The resistive force coefficients can be obtained through the methodology presented in section 4.1.4. Although the coefficients are considered constant for each vehicle, they vary with ambient conditions, thus, additionally the ambient temperature and ambient pressure need to be measured for post processing correction;
3. The tire rolling radius can be obtained through tire nominal size and the addition of a correction factor due to tire deformation in the presence of a vertical load. Tire nominal size is usually given in the form presented in Figure 4.20. The first field (with value 205 in Figure 4.20 example) represents tire width, in millimeters; the second field (valued 65) is the aspect ratio of the tire, meaning that tire side wall length is 65% of the tire width, or $205 \cdot 65/100 = 133.25$ mm; and the last filed, valued 15, is tire rim diameter, in inches ($1\text{in} = 25.4\text{mm}$). To calculate the tire nominal radius, first one need to calculate tire wall:

$$Tire\ wall = Width \cdot \frac{Aspect\ Ratio}{100} \tag{4.43}$$

The tire nominal radius can be then calculated as:

$$Tire\ nominal\ radius = \frac{Rim\ diameter}{2} + Tire\ wall \tag{4.44}$$

The rolling radius is slightly smaller than the nominal radius due to tire deflection under the action of a vertical load (as presented in Figure 4.9). This deflection as a function of the vertical load is presented in Figure 4.22. In a passenger vehicle, the vertical load varies between 2 kN and 5 kN.

4. The total transmission and differential ratio can be obtained directly through vehicle technical specifications or by comparing the engine speed and vehicle speed. The relationship between engine speed and vehicle speed is given by Eq. 4.45:

$$v = \frac{\omega_e \cdot r}{N_{tf}} \tag{4.45}$$

As the engine speed will be measured and the dynamic radius is also calculated, N_{tf} can be obtained. As each gear has a different ratio, N_{tf} will have a value for each gear. In Eq.4.45 it can be seen that, in conditions that the clutch is fully engaged, there is a linear relationship for each gear between vehicle speed and engine speed.

5. The total transmission and differential efficiency will be considered constant. Gillespie (1992) presents values from 0.966 to 0.973 for the transmission efficiency and 0.99 for the differential efficiency.

Figure 4.20 – Example of a vehicle tire nominal size specification (Tyre Town, 2016)

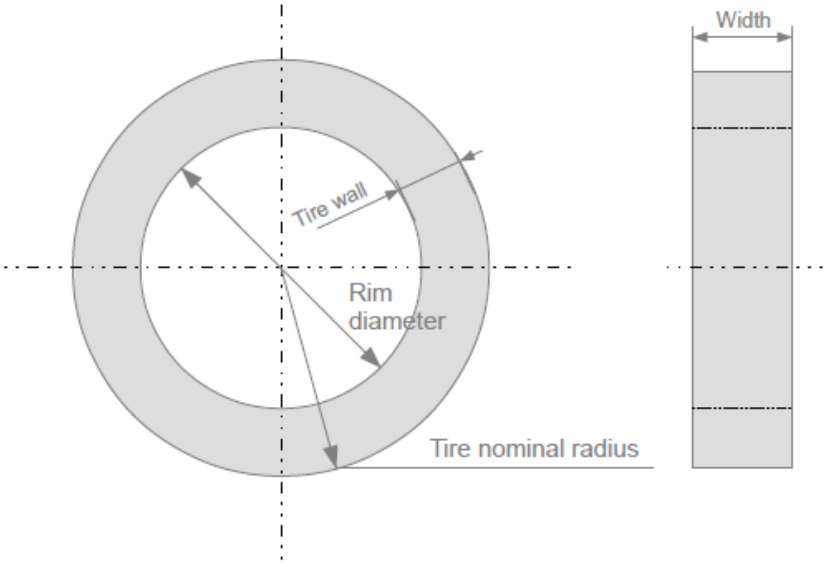

Figure 4.21 – Tire characteristic for nominal diameter calculation

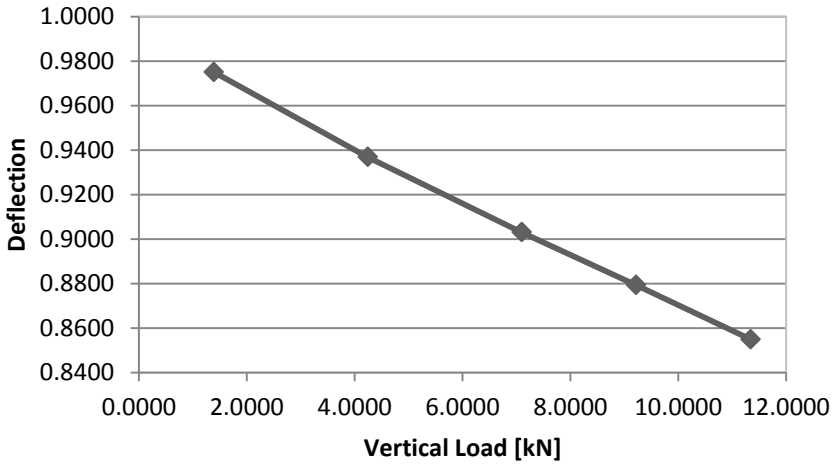

Figure 4.22 – Deflection as a function of vertical load (adapted from Lu et al, 2006)

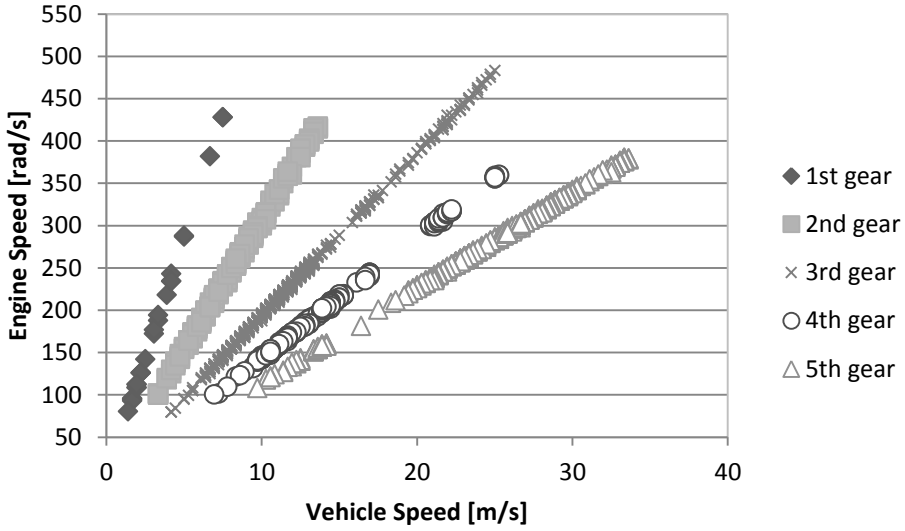

Figure 4.23 – Linear relationship between vehicle speed and engine speed for a 5 gear vehicle

The time-variant parameters directly required to measure the engine torque are vehicle speed, vehicle acceleration and road grade. However, additional parameters are also required for an accurate torque estimation. These parameters are: ambient temperature, ambient pressure and engine speed. Table 4.8 has to be updated in order to add these additional parameters, leading to Table 4.9:

Table 4.9 – Updated parameters for engine torque calculation

Constant parameters	Time-variant parameters

Vehicle mass	Vehicle speed
Constant coefficient of resistive force regression	Vehicle acceleration
Quadratic coefficient of resistive force regression	Road grade
Tire rolling radius	Engine Speed
Total transmission and differential ratio	Ambient Pressure
Total transmission and differential efficiency	Ambient Temperature

Another time-variant parameters that is required for the development of the methodology is the instantaneous fuel consumption in order to relate it to the engine operating conditions.

There are different sources for measuring the parameters presented in Table 4.9. The main sources taken in consideration for the development of the present study is given in Table 4.10:

Table 4.10 – Possible sources of measurement for time-variant parameters

	PEMS	OBD	GPS
Vehicle speed		x	x
Vehicle acceleration		x	x
Road grade			x
Engine Speed		x	
Ambient Pressure		x	
Ambient Temperature		x	
Fuel Consumption	x	x	

With the exception of road grade, all parameters presented in Table 4.10 can be obtained through OBD and therefore will be the basis of data acquisition. PEMS can accurate measure fuel consumption through the analysis of exhaust gases. However, it is an expensive equipment that requires technical knowledge for operation. DeFries, Sabisch and Kishan (2013) and Alessandrini, Filippi and Ortenzi (2012) developed studies based on OBD measurements to monitor fuel consumption. The first study compares the fuel consumption provided from OBD measurement, based on mass air flow (MAF) against the fuel consumption measured through injector fuel rate (which is more accurate, but not accessible through OBD). This comparison is presented in Figure 4.24 and Figure 4.25:

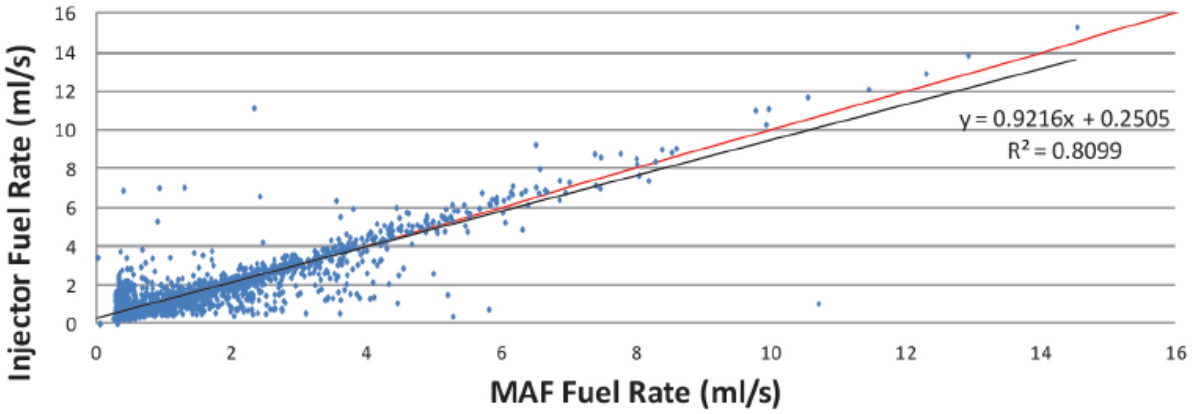

Figure 4.24 – MAF fuel consumption versus injector fuel rates for a 2012 Toyota Camry (DeFries, Sabisch and Kishan, 2013)

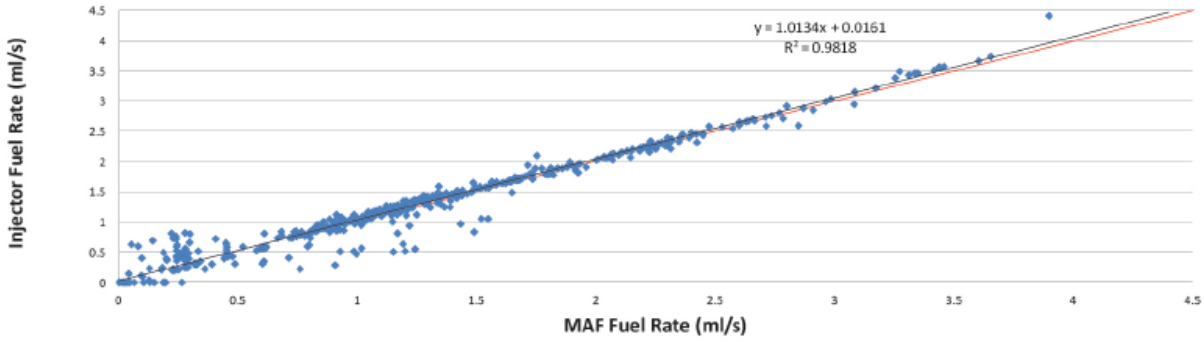

Figure 4.25 – MAF fuel consumption versus injector fuel rates for a 2012 Toyota Prius (DeFries, Sabisch and Kishan, 2013)

It can be seen that a high correlation coefficient is presented in both cases ($R^2 = 0.8099$ for Figure 4.24 and $R^2 = 0.9818$ for Figure 4.25) and therefore it can be considered a reliable source of measurement for fuel consumption.

The fuel consumption based on MAF considers that the engine works in stoichiometric condition (Guzzella and Onder, 2010). In this condition, the amount of oxygen is just enough for converting all the fuel into oxidized products (Heywood, 1988). In this case, the generic chemical reaction for a hydrocarbon is given by Eq. 4.46 (Heywood, 1988):

$$C_aH_b + \left(a + \frac{b}{4}\right)(O_2 + 3.773N_2) \rightarrow aCO_2 + \frac{b}{2}H_2O + 3.773\left(a + \frac{3}{4}\right)N_2 \qquad (4.46)$$

Assuming that regular gasoline is composed of octane, the Eq. 4.46 becomes Eq. 4.47:

$$C_8H_{18} + 12.5(O_2 + 3.773N_2) \rightarrow 8CO_2 + 9H_2O + 47.16N_2 \qquad (4.47)$$

From Eq. 4.47, one can see that each mole of fuel requires 12.5 moles of air. Considering that C_8H_{18} weighs 114.0g for each mole and that $(O_2 + 3.773N_2)$ weighs 137.6 g for each mole, each gram of fuel requires 15.1 grams of air for a complete combustion process. This ratio is known as the stoichiometric air-fuel ratio ($(A/F)_{stoich}$). In spark-ignition engines, the

calibration strategy is to maintain the air-fuel mixture as close as possible to stoichiometric, since in this condition the emission of pollutant gases is minimal and the catalytic efficiency (equipment installed in vehicle exhaust to convert pollutant gases in neutral gases) is the higher possible, as shown in Figure 4.26. It can be seen that the maximum efficiency for all gases is around 14.6. This value is a slightly different from 15.1 since real gasoline is actual a composition of hydrocarbons rather than pure octane.

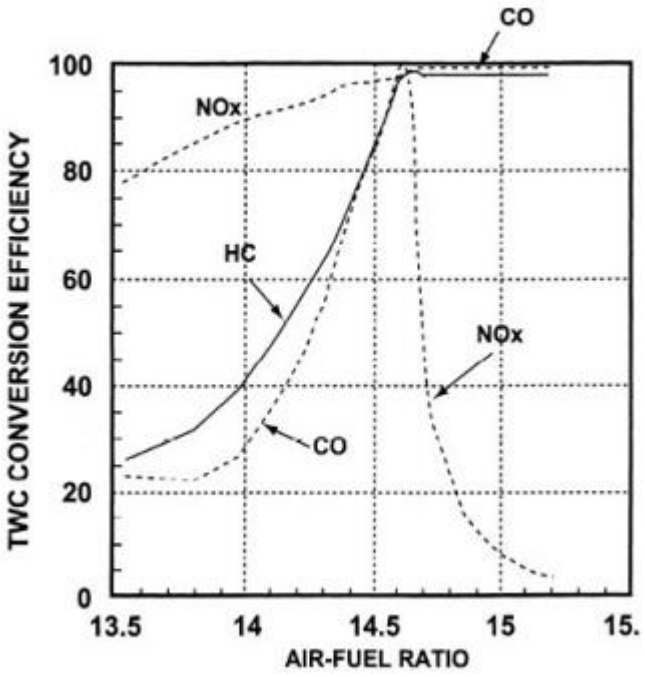

Figure 4.26 – Efficiency of a three-way catalyst (TWC) as function of air-fuel ratio (Yildiz et al, 2010)

In Brazil, according to Faggi (2012), regular gasoline has a composition of C_8H_{13} and an $(A/F)_{stoic}$ of 14.2. However, it is added a 22% of ethanol in volume basis to the gasoline. The reaction for this mixture is presented in Eq. 4.48:

$$0.78C_8H_{13} + 0.22C_2H_5OH + 9.4(O_2 + 3.773N_2) \rightarrow 6.7CO_2 + 5.7H_2O + 35.6N_2 \quad (4.48)$$

The $(A/F)_{stoic}$ in this case will be 13.7. The reaction for ethanol is given by Eq. 4.49:

$$C_2H_5OH + 3(O_2 + 3.773N_2) \rightarrow 2CO_2 + 3H_2O + 11.3N_2 \quad (4.49)$$

The $(A/F)_{stoic}$ for ethanol will be 9.0.

Since there is significant difference in air-fuel ratio for different fuels, it is important to define an air-fuel equivalence ratio (λ), presented in Eq. 4.50:

$$\lambda = \frac{(A/F)_{stoic}}{(A/F)_{actual}} \quad (4.50)$$

For $\lambda < 1$, the mixture is called fuel-rich mixture, which means that there is more fuel per unit of mass of air than stoichiometric condition. Analogously, for $\lambda > 1$ the mixture is called fuel-lean, and for $\lambda = 1$ the mixture is stoichiometric. As spark-ignition engines are calibrated to work as close as possible to stoichiometric conditions, it is a reasonable assumption that $\lambda = 1$ and fuel consumption estimation through MAF is acceptable.

Another comparison between a reliable reference for fuel consumption measurement (an on-board system – OBS – equivalent to PEMS) and OBD-based fuel consumption measured, from Alessandrini, Filippi and Ortenzi (2012) work, is presented in Figure 4.27:

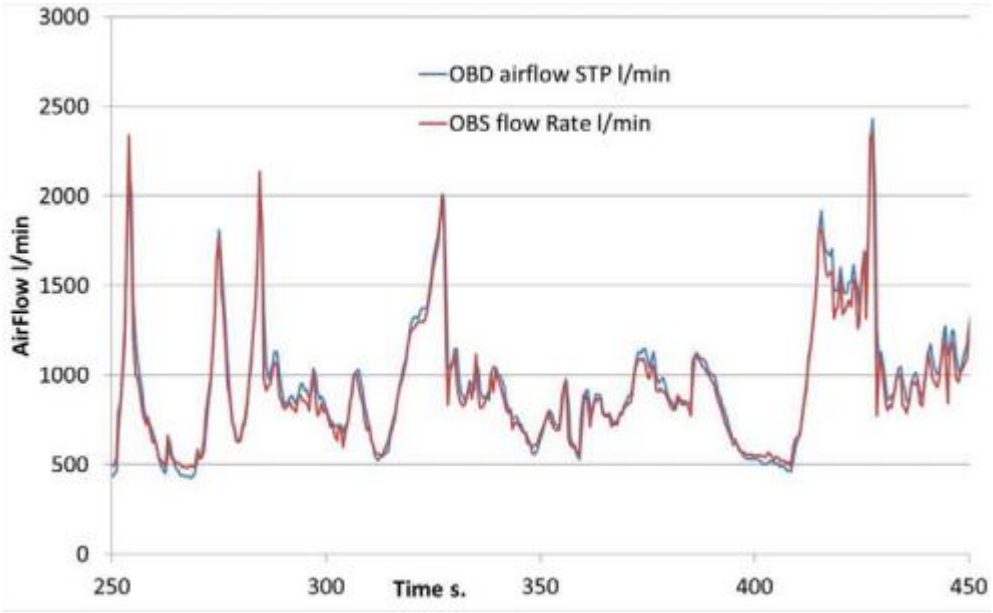

Figure 4.27 – OBD MAF versus OBS MAF for a Citroen C3 1.4L (Alessandrini, Filippi and Ortenzi, 2012)

As OBD data acquiring systems are less expensive and more accessible than PEMS and, as seen in Figure 4.24 to Figure 4.27, they provide good correlation with other measurement techniques, they will be the basis for this study.

The equipment used for the measurements is Racelogic's VBOX 3i, which can be used for OBD parameter acquisition and logging, and also for high accuracy GPS measurement. This equipment is presented in Figure 4.28:

Figure 4.28 – Racelogic VBOX 3i (Racelogic, 2016)

VBOX is capable of acquiring and logging parameter at a rate of 100Hz, which is a good resolution for speed and acceleration measurements. The accuracy for speed measurement is 0.1 km/h, 6m for height measurement and 0.2 km/h for vertical velocity. It will be presented further in this study if the accuracy levels for speed and height are acceptable. A diagram presenting the inputs and outputs for the equipment is presented in Figure 4.29:

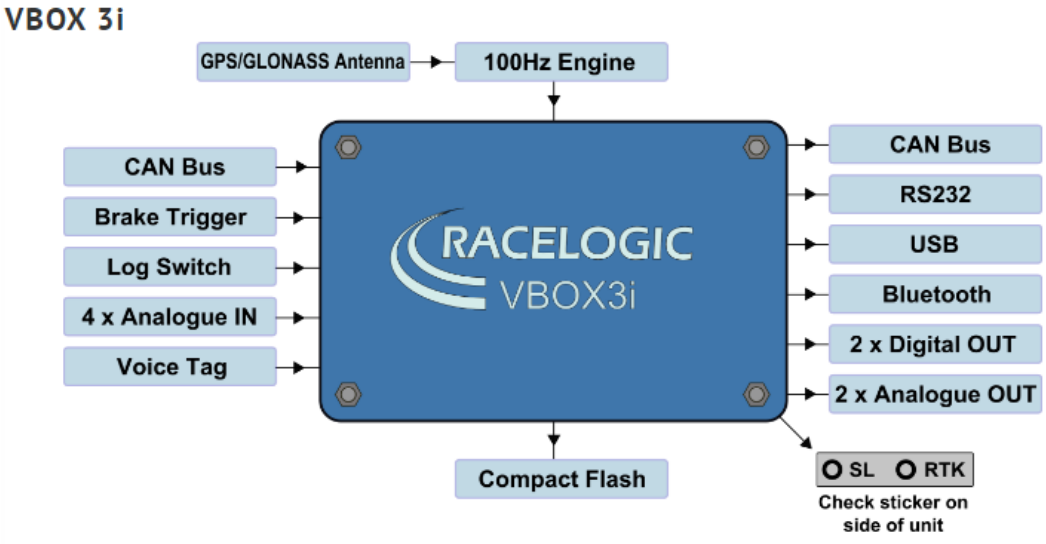

Figure 4.29 – Inputs and Outputs for Racelogic VBOX equipment (Racelogic, 2016)

The ports used for the measurements are:

- GPS Antenna (in order to log GPS data);
- Log Switch (to toggle log on/off);

- CAN Bus (to connect with vehicle OBD port);
- Compact flash (memory card to store acquired data).

The file output format is *.VBO, which is a space delimited text format. An excerpt of this format is presented in Figure 4.30. Files with this extension can be easily processed in Excel or Matlab. The codes generated for post processing and mathematical development of the engine model are Matlab based.

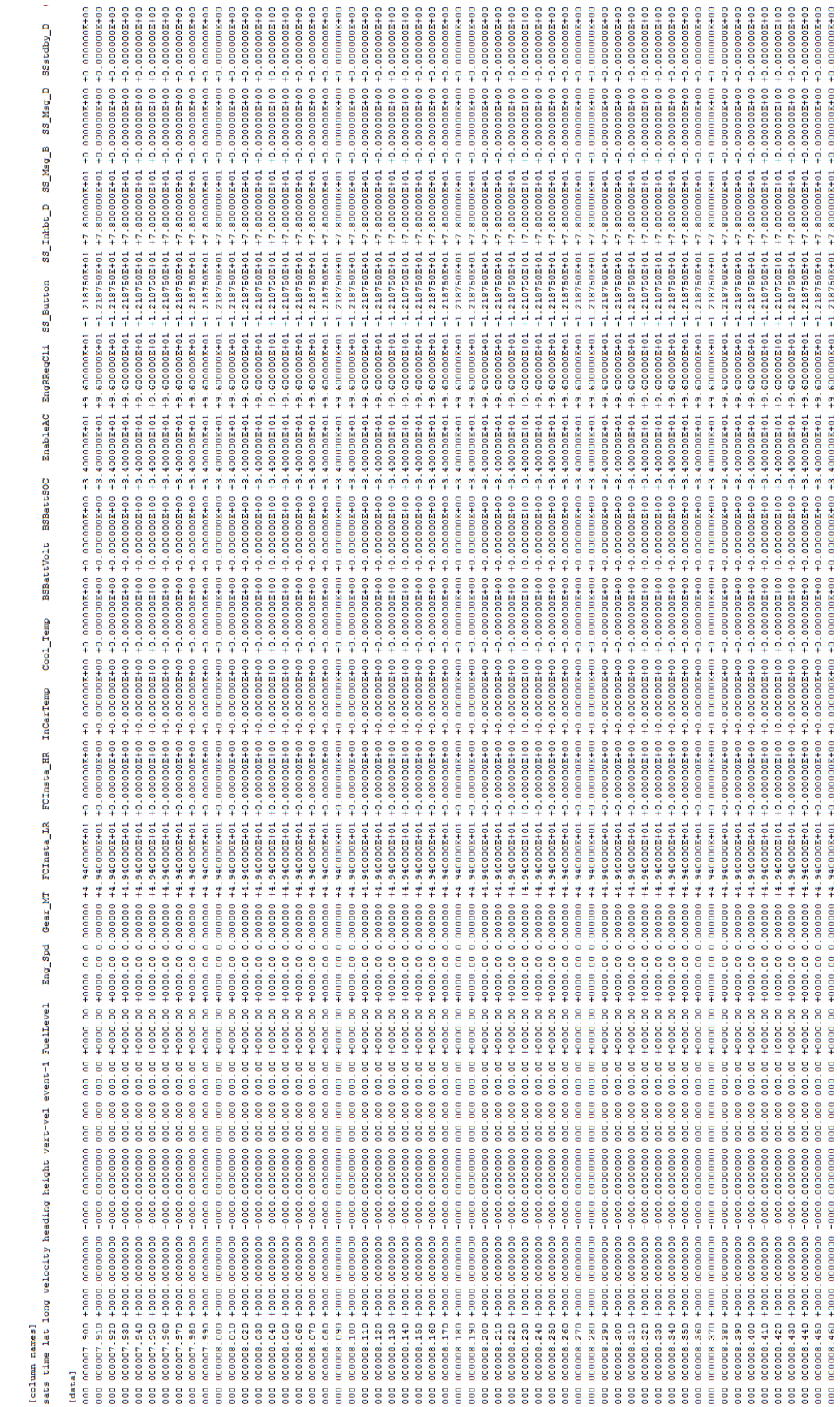

```
[column names]
sats time lat long velocity heading height vert-vel event-1 FuelLevel  Eng_Spd  Gear_MT  FCInsta_LR  FCInsta_HR  InCarTemp  Cool_Temp  BSBattVolt  BSBattSOC  EnableAC  EngReqCli  SS_Button  SS_Inhbt_D  SS_Msg_B  SS_Msg_D  SStndby_D
[data]
000 000007.900 +0000.00000000 -0000.00000000 000.000 000.00 +0000.00 +0.000000 +4.940000E+01 +0.000000E+00 +0.000000E+00 +0.000000E+00 +0.000000E+00 +3.400000E+01 +9.600000E+01 +1.218750E+01 +7.800000E+01 +0.000000E+00
000 000007.910 +0000.00000000 -0000.00000000 000.000 000.00 +0000.00 +0.000000 +4.940000E+01 +0.000000E+00 +0.000000E+00 +0.000000E+00 +0.000000E+00 +3.400000E+01 +9.600000E+01 +1.218750E+01 +7.800000E+01 +0.000000E+00
000 000007.920 +0000.00000000 -0000.00000000 000.000 000.00 +0000.00 +0.000000 +4.940000E+01 +0.000000E+00 +0.000000E+00 +0.000000E+00 +0.000000E+00 +3.400000E+01 +9.600000E+01 +1.218750E+01 +7.800000E+01 +0.000000E+00
000 000007.930 +0000.00000000 -0000.00000000 000.000 000.00 +0000.00 +0.000000 +4.940000E+01 +0.000000E+00 +0.000000E+00 +0.000000E+00 +0.000000E+00 +3.400000E+01 +9.600000E+01 +1.218750E+01 +7.800000E+01 +0.000000E+00
000 000007.940 +0000.00000000 -0000.00000000 000.000 000.00 +0000.00 +0.000000 +4.940000E+01 +0.000000E+00 +0.000000E+00 +0.000000E+00 +0.000000E+00 +3.400000E+01 +9.600000E+01 +1.218750E+01 +7.800000E+01 +0.000000E+00
000 000007.950 +0000.00000000 -0000.00000000 000.000 000.00 +0000.00 +0.000000 +4.940000E+01 +0.000000E+00 +0.000000E+00 +0.000000E+00 +0.000000E+00 +3.400000E+01 +9.600000E+01 +1.218750E+01 +7.800000E+01 +0.000000E+00
000 000007.960 +0000.00000000 -0000.00000000 000.000 000.00 +0000.00 +0.000000 +4.940000E+01 +0.000000E+00 +0.000000E+00 +0.000000E+00 +0.000000E+00 +3.400000E+01 +9.600000E+01 +1.218750E+01 +7.800000E+01 +0.000000E+00
000 000007.970 +0000.00000000 -0000.00000000 000.000 000.00 +0000.00 +0.000000 +4.940000E+01 +0.000000E+00 +0.000000E+00 +0.000000E+00 +0.000000E+00 +3.400000E+01 +9.600000E+01 +1.218750E+01 +7.800000E+01 +0.000000E+00
000 000007.980 +0000.00000000 -0000.00000000 000.000 000.00 +0000.00 +0.000000 +4.940000E+01 +0.000000E+00 +0.000000E+00 +0.000000E+00 +0.000000E+00 +3.400000E+01 +9.600000E+01 +1.218750E+01 +7.800000E+01 +0.000000E+00
000 000007.990 +0000.00000000 -0000.00000000 000.000 000.00 +0000.00 +0.000000 +4.940000E+01 +0.000000E+00 +0.000000E+00 +0.000000E+00 +0.000000E+00 +3.400000E+01 +9.600000E+01 +1.218750E+01 +7.800000E+01 +0.000000E+00
000 000008.000 +0000.00000000 -0000.00000000 000.000 000.00 +0000.00 +0.000000 +4.940000E+01 +0.000000E+00 +0.000000E+00 +0.000000E+00 +0.000000E+00 +3.400000E+01 +9.600000E+01 +1.218750E+01 +7.800000E+01 +0.000000E+00
000 000008.010 +0000.00000000 -0000.00000000 000.000 000.00 +0000.00 +0.000000 +4.940000E+01 +0.000000E+00 +0.000000E+00 +0.000000E+00 +0.000000E+00 +3.400000E+01 +9.600000E+01 +1.218750E+01 +7.800000E+01 +0.000000E+00
000 000008.020 +0000.00000000 -0000.00000000 000.000 000.00 +0000.00 +0.000000 +4.940000E+01 +0.000000E+00 +0.000000E+00 +0.000000E+00 +0.000000E+00 +3.400000E+01 +9.600000E+01 +1.218750E+01 +7.800000E+01 +0.000000E+00
000 000008.030 +0000.00000000 -0000.00000000 000.000 000.00 +0000.00 +0.000000 +4.940000E+01 +0.000000E+00 +0.000000E+00 +0.000000E+00 +0.000000E+00 +3.400000E+01 +9.600000E+01 +1.218750E+01 +7.800000E+01 +0.000000E+00
000 000008.040 +0000.00000000 -0000.00000000 000.000 000.00 +0000.00 +0.000000 +4.940000E+01 +0.000000E+00 +0.000000E+00 +0.000000E+00 +0.000000E+00 +3.400000E+01 +9.600000E+01 +1.218750E+01 +7.800000E+01 +0.000000E+00
000 000008.050 +0000.00000000 -0000.00000000 000.000 000.00 +0000.00 +0.000000 +4.940000E+01 +0.000000E+00 +0.000000E+00 +0.000000E+00 +0.000000E+00 +3.400000E+01 +9.600000E+01 +1.218750E+01 +7.800000E+01 +0.000000E+00
000 000008.060 +0000.00000000 -0000.00000000 000.000 000.00 +0000.00 +0.000000 +4.940000E+01 +0.000000E+00 +0.000000E+00 +0.000000E+00 +0.000000E+00 +3.400000E+01 +9.600000E+01 +1.218750E+01 +7.800000E+01 +0.000000E+00
000 000008.070 +0000.00000000 -0000.00000000 000.000 000.00 +0000.00 +0.000000 +4.940000E+01 +0.000000E+00 +0.000000E+00 +0.000000E+00 +0.000000E+00 +3.400000E+01 +9.600000E+01 +1.218750E+01 +7.800000E+01 +0.000000E+00
000 000008.080 +0000.00000000 -0000.00000000 000.000 000.00 +0000.00 +0.000000 +4.940000E+01 +0.000000E+00 +0.000000E+00 +0.000000E+00 +0.000000E+00 +3.400000E+01 +9.600000E+01 +1.218750E+01 +7.800000E+01 +0.000000E+00
000 000008.090 +0000.00000000 -0000.00000000 000.000 000.00 +0000.00 +0.000000 +4.940000E+01 +0.000000E+00 +0.000000E+00 +0.000000E+00 +0.000000E+00 +3.400000E+01 +9.600000E+01 +1.218750E+01 +7.800000E+01 +0.000000E+00
000 000008.100 +0000.00000000 -0000.00000000 000.000 000.00 +0000.00 +0.000000 +4.940000E+01 +0.000000E+00 +0.000000E+00 +0.000000E+00 +0.000000E+00 +3.400000E+01 +9.600000E+01 +1.218750E+01 +7.800000E+01 +0.000000E+00
000 000008.110 +0000.00000000 -0000.00000000 000.000 000.00 +0000.00 +0.000000 +4.940000E+01 +0.000000E+00 +0.000000E+00 +0.000000E+00 +0.000000E+00 +3.400000E+01 +9.600000E+01 +1.218750E+01 +7.800000E+01 +0.000000E+00
000 000008.120 +0000.00000000 -0000.00000000 000.000 000.00 +0000.00 +0.000000 +4.940000E+01 +0.000000E+00 +0.000000E+00 +0.000000E+00 +0.000000E+00 +3.400000E+01 +9.600000E+01 +1.218750E+01 +7.800000E+01 +0.000000E+00
000 000008.130 +0000.00000000 -0000.00000000 000.000 000.00 +0000.00 +0.000000 +4.940000E+01 +0.000000E+00 +0.000000E+00 +0.000000E+00 +0.000000E+00 +3.400000E+01 +9.600000E+01 +1.218750E+01 +7.800000E+01 +0.000000E+00
000 000008.140 +0000.00000000 -0000.00000000 000.000 000.00 +0000.00 +0.000000 +4.940000E+01 +0.000000E+00 +0.000000E+00 +0.000000E+00 +0.000000E+00 +3.400000E+01 +9.600000E+01 +1.218750E+01 +7.800000E+01 +0.000000E+00
000 000008.150 +0000.00000000 -0000.00000000 000.000 000.00 +0000.00 +0.000000 +4.940000E+01 +0.000000E+00 +0.000000E+00 +0.000000E+00 +0.000000E+00 +3.400000E+01 +9.600000E+01 +1.218750E+01 +7.800000E+01 +0.000000E+00
000 000008.160 +0000.00000000 -0000.00000000 000.000 000.00 +0000.00 +0.000000 +4.940000E+01 +0.000000E+00 +0.000000E+00 +0.000000E+00 +0.000000E+00 +3.400000E+01 +9.600000E+01 +1.218750E+01 +7.800000E+01 +0.000000E+00
000 000008.170 +0000.00000000 -0000.00000000 000.000 000.00 +0000.00 +0.000000 +4.940000E+01 +0.000000E+00 +0.000000E+00 +0.000000E+00 +0.000000E+00 +3.400000E+01 +9.600000E+01 +1.218750E+01 +7.800000E+01 +0.000000E+00
000 000008.180 +0000.00000000 -0000.00000000 000.000 000.00 +0000.00 +0.000000 +4.940000E+01 +0.000000E+00 +0.000000E+00 +0.000000E+00 +0.000000E+00 +3.400000E+01 +9.600000E+01 +1.218750E+01 +7.800000E+01 +0.000000E+00
000 000008.190 +0000.00000000 -0000.00000000 000.000 000.00 +0000.00 +0.000000 +4.940000E+01 +0.000000E+00 +0.000000E+00 +0.000000E+00 +0.000000E+00 +3.400000E+01 +9.600000E+01 +1.218750E+01 +7.800000E+01 +0.000000E+00
000 000008.200 +0000.00000000 -0000.00000000 000.000 000.00 +0000.00 +0.000000 +4.940000E+01 +0.000000E+00 +0.000000E+00 +0.000000E+00 +0.000000E+00 +3.400000E+01 +9.600000E+01 +1.218750E+01 +7.800000E+01 +0.000000E+00
000 000008.210 +0000.00000000 -0000.00000000 000.000 000.00 +0000.00 +0.000000 +4.940000E+01 +0.000000E+00 +0.000000E+00 +0.000000E+00 +0.000000E+00 +3.400000E+01 +9.600000E+01 +1.218750E+01 +7.800000E+01 +0.000000E+00
000 000008.220 +0000.00000000 -0000.00000000 000.000 000.00 +0000.00 +0.000000 +4.940000E+01 +0.000000E+00 +0.000000E+00 +0.000000E+00 +0.000000E+00 +3.400000E+01 +9.600000E+01 +1.218750E+01 +7.800000E+01 +0.000000E+00
000 000008.230 +0000.00000000 -0000.00000000 000.000 000.00 +0000.00 +0.000000 +4.940000E+01 +0.000000E+00 +0.000000E+00 +0.000000E+00 +0.000000E+00 +3.400000E+01 +9.600000E+01 +1.218750E+01 +7.800000E+01 +0.000000E+00
000 000008.240 +0000.00000000 -0000.00000000 000.000 000.00 +0000.00 +0.000000 +4.940000E+01 +0.000000E+00 +0.000000E+00 +0.000000E+00 +0.000000E+00 +3.400000E+01 +9.600000E+01 +1.218750E+01 +7.800000E+01 +0.000000E+00
000 000008.250 +0000.00000000 -0000.00000000 000.000 000.00 +0000.00 +0.000000 +4.940000E+01 +0.000000E+00 +0.000000E+00 +0.000000E+00 +0.000000E+00 +3.400000E+01 +9.600000E+01 +1.218750E+01 +7.800000E+01 +0.000000E+00
000 000008.260 +0000.00000000 -0000.00000000 000.000 000.00 +0000.00 +0.000000 +4.940000E+01 +0.000000E+00 +0.000000E+00 +0.000000E+00 +0.000000E+00 +3.400000E+01 +9.600000E+01 +1.218750E+01 +7.800000E+01 +0.000000E+00
000 000008.270 +0000.00000000 -0000.00000000 000.000 000.00 +0000.00 +0.000000 +4.940000E+01 +0.000000E+00 +0.000000E+00 +0.000000E+00 +0.000000E+00 +3.400000E+01 +9.600000E+01 +1.218750E+01 +7.800000E+01 +0.000000E+00
000 000008.280 +0000.00000000 -0000.00000000 000.000 000.00 +0000.00 +0.000000 +4.940000E+01 +0.000000E+00 +0.000000E+00 +0.000000E+00 +0.000000E+00 +3.400000E+01 +9.600000E+01 +1.218750E+01 +7.800000E+01 +0.000000E+00
000 000008.290 +0000.00000000 -0000.00000000 000.000 000.00 +0000.00 +0.000000 +4.940000E+01 +0.000000E+00 +0.000000E+00 +0.000000E+00 +0.000000E+00 +3.400000E+01 +9.600000E+01 +1.218750E+01 +7.800000E+01 +0.000000E+00
000 000008.300 +0000.00000000 -0000.00000000 000.000 000.00 +0000.00 +0.000000 +4.940000E+01 +0.000000E+00 +0.000000E+00 +0.000000E+00 +0.000000E+00 +3.400000E+01 +9.600000E+01 +1.218750E+01 +7.800000E+01 +0.000000E+00
000 000008.310 +0000.00000000 -0000.00000000 000.000 000.00 +0000.00 +0.000000 +4.940000E+01 +0.000000E+00 +0.000000E+00 +0.000000E+00 +0.000000E+00 +3.400000E+01 +9.600000E+01 +1.218750E+01 +7.800000E+01 +0.000000E+00
000 000008.320 +0000.00000000 -0000.00000000 000.000 000.00 +0000.00 +0.000000 +4.940000E+01 +0.000000E+00 +0.000000E+00 +0.000000E+00 +0.000000E+00 +3.400000E+01 +9.600000E+01 +1.218750E+01 +7.800000E+01 +0.000000E+00
000 000008.330 +0000.00000000 -0000.00000000 000.000 000.00 +0000.00 +0.000000 +4.940000E+01 +0.000000E+00 +0.000000E+00 +0.000000E+00 +0.000000E+00 +3.400000E+01 +9.600000E+01 +1.218750E+01 +7.800000E+01 +0.000000E+00
000 000008.340 +0000.00000000 -0000.00000000 000.000 000.00 +0000.00 +0.000000 +4.940000E+01 +0.000000E+00 +0.000000E+00 +0.000000E+00 +0.000000E+00 +3.400000E+01 +9.600000E+01 +1.218750E+01 +7.800000E+01 +0.000000E+00
000 000008.350 +0000.00000000 -0000.00000000 000.000 000.00 +0000.00 +0.000000 +4.940000E+01 +0.000000E+00 +0.000000E+00 +0.000000E+00 +0.000000E+00 +3.400000E+01 +9.600000E+01 +1.218750E+01 +7.800000E+01 +0.000000E+00
000 000008.360 +0000.00000000 -0000.00000000 000.000 000.00 +0000.00 +0.000000 +4.940000E+01 +0.000000E+00 +0.000000E+00 +0.000000E+00 +0.000000E+00 +3.400000E+01 +9.600000E+01 +1.218750E+01 +7.800000E+01 +0.000000E+00
000 000008.370 +0000.00000000 -0000.00000000 000.000 000.00 +0000.00 +0.000000 +4.940000E+01 +0.000000E+00 +0.000000E+00 +0.000000E+00 +0.000000E+00 +3.400000E+01 +9.600000E+01 +1.218750E+01 +7.800000E+01 +0.000000E+00
000 000008.380 +0000.00000000 -0000.00000000 000.000 000.00 +0000.00 +0.000000 +4.940000E+01 +0.000000E+00 +0.000000E+00 +0.000000E+00 +0.000000E+00 +3.400000E+01 +9.600000E+01 +1.218750E+01 +7.800000E+01 +0.000000E+00
000 000008.390 +0000.00000000 -0000.00000000 000.000 000.00 +0000.00 +0.000000 +4.940000E+01 +0.000000E+00 +0.000000E+00 +0.000000E+00 +0.000000E+00 +3.400000E+01 +9.600000E+01 +1.218750E+01 +7.800000E+01 +0.000000E+00
000 000008.400 +0000.00000000 -0000.00000000 000.000 000.00 +0000.00 +0.000000 +4.940000E+01 +0.000000E+00 +0.000000E+00 +0.000000E+00 +0.000000E+00 +3.400000E+01 +9.600000E+01 +1.218750E+01 +7.800000E+01 +0.000000E+00
000 000008.410 +0000.00000000 -0000.00000000 000.000 000.00 +0000.00 +0.000000 +4.940000E+01 +0.000000E+00 +0.000000E+00 +0.000000E+00 +0.000000E+00 +3.400000E+01 +9.600000E+01 +1.218750E+01 +7.800000E+01 +0.000000E+00
000 000008.420 +0000.00000000 -0000.00000000 000.000 000.00 +0000.00 +0.000000 +4.940000E+01 +0.000000E+00 +0.000000E+00 +0.000000E+00 +0.000000E+00 +3.400000E+01 +9.600000E+01 +1.218750E+01 +7.800000E+01 +0.000000E+00
000 000008.430 +0000.00000000 -0000.00000000 000.000 000.00 +0000.00 +0.000000 +4.940000E+01 +0.000000E+00 +0.000000E+00 +0.000000E+00 +0.000000E+00 +3.400000E+01 +9.600000E+01 +1.218750E+01 +7.800000E+01 +0.000000E+00
000 000008.440 +0000.00000000 -0000.00000000 000.000 000.00 +0000.00 +0.000000 +4.940000E+01 +0.000000E+00 +0.000000E+00 +0.000000E+00 +0.000000E+00 +3.400000E+01 +9.600000E+01 +1.218750E+01 +7.800000E+01 +0.000000E+00
000 000008.450 +0000.00000000 -0000.00000000 000.000 000.00 +0000.00 +0.000000 +4.940000E+01 +0.000000E+00 +0.000000E+00 +0.000000E+00 +0.000000E+00 +3.400000E+01 +9.600000E+01 +1.218750E+01 +7.800000E+01 +0.000000E+00
000 000008.460 +0000.00000000 -0000.00000000 000.000 000.00 +0000.00 +0.000000 +4.940000E+01 +0.000000E+00 +0.000000E+00 +0.000000E+00 +0.000000E+00 +3.400000E+01 +9.600000E+01 +1.218750E+01 +7.800000E+01 +0.000000E+00
```

Figure 4.30 – Excerpt of *.VBO output file

4.1.6 Test Procedure

The measurements will be done in-vehicle and in on-road conditions and, thus, they are subject to diverse sources of variation. A robust procedure is required in order to avoid some of these sources. The main sources the procedure aims to avoid are:

- Ambient related:
  - Rain;
  - Ground surface (roughness and adherence);
- Vehicle operating conditions:
  - Cover only a limited range of engine speed and engine torque;
  - Test under high speeds;
  - Measurement distance;
  - Cold tires;
  - Air conditioning;
  - Opened windows;
- Non-stoichiometric conditions:
  - Accelerator pedal transient;
  - Wide-open-throttle (WOT) enrichment;
  - Engine warm-up.

The ambient can be the source of many variations, including presence of wind, ambient temperature variation, asphalt temperature, presence of rain, humidity, ground and asphalt conditions, amongst others. Most of these sources can be avoided by simply not testing the vehicle in such conditions. However, some of them are inevitable, such as wind, ambient and asphalt temperature variation. In order to mitigate their effect, the vehicle should only be tested within conditions recommended by ABNT standard NBR 10312:2012, the same used for obtaining the resistive force coefficients. These conditions are presented in Table 4.11:

Table 4.11 – Acceptable range for wind speed and ambient temperature according to NBR 10312:2012 (ABNT, 2012)

Parameter	Minimum accepted range	Maximum accepted range
Wind speed	0 m/s	5 m/s
Ambient temperature	5℃	35℃

The vehicle operating conditions may also be source of variation. It is important to observe during the tests that the widest possible range of engine speed and engine torque must be measured, avoiding extrapolation of the mathematical model and, consequently, errors.

The vehicle speed also requires attention in order to avoid speeds greater than 100 km/h, since the vehicle resistive force is not measured above this speed and tire rolling resistance coefficient does not present a constant value above this speed (see Figure 4.11). Tires also do not present a constant rolling resistance coefficient in cold operation (see Figure 4.12), and, thus, it requires a warm-up before the measurement starts. The use of air conditioning affects the engine load, and therefore, the torque estimated Eq. 4.42 will be underestimated if the air conditioning is in use. Opened windows, especially in speeds where the aerodynamic effects are important – above 60 km/h, increases the force needed to overcome aerodynamic resistance and, therefore, also underestimate the engine torque. The distance traveled during the measurements also affects the quality of the results. Post et al (1984) show that the correlation coefficient for power estimative grows rapidly up to 6 km and remain almost steady above this length, as shown in Figure 4.31:

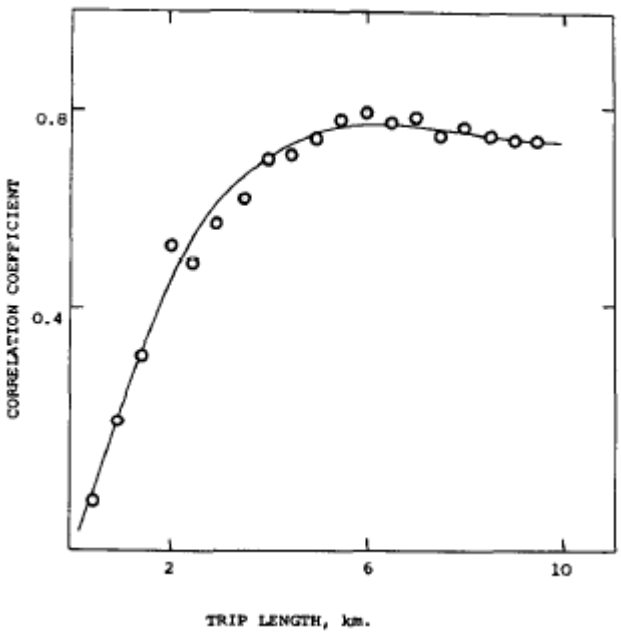

Figure 4.31 – Correlation coefficient for power estimative as a function of drive length (Post et al, 1984)

The trip length effect on fuel consumption is presented by U.S. EPA (1974). It can be observed in Figure 4.32 that fuel economy is highly influenced by trip length for lengths smaller than 5 miles (8.05 km), and is almost stable for greater lengths.

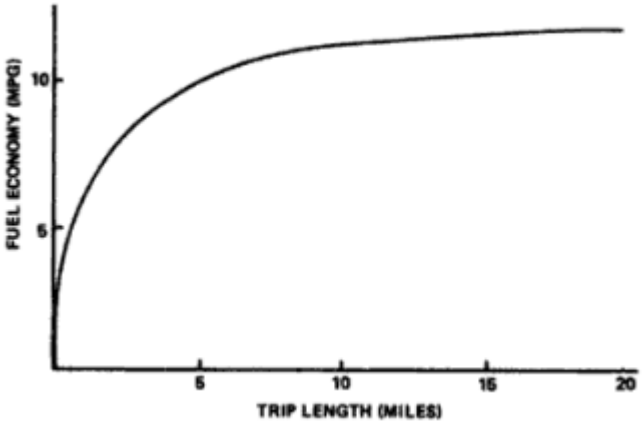

Figure 4.32 – Influence of trip length on fuel economy (U.S. EPA, 1974)

Other important sources of variation are the ones caused by non-stoichiometric operation. Under certain operating conditions, the engine works with rich mixture, affecting the fuel measurement. It is important that the measurements are made with smooth accelerator pedal movements and avoiding WOT condition. The engine operating with coolant temperatures below the normal operating temperature also works with enrichment and, therefore, the warm-up period has a double function of warming up the tires and the engine. DeFries, Sabisch and Kishan (2013) presented the following conditions that forces the engine to work in non-stoichiometric condition:

- Cold start: in this condition, the engine works in open-loop control, which means that the engine receives no feedback from oxygen sensor to indicate if the mixture is lean or rich. Furthermore, in this condition, the engine is programmed to work with richer mixture than stoichiometric to improve cold drivability. As the vehicle does not operate in stoichiometric condition, it will cause an error on fuel consumption calculation based on MAF sensor.
- Wide-open-throttle condition: in this condition, fuel enrichment is used to increase full-load power and cool the engine at high speeds (Guzzella and Onder, 2010).
- Fuel shut-off: during decelerations in closed throttle conditions the engine is providing negative net torque and is helping on vehicle deceleration, which means that no fuel is required. Therefore, the control unit works in shut-off condition and no fuel is injected.

Nose et al (2013) presented a schematic diagram that shows generically the fuel-enrichment zones, presented in Figure 4.33:

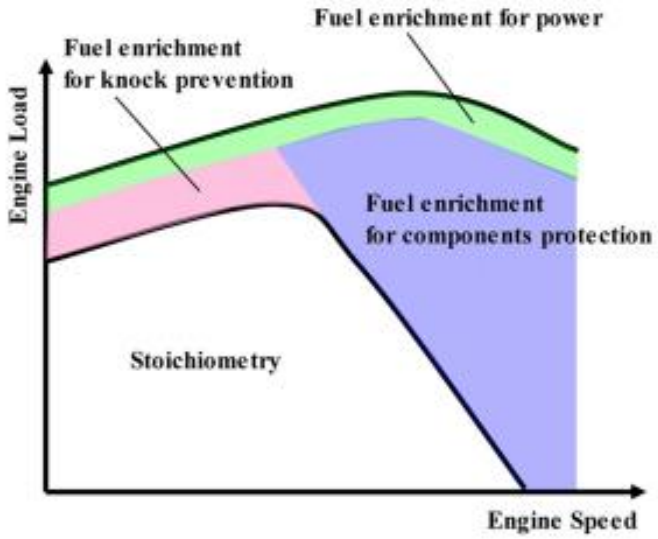

Figure 4.33 – Fuel enrichment zones (Nose et al, 2013)

The aspects that need to be covered by the test procedure are presented in Table 4.12:

Table 4.12 – Aspects covered by present procedure

Sources of variation		**Containment action**
Ambient related	Rain	Do not test in rainy condition or adverse ambient condition (wet asphalt, snow, with alternation of cloudy and sunny conditions, etc.)
	Wind speed	Wind speed $\leq 5 \mathrm{m/s}$
	Ambient temperature	$5℃ \leq$ ambient temperature $\leq 35℃$
	Ground surface	Test vehicle on smooth asphalt surface
Vehicle operating conditions	Engine operating conditions	$1000\ \mathrm{min^{-1}} \leq$ engine speed $\leq 4000\ \mathrm{min^{-1}}$
		$10\% <$ engine load $< 80\%$
	Vehicle speed	Vehicle Speed $\leq 100\ \mathrm{km/h}$
	Trip length	Trip length ≥ 8 km
	Air conditioning	Off
	Windows	Closed
Non-stoichiometric condition	Accelerator pedal transient	Accelerate in smooth pedal movements
	Wide-open-throttle (WOT)	Avoid WOT condition
	Deceleration	Create a post-processing flag to identify this condition

	shutoff	
	Engine warm-up	Trip length ≥ 8 km and engine coolant temperature ≥ 80°C

The measurement procedure proposed is presented in Figure 4.34:

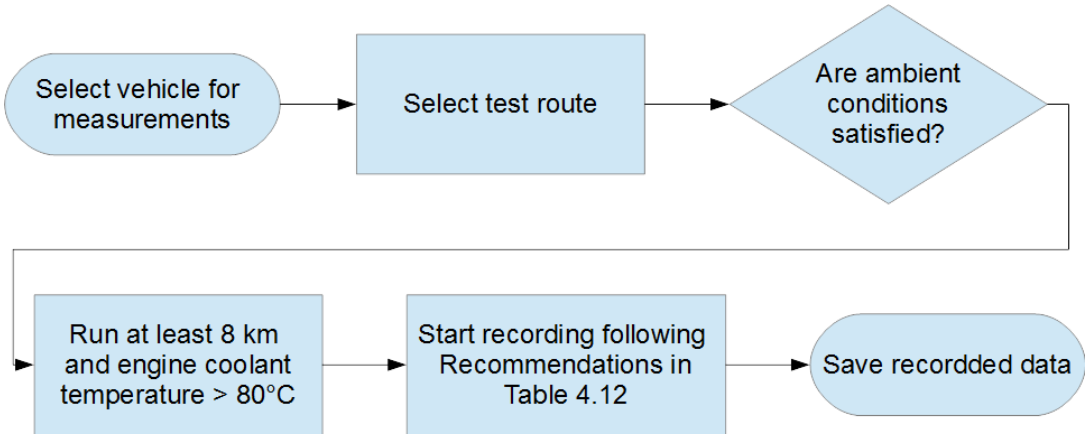

Figure 4.34 – Proposed measurement procedure flowchart

5 EXPERIMENTAL RESULTS

In this section it will be presented the experimental results for five different vehicles. In order to obtain the engine operating conditions for each of these vehicles it is required to obtain the constant- time parameters presented in Table 4.9. In this section it will be presented how the empirical coefficients are measured (constant-time parameters), the post-processing techniques used, and error analysis for the measured parameters.

5.1 MEASUREMENT OF EMPIRICAL COEFFICIENTS

The empirical coefficients that need to be measured are presented in Table 5.1:

Table 5.1 – Empirical coefficients that need to be measured for post-processing

Constant parameters
Vehicle mass
Constant coefficient of resistive force regression
Quadratic coefficient of resistive force regression
Tire rolling radius
Total transmission and differential ratio
Total transmission and differential efficiency

5.1.1 Vehicle Mass

The results for the vehicle mass are measured directly through the weighing machine (see Figure 4.19). The results are presented in Table 5.2:

Table 5.2 – Measured test mass for vehicles 1 to 5

Vehicle 1	Vehicle 2	Vehicle 3	Vehicle 4	Vehicle 5
1085 ± 2.5 kg	1410 ± 2.5 kg	1375 ± 2.5 kg	1525 ± 2.5 kg	1710 ± 2.5 kg

5.1.2 Vehicle Resistive force coefficients

The measurement of the resistive force regression coefficients is done following procedure normatized by ABNT Standard NBR 10312:2012. The speed versus time coastdown measurement was done in a flat track of 2.4 km length near the city of Ibiaí in

Brazilian state of Minas Gerais. A total of 10 coastdown runs (5 in each way) were done, generating a table similar to Table 4.5, but with 10 lines of data instead of only one line, and each data line generating a similar table to Table 4.7, and, consequently, a value for f_0 and a value for f_2 for each line. The speed versus time measurements are presented in Figure 5.1:

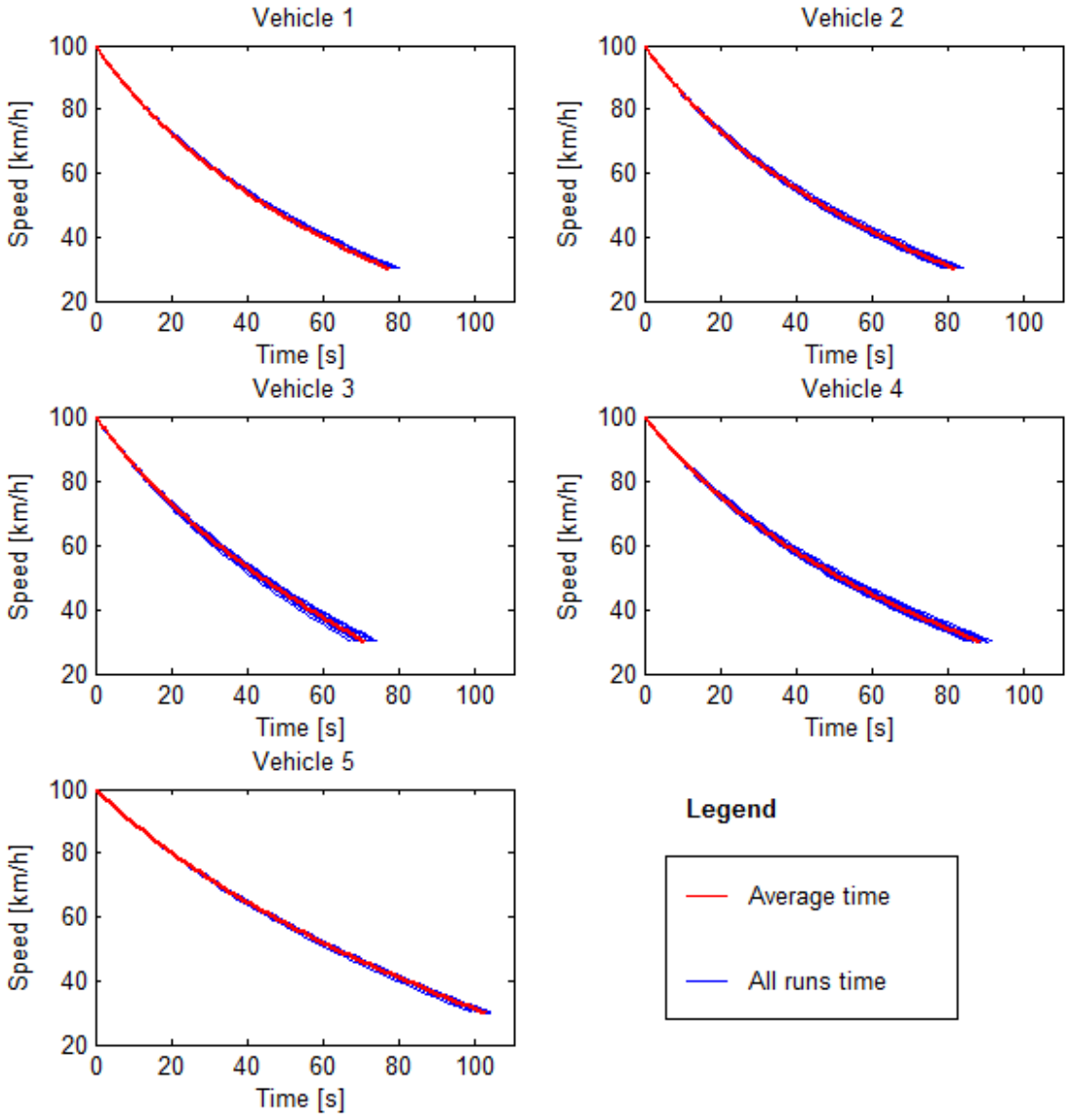

Figure 5.1 – Coastdown speed versus time measurements

The results of the coastdown test are the average coefficients (μ_{f_0}, μ_{f_2}), coefficients standard deviation $(\sigma_{f_0}, \sigma_{f_2})$ and relative standard deviation $(\sigma_{f_0}/\mu_{f_0}, \sigma_{f_2}/\mu_{f_2})$ corrected for standard ambient condition of 101.325 kPa and 25℃, presented in Table 5.3 and in Table 5.4:

Table 5.3 – Coastdown test results for f_0 corrected for 101.325 kPa and 25°C

	Vehicle 1	Vehicle 2	Vehicle 3	Vehicle 4	Vehicle 5
μ_{f_0} [N]	121.2	142.4	213.8	141.6	184.4
σ_{f_0} [N]	10.9	9.1	23.5	8.6	7.9
σ_{f_0}/μ_{f_0}	9.0%	6.4%	11.4%	6.1%	4.3%

Table 5.4 – Coastdown test results for f_2 corrected for 101.325 kPa and 25°C

	Vehicle 1	Vehicle 2	Vehicle 3	Vehicle 4	Vehicle 5
$\mu_{f_2}[\mathrm{Ns^2/m^2}]$	0.5237	0.6708	0.5372	0.6366	0.4601
$\sigma_{f_2}[\mathrm{Ns^2/m^2}]$	0.02251	0.04830	0.03277	0.05029	0.02623
σ_{f_2}/μ_{f_2}	4.3%	7.2%	6.1%	7.9%	5.7%

The resistive force for each vehicle is presented on Figure 5.2:

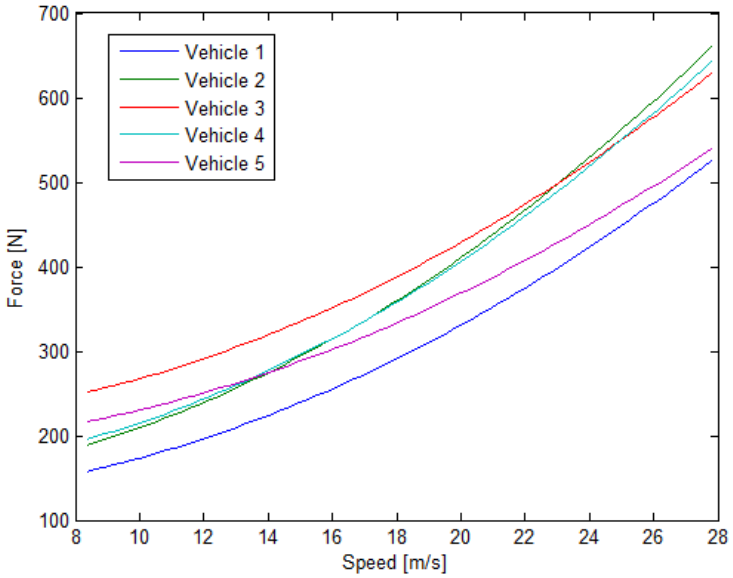

Figure 5.2 – Resistive force for the studied vehicles

It is important to notice that there is an uncertainty in the coefficients that describe the resistive force regression. This causes an uncertainty on the force calculation. As the total uncertainty on force is unknown but the standard deviation of the coefficients is measured, and as the force regression equation is also known, the uncertainty for the force can be

estimated. Bevington and Robinson (2003) present a generic equation to estimate the variance of a quantity x that is a function of at least two variables u and v (Eq. 5.1):

$$\sigma_x^2 \cong \sigma_u^2 \left(\frac{\partial x}{\partial u}\right)^2 + \sigma_v^2 \left(\frac{\partial x}{\partial v}\right)^2 + \cdots \tag{5.1}$$

In the present case, the quantity represented by x in Eq. 5.1 is the resistive force (R_x), and the variables that affect this force are f_0 and f_2. Therefore, Eq. 5.1 can be rewritten into Eq. 5.2:

$$\sigma_{R_x}^2 \cong \sigma_{f0}^2 \left(\frac{\partial R_x}{\partial f_0}\right)^2 + \sigma_{f2}^2 \left(\frac{\partial R_x}{\partial f_2}\right)^2 \tag{5.2}$$

The standard deviation for the resistive force is the square root of the variance, leading to Eq. 5.3:

$$\sigma_{R_x} = \sqrt{\sigma_{f0}^2 \left(\frac{\partial R_x}{\partial f_0}\right)^2 + \sigma_{f2}^2 \left(\frac{\partial R_x}{\partial f_2}\right)^2} \tag{5.3}$$

The partial differentiation of R_x with respect to f_0 and f_2 leads to Eq. 5.4:

$$\sigma_{R_x} = \sqrt{\sigma_{f0}^2 + \sigma_{f2}^2 v_x^4} \tag{5.4}$$

The resistive force and the errors for each vehicle is presented in Figure 5.3:

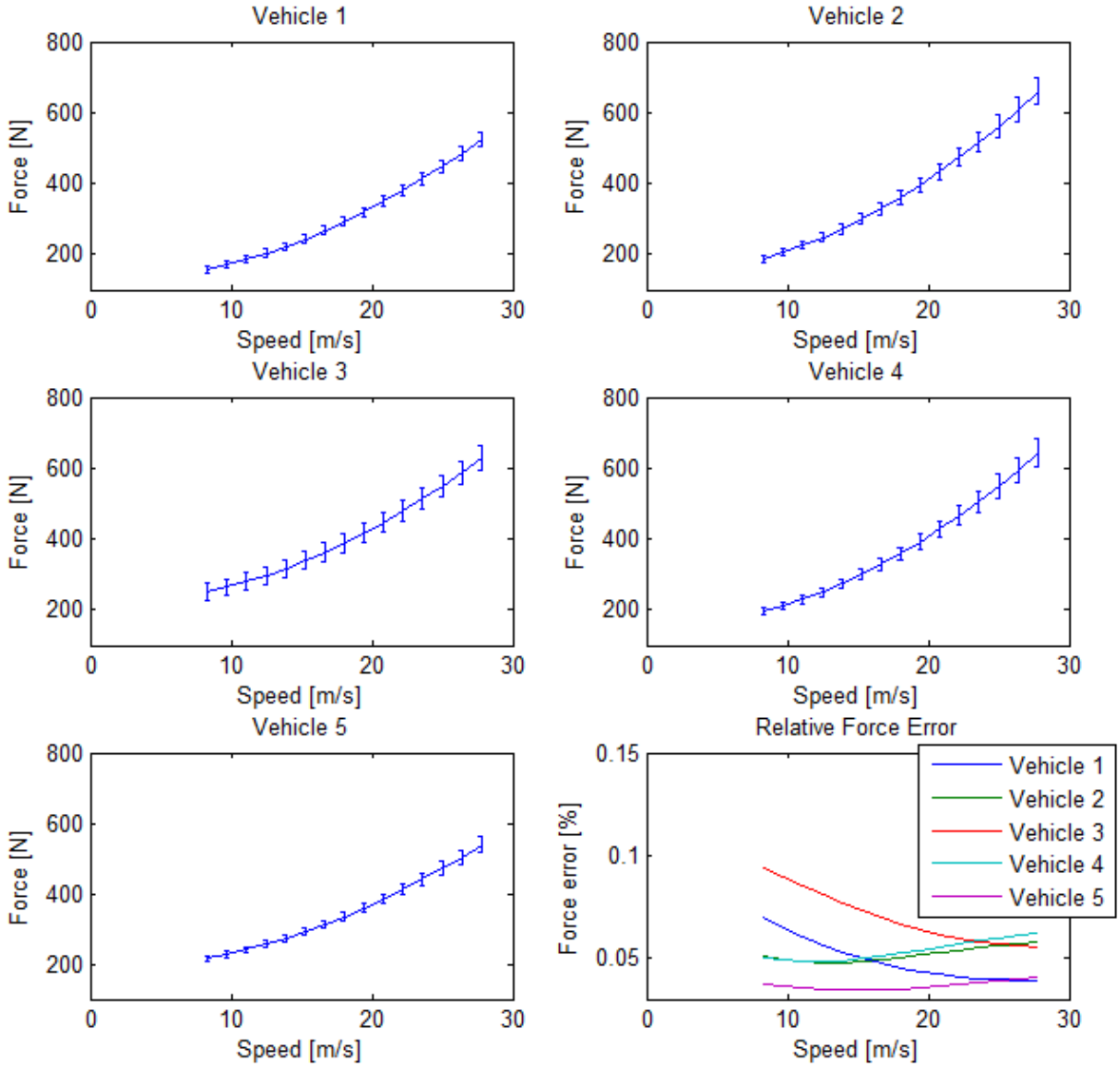

Figure 5.3 – Resistive force with error bars and relative error of resistive force for vehicles 1 to 5

5.1.3 Tire rolling radius

The tire rolling radius can be calculated through the nominal size of the tires, presented in Table 5.5:

Table 5.5 – Tire dimension properties for measured vehicles

Vehicle	Vehicle 1	Vehicle 2	Vehicle 3	Vehicle 4	Vehicle 5
Tire nominal size	175/65 R14	205/60 R16	205/55 R16	235/55 R17	235/45 R18
Tire load [kN]	2.66	3.46	3.37	3.74	4.19

Deflection	0.958	0.948	0.949	0.945	0.939
Tire rolling radius [m]	0.279	0.309	0.300	0.326	0.314

The uncertainty on tire rolling radius due to weight measurement uncertainty was found to be less than 0.1% and therefore it will not be considered.

5.1.4 Transmission and Differential ratio and efficiency

Specific tests were made in order to measure the transmission and differential ratio. These tests consist of engaging a gear and acquire engine speed and vehicle speed in that gear only, and repeat the procedure for all gears. The results are similar to the example presented in Figure 4.23. Adapting Eq. 4.45 to isolate eN_{tf}, one can obtain Eq. 5.5:

$$N_{tf} = \frac{\omega_e \cdot r}{v} \tag{5.5}$$

It is important to notice that as the ratio ω_e/v is measured, even if there is an error in the measurement of the rolling radius, N_{tf} will compensate in order to maintain the ratio N_{tf}/r equals to ω_e/v.

The final empirical coefficient to be obtained is the transmission and differential efficiency. However, this parameter is difficult to measure without the use of a dynamometer. In this work, it will be used a constant coefficient. Gillespie (1992) presents an example for manual transmissions in which the minimal efficiency for transmission is 0.966 and for differential, 0.99. A global efficiency will be considered 0.95 in this study.

5.2 TIME-VARIANT PARAMETERS MEASUREMENT AND POST PROCESSING

The measurement of time-variant parameters is done through the use of VBOX equipment. It can acquire both high precision GPS signal and OBD data. Each of the time-variant parameters (instantaneous fuel consumption and the ones that will be used to estimate engine torque) will be presented in this section.

5.2.1 Speed signal

Two measurements of speed signal are measured, with one being measured through GPS, and the other one, measured through ABS speed sensor, which is the signal that the

engine control unit uses for its internal calculations. These two signals are complementary, since GPS signal has higher resolution (0.01 km/h) than ABS sensor measured (0.5 km/h).

This difference is important for the calculation of acceleration, especially in low speeds. However, GPS signal is sensitive to external disturbances that cause signal errors that affect speed measurement. Thus, combining these two signals improves overall quality of the acquisition. This issue is presented on Figure 5.4:

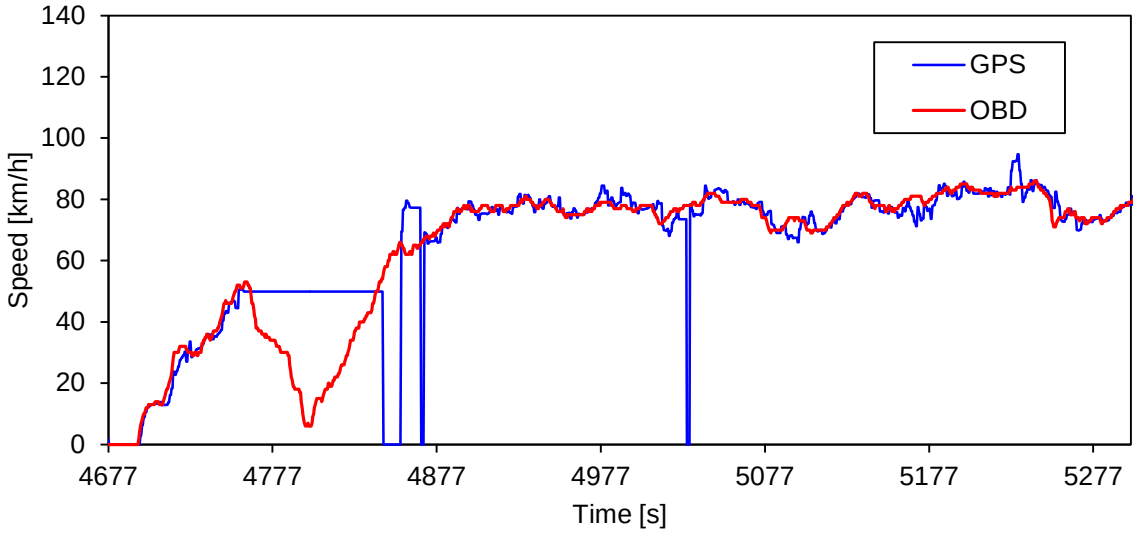

Figure 5.4 – GPS speed and OBD Speed versus time

It can be seen a significant error from time of 4754s to 4867s due probably to some external interference and a signal loss in time 5029s. In order to identify regions of possible error in GPS speed signal, two additional measurements will be required: 1) Satellite count and 2) Horizontal dilution of precision.

The satellite count is to account possible signal errors due to physical obstacles in the path from the GPS receiver to the satellite. The dilution of precision (DOP) is a measure of the satellite geometry error sensitivity (Lasky et al, 2006). The principle of the DOP is presented in Figure 5.5:

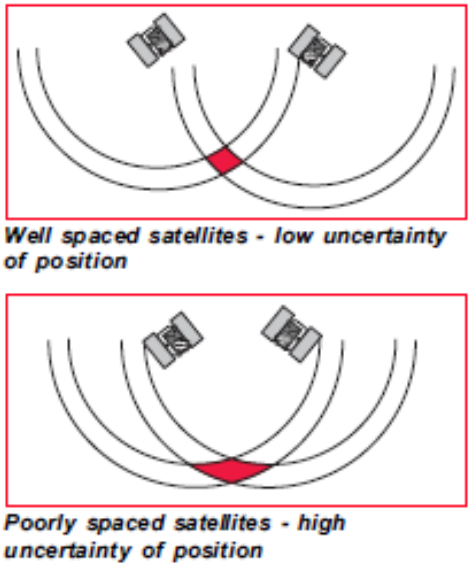

Figure 5.5 – Illustration of Dilution of Precision (Leica, 1999)

An excerpt of a GPS speed measurement with the number of satellites and the DOP is presented in Figure 5.6:

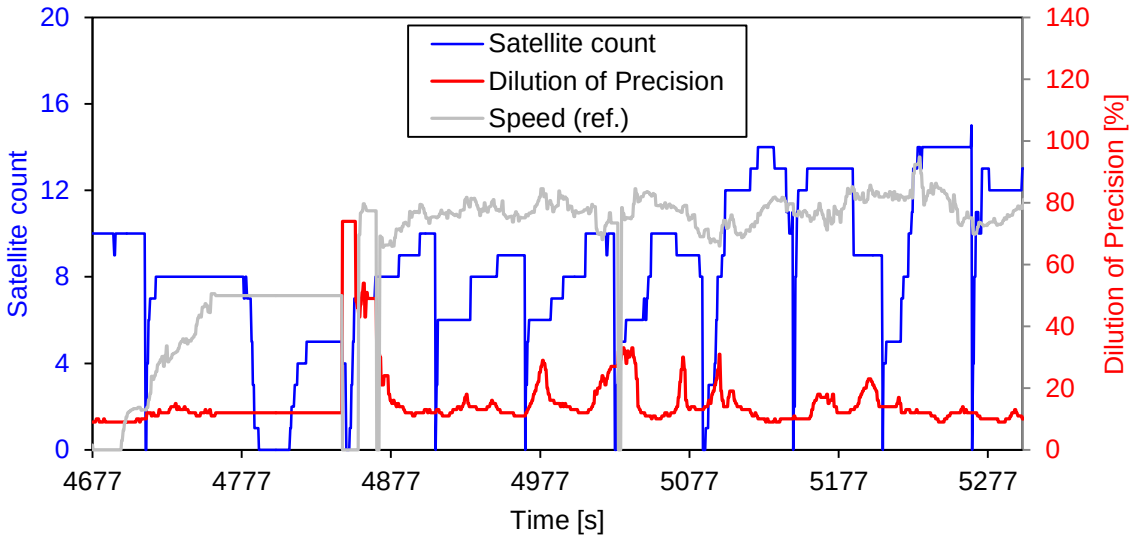

Figure 5.6 – Excerpt of GPS speed measurement with DOP and satellite counts signals

In order to avoid speed measurement errors, for satellite count lower than 9 and for DOP higher than 20 the speed will be considered the OBD speed. In other conditions, the speed considered is the GPS speed. The combined speed signal for the excerpt presented in Figure 5.4 and Figure 5.6 is showed in Figure 5.7:

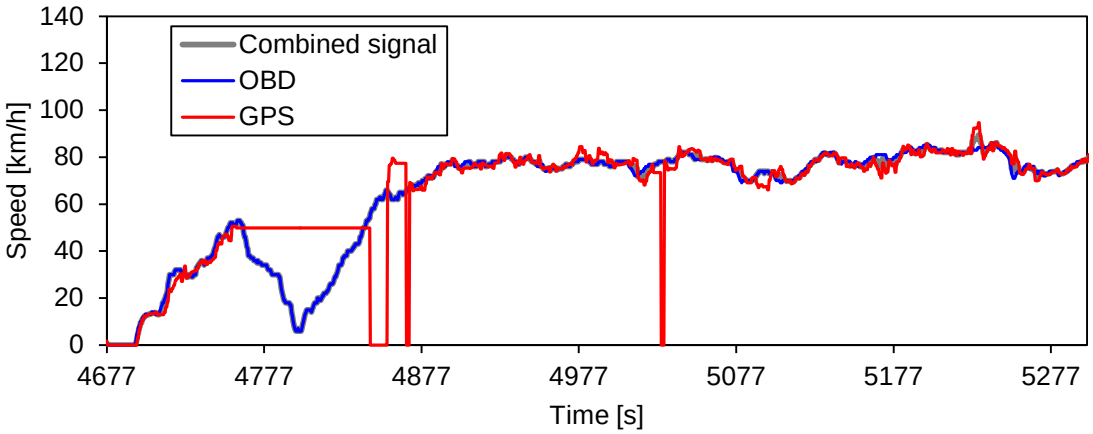

Figure 5.7 – Excerpt of combined speed signal

Speed signal noises need to be avoided. Some techniques are applied in order to avoid the effect of the noises in torque calculation. One frequent signal noise present in GPS-based acquisitions is called "zero-speed drift" (Duran and Earleywine, 2012). This error occurs when vehicle is stopped in idle condition and GPS records small speed disturbances (from 0.1 km/h to 0.3 km/h), although the vehicle is static, as presented in Figure 5.8. To avoid these errors, whenever the total distance of a microtrip (interval between an idle condition and the next idle condition) is lower than 1.5 m the total microtrip will not be considered and the speeds in this microtrip will be automatically set to zero.

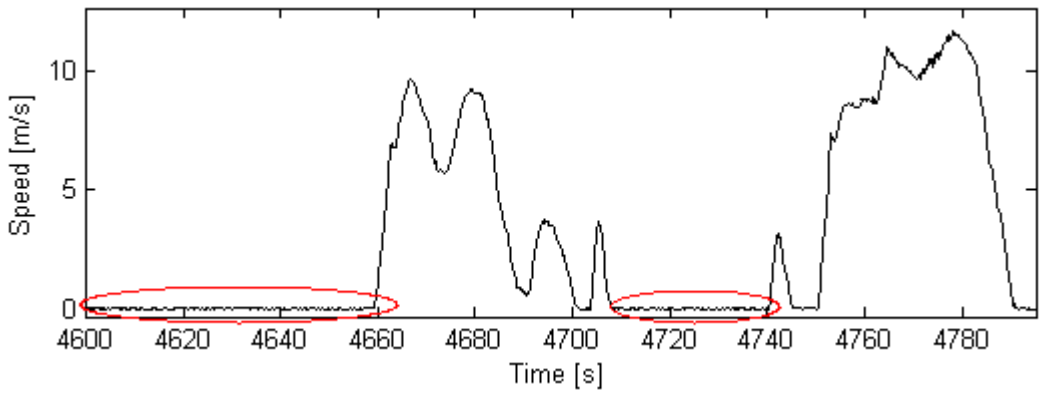

Figure 5.8 – Excerpt of speed measurement containing zero-speed drift effect

Another common noise present in GPS-based acquisitions is called "false zero" noise. In this case, a sudden signal drop-out creates false zero speed signals, as shown in Figure 5.9. Although combination with OBD signal can mitigate almost completely this error, it can still happen and, therefore, a signal processing technique must be used to avoid it. The technique

applied consists in identifying the points of zero-speed with non-zero neighbors and replace the zero speed value with a linear interpolation of its neighbors speeds.

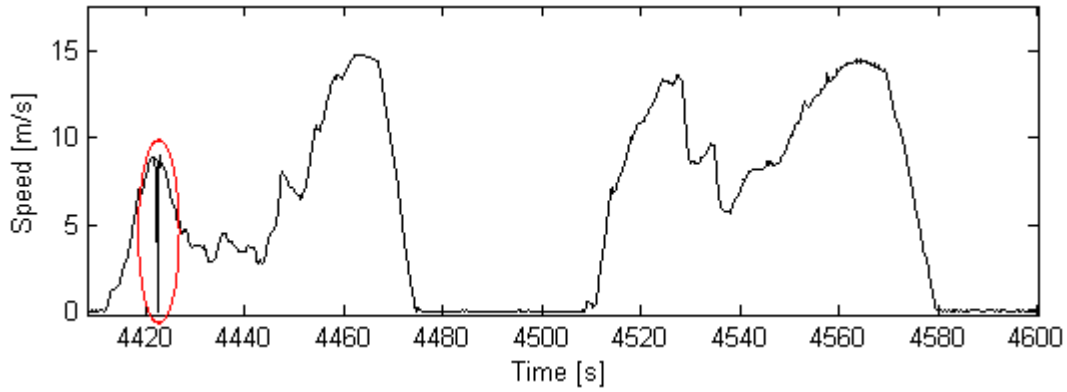

Figure 5.9 – Excerpt of speed measurement containing false zero noise

Speed signal measurement is also subject to random white noise, as presented in Figure 5.10. Low-pass filters are applied to speed signals in order to remove this type of noise. According to Smith (1999), digital filters have two uses: signal separation and signal restoration. In the present case, the aim to use a digital filter is to separate noise from the original signal. In the present work, two types of filter studied are: 1) moving average (MA) filter and 2) Butterworth infinite impulse response filter. These filters were selected since they are the simplest filters to apply (Proakis and Manolakis, 1996).

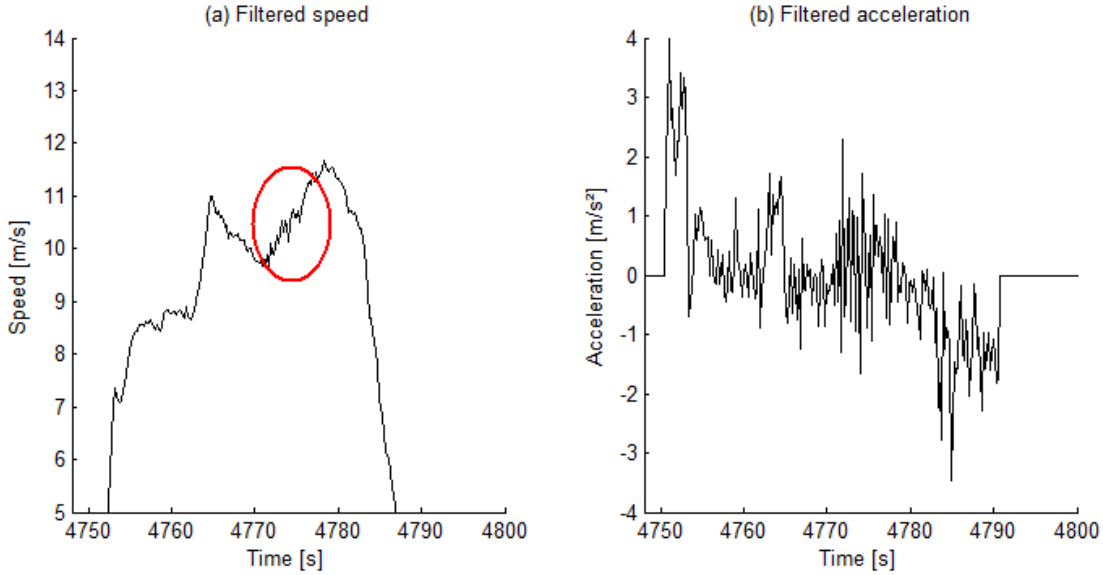

Figure 5.10 – Excerpt of containing random white noise for (a) speed and (b) acceleration

The analysis of these two types of filter is presented below:

- Moving average filter:

The MA filter is a time-domain filter and, therefore, no domain transform such as discrete Fourier transform (DFT) or fast Fourier transform (FFT) is required. Also, as it operates in time-domain, it is not recommended to separate band frequencies. However, this filter is one of the most commonly used since it is the easiest digital filter to understand and apply. In applications where the main relevant aim is to reduce white noise and maintain the original signal shape rather than separate frequencies, it has optimal performance (Smith, 1999). In equation form, this filter can be written as Eq. 5.6:

$$y[i] = \frac{1}{k}\sum_{j=0}^{k-1} x[i+j] \tag{5.6}$$

Where x is the input signal, y is the output signal, M is the number of points used in the MA. Alternatively, the points of the MA can be chosen symmetrically to the output point, as in Eq. 5.7:

$$y[i] = \frac{1}{k}\sum_{j=-\frac{(k-1)}{2}}^{\frac{(k-1)}{2}} x[i+j] \tag{5.7}$$

According to Smith (1999), the MA filter has an exceptionally performance for smoothing signal (the action in time-domain), but it is an exceptionally bad low-pass filter (the action in frequency domain). The smoothing action of a MA filter can be further improved through multiple-pass filtering at a cost of increased computational time. Figure 5.11 presents the frequency response of a moving average filter for different number of average points. It can be seen that it has poor capability of eliminating specific frequencies. Figure 5.12 presents a seven point multiple pass moving average filter for 1, 2 and 4 passes. It can be seen that increasing number of passes improves the band attenuation of the moving average filter, with faster amplitude decay.

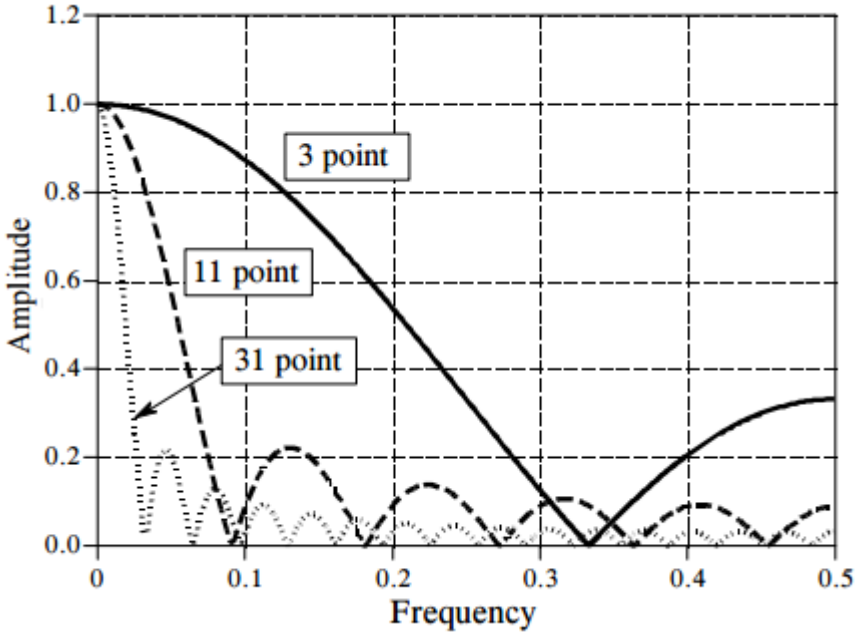

Figure 5.11 – Frequency response of a moving average filter for different averaging points (Smith, 1999)

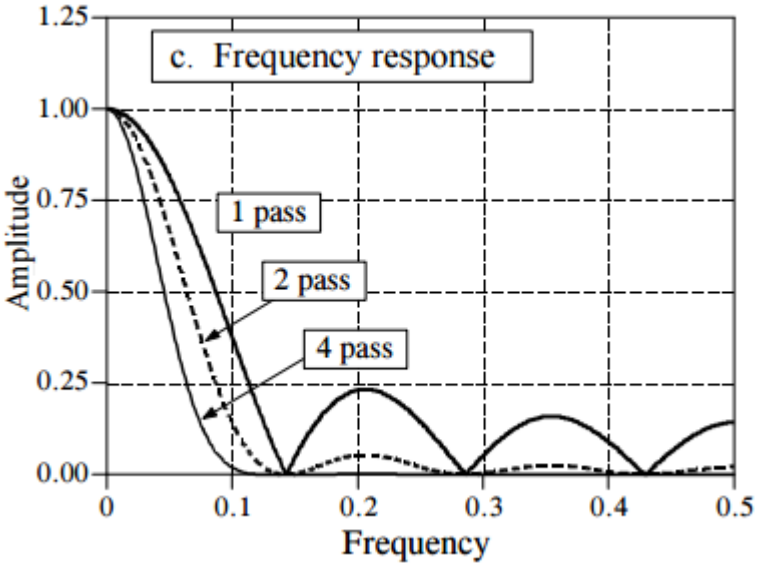

Figure 5.12 – Frequency response of a moving average filter for multiple pass moving average filter with 7 points average filter (Smith, 1999)

- Butterworth IIR filter:

Butterworth filters are designed to have a flat frequency response in the passband. It is originally an analog filter mapped into digital filter (Proakis and Manolakis, 1996). Differently from MA filter, the Butterworth filter is a frequency-domain filter, therefore its equation is described as function of frequency in form of a

transfer function instead of samples (or time). Its transfer function is presented in Eq. 5.8:

$$|H(\Omega)|^2 = \frac{1}{1 + \left(\frac{\Omega}{\Omega_c}\right)^{2N}} \tag{5.8}$$

Where Ω is the frequency, Ω_c is the cutoff frequency, which is the frequency where the magnitude of the filter reaches -3 dB, and N is the filter order. The filter order determines the decay rate of the filter. Figure 5.13 presents the frequency response of a low-pass Butterworth filter for a generic cutoff frequency and different orders.

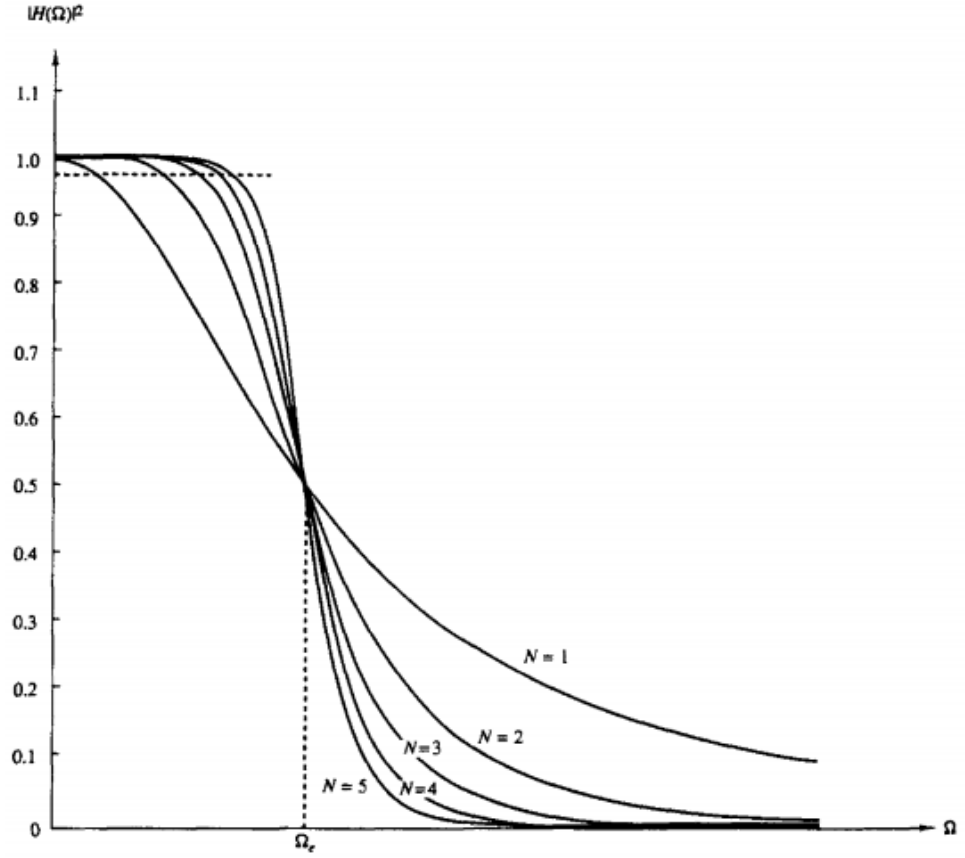

Figure 5.13 – Frequency response of a Butterworth low-pass digital filter (Proakis and Manolakis, 1996)

The filter selection depends on the characteristic of the signal one will measure and the instrument used in the measurement. An analysis of the acquisition signal is required in order to properly select the filter. In the present case, the signal that will be filtered is the vehicle speed. On the excerpt presented in Figure 5.10, it can be observed the oscillating acceleration between -1 to 1 m/s² in short intervals of time. However, it is highly unlikely that one would

drive in this condition. This acceleration amplitude is strong enough to be sensed by the human body (as a reference, the maximum acceleration on EPA city cycle is 1.5 m/s²) and these variations within short amount of time – a comfort measure called jerk – would be highly uncomfortable. Therefore, it is most likely that these variations are consequence of white noise and not a desired signal output. The main aspect that should be considered in this case is if the filter used should be a time-domain filter or a frequency-domain filter.

A comparison of the standard EPA-75 speed schedule against a measurement of a vehicle performing this schedule is done in order to identify a baseline for the real signal and differentiate it from white noise. Figure 5.14 presents the speed and acceleration signal comparison in time domain and Figure 5.15 presents the comparison of the same signals in frequency domain.

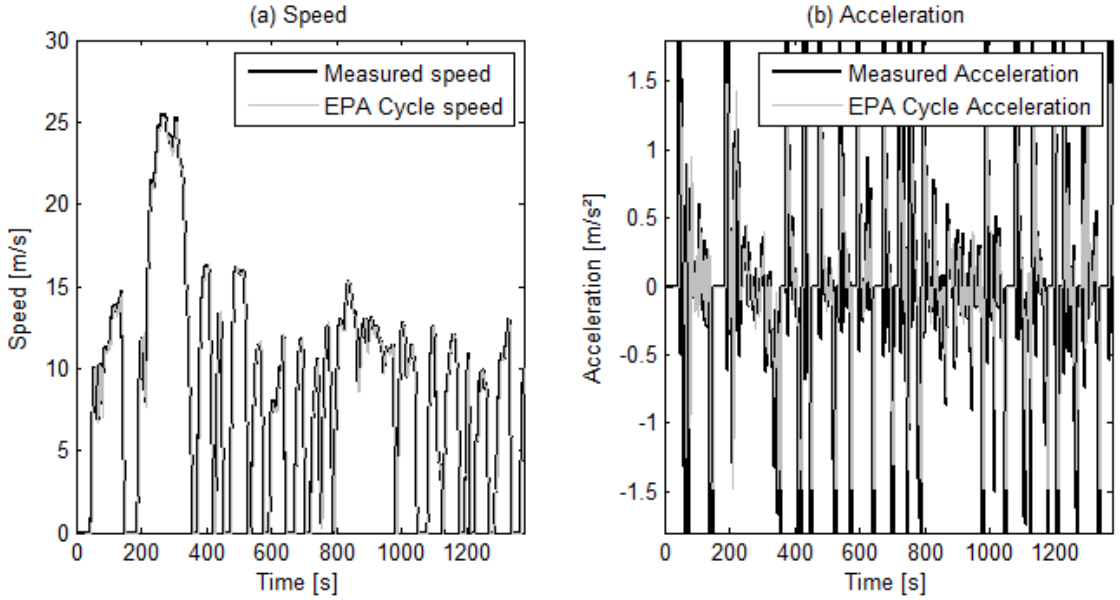

Figure 5.14 – Comparison of a time domain signals for EPA -75 schedule cycle versus an in-lab measured test for (a) speed and (b) acceleration

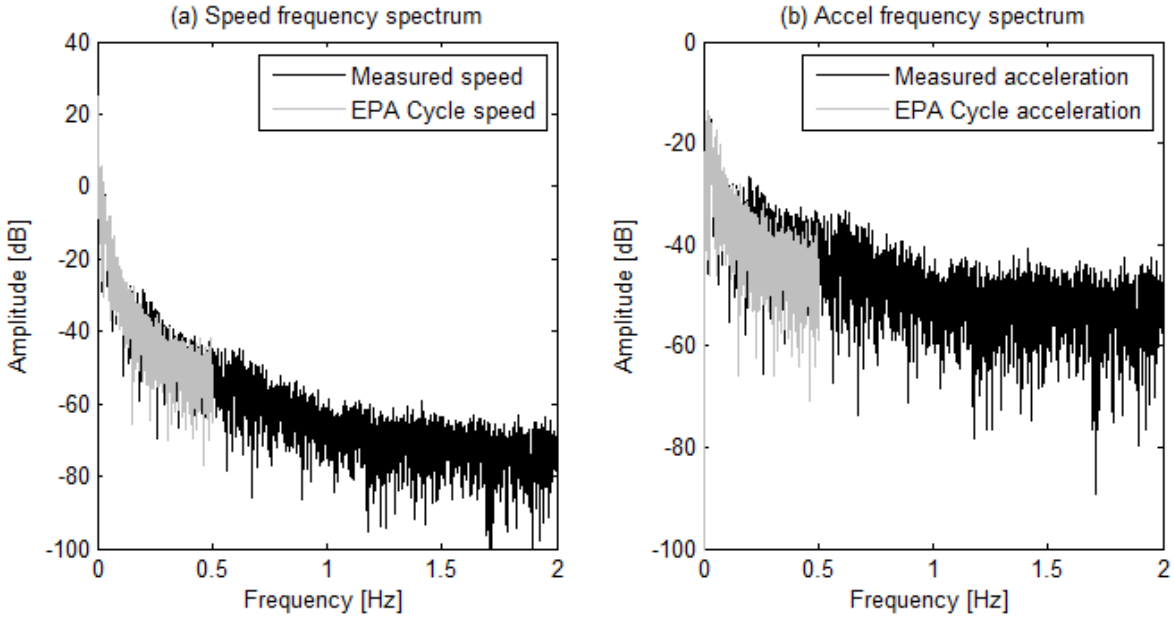

Figure 5.15 – Comparison of frequency domain signals for EPA -75 schedule cycle versus an in-lab measured test for (a) speed and (b) acceleration

It is important to notice that the EPA-75 speed schedule has a sample frequency of 1 Hz and therefore the positive frequency spectrum can only be presented up to 0.5 Hz. Still, it can be seen that the behavior of measured and scheduled signals for both time domain and frequency domain, and for speed and acceleration signals are similar. Now, making the same comparison, but considering a real world speed signal instead of an in-lab measured signal, there is a significant difference in speed and acceleration frequency spectrum (Figure 5.16).

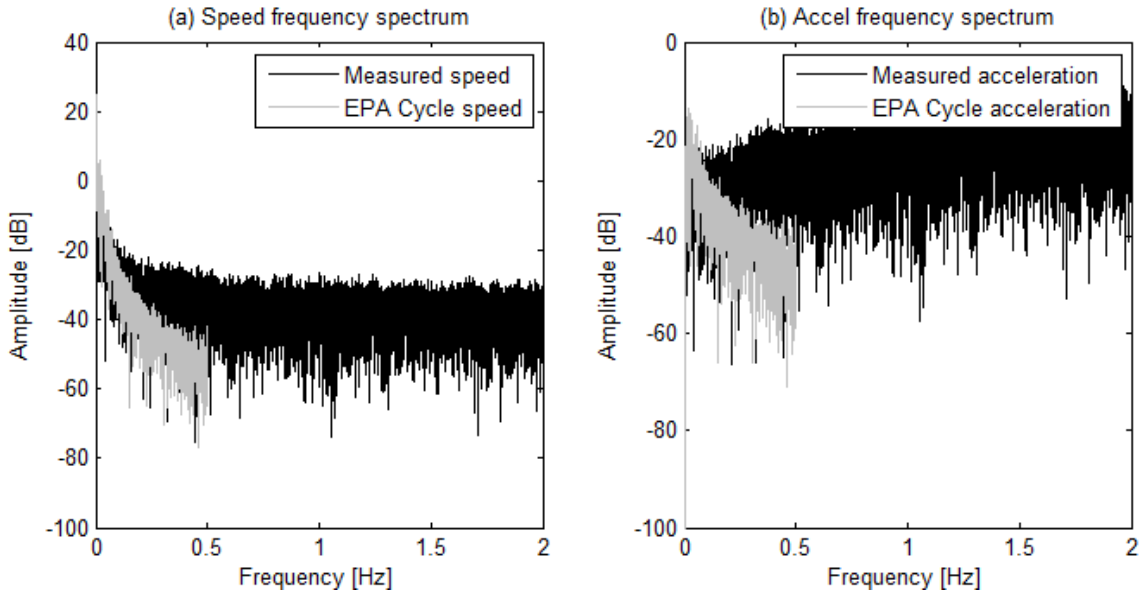

Figure 5.16 – Comparison of frequency domain signals for EPA -75 schedule cycle versus a real world measured test for (a) speed and (b) acceleration

In Figure 5.16, there is a clear difference between the measured and scheduled signals for both speed and acceleration. However, in none of the cases (EPA-75 cycle schedule, in-lab measurement and real world measurement) it is possible to identify clearly the frequency of the undesirable white noise – it seems to be present in all frequency range. This weighs in favor of the MA filter, since it is not clear what should be considered as a cutoff frequency.

The two aforementioned filters are compared with regard to their time-domain responses for both speed and acceleration. The filter design parameters were chosen in order to minimize acceleration variations and preserve the speed shape. The design parameters obtained for both filters are presented in Table 5.6:

Table 5.6 – Filter design parameters

Moving Average filter		**Butterworth filter**	
Average points	6	Cutoff frequency	1 Hz
Number of passes	6	Filter order	5

Applying these filters to speed signal presented in Figure 5.10, the results are as follow in Figure 5.17 and Figure 5.18:

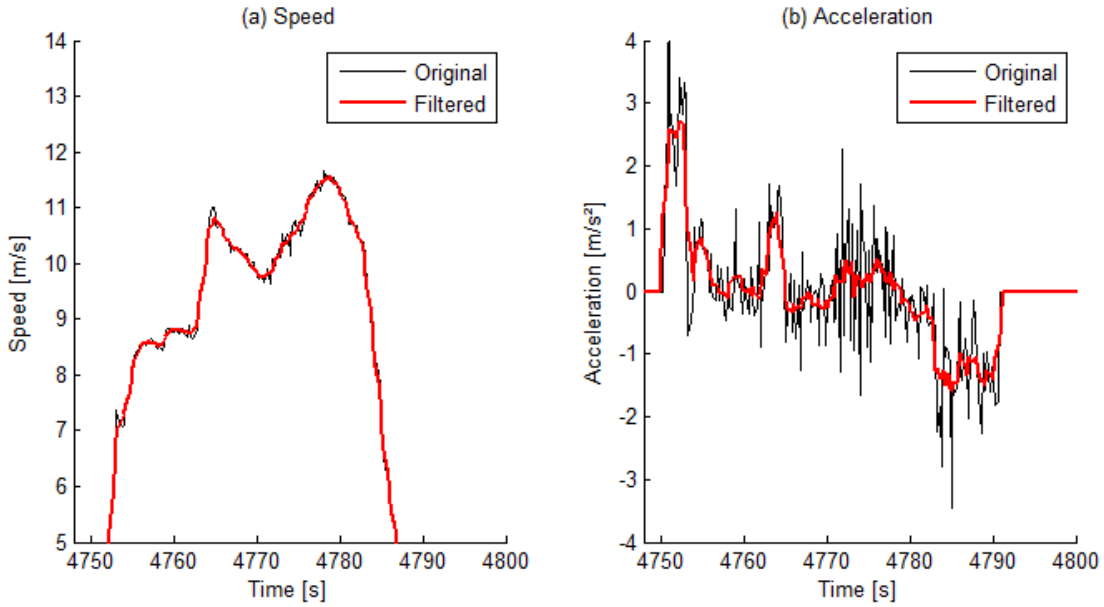

Figure 5.17 – Speed signal filtered through a MA filter

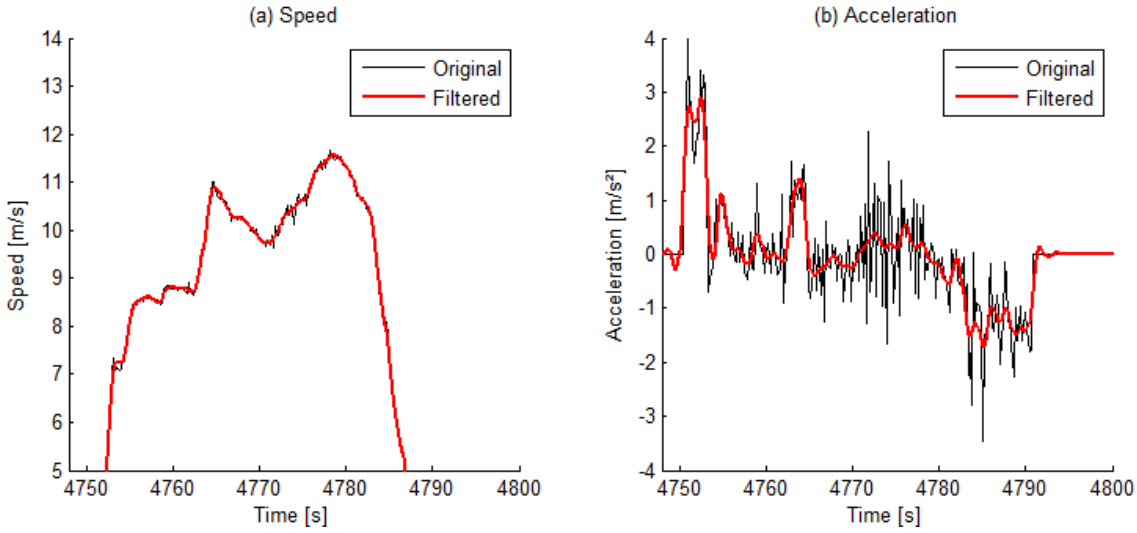

Figure 5.18 – Speed signal filtered through a Butterworth filter

Although both filtering results look similar, there is an undesired effect caused by the Butterworth filter. A detail of the acceleration around 4790s is presented in Figure 5.19 to illustrate this effect.

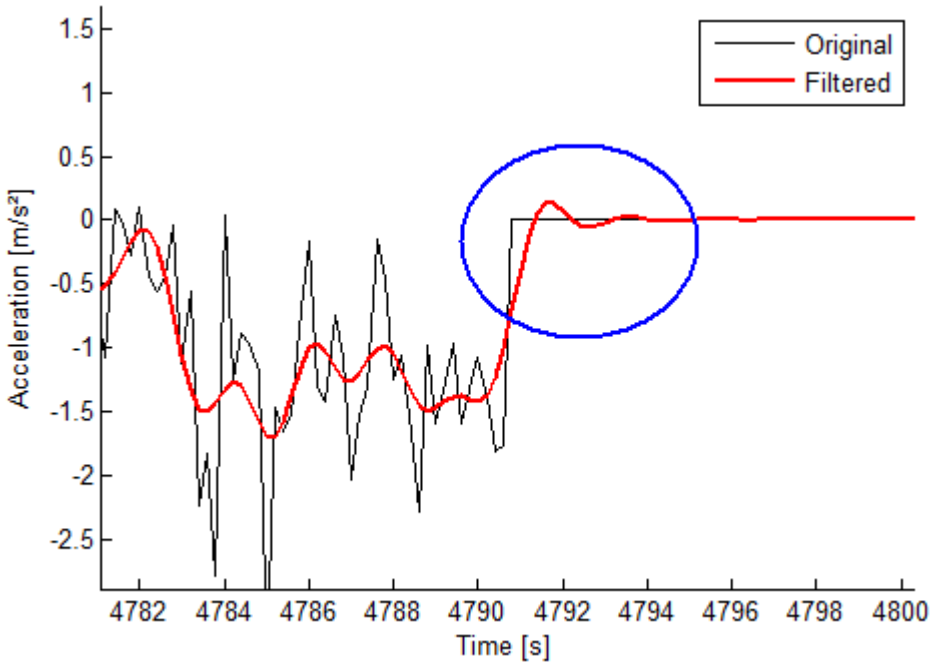

Figure 5.19 – Illustration of undesired effect of Butterworth filtering in acceleration signal

The area highlighted by the ellipse shows an acceleration oscillation in a condition where the vehicle is static, and, therefore, no acceleration would be expected. As the acceleration is obtained by deriving speed signal, this can be also seen in the speed signal, as presented in Figure 5.20:

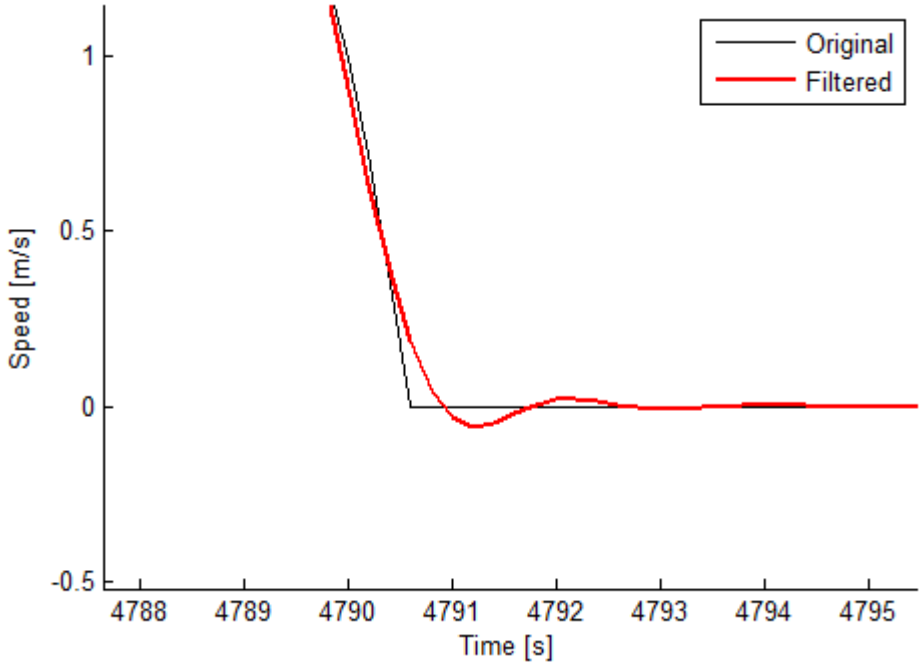

Figure 5.20 – Illustration of undesired effect of Butterworth filtering in speed signal

This oscillation causes the appearance of negative speeds, which does not make sense since what is measured is the magnitude of the speed, regardless of the way and direction. Any attempt to exclude these negative speeds causes disturbances and noises on the signal, especially when deriving speed to calculate acceleration. Therefore, a time-domain moving average filter is more suitable in this case.

Figure 5.21 presents the speed signal after all post-processing techniques presented in this section. It can be seen a huge improvement in signal quality, without losing original signal characteristic.

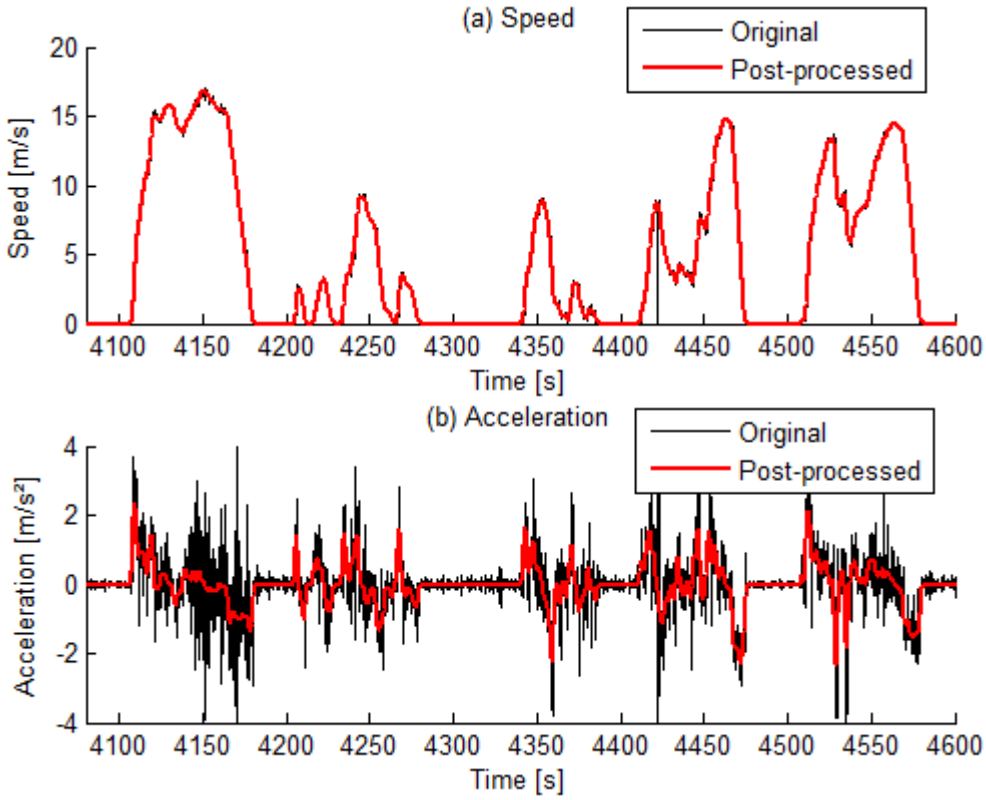

Figure 5.21 – Speed signal after post processing

5.2.2 Road grade signal

In theory, road grade signal could be obtained through 3 different methods without measuring the torque acting on wheels:

- GPS elevation signal;
- High precision accelerometer;
- Measuring barometric pressure.

GPS elevation signal is not as accurate as GPS latitude and longitude positioning or GPS speed measurement due to insufficient positioning and availability of satellite network (Wood et al, 2014). Some techniques can be used in order to improve the quality of this signal. Wood et al (2014) cites the use of Kalman filters, performing multiple runs on same location and the use of a technology called Lidar (laser based measurements). Bae, Ryu and Gerdes (2001) have obtained good results for road grade estimation just by using low-pass filters, since road grade variation is concentrated in frequencies below 0.5 Hz. Sahlholm and Johansson (2010) have improved the road grade signal by comparing the measured grade with high precision digital topographic maps.

Accelerometer measurement is subject to diverse range of noises, which makes it difficult to use its signal for this purpose (EPA, 2012). There are, however, works that combine GPS signal with accelerometer signal (Wang et al, 2013) with satisfactory results.

Barometric measurements are not recommended for the range in study. It is difficult to measure difference in barometric pressure for only few meters in height difference. Therefore, this technique will not be considered.

The GPS signal will be studied and some techniques will be applied in order to improve its quality. The first step to identify where the signal must be improved is to obtain the road grade based on height measurement. The road grade can be described in equation form as Eq. 5.9:

$$\theta = \tan^{-1}\left(\frac{ds_z}{ds_x}\right) \tag{5.9}$$

Where s_x is the space run in x direction and s_Z is the space run in z direction.

Alternatively, the GPS can provide the vertical speed instead of the altitude, leading to an alternate form of Eq. 5.9, presented in Eq. 5.10:

$$\theta = \tan^{-1}\left(\frac{d\dot{s}_z}{d\dot{s}_x}\right) \tag{5.10}$$

The option to use Eq. 5.9 or Eq. 5.10 depends on GPS equipment in use, since different equipment have different output forms. In the present work, it is used Eq. 5.9.

An acquisition of the measured altitude is presented in Figure 5.22:

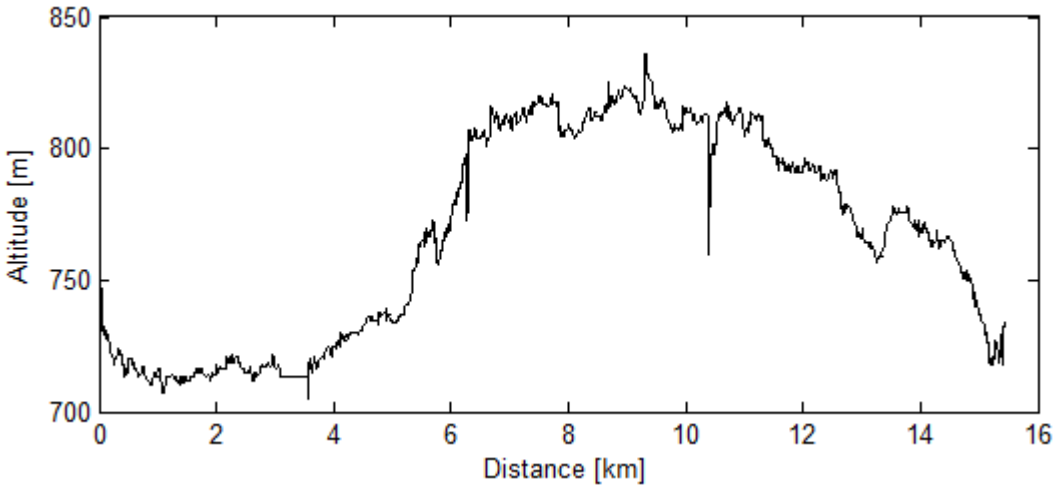

Figure 5.22 – Measured altitude as a function of measured distance

It can be noticed some noises that jeopardizes the altitude signal quality:

- Zero-speed altitude drift:

This noise has the same source of zero-speed drift presented in Section 5.2.1. When the vehicle is stopped in idle condition the altitude signal drifts instead of remaining static, as presented in Figure 5.23:

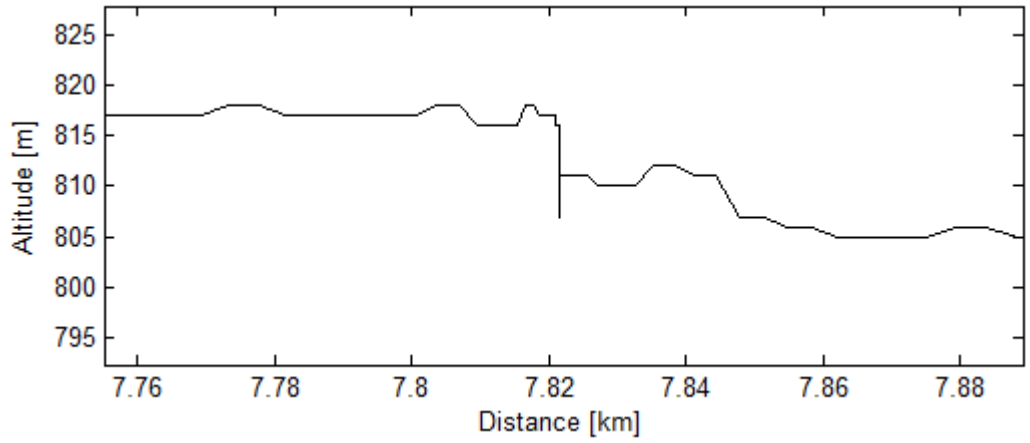

Figure 5.23 – Zero-speed altitude drift

- High variation in altitude within short distance (detail presented in Figure 5.24):

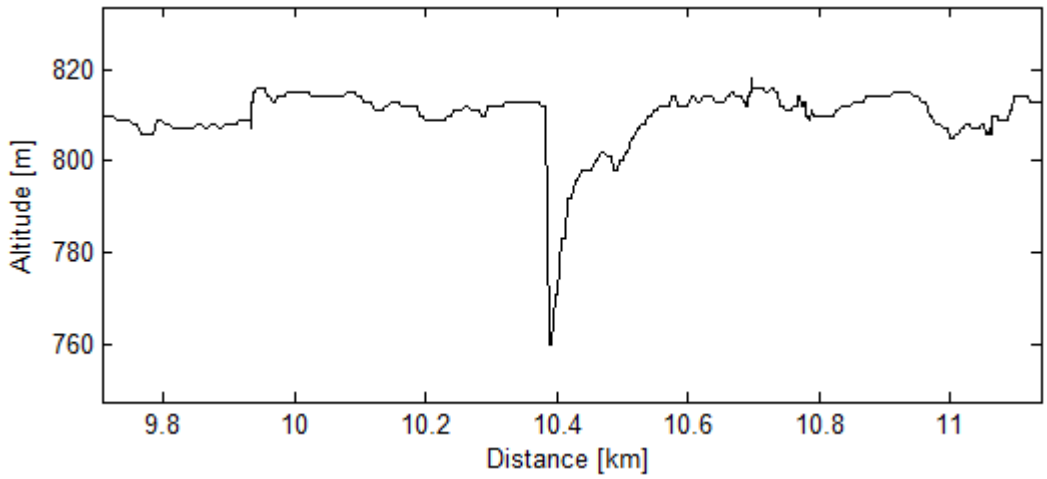

Figure 5.24 – Detail containing excessive altitude variation in 10.4 km surroundings

This signal noise is probably due to GPS signal loss or high DOP, which increases the GPS uncertainty;

- High-frequency oscillation:

The road grade of asphalted surfaces are not expected to present high spatial frequency (spatial frequency because it is related to space, instead of time). This effect can be seen in the whole measurement extension in Figure 5.22.

In order to correct these undesired effects, the following steps are proposed:

1. Derive altitude and distance with respect to time in order to obtain $d\dot{s}_z/d\dot{s}_x$, presented in Figure 5.25. It can be seen that due to noise and discontinuities, the magnitude of ds_z/ds_x frequently reaches values higher than 5. As reference, $ds_z/ds_x = 1$ is a 45° slope, which most of the vehicles are unable to transpose.

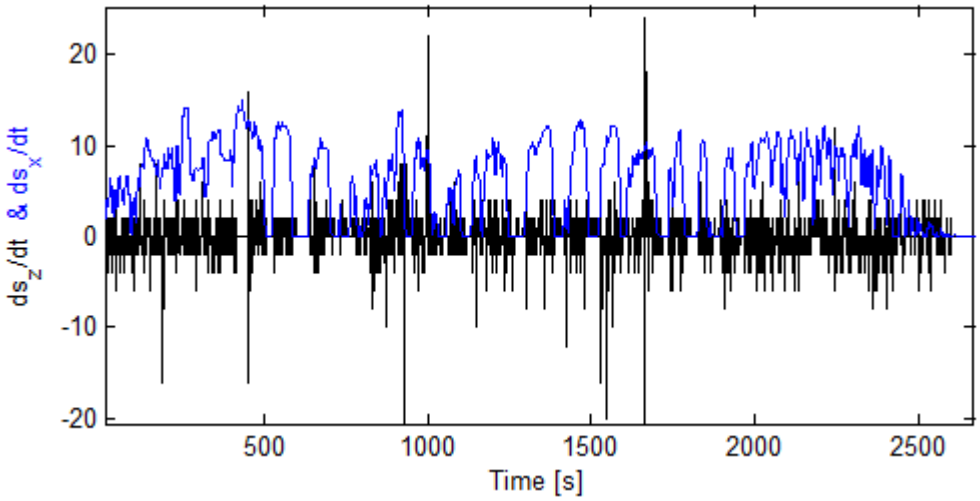

Figure 5.25 – ds_x/dt and ds_z/dt as function of time

2. Whenever vehicle speed is zero, $\dot{s}_z$ will be automatically set to zero. This will eliminate zero-drift speed and set $d\dot{s}_z/d\dot{s}_x$ zero for $d\dot{s}_x$ in order to avoid infinite results;
3. Saturate $d\dot{s}_z/d\dot{s}_x$ to -0.15 as minimum allowed value and +0.15 as maximum allowed value (it is very uncommon in urban conditions the presence of slopes higher than 10%, and almost inexistent higher than 15% slopes – test route should be changed if higher slopes are present);
4. Integer the resultant signal for $d\dot{s}_z/d\dot{s}_x$ in order to obtain a new altitude curve (s_z). The result for the measurement presented in Figure 5.22 after the application of this procedure is presented in Figure 5.26:

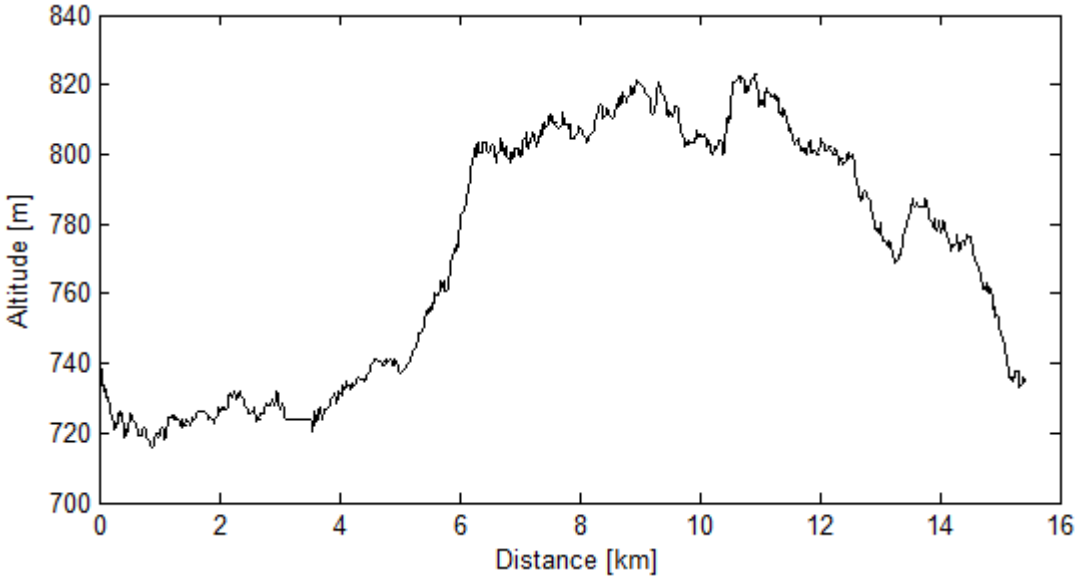

Figure 5.26 – GPS altitude corrected signal

5. Apply a MA filter (the aim here is the same as vehicle speed – smooth signal and reduce random white noise). In this case, however, the altitude signal is not time-domain but space-domain instead. The procedure is similar to procedure presented in time-domain but an additional step is required. The MA filter can be applied directly in time domain because the measurements were made in fixed time steps. However, as speed varies, the distance has no fixed steps, which leads to errors and output signal discontinuities. In order to apply the MA filter in space domain an auxiliary signal of constant space interval is created and another auxiliary signal that interpolates the altitude signal into the auxiliary distance signal. These signals are compared with base signals in Figure 5.27. As expected, both signals are coincident as no other operation was made. The MA filter must be applied to the auxiliary interpolated signal, as presented in Figure 5.28. The interpolation was made considering 100000 points in order to have greater order than the original signal. The filter parameters chosen are 50 points and 5 passes. These parameters were chosen in order to reduce spatial frequencies higher than 0.1 m^{-1} (or, in a more comprehensive way, to avoid oscillations with periods lower than 10 m in x axis), with minimal cost to overall shape.

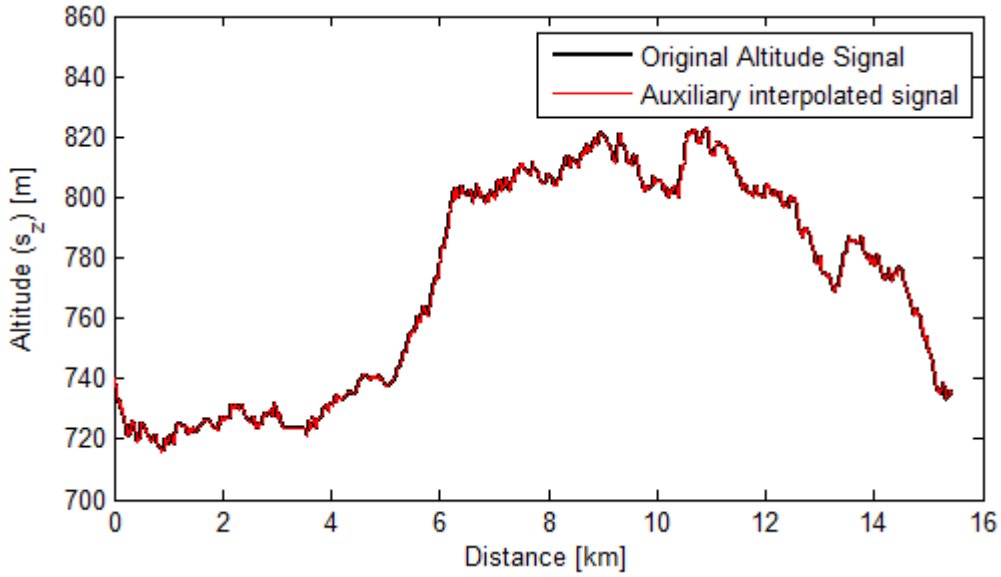

Figure 5.27 – Original altitude signal versus interpolated signal

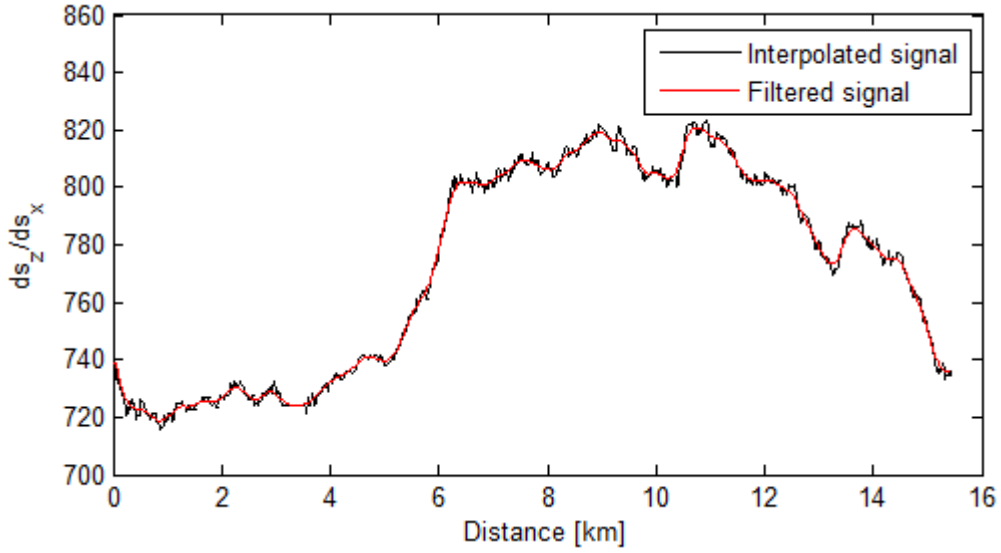

Figure 5.28 – Interpolated signal versus filtered signal

In order to confront the accuracy of the methodology, some points were verified through map georeferencing. The comparison data was done using Google Maps height based on latitude and longitude inputs. Eleven points were used for the comparison, and the results are presented in Figure 5.29:

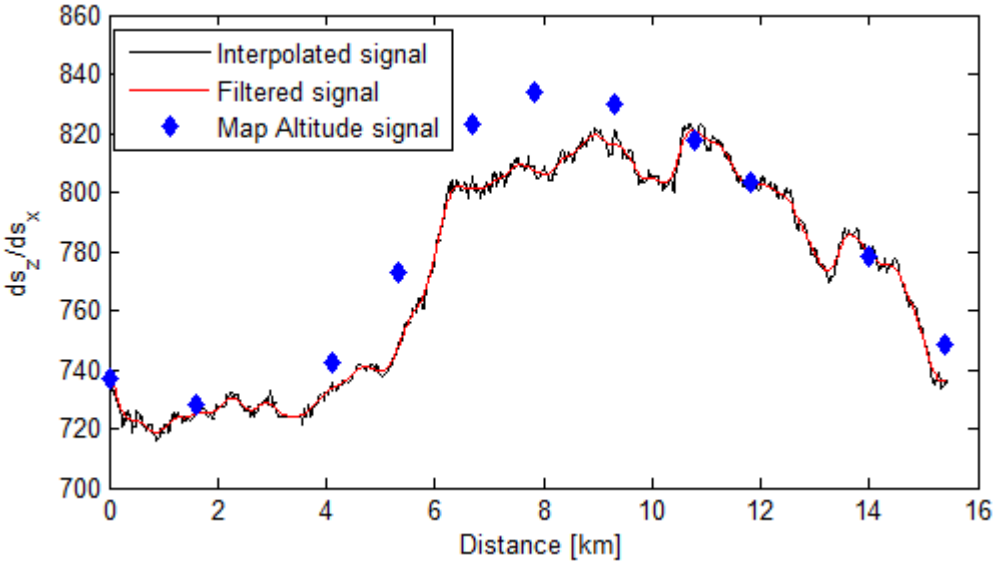

Figure 5.29 – Comparison with measured altitude methodology versus georeferencing

In general, the georeferenced points present a similar shape with the measured road grade signal. However, discrepancies of almost 20 m are observed in the distance interval of 6 km to 9 km. Although this error is greater than the 6 m presented in Section 4.1.5, the other points present a good match. The height error will be considered the ± 6 m informed by VBOX (the same as presented in Section 4.1.5).

5.2.3 Engine Speed

The information of engine speed is provided to OBD directly. This means that the signal acquired is a signal provided by the crankshaft speed sensor. The sensor type used for engine speed measurement is a Hall sensor, in which an electric signal is generated through a permanent magnet under the magnetic effect of a toothed wheel (presented in Figure 5.30).

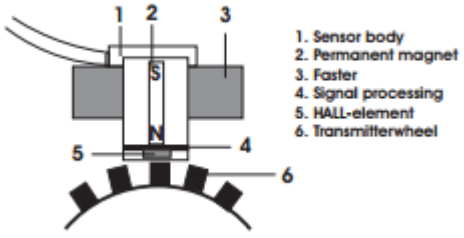

Figure 5.30 – Hall sensor (Hellström, 2005)

The electric signal will vary from maximum (when gear tooth is in closest possible position to sensor) to minimum (in interval between two gear teeth) for each gear tooth. This will generate a periodic signal with a frequency as higher as the number of teeth per revolution than the engine speed (note that RPM – m^{-1} – is actually a unit of frequency). Therefore, measuring the signal frequency and dividing by the number of teeth provides the engine speed. According to Turner (2009), the required accuracy for engine control is 1% of absolute signal.

The only post-processing step required to engine speed signal is the application of filter to reduce noise. However, in this case, the Butterworth filter is more suitable than the moving average filter. To explain the reason, an excerpt of an engine speed measurement is presented in Figure 5.31:

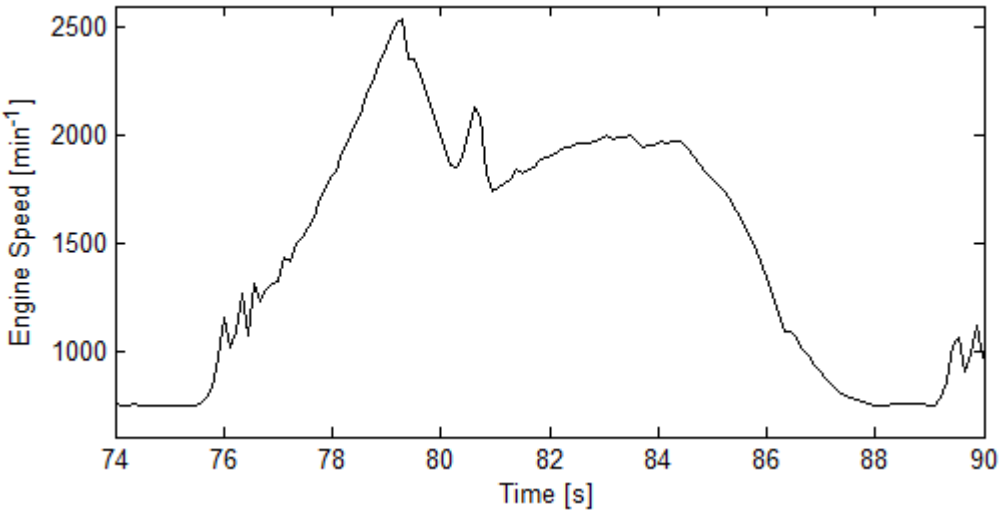

Figure 5.31 – Excerpt of engine speed measurement

It can be observed the presence of an oscillation near 76 s to 77 s. This oscillation is a dynamic effect called judder that happens due to component elasticity during clutch coupling. This effect should not affect fuel consumption since it is a mechanical response to engine torque input on transmission and driveline systems that happens at relatively short high frequency (around 4 Hz). There is, however, a second oscillation, in the surroundings of 81 s. This oscillation is due to gear shift from 1st gear to 2nd gear and from 2nd gear to 3rd gear. Figure 5.32 presents the same excerpt of Figure 5.31 with highlights to the operating conditions. The first operating condition highlighted is idling condition (1); the second operating condition is when the vehicle starts the movement, and therefore clutch is coupling engine and transmission (2), or during gear shifts, since in those conditions the clutch is also coupling and decoupling engine and transmission; the other three conditions (3), (4) and (5),

are conditions with gears engaged, where the linear relationship between vehicle speed and engine speed is linear, respectively for first gear engaged, second gear engaged and third gear engaged.

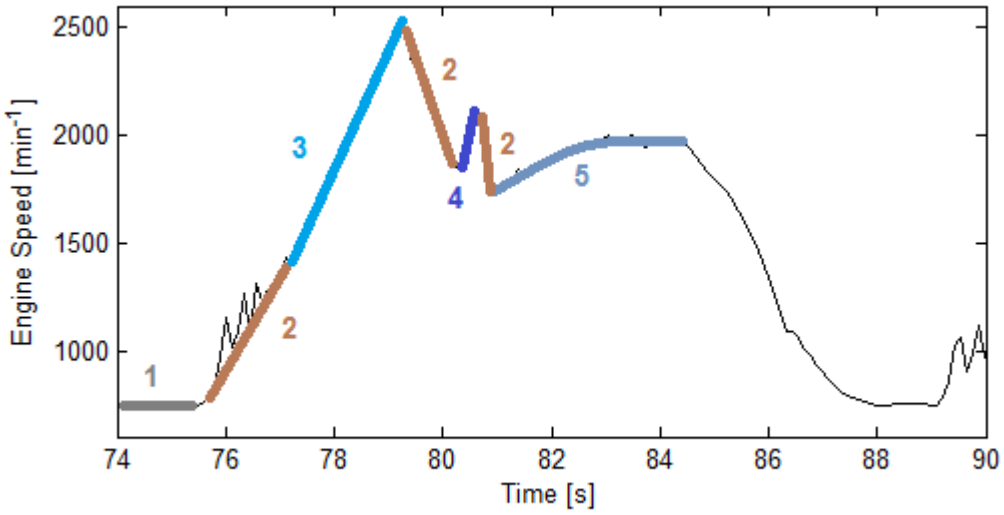

Figure 5.32 – Excerpt of engine speed with operating conditions highlighs: 1) idle; 2) clutch coupling; 3) 1st gear engaged; 4) 2nd gear engaged; and 5) 3rd gear engaged.

It is important to notice that the second gear is engaged for only a short period (around 0.5 s), but this is an important effect to fuel consumption since fuel is used to accelerate the engine from 1800 RPM to 2100 RPM. However, it is unlikely that a driver will maintain a gear engaged in less than 0.5 s (maximum frequency of 2 Hz). The filter design must take into account that frequencies higher than 4 Hz are considered noise and that frequencies lower than 2 Hz are part of the study object. A high order filter is required in order to avoid the attenuation of the desired signals. The design parameters of the Butterworth filter chosen are presented in Table 5.7:

Table 5.7 – Butterworth filter design parameters for engine speed signal

Butterworth filter for engine speed	
Cutoff frequency	3 Hz
Filter order	9

The filter frequency attenuation is presented in Figure 5.33:

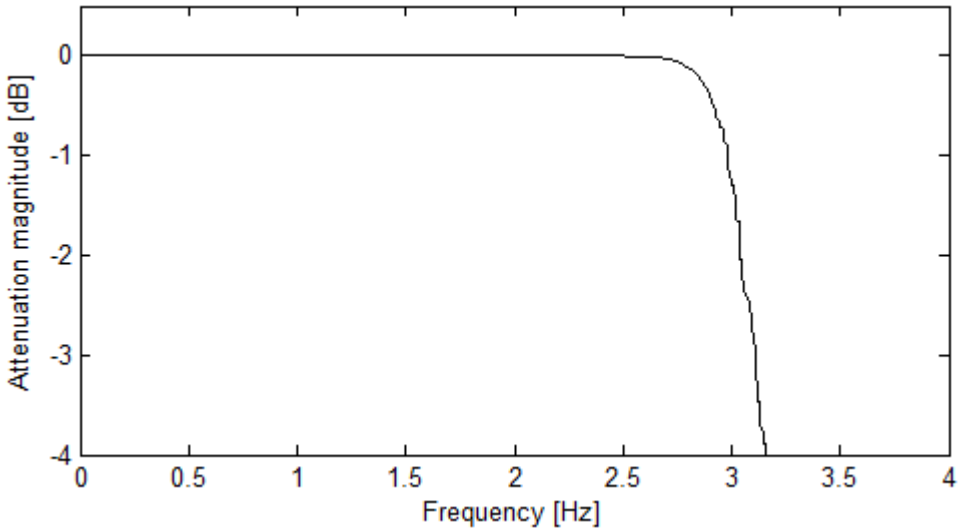

Figure 5.33 – Filter frequency attenuation for engine speed

It can be noticed the attenuation is 0 dB for frequencies below 2 Hz (object of interest) and decays rapidly above 2.5 Hz, with -3 dB frequency equals to 3 Hz (noise).

The engine speed minimum required accuracy for engine control and calibration is 1%, according to Turner (2009). This value may vary from vehicle to vehicle and from technology to technology, but it will be assumed a maximum of 1% error for this signal.

5.2.4 Ambient temperature and barometric pressure

Vehicles are equipped with ambient temperature and barometric pressure sensors in the fuel and throttle control. Engine management system relies on these parameters to properly control the engine to obtain maximum performance and efficiency, enhance drivability and control emissions (Turner, 2009). The most common temperature sensors are thermistors, and most of vehicles use this type of sensor for measuring ambient temperature. Thermistors are semiconducting materials whose resistance is dependent of the temperature. The required accuracy for the temperature measurement for engine control purposes is 2%.

The barometric pressure measurement is used for altitude calculation and for measuring pressure difference between ambient and manifold air pressure in order to correct air-fuel ratio. At higher altitudes, the air is thinner and therefore the amount of fuel injected need to take it into account in order to avoid fuel-rich mixtures. The required accuracy for this sensor for engine control purposes is 3%.

Although both ambient temperature and barometric pressure are time-variant parameters, their instantaneous effect on vehicle dynamics and longitudinal forces are

complicated to measure and to verify, and very complex and integrated models are required. The ambient temperature has an effect on aerodynamic force, on tire resistive force, engine and transmission time to reach fluids operating temperatures and others. Barometric pressure affects aerodynamic forces as well. It is not the purpose of this work to develop a model to capture all these effects and their sensitivity on engine torque. Instead of a complicated transient model to correct the resistive forces instantly by temperature and pressure, a mean value for these parameters will be considered and the force coefficients will be corrected based on these mean values on Eq. 4.39 and Eq. 4.40. This assumption is reasonable if there is no excessive variation on these parameters (± 10 ℃ and ± 10 kPa).

5.2.5 Fuel consumption signal measurement

As mentioned in Section 4.1.5, the fuel consumption procedure used in the present work is based on mass air flow sensor. This methodology considers that the engine works in stoichiometric conditions. This assumption is reasonable depending on the operating conditions, since the engine is controlled electronically to maintain this condition whenever possible due to emission gas control. The fuel consumption equation based on MAF is presented in Eq. 5.11:

$$\dot{m}_f = \frac{\dot{m_{air}}}{\lambda_{comm}} \tag{5.11}$$

Where $\dot{m}_f$ is the mass fuel flow, $\dot{m_{air}}$ is the mass air flow and λ_{comm} is the commanded air flow, which is the same as the λ_{stoic}.

The fuel consumption signal is not filtered since the original signal has low undesired high frequency noise. In fact, some of the high frequency measurements are relevant measurements since fuel flow has quicker response time than acceleration, for example. This is explained due to the fact that the fuel mass is directly related to throttle opening and closing and, thus, the signal response is almost instantaneous to throttle inputs. On the other hand, it takes some time after throttle opening, for example, for the whole mechanical systems react and accelerate the vehicle. An excerpt of a fuel consumption measurement is presented in Figure 5.34:

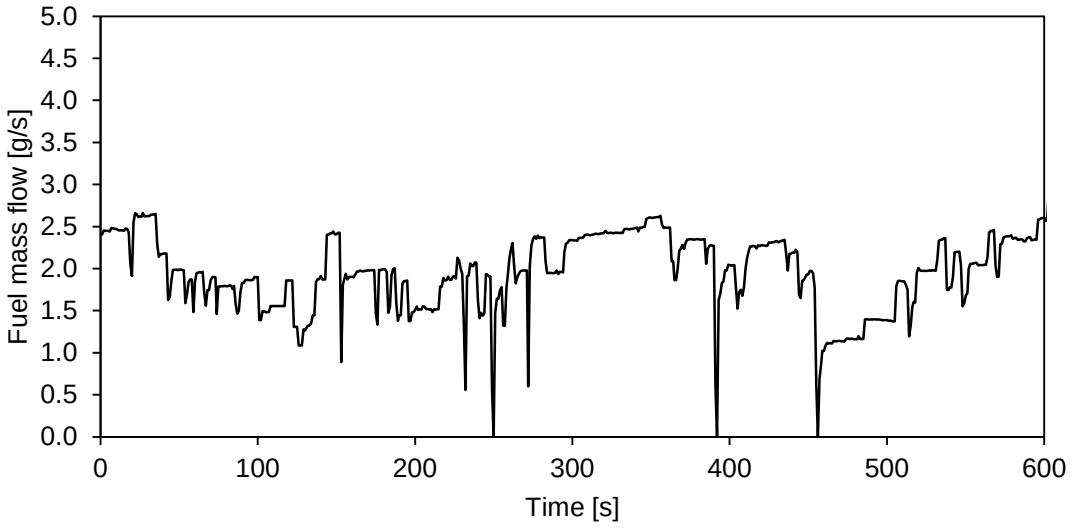

Figure 5.34 – Excerpt of fuel consumption signal

Alessandrini, Fillipo and Ortenzi (2012) found errors of 2% to 4% using MAF-based fuel consumption when compared to laboratory fuel consumption tests for three different vehicles using gasoline.

5.3 ENGINE TORQUE CALCULATION

In this section it will be presented the torque calculation for the vehicles studied and the effect of the intrinsic measurement errors. Eq. 4.42 is presented again for didactical purposes:

$$\tau_e = \frac{(M_e \cdot \dot{v} + f_0 + f_2 \cdot v^2 + W \cdot \sin\theta) \cdot r}{N_{tf} \cdot \eta_{tf}} \tag{4.42}$$

The procedure proposed in the present work for calculating engine torque is presented in flowchart form in Figure 5.35:

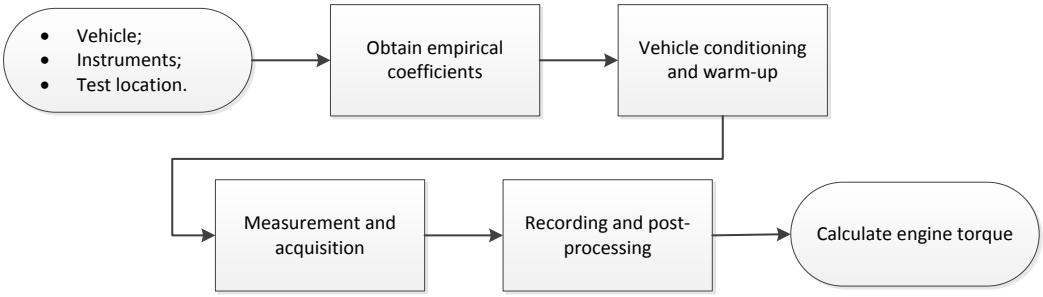

Figure 5.35 – Summarized flowchart of proposed procedure to measure engine torque

An important consideration to be made is how individual parameters uncertainties causes uncertainties in torque calculation. In order to obtain the torque uncertainty, Eq. 5.1 will be used. This equation is repeated below:

$$\sigma_x^2 \cong \sigma_u^2 \left(\frac{\partial x}{\partial u}\right)^2 + \sigma_v^2 \left(\frac{\partial x}{\partial v}\right)^2 + \cdots \tag{5.1}$$

The total uncertainties will be calculated by re-writing torque equation and breaking it down in parts. The first step will be to re-write it in order to eliminate N_{tf} and r since these parameters uncertainties are unknown. By rearranging Eq. 5.5 one can obtain Eq. 5.12:

$$\frac{N_{tf}}{r} = \frac{\omega_e}{v} \tag{5.12}$$

Replacing the left side of equation by the right side, the Eq. 5.13 is obtained:

$$\tau_e = \frac{(M_e \cdot \dot{v} + f_0 + f_2 \cdot v^2 + W \cdot \sin\theta)}{\eta_{tf}} \left(\frac{v}{\omega_e}\right) \tag{5.13}$$

Eq. 5.13 is more convenient because all terms have known errors (with the exception of η_{tf}, which will be explained later). It is also convenient to define, for didactical purposes, the following relationships:

$$P_{kin} = M_e \cdot \dot{v} \cdot v \tag{5.14}$$

$$P_{res} = (f_0 + f_2 \cdot v^2) \cdot v \tag{5.15}$$

$$P_g = M \cdot g \cdot v \cdot \sin\theta \tag{5.16}$$

$$P_{wheel} = P_{kin} + P_{res} + P_g \tag{5.17}$$

$$P_e = \frac{P_{wheel}}{\eta_{tf}} \tag{5.18}$$

Where P_{kin} is the kinetic power (the power required to accelerate the vehicle from a speed to another speed); P_{res} is the resistive power (required to overcome the aerodynamic and rolling resistance effects); P_g is the grade power (required to overcome road uphill or power absorbed during downhill); P_{wheel} is the effective power sensed on vehicle wheels; and P_e is the power that must be provided by the engine to deliver a certain level of wheel power.

Rearranging Eq. 5.13 using relationships presented from Eq. 5.14 to Eq. 5.16, one can obtain Eq. 5.19:

$$\tau_e = \frac{\left(P_{kin} + P_{res} + P_g\right)}{\eta_{tf} \cdot \omega_e} = \frac{P_{wheel}}{\eta_{tf} \cdot \omega_e} \tag{5.19}$$

The uncertainties can be calculated individually for each power component and propagated through Eq. 5.1 until all errors are accounted for engine torque. The uncertainty calculation for P_{kin} is presented in Eq. 5.20 and Eq. 5.21:

$$\sigma_{P_{kin}} = \sqrt{\sigma_{M_e}^2 \left(\frac{\partial_{P_{kin}}}{\partial M_e}\right)^2 + \sigma_{\dot{v}}^2 \left(\frac{\partial_{P_{kin}}}{\partial \dot{v}}\right)^2 + \sigma_v^2 \left(\frac{\partial_{P_{kin}}}{\partial v}\right)^2} \tag{5.20}$$

$$\sigma_{P_{kin}} = \sqrt{\sigma_{M_e}^2 \, (\dot{v} \cdot v)^2 + \sigma_{\dot{v}}^2 \, (M_e \cdot v)^2 + \sigma_v^2 \, (M_e \cdot \dot{v})^2} \tag{5.21}$$

The uncertainty in kinetic power calculation for the vehicles studied in this work, considering an acceleration of 1 m/s² and four different speeds is presented on Table 5.8:

Table 5.8 – Kinetic power uncertainties for the studied vehicles

	Units	Vehicle 1	Vehicle 2	Vehicle 3	Vehicle 4	Vehicle 5
M_e	[kg]	1085	1410	1375	1525	1710

σ_{M_e}	[kg]	2.50	2.50	2.50	2.50	2.50
σ_v	[m/s]	0.028	0.028	0.028	0.028	0.028
$\sigma_{\dot{v}}$	[m/s²]	0.028	0.028	0.028	0.028	0.028
$\dot{v}$	[m/s²]	1				

v [m/s]	P_{kin} uncertainty [W]				
	Vehicle 1	Vehicle 2	Vehicle 3	Vehicle 4	Vehicle 5
5	155.4	201.7	196.7	218.1	244.5
10	315.5	409.4	399.3	442.7	496.3
15	471.9	612.5	597.3	662.2	742.3
20	628.6	815.8	795.7	882.1	988.8

v [m/s]	Relative P_{kin} uncertainty [%]				
	Vehicle 1	Vehicle 2	Vehicle 3	Vehicle 4	Vehicle 5
5	2.73%	2.72%	2.72%	2.72%	2.72%
10	2.77%	2.77%	2.77%	2.76%	2.76%
15	2.76%	2.76%	2.76%	2.76%	2.76%
20	2.76%	2.76%	2.76%	2.75%	2.75%

It can be observed that since σ_{M_e}, σ_v and $\sigma_{\dot{v}}$ are similar for all vehicles, the relative P_{kin} uncertainty are also similar (around 2.8%) independently of speed. This behavior is also noticed for different acceleration levels.

The uncertainty for resistive power is expressed in Eq. 5.22 and Eq. 5.23:

$$\sigma_{P_{res}} = \sqrt{\sigma_v^2 \left(\frac{\partial_{P_{res}}}{\partial v}\right)^2 + \sigma_{f_0}^2 \left(\frac{\partial_{P_{res}}}{\partial f_0}\right)^2 + \sigma_{f_2}^2 \left(\frac{\partial_{P_{res}}}{\partial f_2}\right)^2} \tag{5.22}$$

$$\sigma_{P_{res}} = \sqrt{\sigma_v^2 \, (f_0 + 3f_2 \cdot v^2)^2 + \sigma_{f_0}^2 \, (v)^2 + \sigma_{f_2}^2 \, (v^3)^2} \tag{5.23}$$

The results for the vehicles studied are presented in Table 5.9:

Table 5.9 - Kinetic power uncertainties for the studied vehicles

	Units	Vehicle 1	Vehicle 2	Vehicle 3	Vehicle 4	Vehicle 5
M_e	[kg]	1085	1410	1375	1525	1710
f_0'	[N]	121.2	142.4	213.8	141.6	184.4
f_2'	[Ns²/m²]	0.5237	0.6708	0.5372	0.6366	0.4601
$\sigma f_0'$	[%]	9.0%	6.4%	11.4%	6.1%	4.3%
$\sigma f_2'$	[%]	4.3%	7.2%	6.1%	7.9%	5.7%

v [m/s]	P_{res} uncertainty [W]				
	Vehicle 1	Vehicle 2	Vehicle 3	Vehicle 4	Vehicle 5
5	54.8	46.3	122.1	44.0	40.3
10	111.7	103.6	246.1	100.4	84.0
15	180.9	213.4	382.3	214.1	148.9
20	283.7	428.0	554.0	438.6	263.8

v [m/s]	Relative P_{res} uncertainty [%]				
	Vehicle 1	Vehicle 2	Vehicle 3	Vehicle 4	Vehicle 5
5	8.16%	5.82%	10.75%	5.58%	4.11%
10	6.43%	4.95%	9.20%	4.89%	3.65%
15	5.05%	4.85%	7.62%	5.01%	3.45%
20	4.29%	5.21%	6.46%	5.53%	3.58%

For the uncertainty calculation of grade power a simplification will be used: $\sin\theta \approx \tan\theta \approx \theta$. This simplification is used only for uncertainty calculation and it is based on the almost linear behavior of these trigonometric functions for small angles. Another simplification is that gravitational acceleration is considered a constant ($\sigma_g = 0$). These simplifications are already taken into account in Eq. 5.24 and 5.25 where the uncertainty for grade power is presented:

$$\sigma_{P_g} = \sqrt{\sigma_M^2 \left(\frac{\partial_{P_g}}{\partial M}\right)^2 + \sigma_\theta^2 \left(\frac{\partial_{P_g}}{\partial \theta}\right)^2} \tag{5.24}$$

$$\sigma_{P_g} = \sqrt{\sigma_M^2 \, (g \cdot \theta)^2 + \sigma_\theta^2 \, (M \cdot g)^2} \tag{5.25}$$

The results for Eq. 5.24 and 5.25 for the studied vehicles is presented on Table 5.10:

Table 5.10 – Grade power uncertainties for the studied vehicles

	Units	Vehicle 1	Vehicle 2	Vehicle 3	Vehicle 4	Vehicle 5
M_e	[kg]	1085	1410	1375	1525	1710
σ_θ	[%]	6.0%	6.0%	6.0%	6.0%	6.0%

θ [rad]	P_g uncertainty [W]				
	Vehicle 1	Vehicle 2	Vehicle 3	Vehicle 4	Vehicle 5
0.010	6.6	8.5	8.3	9.2	10.4
0.027	17.5	22.8	22.2	24.7	27.6
0.043	28.5	37.0	36.1	40.1	44.9
0.060	39.5	51.3	50.0	55.5	62.2

θ [rad]	Relative P_g uncertainty [%]				
	Vehicle 1	Vehicle 2	Vehicle 3	Vehicle 4	Vehicle 5
0.010	6.18%	6.18%	6.18%	6.18%	6.18%
0.027	6.18%	6.18%	6.18%	6.18%	6.18%
0.043	6.18%	6.18%	6.18%	6.18%	6.18%
0.060	6.18%	6.18%	6.18%	6.18%	6.18%

Two aspects can be concluded from Table 5.10: 1) the relative error does not depend on θ; and 2) the error due to vertical velocity (or relative height) is much more important than the error due to vehicle mass measurement.

As $\sigma_{P_{kin}}$, $\sigma_{P_{res}}$ and σ_g are known, the uncertainty for P_{wheel} can be calculated (Eq.26):

$$\sigma_{P_{wheel}} = \sqrt{\sigma_{P_{kin}}^2 + \sigma_{P_{res}}^2 + \sigma_{P_g}^2} \tag{5.26}$$

The engine torque uncertainty, following the same procedure, is given by Eq. 5.27:

$$\sigma_{\tau_e} = \sqrt{\sigma_{P_e}^2 \left(\frac{1}{\omega_e}\right)^2 + \sigma_{\omega_e}^2 \left(-\frac{P_e}{\omega_e^2}\right)^2} \tag{5.27}$$

The approximation $\sigma_{P_e} \approx \sigma_{P_{wheel}}$ is reasonable since $\eta_{tf} \approx 1$ and saves calculation steps. It can be observed that the η_{tf} term was not included in the calculation. It is a great challenge to calculate the efficiency uncertainty. Additionally, this term is a gain function that amplifies the torque or power signal equally along their whole extension in order to compensate for the torque loss in transmission and differential. If the value of n_{tf} is incorrect, the proportions and shape of the curve is maintained and the proportional error is also maintained. However, this factor is useful when comparing two vehicles whose transmission efficiencies are known, because the effect of engine and transmission on fuel consumption can be isolated.

The results obtained for the studied vehicles for torque calculation uncertainties within a range of $\dot{v}$ and v at road grade of 0.01 rad are presented in Figure 5.36.

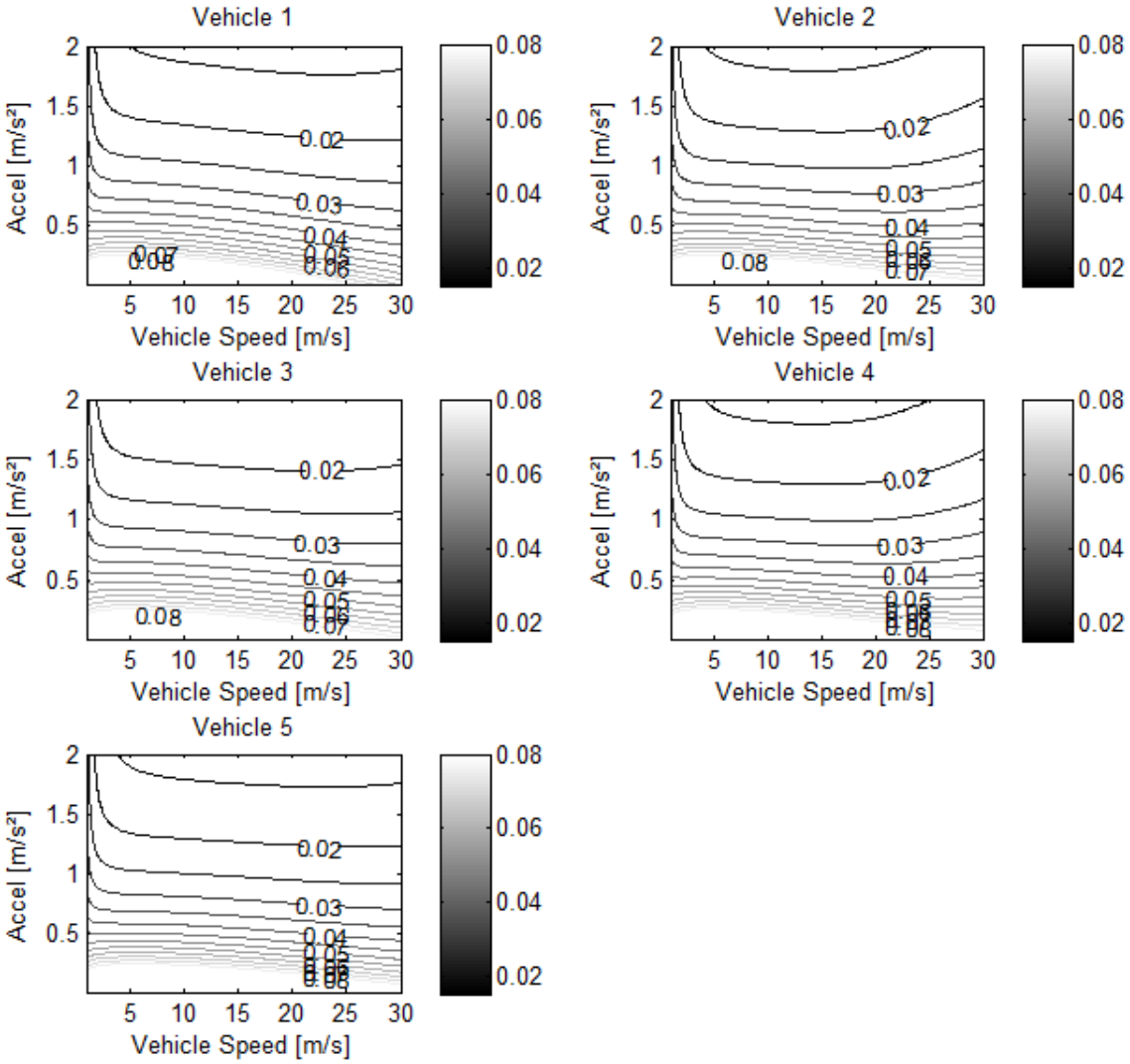

Figure 5.36 – Torque calculation uncertainties for $\theta = 0.01$ rad

The main conclusion that can be drawn from Figure 5.36 is that for higher levels of acceleration there is a general trend to reduce torque uncertainty. It is also a reasonable assumption to consider that $\sigma_{\tau_e} \leq 5\%$ for accelerations higher than 0.5 m/s². In order to comprehend how the engine torque uncertainty would be reduced by increasing accuracy and precision of acquired signals the torque uncertainty was calculated considering each individual measurement with zero uncertainty, and also considering that each of the power components introduced by Eq. 5.14 to Eq. 5.16 have no uncertainty in their calculations considering a speed of 10 m/s, an acceleration of 0.5 m/s² and a road grade of 0.06. The results are presented on Table 5.11 in the form of torque uncertainty reduction (as a percentage of total absolute uncertainty) by considering each parameter or power component as zero uncertainty.

Table 5.11 – Torque uncertainty reduction by eliminating measured parameters uncertainty for $v = 10\ \mathrm{m/s}$ and $\dot{v} = 0.05\ \mathrm{m/s^2}$

	$\sigma_v = 0$	$\sigma_{\dot{v}} = 0$	$\sigma_M = 0$	$\sigma_{f_0} = 0$	$\sigma_{f_2} = 0$	$\sigma_{p_{kin}} = 0$	$\sigma_{p_{res}} = 0$	$\sigma_{p_g} = 0$ $\sigma_\theta = 0$
Vehicle 1	0.0%	64.7%	0.0%	5.5%	0.2%	64.7%	5.7%	0.7%
Vehicle 2	0.0%	72.8%	0.0%	2.4%	0.7%	72.8%	3.1%	0.7%
Vehicle 3	0.0%	46.5%	0.0%	14.5%	0.2%	46.5%	14.9%	0.5%
Vehicle 4	0.0%	74.9%	0.0%	1.8%	0.6%	74.9%	2.5%	0.7%
Vehicle 5	0.0%	79.5%	0.0%	1.2%	0.1%	79.5%	1.4%	0.7%

It can be observed from Table 5.11 that the parameters that has higher contribution on torque uncertainty is acceleration (and, therefore, the kinetic power component), followed by f_0. The same study was made considering the same acceleration (0.5 m/s²) and a speed of 30 m/s (presented in Table 5.12).

Table 5.12 – Torque uncertainty reduction by eliminating measured parameters uncertainty for $v = 30\ \mathrm{m/s}$ and $\dot{v} = 0.05\ \mathrm{m/s^2}$

	$\sigma_v = 0$	$\sigma_{\dot{v}} = 0$	$\sigma_M = 0$	$\sigma_{f_0} = 0$	$\sigma_{f_2} = 0$	$\sigma_{p_{kin}} = 0$	$\sigma_{p_{res}} = 0$	$\sigma_{p_g} = 0$ $\sigma_\theta = 0$
Vehicle 1	0.1%	40.6%	0.0%	4.0%	14.7%	40.6%	19.5%	0.1%
Vehicle 2	0.0%	26.2%	0.0%	1.1%	30.7%	26.2%	32.5%	0.0%
Vehicle 3	0.0%	30.5%	0.0%	10.3%	15.5%	30.5%	28.0%	0.0%
Vehicle 4	0.0%	27.6%	0.0%	0.9%	29.6%	27.6%	31.0%	0.0%
Vehicle 5	0.0%	54.8%	0.0%	1.0%	9.6%	54.8%	10.7%	0.1%

In this condition acceleration is still the highest contributor to torque uncertainty, but the significance of f_2 contribution is highly increased, with highlight to vehicles 2 and 4, whose f_2 uncertainty contributes more to torque uncertainty than $\dot{v}$ uncertainty.

A final consideration in the calculation of engine torque is that Eq. 4.42 and Eq. 5.13 can be negative since the kinetic component and grade component can be negative. In these conditions, it means that the engine is delivering no net torque to the clutch and transmission; the engine operates in cut-off mode and no fuel is injected. For this reason, the calculated torque will be considered zero in these conditions (which is equivalent to say that the engine torque will be null whenever $P_{wheel} < 0$). The Eq. 4.42 is modified in order to account for this logical condition (Eq. 5.28):

$$\tau_e = \begin{cases} \dfrac{(M_e \cdot \dot{v} + f_0 + f_2 \cdot v^2 + W \cdot \sin\theta) \cdot r}{N_{tf} \cdot \eta_{tf}}, \tau_e > 0 \\ 0, \tau_e \leq 0 \end{cases} \quad (5.28)$$

An excerpt of engine torque calculation for vehicle 1 is presented on Figure 5.38.

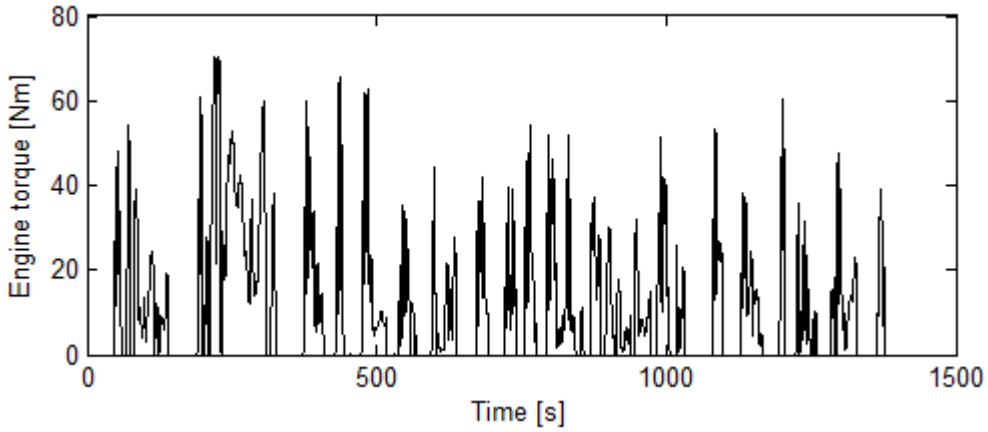

Figure 5.37 – Excerpt of calculated torque for vehicle 1

The detailed flow chart that shows all calculation steps to obtain the engine torque is presented on Figure 5.38.

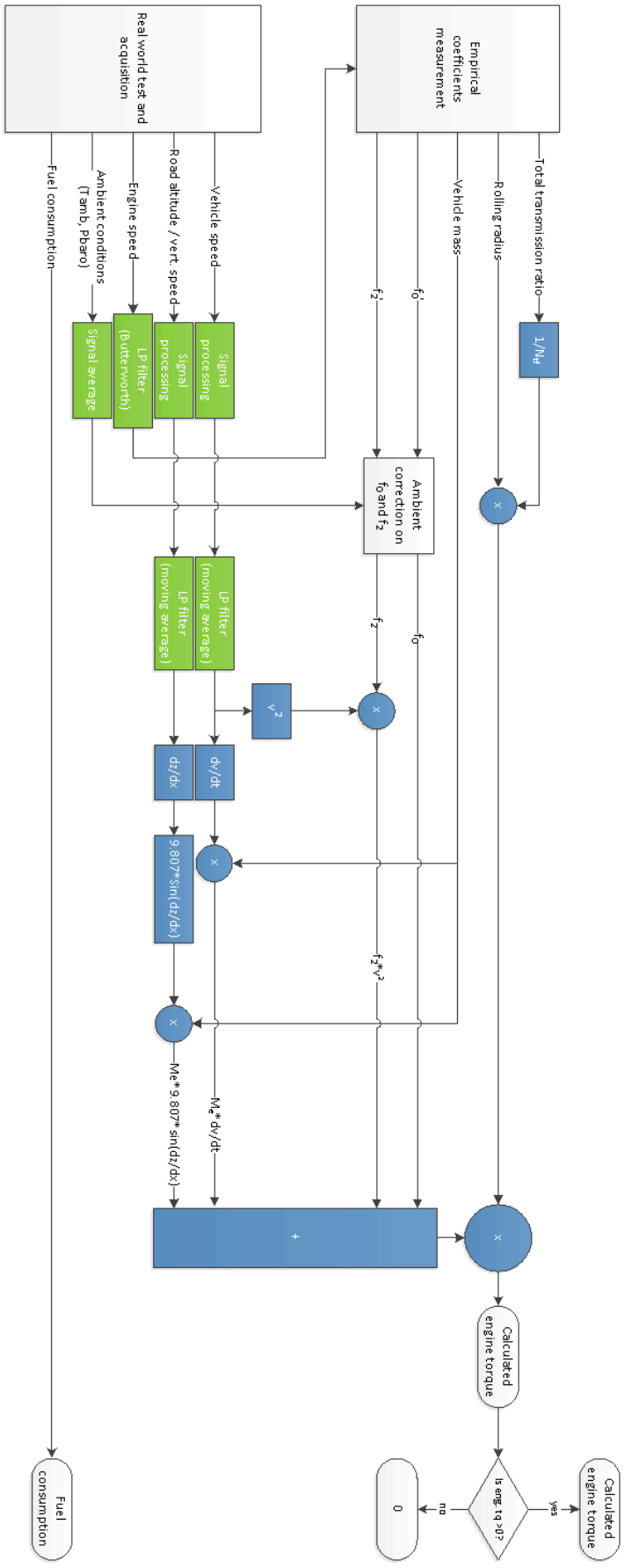

Figure 5.38 – Flowchart of the torque calculation procedure

6 ENGINE PERFORMANCE MAP MODEL DEVELOPMENT

In this section it will be presented a mathematical model used to describe the engine fuel consumption as a function of engine speed and engine torque. It will be presented the measurements done according to Section 5 and the corresponding map fitted to each of the measurements, as well as a comparison of fuel estimated using those maps in different measurements.

6.1 ENGINE FUEL CONSUMPTION MATHEMATICAL MODEL

The most common models used to describe the engine fuel consumption are polynomial models and neural network models. As presented in Section 3.4, there is great diversity of models that can be used for this purpose with satisfactory results. Therefore, the quality of the data used to fit or train the model is more important than the type of model used.

In this work, the model chosen is polynomial models. The reasons why this model was chosen are listed below:

- They are simple to comprehend and to implement, requiring low processing effort;
- They are parametric and the parameters may have physical meanings;
- They have presented correlation coefficient as high as neural networks and genetic programming approaches (as presented in Section 3.4).

The polynomial model is defined by the number of independent variables and the order of the polynomial. In this case, there are two independent variables (fuel consumption and engine torque). The order of the polynomial will be chosen between a second order polynomial, a third order polynomial and a fourth order polynomial. The generic equation for a two independent variables polynomial with order n is presented in Eq. 6.1:

$$f = a_{00} + \sum_{i,j=1}^{i+j=n} a_{ij} x^i y^j \tag{6.1}$$

High order polynomials often increase the correlation coefficient of the fit and reduce the residual errors (Rawlings, Pantula and Dickey, 1998). However, they have as side effect the appearance of wild oscillations, as presented by the authors in Figure 6.1:

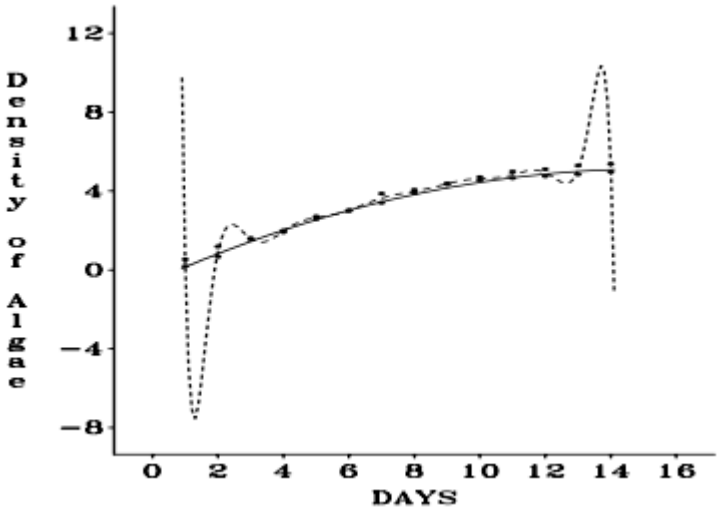

Figure 6.1 – Example of a data fitted with a second order polynomial (continuous line) and a 13th order polynomial (dotted line) (Rawlings, Pantula and Dickey, 1998)

The performance of the polynomial regression fit to describe an engine fuel map will be verified by comparing a fitted model to a measured map. The studied map is presented by Çay et al (2012). The engine speed, engine torque and fuel consumption is presented in Table 6.1:

Table 6.1 – Engine normalized values for ω_e, τ_e and absolute $\dot{m}_f$ (Çay et al, 2012)

	ω_e	τ_e	$\dot{m}_f$		ω_e	τ_e	$\dot{m}_f$		ω_e	τ_e	$\dot{m}_f$
	min^{-1}	Nm	g/s		min^{-1}	Nm	g/s		min^{-1}	Nm	g/s
1	0.1	0.1	0.100	20	0.3	0.2	0.184	38	0.6	0.2	0.317
2	0.1	0.2	0.120	21	0.3	0.3	0.233	39	0.6	0.3	0.402
3	0.1	0.3	0.152	22	0.3	0.4	0.249	40	0.6	0.4	0.539
4	0.1	0.4	0.164	23	0.3	0.5	0.260	41	0.6	0.5	0.607
5	0.1	0.5	0.181	24	0.3	0.6	0.300	42	0.6	0.6	0.642
6	0.1	0.6	0.191	25	0.3	0.7	0.352	43	0.6	0.7	0.711
7	0.1	0.7	0.212	26	0.3	0.8	0.389	44	0.6	0.8	0.776
8	0.1	0.8	0.244	27	0.3	0.9	0.405	45	0.8	0.1	0.361
9	0.1	0.9	0.272	28	0.5	0.1	0.162	46	0.8	0.2	0.470
10	0.2	0.1	0.113	29	0.5	0.2	0.315	47	0.8	0.3	0.553
11	0.2	0.2	0.138	30	0.5	0.3	0.404	48	0.8	0.4	0.684
12	0.2	0.3	0.186	31	0.5	0.4	0.471	49	0.8	0.5	0.747
13	0.2	0.4	0.187	32	0.5	0.5	0.503	50	0.8	0.6	0.900
14	0.2	0.5	0.210	33	0.5	0.6	0.573	51	0.9	0.1	0.545
15	0.2	0.6	0.220	34	0.5	0.7	0.621	52	0.9	0.2	0.675
16	0.2	0.7	0.258	35	0.5	0.8	0.643	53	0.9	0.3	0.734
17	0.2	0.8	0.293	36	0.5	0.9	0.671	54	0.9	0.4	0.765
18	0.2	0.9	0.331	37	0.6	0.1	0.238	55	0.9	0.5	0.861
19	0.3	0.1	0.123								

Although the engine data presented in Table 6.1 are normalized for engine torque and engine speed, the polynomial fit is still valid since the proportions are maintained. The data was fitted with a second order, third order and fourth order polynomial. The coefficients obtained for each fit with 95% confidence bounds are presented in Table 6.2:

Table 6.2 – Polynomial fit coefficients for data presented in Table 6.1

2nd order polynomial

Coefficient	Value	95% Conf. bounds
a00	0.0585	(-0.006253,0.1233)
a10	-0.0720	(-0.2771,0.1331)
a01	0.2178	(0.01396,0.4217)
a20	0.4888	(0.3128,0.6649)
a11	1.0160	(0.8319,1.2)
a02	-0.1346	(-0.3104,0.04113)

3rd order polynomial

Coefficient	Value	95% Conf. bounds
a00	0.1502	(0.01674,0.2837)
a10	-0.7723	(-1.503,-0.04137)
a01	0.0467	(-0.6482,0.7417)
a20	1.5400	(0.2006,2.88)
a11	2.5310	(1.086,3.977)
a02	-0.2712	(-1.583,1.04)
a30	-0.4600	(-1.249,0.3292)
a21	-1.0840	(-2.081,-0.08763)
a12	-0.7077	(-1.619,0.2036)
a03	0.2292	(-0.5726,1.031)

4th order polynomial

Coefficient	Value	95% Conf. bounds
a00	0.0456	(-0.18,0.2713)
a10	-0.3250	(-2.081,1.431)
a01	0.9023	(-0.7968,2.601)
a20	1.5340	(-3.696,6.763)
a11	-0.1652	(-6.07,5.74)
a02	-2.6110	(-7.815,2.592)
a30	-2.8780	(-9.63,3.875)
a21	5.1560	(-3.229,13.54)
a12	0.8019	(-7.138,8.742)
a03	3.2010	(-3.646,10.05)
a40	2.3650	(-0.8073,5.537)
a31	-5.1800	(-9.108,-1.253)
a22	1.0170	(-3.887,5.922)
a13	-1.9780	(-5.661,1.705)
a04	-1.0990	(-4.327,2.129)

The parameters used to indicate the quality of the fit are the correlation coefficient (R^2), the square sum of errors (SSE) and the root mean square error ($RMSE$). According to Rawlings, Pantula and Dickey (1998), the $RMSE$ is a measure of the standard deviation of the differences between predicted and observed values. SSE is a measure of the distance between predicted and observed values. The R^2 is the proportion of the sum of squares that are

explained by the model with relation to the total sum of squares. A model that explains perfectly the observed data has a $R^2 = 1$, $RMSE = SSE = 0$.

The quality parameters for the polynomial fits presented in Table 6.2 are presented on Table 6.3:

Table 6.3 – Quality parameters for polynomial fits presented in Table 6.2

	R^2	SSE	$RMSE$
2nd order	0.9762	0.0973	0.0348
3rd order	0.9788	0.0869	0.0347
4th order	0.9922	0.0318	0.0218

It can be seen that the correlation coefficient increases with the order of the polynomial, while both $RMSE$ and SSE decreases. However, all of the models present high correlation coefficient, and the second order polynomial (simpler implementation, less time required for coefficient determination) is suitable enough for the purposes of this work. The fuel maps generated by the regressions in Table 6.2 are presented in Figure 6.2, Figure 6.3 and Figure 6.4:

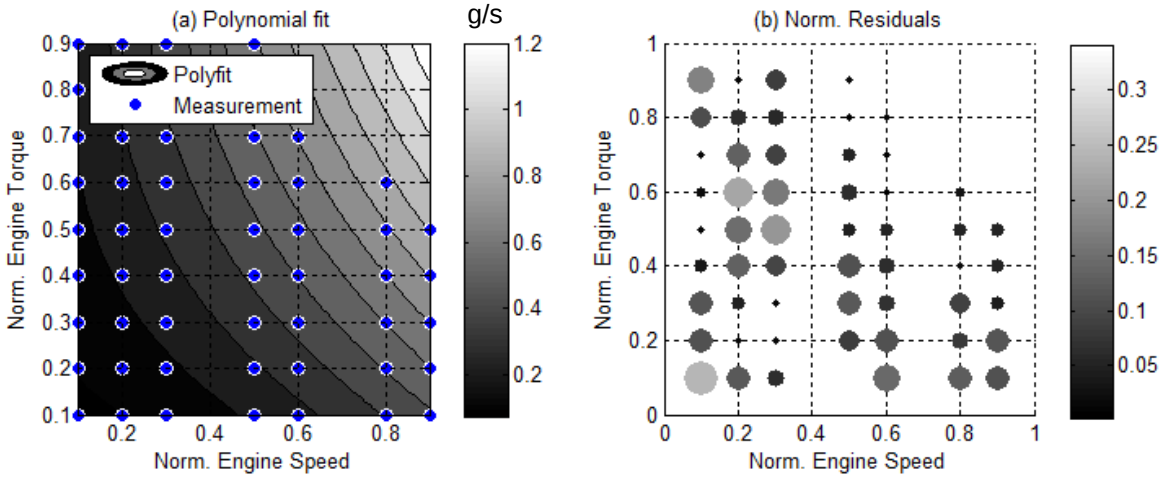

Figure 6.2 – Fuel map generated by 2nd order polynomial fit

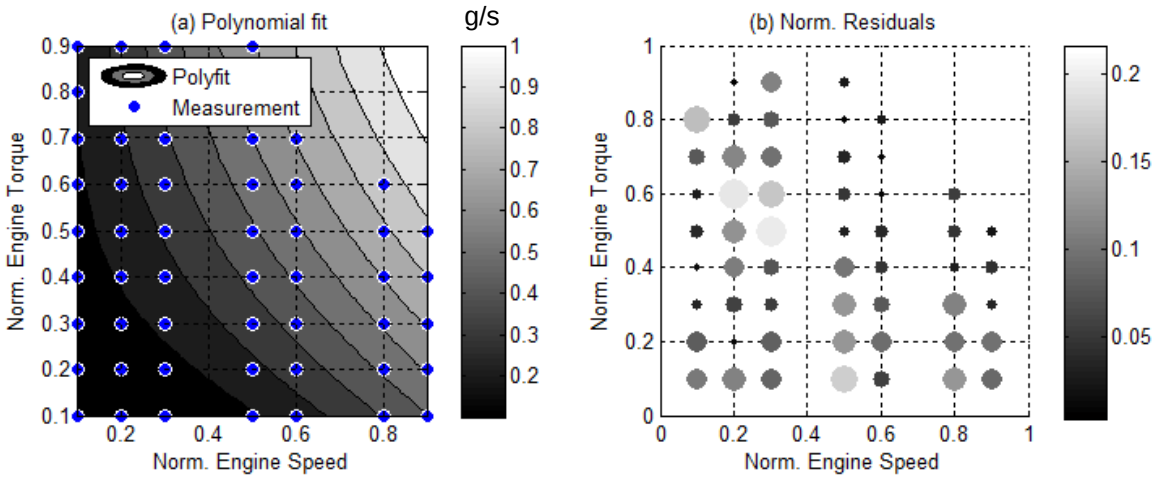

Figure 6.3 – Fuel map generated by 3rd order polynomial fit

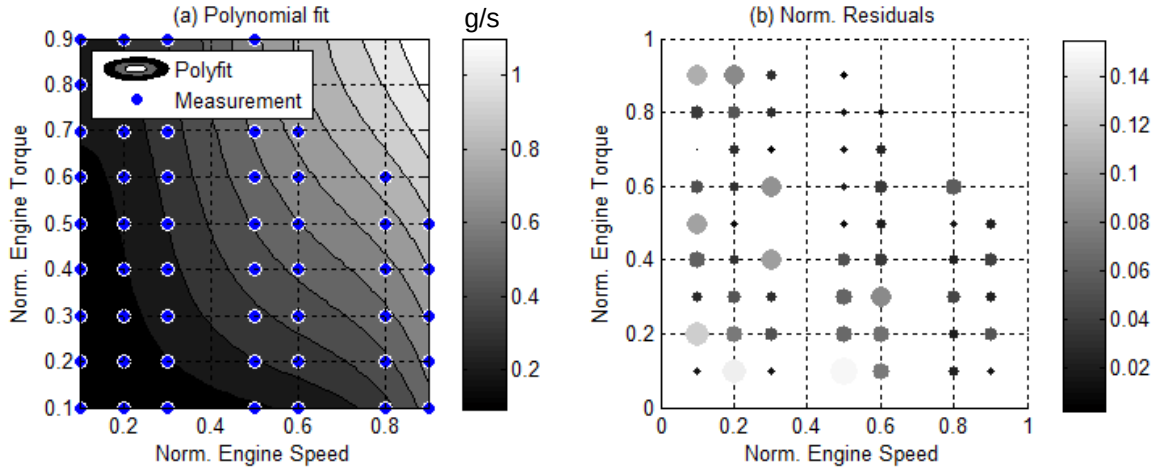

Figure 6.4 – Fuel map generated by 4th order polynomial fit

The absolute and normalized residuals histograms for each of the polynomial regressions are presented in Figure 6.5, Figure 6.6 and Figure 6.7. It can be seen that the maximum and minimum errors are closer to zero for the 4th order polynomial fit. Another important aspect to be considered is if the normalized residuals follow a specific trend. It can be seen that not trend is observed from chart (b) in Figure 6.5, Figure 6.6 and Figure 6.7, which contributes to the conclusion that the errors are random and not systemic.

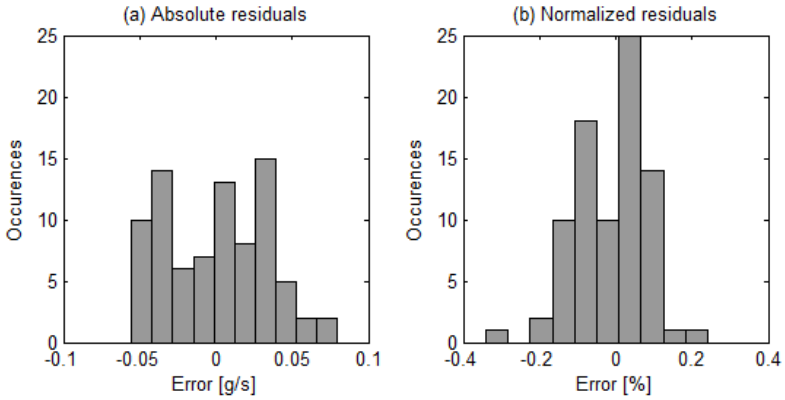

Figure 6.5 – (a) Absolute and (b) normalized error histogram for the 2nd order polynomial regression

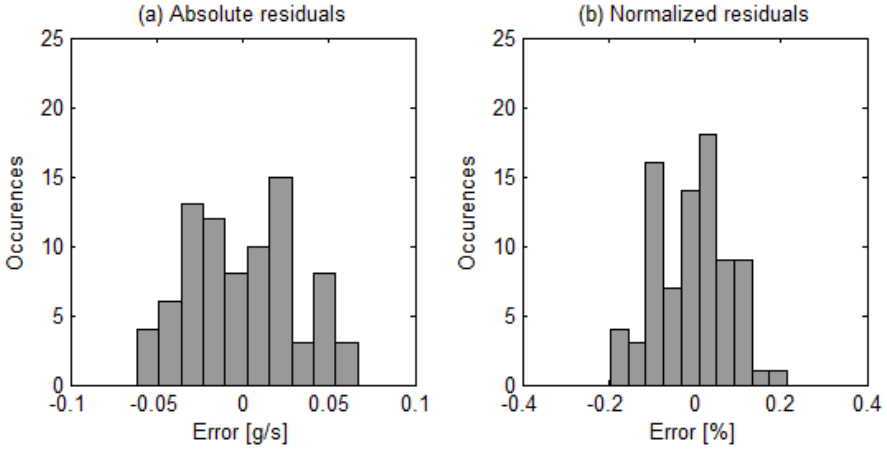

Figure 6.6 – (a) Absolute and (b) normalized error histogram for the 3rd order polynomial regression

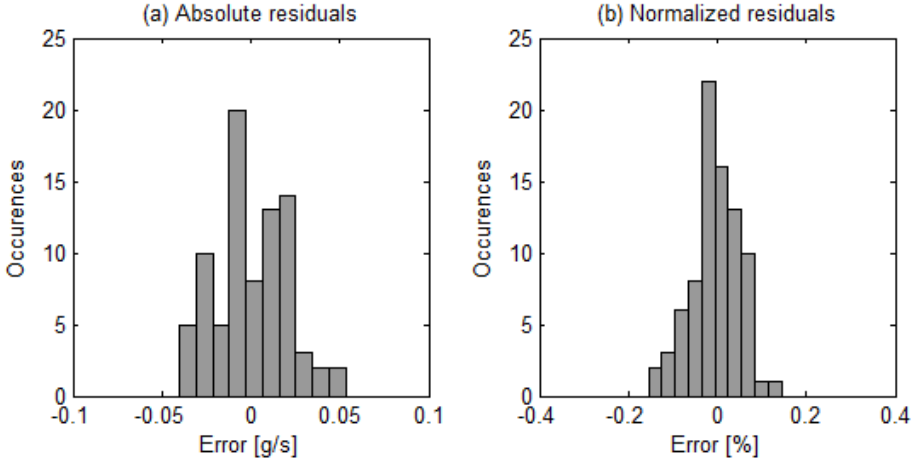

Figure 6.7 – (a) Absolute and (b) normalized error histogram for the 4th order polynomial regression

In order to properly evaluate the order of the polynomial the F-test is used. The F-test is used to test the null hypothesis of a combination of polynomial coefficients are zero (Rawlings, Pantula and Dickey, 1998). This test compares the calculated F-statistic for the regressions that are being analyzed against the F-distribution for the set of tests. Assuming, for example, that a fourth order polynomial is an adequate fit, a test is made to check if reducing the order of the polynomial would still be adequate. The F-test equation is presented in Eq. 6.2:

$$F_{test} = \frac{(SSE_{red} - SSE_{full})/(k - 1 - q)}{SSE_{full}/\ (\sum n_i - k)} \tag{6.2}$$

Where SSE_{red} is the sum of square errors for the reduced order polynomial, SSE_{full} is the sum of square errors for the full order polynomial, $k - 1$ is the order of the full polynomial, q is the order of the reduced polynomial and $\sum n_i$ is the number of measurements. For example, to understand if it is reasonable to reduce the order of the polynomial from fourth to third it must be assumed that all terms a_{ij} with higher order than 3 are zero: $a_{ij}(i + j > 3) = 0$. This is considered as the null hypothesis, i. e., the hypothesis under proof. To accept or reject this hypothesis the F-ratio calculated using Eq. 6.2 is compared against the F-distribution for the degrees of freedom considered in the analysis. In the present case, $SSE_{red} = 0.0521$, $SSE_{full} = 0.0313$, $k - 1 = 14$ (the fourth order polynomial has 15 coefficients counting the constant coefficient), $q = 9$ (the third order polynomial has 10 coefficients counting the constant coefficient), $\sum n_i = 82$. Therefore,

$$F_{test} = \frac{(0.0869 - 0.0318)/(5)}{0.0318/\ (82 - 15)} = 23.218$$

The F-distribution parameters to compare are presented in Eq. 6.3:

$$F_{test_{(\alpha;k-1-q,\sum n_i-k)}} \tag{6.3}$$

Where α is the confidence interval unitary complement (it is a common practice to consider 95% confidence interval, therefore, $\alpha = 5\%$). If the F calculated is larger than F-distribution, the hypothesis must be rejected, i. e., $a_{ij}(i + j > q) \neq 0$. In the present case, the F-distribution is given by $F_{test_{(0.05;5,67)}} = 6.256$. Hence, as $F_{test} = 23.218$ the hypothesis is rejected, which means that the terms of order higher than 3 are important to the estimative. Comparing a reduction from order 4 to order 2, $F_{test} = 15.334$ and $F_{test_{(0.05;9,67)}} = 3.388$ and the hypothesis is also rejected. Reducing from order 3 to order 2 presents a different results, with $F_{test} = 2.154$ and $F_{test_{(0.05;4,72)}} = 9.117$ which means that the hypothesis is accepted. This occurs because the SSE of third order polynomial is just a little smaller than

the SSE of the second order polynomial. However, as it was once rejected the hypothesis of a third order polynomial, the fourth order polynomial. The comparison of a fifth order polynomial against a fourth order polynomial gives the following result: $F_{test} = 3.248$ and $F_{test_{(0.05;6,61)}} = 4.950$. Therefore, the fourth order polynomial presents the best of the alternatives to describe the measured data.

The equation proposed for this model is presented in Eq. 6.1a:

$$\begin{aligned} f = {} & 0.046 - 0.325\omega_e + 0.902\tau_e + 1.534\omega_e^2 - 0.156\tau_e\omega_e - 2.611\tau_e^2 - 2.878\omega_e^3 \\ & + 5.156\omega_e^2\tau_e + 0.802\omega_e\tau_e^2 + 3.201\tau_e^3 + 2.356\omega_e^4 - 5.180\omega_e^3\tau_e \\ & + 1.017\omega_e^2\tau_e^2 - 1.978\omega_e\tau_e^3 - 1.099\tau_e^4 \end{aligned} \quad (6.1a)$$

6.2 ENGINE FUEL CONSUMPTION MAPS FOR STUDIED VEHICLES

This section presents the results of the measurements applied to the mathematical model presented in Section 6.1. Two measurements per vehicle were made, and they will be presented in the same form of the engine model used for the definition of the mathematical model.

In order to avoid the regions in which the engine is not working in stoichiometric condition, it will only be considered engine speeds above a certain threshold, as well as for engine torque. The threshold used is idle engine speed plus 150 RPM in order to avoid oscillations and 5 Nm of torque in order to avoid torques close to 0 Nm which causes large relative errors due to low absolute value of torque.

The fuel consumption map presented on Figure 6.8 was measured on vehicle 3. It can be seen a huge amount of points used for the measurement, which is an essential characteristic of a real-world measurement at high sampling frequency (in this case, 10 Hz).

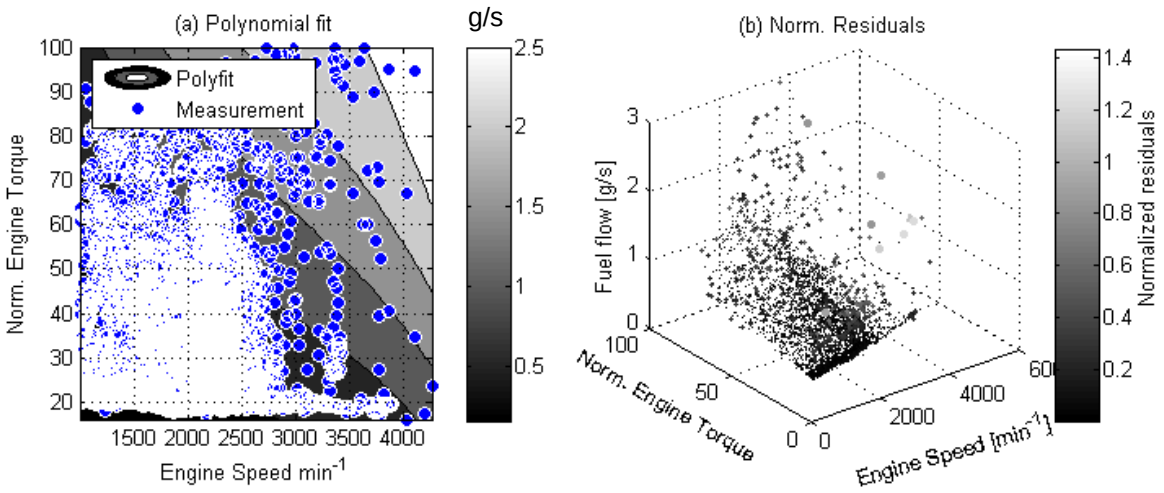

Figure 6.8 – Fuel consumption map measured for Vehicle 3

The R^2 for this measurement is 0.8424 and the SSE is 81.626. The histogram distribution of the residuals is presented in Figure 6.9:

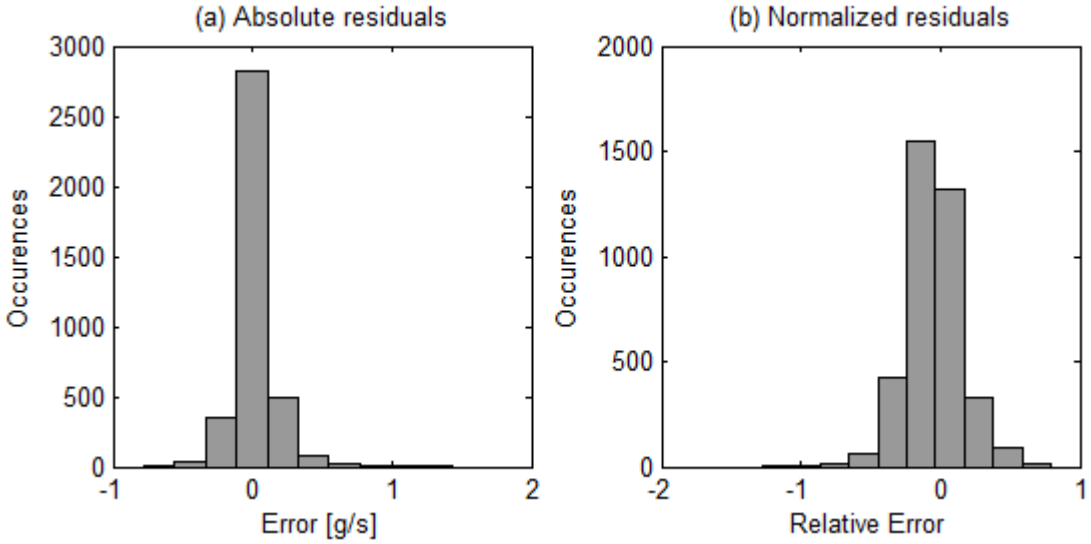

Figure 6.9 – Distribution of residuals for engine fuel map model presented in Figure 6.8

It can be seen that the residuals are centered in zero, which means that there is no bias in the fuel consumption calculation. However, the relative residuals are relatively high, with part of the residuals being higher than the magnitude of the fuel flow itself. The analysis of the empirical cumulative distribution () function with 5% bounds shows that 90% of the residuals are within [-0.32,0.30].

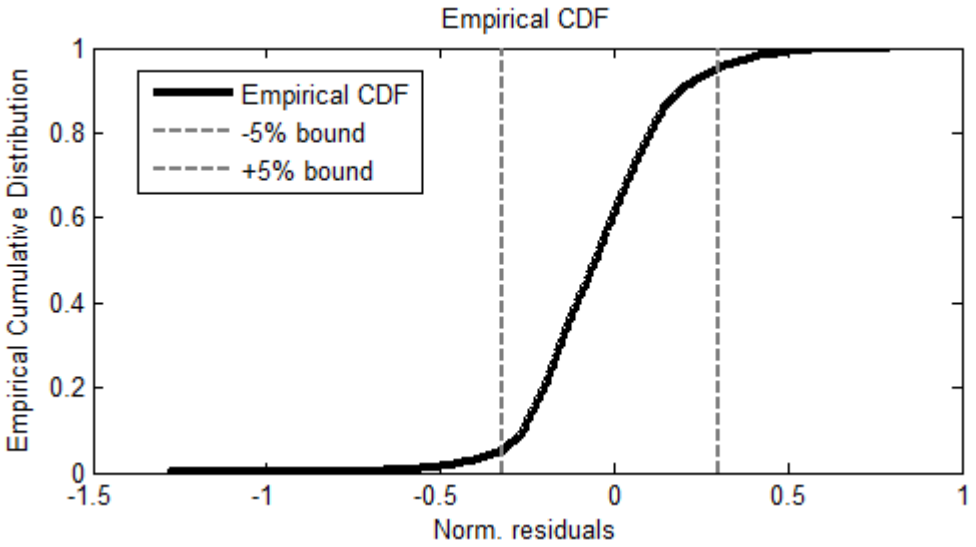

Figure 6.10 – Empirical Cumulative Distribution Function of residuals of the polynomial regression presented in Figure 6.8

Applying the fuel map regression obtained for the measured engine speed and torque calculation, one can calculate the instantaneous fuel consumption. This calculated fuel consumption can be compared with the measured fuel consumption. The result is presented in Figure 6.11.

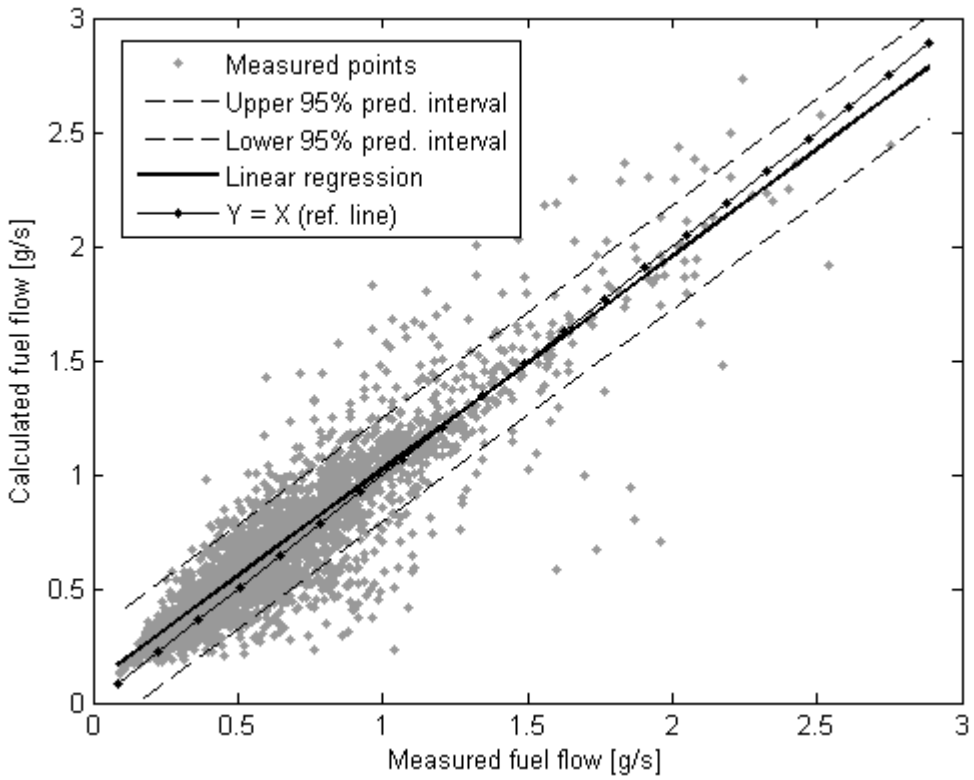

Figure 6.11 – Calculated versus measured fuel flow with 95% confidence interval

It can be observed that although there is high variation in normalized residuals, the linear trend between calculated and measured fuel consumption is close to $y = x$ line, which indicates a perfect correlation between measured and calculated signals. The total measured fuel consumed versus the total calculated fuel consumption is presented in Figure 6.12:

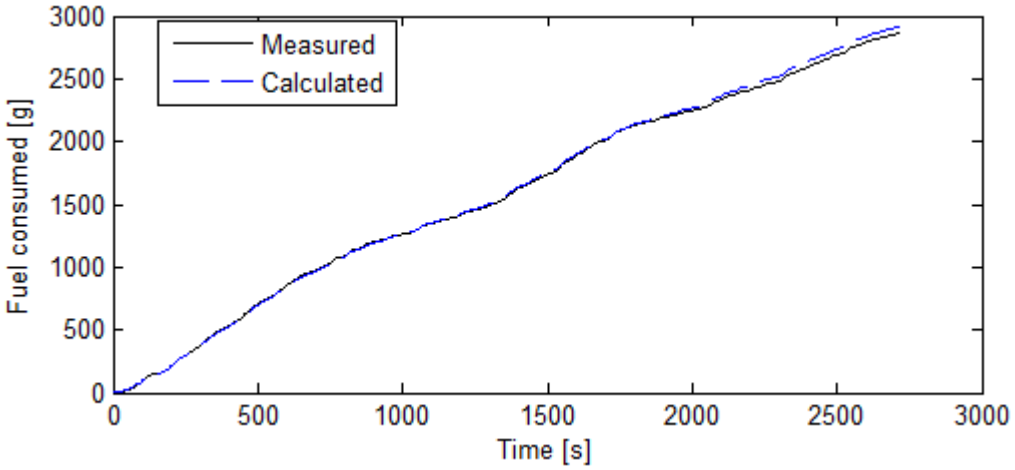

Figure 6.12 – Total measured fuel consumed versus total calculated fuel consumed

The total measured fuel consumed is 2860 g, and the total calculated fuel consumption is 2911 g, and therefore, the total relative error is 1.78%. The results for each measurement and for each vehicle will be reported by showing the polynomial coefficients and a chart of fuel map and the calculated versus measured instantaneous fuel flow.

The fuel map coefficients for measurements of vehicles 1 to 3 are presented in Table 6.4:

Table 6.4 – Coefficients of polynomial regression for vehicles 1 to 3

	Vehicle 1		Vehicle 2		Vehicle 3	
Coefficient	Run 1	Run 2	Run 1	Run 2	Run 1	Run 2
a00	-7.666E-02	-3.416E-01	-1.068E+00	-9.544E-01	-1.672E-01	1.553E+00
a10	4.340E-04	9.349E-04	4.644E-03	1.248E-03	-2.987E-04	-1.452E-03
a01	-2.984E-03	2.071E-02	-4.554E-02	4.279E-02	3.363E-02	-7.502E-02
a20	-1.726E-07	-4.886E-07	-4.997E-06	-1.164E-06	5.106E-07	4.417E-07
a11	6.120E-06	-1.554E-05	4.767E-05	3.147E-06	-1.336E-05	6.147E-05
a02	1.970E-04	-4.651E-04	7.126E-04	-1.007E-03	-7.078E-04	1.260E-03
a30	2.758E-11	1.024E-10	1.909E-09	4.144E-10	-1.975E-10	-4.735E-11
a21	6.151E-10	6.799E-09	-3.831E-09	5.502E-09	3.404E-09	-8.821E-09
a12	-1.938E-07	2.211E-07	-4.619E-07	-3.904E-08	3.437E-07	-6.134E-07
a03	3.598E-06	7.480E-06	-3.475E-06	1.106E-05	4.176E-06	-1.011E-05
a40	-6.781E-17	-5.087E-15	-2.500E-13	-5.498E-14	2.459E-14	6.211E-15
a31	-1.984E-13	-7.683E-13	1.048E-12	-1.164E-13	-1.251E-13	-6.909E-13
a22	2.844E-11	-4.058E-11	-6.140E-11	-4.112E-11	-3.682E-11	1.143E-10

a13	1.090E-09	2.061E-10	4.301E-09	1.073E-09	-1.267E-09	7.236E-10
a04	-6.097E-08	-7.132E-08	-2.419E-08	-5.209E-08	-3.269E-09	4.470E-08

The coefficients for vehicles 4 and 5 are presented in Table 6.5:

Table 6.5 – Coefficients of polynomial regression for vehicles 4 and 5

	Vehicle 4		Vehicle 5	
Coefficient	Run 1	Run 2	Run 1	Run 2
a00	-2.067E+00	-1.613E+00	-8.103E-01	-1.248E+00
a10	5.974E-03	4.246E-03	1.494E-03	2.567E-03
a01	2.345E-02	6.632E-02	2.104E-02	3.900E-02
a20	-5.521E-06	-3.361E-06	-1.163E-06	-2.279E-06
a11	-6.265E-06	-5.209E-05	1.162E-05	4.847E-07
a02	-5.704E-04	-1.394E-03	-4.935E-04	-1.226E-03
a30	2.169E-09	1.150E-09	2.215E-10	6.828E-10
a21	-9.219E-10	2.292E-08	1.161E-08	2.110E-08
a12	3.891E-07	3.795E-07	-1.956E-07	-1.893E-07
a03	1.566E-06	1.629E-05	5.737E-06	1.858E-05
a40	-2.937E-13	-1.380E-13	1.483E-14	-3.252E-14
a31	4.119E-13	-4.219E-12	-4.206E-12	-7.449E-12
a22	-7.521E-11	9.333E-12	9.484E-11	1.080E-10
a13	-1.152E-10	-2.520E-09	-1.061E-09	-1.217E-09
a04	-1.352E-09	-6.036E-08	-8.670E-09	-7.834E-08

Table 6.6 presents an analysis of the quality parameters for the polynomial regression for all vehicles and measurements. It can be seen that minimum $R^2 = 0.797$ and for vehicles 1, 2 and 5 the minimum R^2 is 0.913, which is a very good correlation coefficient. The terms $\dot{mf}_c$, $\dot{mf}_m$ and $\Delta_{m/c}$ are, respectively, the calculated fuel flow, the measured fuel flow and the relative delta between them. It is important to observe that all measurements are lower than 4% and, with the exception of the vehicle 3, all vehicles present this delta lower than 0.2%.

Table 6.6 – Regression quality parameters for the polynomial regression

	Vehicle 1		Vehicle 2		Vehicle 3		Vehicle 4		Vehicle 5	
	Run 1	Run 2	Run 1	Run 2	Run 1	Run 2	Run 1	Run 2	Run 1	Run 2
SSE	33.63	12.14	179.92	241.33	81.63	237.74	67.10	26.65	22.78	9.01
R^2	0.9687	0.9859	0.9133	0.9391	0.8424	0.7973	0.7972	0.8992	0.9968	0.9959
$RMSE$	0.082	0.040	0.218	0.216	0.147	0.319	0.139	0.095	0.068	0.043
$\sum \dot{mf}_c [g]$	2896	6268	4856	5799	2911	2279	1278	1182	8383	4048
$\sum \dot{mf}_m [g]$	2895	6270	4854	5798	2860	2192	1276	1184	8383	4048
$\Delta_{m/c}$	0.03%	-0.03%	0.04%	0.02%	1.78%	3.97%	0.16%	-0.17%	0.00%	0.00%

g/s

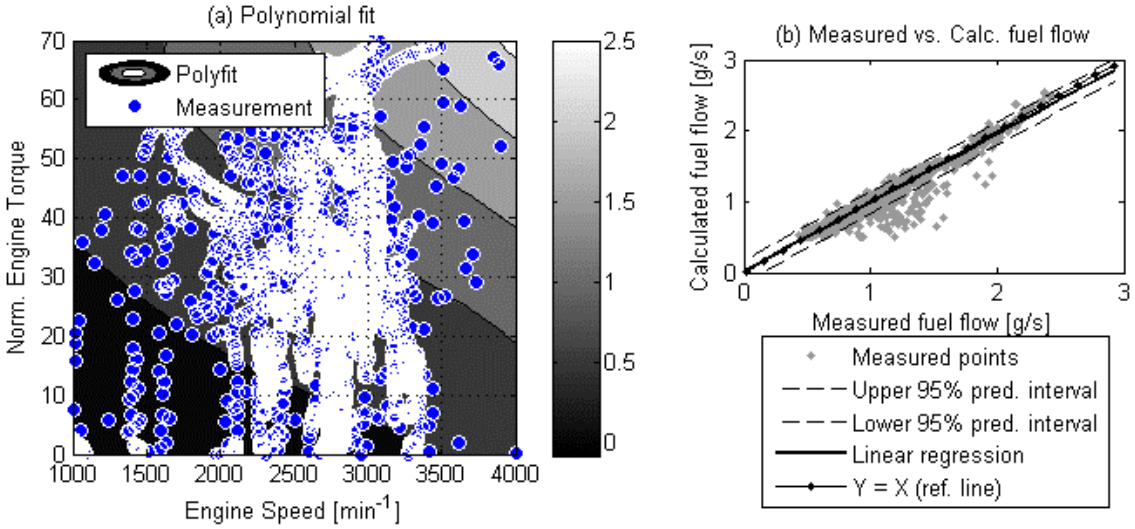
(a) Polynomial fit
Polyfit
Measurement
Norm. Engine Torque
Engine Speed [min-1]
(b) Measured vs. Calc. fuel flow
Calculated fuel flow [g/s]
Measured fuel flow [g/s]
Measured points
Upper 95% pred. interval
Lower 95% pred. interval
Linear regression
Y = X (ref. line)

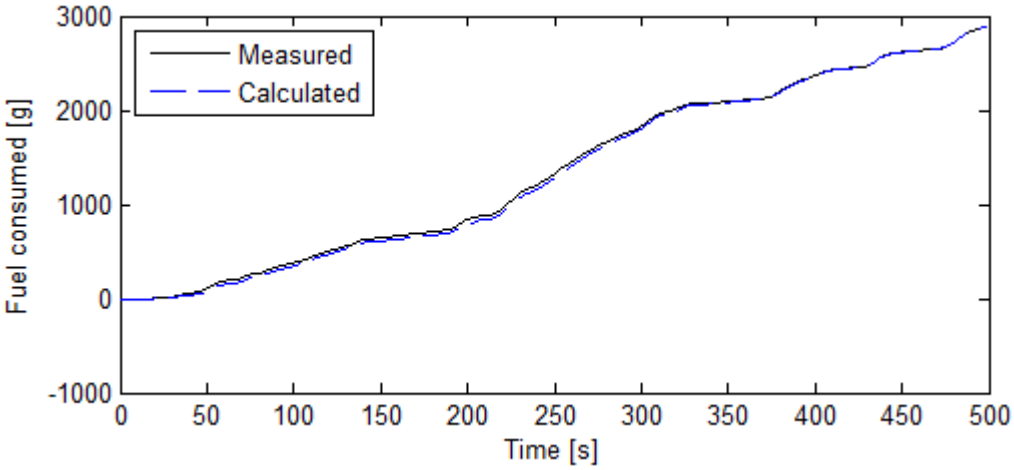
Measured
Calculated
Fuel consumed [g]
Time [s]

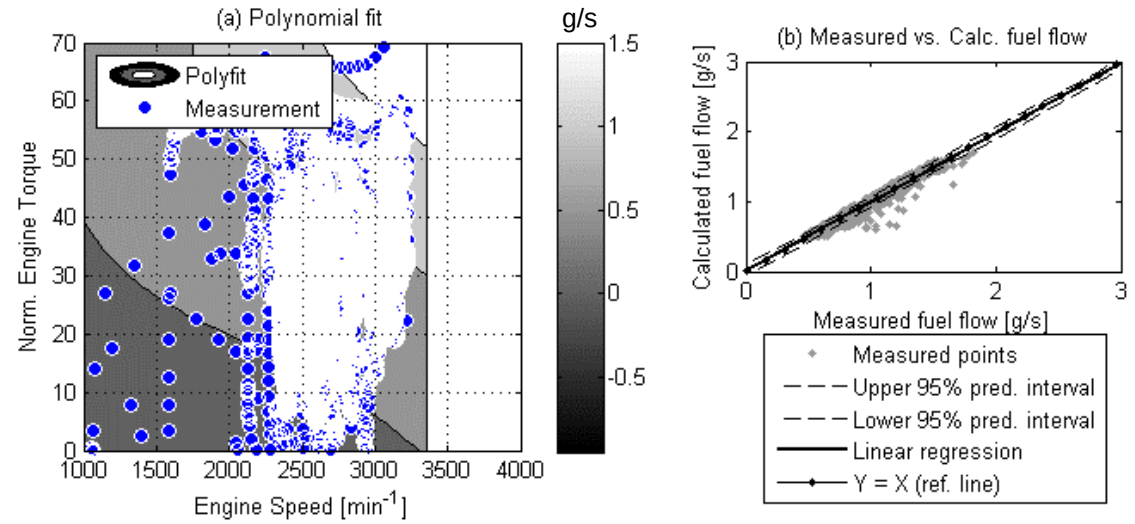
(a) Polynomial fit
g/s
Polyfit
Measurement
Norm. Engine Torque
Engine Speed [min-1]
(b) Measured vs. Calc. fuel flow
Calculated fuel flow [g/s]
Measured fuel flow [g/s]
Measured points
Upper 95% pred. interval
Lower 95% pred. interval
Linear regression
Y = X (ref. line)

7 CONCLUSION

In this work it was presented a methodology for using GPS and OBD-II signals to calculate the engine operating conditions and fuel consumption. A broad literature review was presented, showing a diversity of models used to describe the fuel consumption of an engine, real world measuring and laboratory fuel consumption measurements. A model for modeling the fuel consumption as a function of engine speed and engine torque is proposed and validated. Experimental results for five different vehicles are presented and the fuel consumption calculated through the engine model proposed is compared against measured fuel consumption.

It was showed from the literature review that most of the engine fuel consumption models present satisfactory results if the problem is correctly stated and the input data is reliable. That information permitted the use a mathematical model as simple as a two variable polynomial regression to describe the engine fuel consumption as a function of engine torque and engine speed.

The combination of GPS speed with OBD-II speed can provide reliable speed information. The speed is an important input data for engine torque calculation and a useful signal to cross check the engine speed signal due to the linear relationship of these signals when the vehicle is with clutch engaged.

It was presented a methodology to avoid possible error states and undesired operating conditions, such as cold engine coolant temperature, cold tires, fuel enrichment, low distance driven and speeds above tire constant behavior of the rolling resistance coefficient.

An important contribution of the present work is the breakdown of uncertainty propagation of individual parameters uncertainty to engine torque calculation. The conclusion of this study is that the greatest contributor to torque uncertainty is the acceleration (which is calculated through speed signal) for low and moderate speeds (lower than 30 m/s), while the quadratic coefficient of the resistive force regression has as much influence of acceleration on torque uncertainty for high speeds (higher than 30 m/s). The total uncertainty for calculated engine torque using a similar equipment of this work is smaller than 5% for acceleration levels greater than 0.5 m/s^2.

The combination of signal quality enhancing techniques with high accuracy equipment lead to high level of correlation coefficient for the polynomial regression models (in a range varying from 0.797 to 0.997, depending on the vehicle) and a good accuracy for fuel consumption estimation, presenting errors lower than 4% in all studied cases.

The methodology proposed was proven robust, being tested in five different vehicles, in different test routes, presenting repeatedly consistent results, and is able to be used in several applications, such as product development activities, engines efficiency comparison, optimization studies such as shift schedule and final drive ratio optimization.

REFERENCES

ABNT. 2014. *NBR 10312:2014.* 2014.

—. 2012. *NBR 6601:2012.* 2012.

Ahlawat, R., J., Bredenbeck and Ichige, T. 2013. Estimation of road load parameters via on-road vehicle testing. *Tire Technology Expo.* Cologne, Germany, 2013.

Ahn, K. 1998. *Microscopic fuel consumption and modeling.* Blacksburg, VI : Virginia Polytechnic Institute and State University, 1998.

Akcelik, R. 1989. Efficiency and Drag in the Power-Based Model of Fuel Consumption. *Transportation Research, Part B.* 23, 1989, Vol. 5, 375-385.

Alessandrini, A., Filippi, F. and Ortenzi, F. 2012. Consumption calculation of vehicles using OBD data. Tampa, FL : International Emission Inventory Conference: Session 8, 2012.

An, F., Earley, R. and Green-Weiskel, L. 2011. *Global overview on fuel efficiency and motor vehicle emission standards: policy options and perspectives for international cooperation.* Beijing, Los Angeles and New York : United Nations. Department of Economic and Social Affairs. Commission on Sustainable Development. The Innovation Center for Energy and Transportation, 2011. CSD19/2011/BA3.

André, M., et al. 2006. Real-world European driving cycles, for measuring pollutant emissions from high- and low-powered cars. *Atmospheric Environment.* 40, 2006, p.5944-5953.

Ashgriz, N. and Mostaghimi, J. 2002. An Introduction to Computational Fluid Dynamics. [book auth.] J. Saleh. *Fluid Flow Handbook.* s.l. : Mc Graw-Hill Professional, 2002.

Bae, H., Ryu, J. and Gerdes, J. 2001. Road Grade and Vehicle Parameter Estimation for Longitudinal Control Using GPS. *IEEE Conference on Intelligent Transportation Systems, Proceedings, ITSC.* 2001, p. 166-171.

Barth, M., et al. 1996. *Modal emission modeling: a physical approach.* s.l. : Transportation Research Record 1520, 1996.

Benajesa, J., et al. 2016. Optimization of the combustion system of a medium duty direct injection diesel engine by combining CFD modeling with experimental validation. *Energy Conversion and Management.* 2016, Vol. 110, p. 212-229.

Bevington, P. R. and Robinson, D. K. 2003. *Data Reduction and Error Analysis for the Physical Sciences.* New York : McGraw-Hill, 2003. ISBN 0-07 247227-8.

Birrell, S., et al. 2014. Analysis of three independent real-world driving studies: A data driven and expert analysis approach to determining parameters affecting fuel economy. *Transportation Research: Part D.* 2014, Vol. 33, p. 74-86.

Blagojević, I., et al. 2012. A Model for Gear Shifting Optimization in Motor Vehicles. *Transactions of FAMENA - XXXVI-2.* ISSN: 1333-1124, 2012.

Bonnel, P., Kubelt, J. and Provenza, A. 2011. Heavy-duty engines conformity testing based on PEMS. *European Commission: Joint Research Centre.* ISBN: 978-92-79-21039-6, 2011.

Bosgra, O. H. 2010. *Physical Modelling for Systems and Control.* Delft : Delft University of Technology, 2010.

Brinkman, N., et al. 2005. *Well-to-Wheels analysis of advanced fuel/vehicle systems — a North American study of energy use, greenhouse gas emissions, and criteria pollutant emissions.* Washington, DC : Office of Energy Efficiency & Renewable Energy, 2005.

Cay, Y. 2013. Prediction of a gasoline engine performance with artificial neural network. *Fuel.* 111, 2013, 324-331.

Çelik, V. and Arcaklioglu, E. 2005. Performance maps of a diesel engine. *Applied Energy.* 81, 2005, p. 247-259.

Chakraborty, A., Roy, S. and Banerjee, R. 2016. An experimental based ANN approach in mapping performance-emission characteristics of a diesel engine operating in dual-fuel mode with LPG. *Journal of Natural Gas Science and Engineering.* 28, 2016, p. 15-30.

Cheikh, K., et al. 2016. Experimental assessment of performance and emissions maps for biodiesel fueled compression ignition engine. *Applied Energy.* 1, 2016, Vol. 161, p. 320-329.

Chiara, F. and Canova, Marcello. 2013. A review of energy consumption, management and recovery in automotive systems with considerations on future trends. *Proceedings of the Institution of Mechanical Engineers Part D Journal of Automobile Engineering.* 6, 2013, Vol. 22, p. 914-936.

Clark, S. K. and Dodge, R. N. 1979. *A Handbook for the Rolling Resistance of Pneumatic Tires.* Ann Arbor, MI : Institute of Science and Technology, University of Michigan, 1979.

Clark, S. K. 1978. Rolling Resistance of Pneumatic Tires. *Tire Science and Technology.* TSTCA, 1978, Vol. 6, 3.

Crolla, D. and Mashadi, B. 2012. *Vehicle Powertrain Systems: Integration and Optimization.* West Sussex, United Kingdom : John Wiley & Sons, 2012. ISBN 978-0-470-66602-9.

DeFries, T. H., Sabisch, M. A. and Kishan, S. 2013. Light-Duty Vehicle In-Use Fuel Economy Data Collection: Pilot Study. Austin, TX : Eastern Research Group, 2013. Version 8.

DeFries, T., et al. 2014. In-use fuel economy and CO2 emissions measurement using OBD data on US light-duty vehicles. *SAE International Journal of Engines.* 7, 2014, Vol. 3, doi: 10.427/2014-01-1623.

Denton, T. 2009. *Automobile Electrical and Electronic Systems, 3rd Ed.* Burlington, MA : Butterworth-Heinemann, 2009. ISBN: 0750662190.

Duran, A. and Earleywine, M. 2012. GPS Data Filtration Method for Drive Cycle Analysis Applications. *SAE World Congress & Exhibition.* DOI: 10.4271/2012-01-0743, 2012.

Earleywine, M., et al. 2011. Simulated Fuel Economy and Performance of Advanced Hybrid Electric and Plug-in Hybrid Electric Vehicles Using In-Use Travel Profiles. *IEEE - Vehicle Propulsion and Power Conference.* 2011.

Eckert, J. J., et al. 2014. Vehicle Gear Shifting Co-Simulation To Optimize Performance And Fuel Consumption In The Brazilian Standard Urban Driving Cycle. *Blucher Engineering Proceedings - SIMEA.* 2014.

Empresa de Pesquisa Energética - EPE. 2015. *Balanço Energético Nacional: Ano Base 2014: Relatório Final.* Rio de Janeiro : EPE, 2015.

Eriksson, L. and Nielsen, L. 2014. *Modeling and Control of Engines and Drivelines.* West Sussex, UK : Wiley & Sons Press, 2014. ISBN 978-1-118-47999-5.

European Community. 1999. Regulation of the european parliament and of the council. *Setting emission performance standards for new passenger cars as part of the Community's integrated approach to reduce CO2 emissions from light-duty vehicles.* Brussels : s.n., 1999. 1999/125/EC.

Faggi, R. 2012. Formação de Mistura Ar Combustível em Motores de Ignição por Faísca a Quatro Tempos. São Caetano do Sul : Dissertação. Instituto Mauá de Tecnologia. , 2012.

Fonseca, H., Ferreira, C. and Fernandes, T. 2012. New Consumption Methodologies to Measure in Real Time Fuel Consumption of Internal Combustion Engines. *15th International Conference on Experimental Mechanics.* 2012.

Fontaras, G., Pistikopoulos, P. and Samaras, Z. 2008. Experimental evaluation of hybrid vehicle fuel economy and pollutant emissions over real-world simulation driving cycles. *Atmospheric Environment.* 2008, Vol. 42, 4023-4035.

Foster, I. and Koscher, K. 2015. Exploring Controller Area Networks. San Diego: Usenix, 2015, Vol. 40, 6.

Fox, R. W., McDonald, A. T. and Pritchard, P. J. 2006. *Introdução à Mecânica dos Fluidos.* Rio de Janeiro, RJ : LTC Editora, 2006. ISBN 978-85-216-1468-5.

Frey, H. C., et al. 2003. On-Road Measurement of Vehicle Tailpipe Emissions Using a Portable Instrument. *Journal of the Air & Waste Management Association.* 2003, p. 992-1002.

Ghazikhani, M. and I., Mirzaii. 2011. Soot emission prediction of a waste-gated turbo-charged DI diesel engine using artificial neural network. *Neural Computing and Applications.* 2, 2011, Vol. 20, p. 303-308.

Gillespie, T. D. 1992. *Fundamentals of Vehicle Dynamics.* Warrendale, PA : Society for Automotive Engineers, 1992.

Goering, C. E. and Cho, H. 1988. Engine model for mapping BSFC contours. *Mathematical and Computer Modelling.* 1988, Vol. 11, p. 514-518.

Goharimanesh, M., et al. 2014. More efficiency in fuel consumption using gearbox optimization based on Taguchi method. *Journal of Industrial Engineering International.* 2014, Vol. 2, 2251-712X.

Guimarães, A. A. 2003. Análise da norma ISO11783 e sua utilização na implementação do barramento do implemento de um monitor de semeadora. São Paulo, SP : Escola Politécnica da Universidade de São Paulo, 2003.

Guo, H., Ang, J. J. and Wu, Y. 2009. Extracting Controller Area Network Data for Reliable Car Communications. *IEEE Intelligent Vehicle Symposium.* ISBN 978-1-4244-3503-6, 2009.

Guzzella, L. and Onder, C. H. 2010. *Introduction to Modeling and Control of Internal Combustion Engine Systems.* Heidelberg : Springer, 2010. ISBN 978-3-642-10774-0.

Guzzella, L. and Sciarretta, A. 2013. *Vehicle Propulsion Systems: Introduction to Modeling and Optimization.* New York : Springer, 2013. ISBN 978-3-642-35912-5.

Guzzella, L. 2007. Modeling and Control of Advanced Propulsion Systems. *Oil & Gas Science and Technology – Rev. IFP.* 4, 2007, Vol. 62, p. 585-594.

Hellström, M. 2005. Engine Speed Based Estimation of the Indicated Engine Torque. *Master's thesis.* Linkopings : Dept. of Electrical Engineering, Linkopings universitet , 2005.

Heywood, J. B. 1988. *Internal Combustion Engines Fundamentals.* New York, NY : McGraw-Hill Inc., 1988.

Hofman, T. and van Leeuwen, D. 2009. Analysis of modeling and simulation methodologies for vehicular propulsion systems. ISBN: 978-1-4244-2600-3, 2009.

How Stuff Works. How Stuff Works: Auto. [Online] [Cited: May 05, 2016.] http://auto.howstuffworks.com/transmission4.htm.

Hu, J., et al. 2012. Real-world fuel efficiency and exhaust emissions of light-duty diesel vehicles and their correlation with road conditions. *Journal of Environmental Sciences.* 24, 2012, Vol. 5, p. 865-874.

Huo, H., et al. 2011. Fuel consumption rates of passenger cars in China: labels versus real-world. *Energy Policy.* 39, 2011, 7130-7135.

Igarashi, H. 2011. Precise Speedometer Using the GPS and IMU. *Journal of the Society of Automotive Engineers of Japan.* 2011, Vol. 65, 7.

INMETRO, Divisão de Programas de Avaliação da Conformidade. 2011. Requisitos de avaliação da conformidade para veículos. Rio de Janeiro, RJ : s.n., 2011. Portaria 377/2011.

International Council for Clean Transportation. 2013. *From laboratory to road: A comparison of official and 'real-world' fuel consumption and CO2 values for cars in Europe and the United States.* Washington, DC : s.n., 2013.

International Council on Clean Transportation. 2014. *Global Comparison of Passenger Car and Light-commercial Vehicle Fuel Economy/GHG Emissions Standards .* Washington, DC : s.n., 2014.

Jahns, G. 1983. A Method of describing Diesel Engine performance maps. *ASAE Paper, NCR 83-103.* 1983.

Johnson, K. C., et al. 2009. On-road comparison of a portable emission measurement system with a mobile reference laboratory for a heavy-duty diesel vehicle. *Atmospheric Environment.* 2009, Vol. 43, p. 2877-2883.

Katz, J. 1995. *Race car aerodynamics.* San Diego : Department of Aerospace Engineering, San Diego State University, 1995.

Keller, J. 2014. *A Cost Effective Method to Create Accurate Engine Performance Maps & Updating the Nebraska Pumping Plant Performance Criteria.* Lincoln, Nebraska : University of Nebraska, 2014.

Kent, J. H., Allen, G. H. and Rule, G. 1977. A driving cycle for sydney. *Transportation Research.* 1977, Vol. 12, 147-152.

Kumar, N. and Pandey, K. P. 2015. A visual basic program for predicting optimum gear and throttle position for best fuel economy for 32 kW tractor. *Computers and Electronics in Agriculture.* 119, 2015, p. 217-227.

Lasky, T. Y., et al. 2006. *Development of vehicular and personal universal longitudinal travel diary systems using GPS and new technology.* Davis, California : University of California at Davis, 2006. UCD-ARR-06-12-31-01.

Leica. 1999. Introduction to GPS (Global Positioning System). Heerbrugg, Switzerland : Leica Geosystems AG, 1999.

Liu, J., Wang, X. and Khattak, A. 2016. Customizing driving cycles to support vehicle purchase and use decisions: Fuel economy estimation for alternative fuel vehicle users. *Transportation Research: Part C.* 2016, Vol. 67, 280-298.

Lotfan, R. S., et al. 2016. ANN-based modeling and reducing dual-fuel engine's challenging emissions by multi-objective evolutionary algorithm NSGA-II. *Applied Energy.* 2016, Vol. 175, p. 91-99.

Lu, D., et al. 2006. Modelling of tire overturning moment and loaded radius. *Vehicle System Dynamics.* 2006, Vol. 44, p. 104-114.

Lucas, G. G. and Emtage, A. L. 1987. A New Look at the Analysis of Coast-Down Test Results. *Proceedings of the Institution of Mechanical Engineers, Part D: Journal of Automobile Engineering.* 201, 1987, 91.

Luo, Z., et al. 2016. Multi-objective optimization for GPU3 Stirling engine by combining multi-objective algorithms. *Renewable Energy.* 2016, Vol. 94, p. 114-125.

Mahlia, T. M. I., Tohno, S. and Tezuka, T. 2012. A review on fuel economy test procedure for automobiles: Implementation possibilities in Malaysia and lessons for other countries. *Renewable and Sustainable Energy Reviews.* 16, 2012, p. 4029-4046.

Maloney, P. and Nursilo, W. 2011. *Optimizing Performance and Fuel Economy of a Dual-Clutch Transmission Powertrain with Model-Based Design.* s.l. : Mathworks, 2011. 91968.

Manzoli, A. 2009. *Análise das emissões veiculares em trajetos urbanos curtos com localização por GPS.* São Carlos, SP : Escola de Engenharia de São Carlos, Universidade de São Paulo, 2009.

Maroteaux, F., Saad, C. and Aubertin, F. 2015. Development and validation of double and single Wiebe function for multi-injection mode Diesel engine combustion modelling for hardware-in-the-loop applications. *Energy Conversion and Management.* 2015, Vol. 105, p. 630-641.

Mashadi, B. and Crolla, D. 2011. *Vehicle Powertrain Systems.* Essex, United Kingdom : Wiley, 2011. ISBN: 9780470666029.

McKiernan, M., et al. 1987. Estimating Diesel engine performance by indirect methods. *SAE Technical Paper Series, 871606.* ISSN 0148-7191, 1987.

Meiden automotive test systems. 2011. Chassis Dynamometer system. [Online] 2011. [Cited: Abril 21, 2015.] http://automotive.meidensha.co.jp/en/system/index01.html.

Mellios, G., et al. Parametrisation of fuel consumption and CO2 emissions of passenger cars and light commercial vehicles for modelling purposes. *JRC Scientific and Technical Reports.* p. 116.

Meywerk, M. 2015. *Automotive Series: Vehicle Dynamics.* West Sussex, United Kingdom : John Wiley & Sons, 2015. ISBN 9781118971352.

Mock, P., et al. 2012. 2012. *International Council on Clean Transportation Working Paper.* 2012.

Moran, M. J. and Shapiro, H. W. 2000. *Princípios de Termodinâmica para Engenharia.* Rio de Janeiro, RJ : LTC Editora, 2000.

Mr. Clutch. Mr. Clutch. *Services: Differential Rebuilding.* [Online] [Cited: July 05, 2016.] http://www.mrclutchnw.com/services/differential-rebuilding/.

National Highway Traffic Safety Administration (NHTSA). 1978. Code of Federal Regulations. *Procedures for considering environmental impacts.* Washington, DC : s.n., 1978. 49 CFR Part 520-538.

Navet, N. and Simonot-Lion, F. 2008. *Automotive Embedded Systems Handbook.* Boca Raton : CRC Press, 2008. ISBN-10: 0-8493-8026-X.

Necula, E. 2015. Analyzing Traffic Patterns on Street Segments Based on GPS Data Using R. *Transportation Research Procedia.* 2015, Vol. 10, p. 276-285.

Nose, H., et al. 2013. Fuel Enrichment Control System by Catalyst Temperature Estimation to Enable Frequent Stoichiometric Operation at High Engine Speed/Load condition. Detroit, MI : SAE World Congress & Exhibition, 2013. ISSN: 0148-7191.

Ntziachristos, L., et al. 2014. In use vs. type-approval fuel consumption of current passenger cars in Europe. *Energy Policy.* 2014, Vol. 67, 403-411.

Oh, Y., et al. 2014. Modeling effects of vehicle specifications on fuel economy based on engine fuel consumption map and vehicle dynamics. *Transportation Research: Part D.* 32, 2014, p. 287-302.

Palocz-Andresen, M. 2012. *Decreasing Fuel Consumption and Exhaust Gas Emissions in Transportation.* Berlin : Springer, 2012. ISBN 978-3-642-11975-0.

Papaioannou, I. N. 2005. Estudo da eletrônica embarcada automotiva e sua situação atual no Brasil. *Dissertação de Mestrado.* São Paulo, SP : Escola Politécnica da Universidade de São Paulo, 2005.

Pennsylvania State University. Global Positioning Systems. *Pennsylavania e-education site.* [Online] [Cited: 05 20, 2016.] https://www.e-education.psu.edu/geog160/node/1923.

Post, K., et al. 1984. Fuel Consumption and Emission Modelling by Power Demand and a Comparison with Other Models. *Transportation Research: Part A.* 3, 1984, Vol. 18A, p. 191-213.

Post, K., et al. 1981. *Fuel economy and emission research annual report by the University of Sydney for 1980-1981.* Sydney : Charles Kolling Res. Lab., University of Sidney, 1981.

Proakis, J. and Manolakis, D. G. 1996. *Digital Signal Processing: Principles, Algorithms and Applications. 3rd edition.* Upper Saddle River, New Jersey : Prentice-Hall, Inc., 1996. ISBN 0-13-394338-9l.

Racelogic. 2016. Performance Testing. *VBOX Automotive.* [Online] July 15th, 2016. [Cited: July 15th, 2016.] https://www.vboxautomotive.co.uk/index.php/en/applications/performance-testing.

—. 2014. VBOX 3i v3 100Hz Data Logger. [Online] Novembro 28, 2014. [Cited: Abril 17, 2015.] http://www.racelogic.co.uk/_downloads/vbox/Datasheets/Data_Loggers/RLVB3i_Data.pdf.

Rawlings, J. O., Pantula, S. G. and Dickey, D. A. 1998. *Applied Regression Analysis: A Research Tool.* New York : Springer, 1998. ISBN 0-387-98454-2.

Ribbens, W. B. 2013. *Understanding Automotive Electronics. 7th Ed.* Waltham, MA : Butterworth–Heinemann, 2013. ISBN: 978-0-7506-7599-4.

Saerens, B., et al. 2009. Minimization of the fuel consumption of a gasoline engine using dynamic optimization. *Applied Energy.* 86, 2009, p. 1582-1588.

Sahlholm, P. and Johansson, K. H. 2010. Road Grade Estimation for Look-ahead Vehicle Control Using Multiple Measurement Runs. *Control Engineering Practice.* 18, 2010, p. 1328-1341.

Sandoval, D. and Heywood, J. B. 2003. An improved friction model for spark-ignition engines. *SAE International.* 2003.

Sayin, C., et al. 2006. Performance and exhaust emissions of a gasoline engine using artificial neural network. *Applied Thermal Engineering.* 1, 2006, Vol. 27, p. 46-54.

Schmid, C. 1938. *Die Fahrwiderstaende beim Kraftfahrzeug und die Mittel zu Ihrer Verringerung.* Stuttgart : ATZ, 1938.

Shan, Z. and Zhu, Q. 2015. Camera location for real-time traffic state estimation in urban road network using big GPS data. *Neurocomputing.* 2015, Vol. 169, p. 134-143.

Silva, L. R. T. and Araújo, T. S. 2010. Ferramenta de diagnóstico automotivo OBD-II. Santo André, SP : Centro Paula Souza Faculdade de Tecnologia , 2010.

Sivak, M. and Schoettle, B. 2012. Eco-driving: Strategic, tactical, and operational decisions of the driver that. *Transport Policy.* 22, 2012, p. 96-99.

Skog, I. and Handël, P. 2014. Indirect Instantaneous Car-Fuel Consumption Measurements. *IEEE Transactions on Instrumentation and Measurement.* 2014, Vol. 63, 12.

Smith, R., et al. 2011. GPS-based optimization of plug-in hybrid electric vehicles' power demands in a cold weather city. *Transportation Research: Part D.* 2011, Vol. 16, p. 614-618.

Smith, S. W. 1999. *The Scientist and Engineer's Guide to Digital Signal Processing.* San Diego, CA : California Technical Publishing, 1999.

—. 1999. *The Scientist and Engineer's Guide to Digital Signal Processing. 2nd Edition.* San Diego, California : California Technical Publishing, 1999. ISBN 0-9660176-7-6.

Society for Automotive Engineering - SAE. 1995. *Procedure for Mapping Engine Performance-Spark Ignition and Compression Ignition Engines.* 1995.

Tatschla, R., et al. 2014. A scalable simulation methodology for assessment of SI-engine performance and fuel consumption on component, subsystem and system level. 2014.

Teixeira, F. C. R. and Tournier, D. R. 2015. Utilização de telemetria para diagnóstico automotivo à distância. *XXIII Simpósio Internacional de Engenharia Automotiva.* 1, 2015, Vol. 2.

The International Council on Clean Transportation. 2014. *Global Comparison of Passenger Car and Light-commercial Vehicle Fuel Economy/GHG Emissions Standards.* 2014.

Togun, N. and Baysec, S. 2010. Genetic programming approach to predict torque and brake specific fuel consumption of a gasoline engine. *Applied Energy.* 2010, Vol. 87, p. 3401-3408.

Tong, H. Y., Hung, W. T. and Cheung, C. S. 1999. Development of a driving cycle for Hong Kong. *Atmospheric Environment.* 1999, Vol. 33, 2323-2335.

Tong, H. Y., Hung, W. T., Cheung, C. S. 2011. On-Road Motor Vehicle Emissions and Fuel Consumption in Urban Driving Conditions. *Journal of the Air & Waste Management Association.* 2011.

Turkson, R. F., et al. 2016. Artificial neural network applications in the calibration of spark-ignition engines: An overview. *Engineering Science and Technology, an International Journal.* 2016.

Turner, J. 2009. *Automotive Sensors.* New York : Momentum Press, LLC., 2009. ISBN 1-60650-009-0.

Tyretown. Record Your Car Tire Size. *Tyre town.* [Online] [Cited: June 21, 2016.] http://www.tyretown.com/my_record_tyre_size_car.htm.

U.S. Energy Information Administration. 2012. Annual Energy Review. Washington, DC : s.n., 2012. 2011. DoE/EIA-0384(2011).

U.S. Environmental Protection Agency. 1974. *A Report on Automotive Fuel Economy.* Washington, DC : University of California. Institute of Transportation and Traffic Engineering , 1974.

—. 1974. *A Report on Automotive Fuel Economy.* Washington, D : University of California. Institute of Transportation and Traffic Engineering, 1974.

—. 1993. *Federal test procedure review project: preliminary technical report.* Washington, D.C. : U. S. Environmental Protection Agency, Certification Division, Office of Mobile Sources, Office of Air & Radiation, 1993. EPA 420-R-93-007.

—. 2013. *Fuel Economy Labels in EPA and DOT Final Rulemaking "Revisions and Additions to Motor Vehicle Fuel Economy Label".* Washington, DC : EPA, 2013.

—. 2012. Use of Data from "Development of Generic Link-Level Driving Cycles", Sierra Research, May 5, 2009. Washington, DC : Sierra Research, Inc., 2012. EPA-420-B-12-050.

Wallner, T., Scarcelli, R. and Matthias, N. 2011. Optimization of Direct-Injection H2 Combustion Engine Performance, Efficiency, and Emissions. *Argonne National Laboratory.* 2011.

Walter, R. 2014. Acquiring Data from In-Vehicle Networks. *University of California, Riverside.* 2014.

Wang, H., Shi, Z. and Ren, Z. 2013. Instantaneous Road Grade Estimation Based on GPS/IMU. *Journal of Computational Information Systems.* 9, 2013, Vol. 18, p. 7207-7214.

Wang, Q., et al. 2008. Characterization of vehicle driving patterns and development of driving cycles in Chinese cities. *Transportation Research: Part D.* 2008, Vol. 13, 289-297.

Weiss, M., et al. 2011. Analyzing on-road emissions of light-duty vehicles with Portable Emission Measurement Systems (PEMS). *European Commission: Joint Research Centre.* ISBN: 978-92-79-19072-8, 2011.

Wood, E., et al. 2014. Appending High-Resolution Elevation Data to GPS Speed Traces for Vehicle Energy Modeling and Simulation. Golden, Colorado : U.S. National Renewable Energy Laboratory, 2014. NREL/TP-5400-61109.

Wu, X., et al. 2015. Real-world emissions and fuel consumption of diesel buses and trucks in Macao: From on-road measurement to policy implications. *Atmospheric Environment.* 2015, Vol. 120, 393-403.

Xu, Y., et al. 2015. Assessment of alternative fuel and powertrain transit bus options using real world operating data: life-cycle fuel and emissions modeling. *Applied Energy.* 2015, Vol. 154, 143-159.

Yasin, T. P. 1978. The analytical basis of automobile coastdown testing. *Society of Automotive Engineers.* 1978.

Yldiz, Y., et al. 2010. Spark Ignition Engine Fuel-to-Air Ratio Control: An Adaptive Control Approach. *Control Engineering Practice.* 12, 2010, Vol. 18, p. 1369-1378.

Yu, Q., Li, T. and Li, H. 2016. Improving urban bus emission and fuel consumption modeling by incorporating passenger load factor for real world driving. *Applied Energy*. 2016, Vol. 161, 101-111.

Zhang, S., et al. 2014. Real-world fuel consumption and CO2 emissions of urban public buses in Beijing. *Applied Energy*. 2014, Vol. 113, p. 1645-1655.

Zhao, J. and Xu, M. 2013. Fuel economy optimization of an Atkinson cycle engine using genetic algorithm. *Applied Energy*. 105, 2013, p. 335-348.

APPENDIX – FUEL MAPS AND ACCUMULATIVE FUEL CONSUMPTION CHARTS

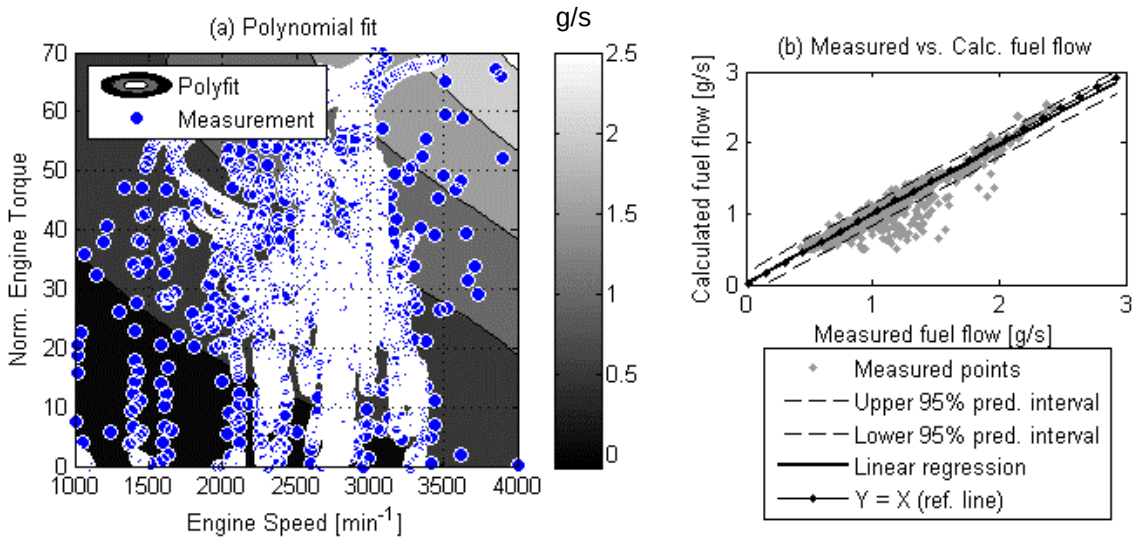

Figure A.1 –Engine map polynomial fit (1) and measurement versus calculation fuel flow plot (b) for vehicle 1, run 1

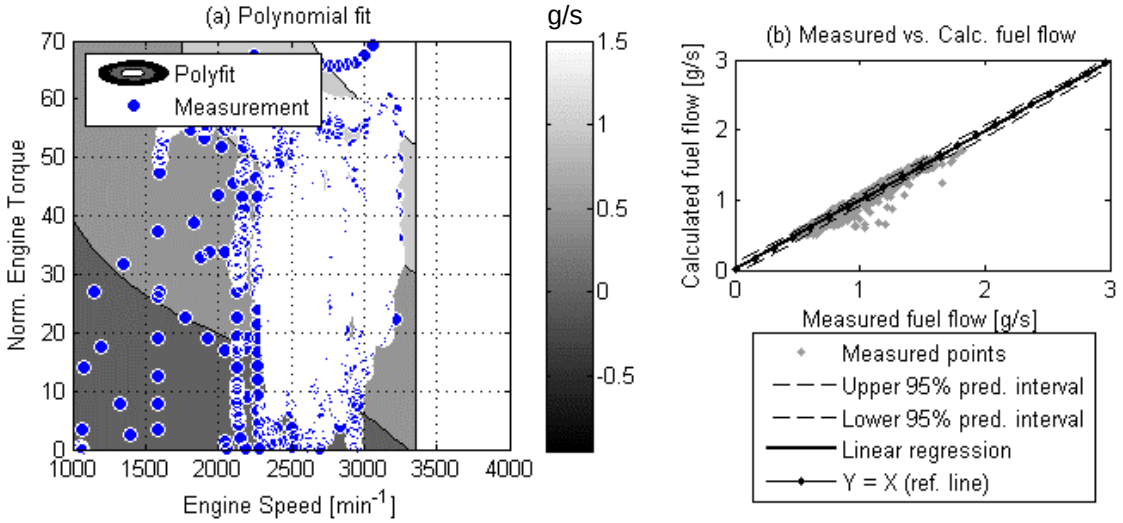

Figure A.2 –Engine map polynomial fit (1) and measurement versus calculation fuel flow plot (b) for vehicle 1, run 2

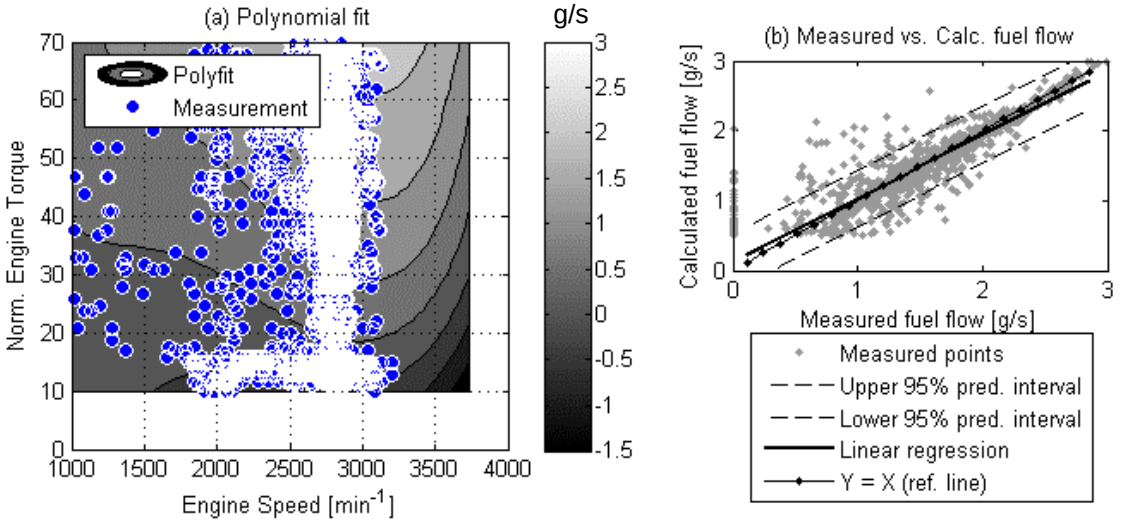

Figure A.3 –Engine map polynomial fit (1) and measurement versus calculation fuel flow plot (b) for vehicle 2, run 1

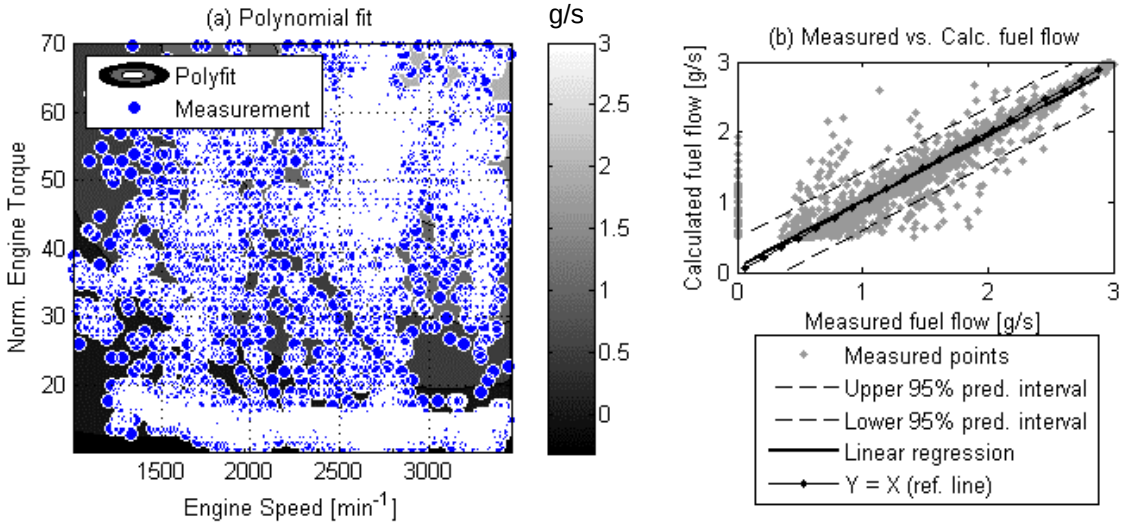

Figure A.4 –Engine map polynomial fit (1) and measurement versus calculation fuel flow plot (b) for vehicle 2, run 2

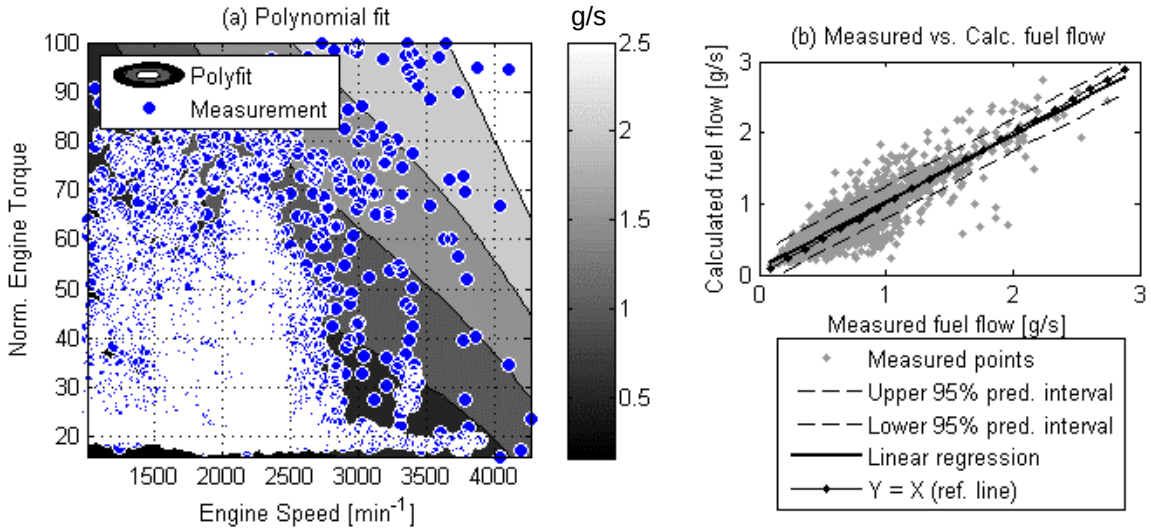

Figure A.5 –Engine map polynomial fit (1) and measurement versus calculation fuel flow plot (b) for vehicle 3, run 1

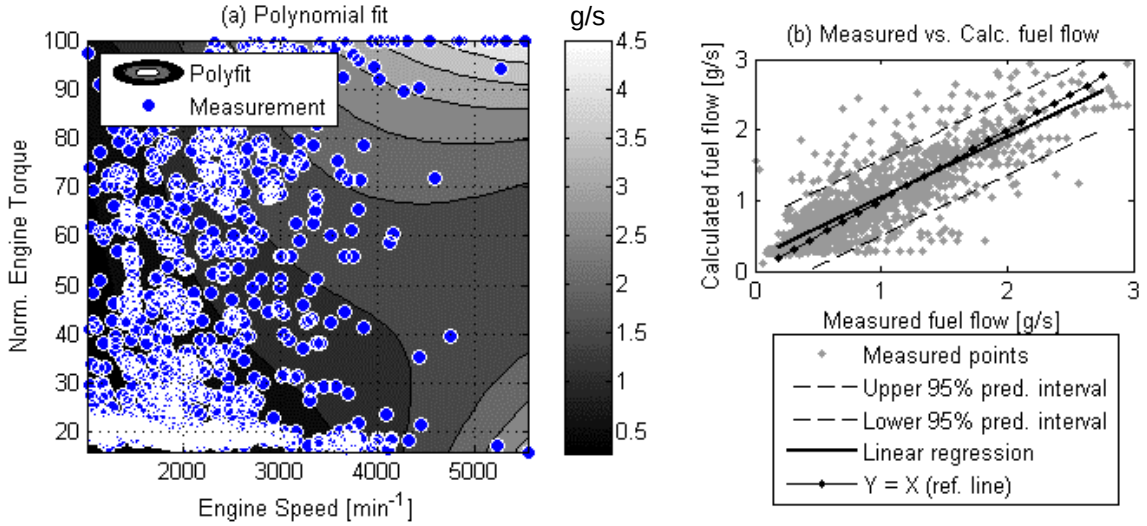

Figure A.6 –Engine map polynomial fit (1) and measurement versus calculation fuel flow plot (b) for vehicle 3, run 2

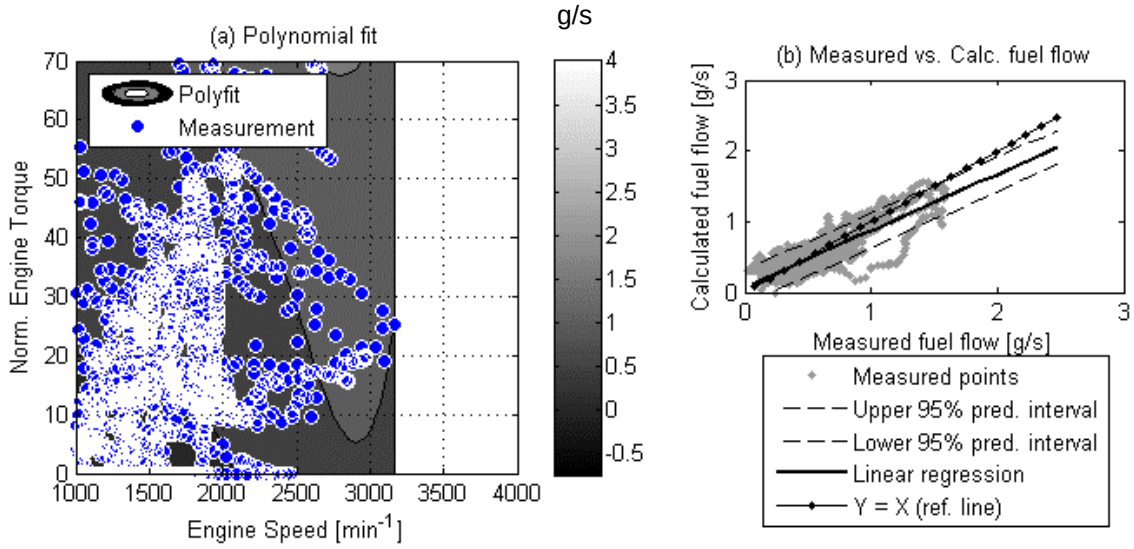

Figure A.7 –Engine map polynomial fit (1) and measurement versus calculation fuel flow plot (b) for vehicle 4, run 1

g/s

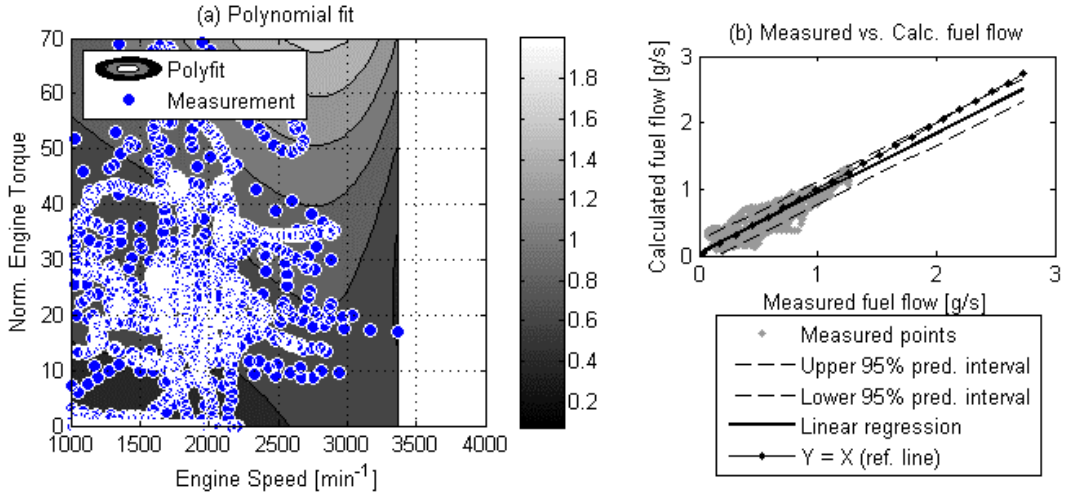

Figure A.8 –Engine map polynomial fit (1) and measurement versus calculation fuel flow plot (b) for vehicle 4, run 2

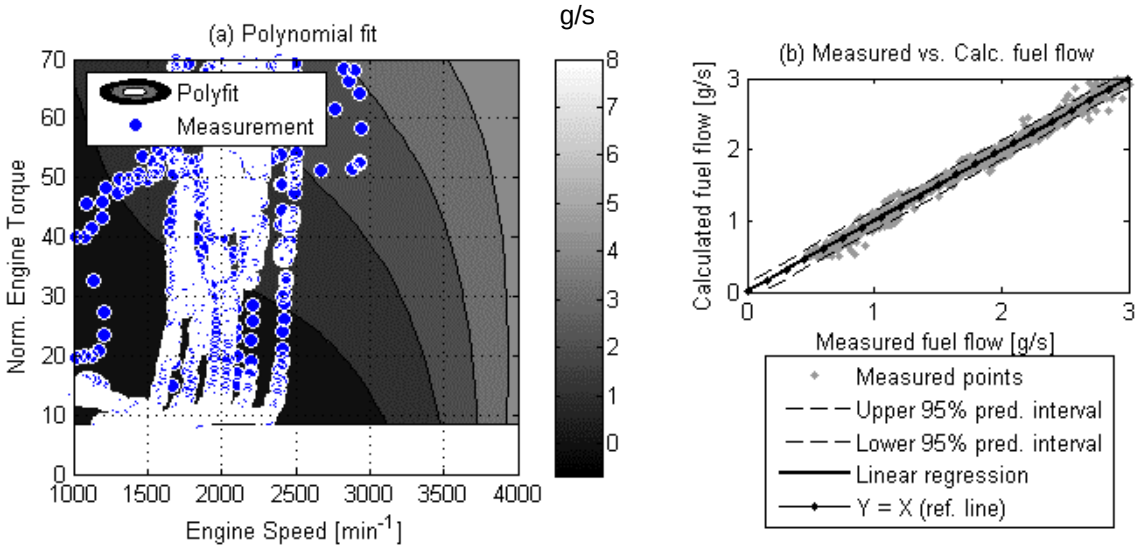

Figure A.9 –Engine map polynomial fit (1) and measurement versus calculation fuel flow plot (b) for vehicle 5, run 1

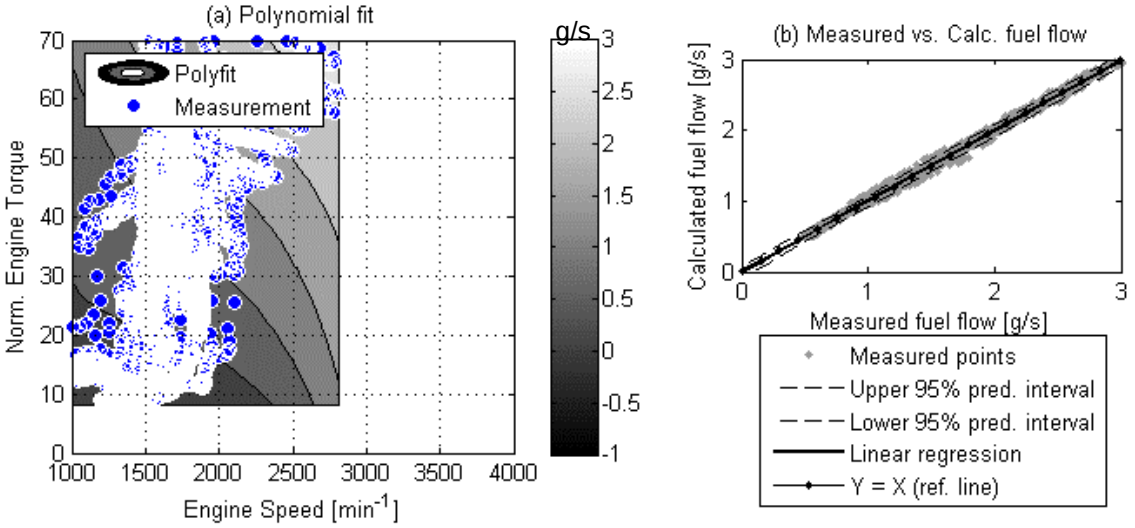

Figure A.10 –Engine map polynomial fit (1) and measurement versus calculation fuel flow plot (b) for vehicle 5, run 2

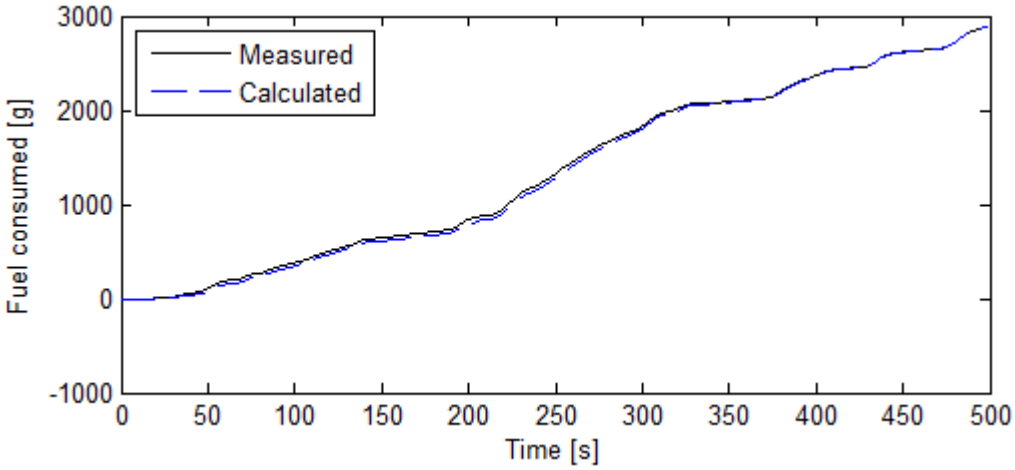

Figure A.11 – Total measured fuel flow versus calculated fuel flow for vehicle 1, run 1

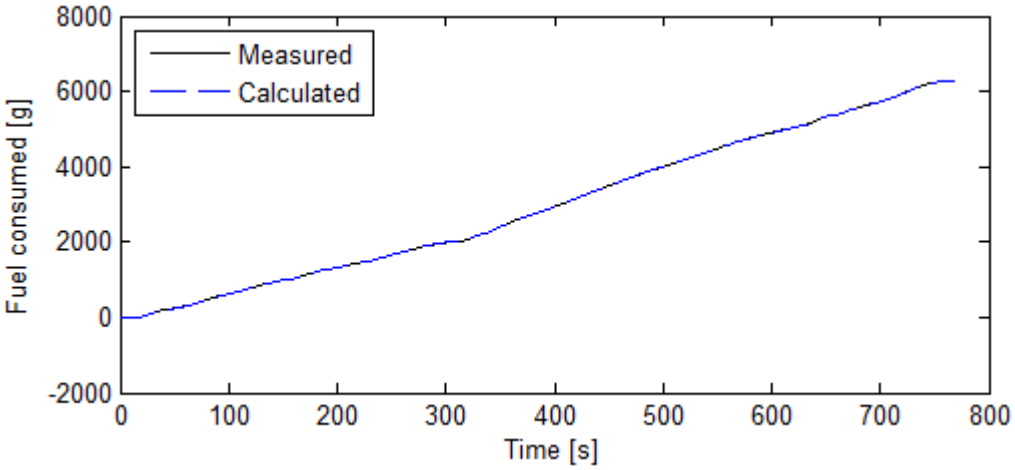

Figure A.12 – Total measured fuel flow versus calculated fuel flow for vehicle 1, run 2

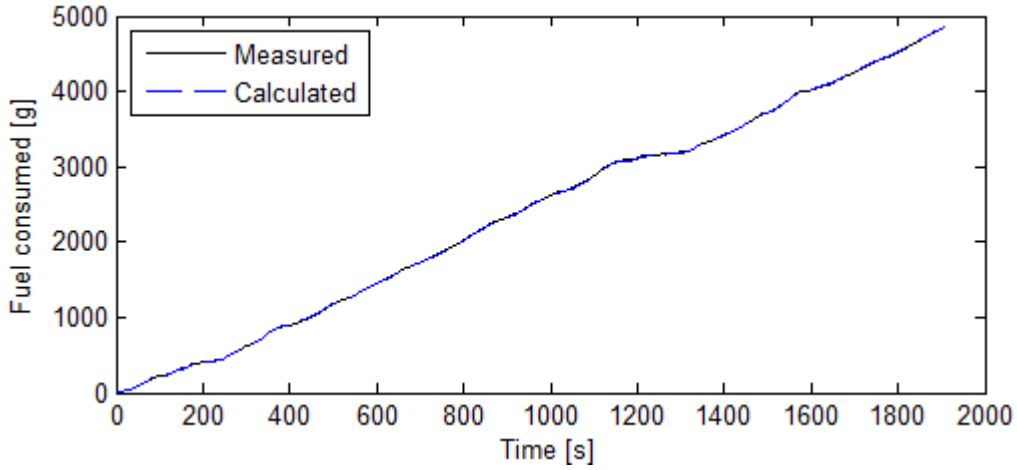

Figure A.13 – Total measured fuel flow versus calculated fuel flow for vehicle 2, run 1

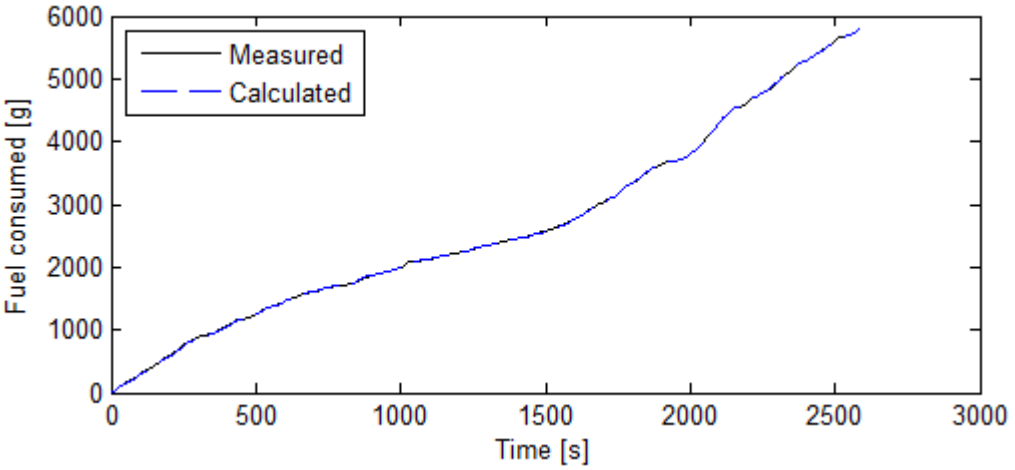

Figure A.14 – Total measured fuel flow versus calculated fuel flow for vehicle 2, run 2

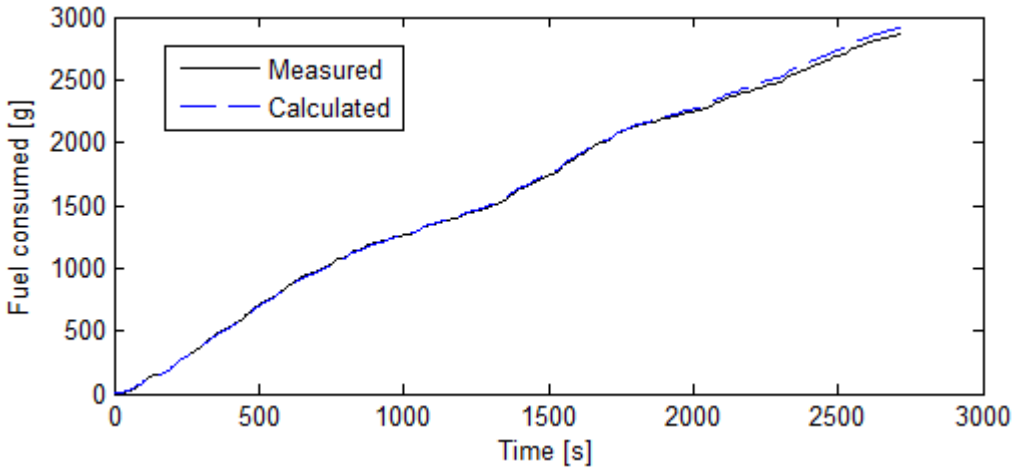

Figure A.15 – Total measured fuel flow versus calculated fuel flow for vehicle 3, run 1

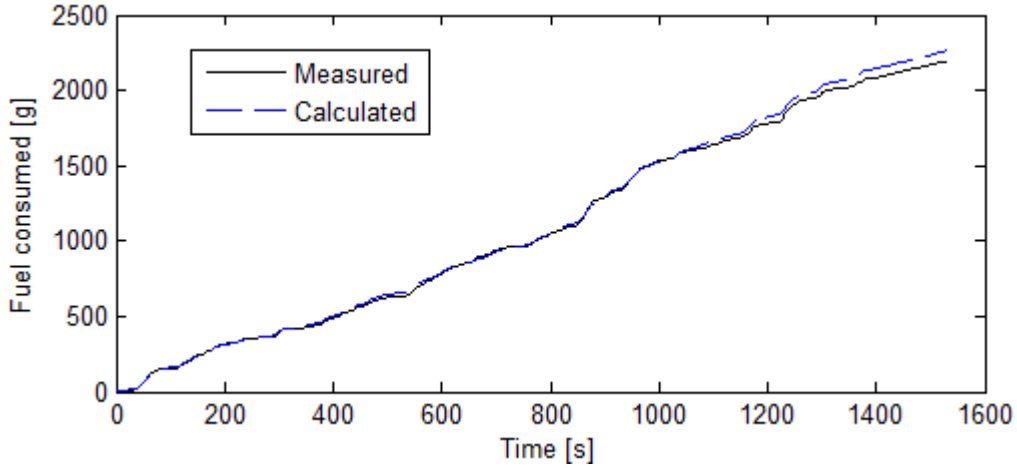

Figure A.16 – Total measured fuel flow versus calculated fuel flow for vehicle 3, run 2

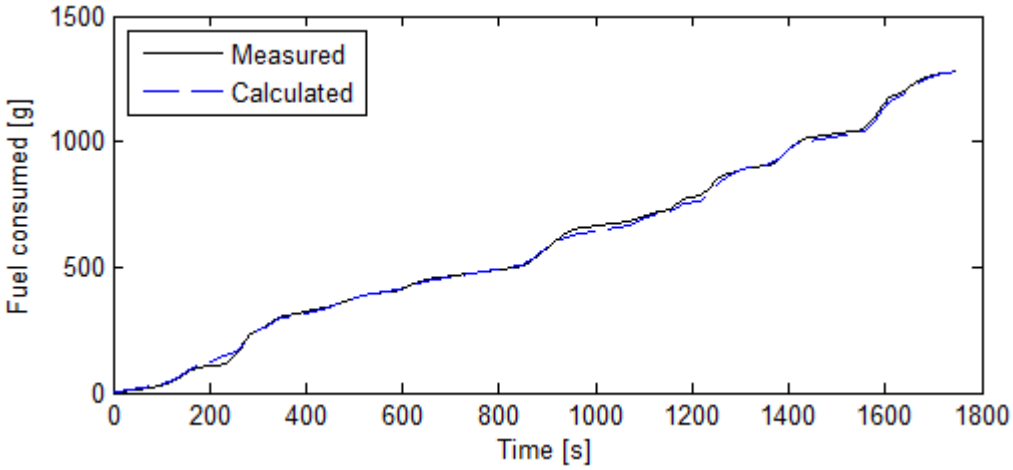

Figure A.17 – Total measured fuel flow versus calculated fuel flow for vehicle 4, run 1

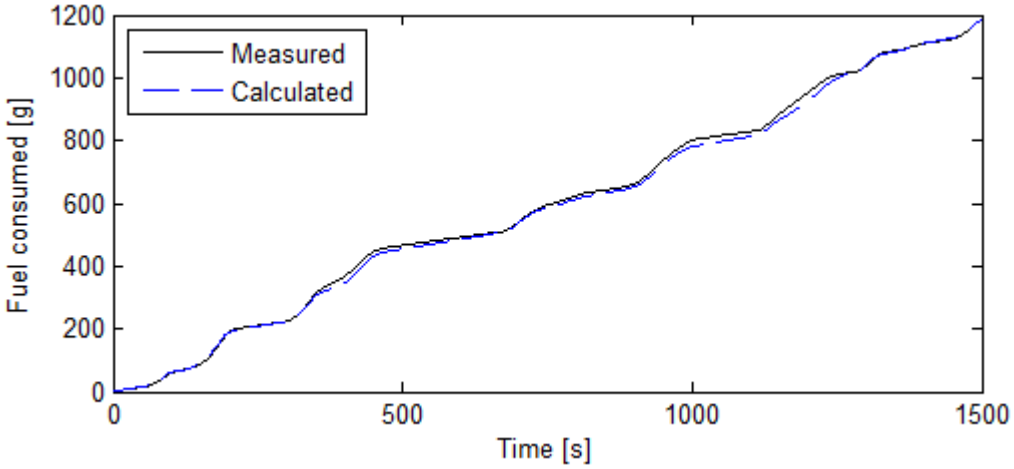

Figure A.18 – Total measured fuel flow versus calculated fuel flow for vehicle 4, run 2

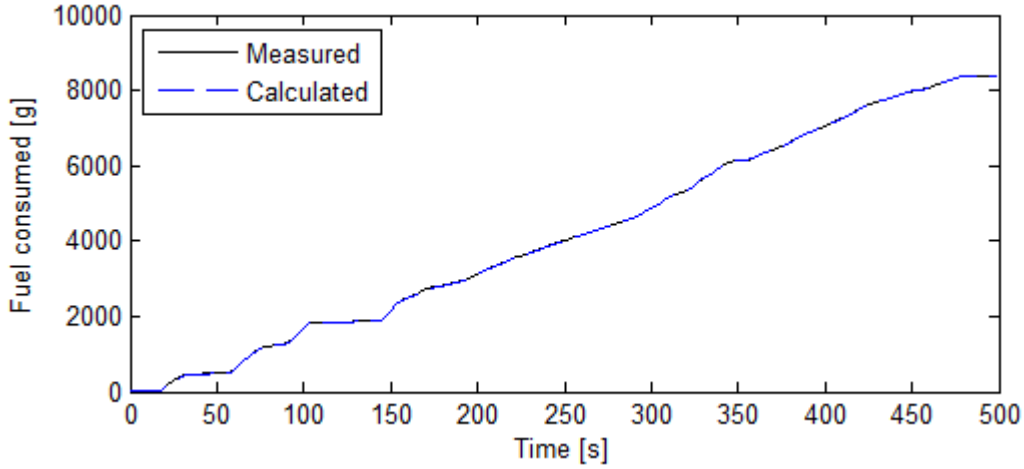

Figure A.19 – Total measured fuel flow versus calculated fuel flow for vehicle 5, run 1

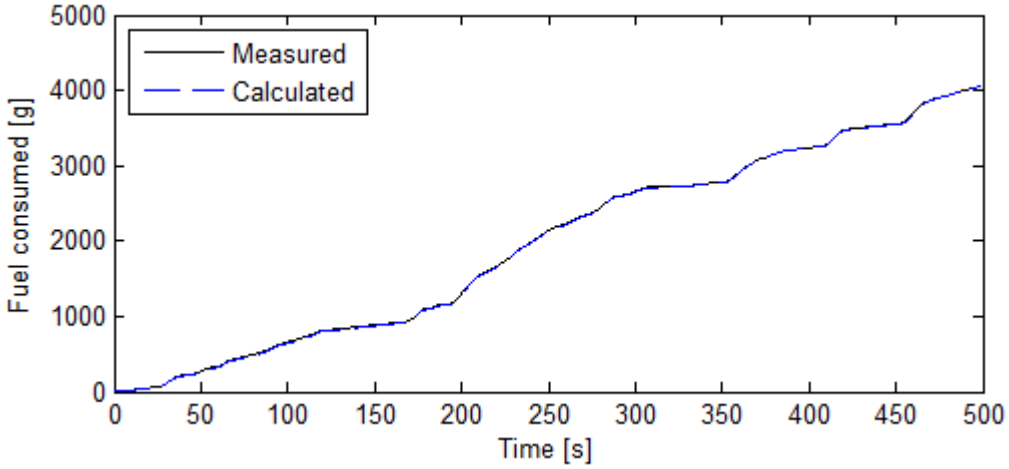

Figure A.20 – Total measured fuel flow versus calculated fuel flow for vehicle 5, run 2